Dynamic Bonding in Soft Matter Materials and on Surfaces

Zur Erlangung des akademischen Grades eines

DOKTOR DER NATURWISSENSCHAFTEN

(Dr. rer. nat)

Karlsruhe Institut für Technologie (KIT),

Fakultät für Chemie und Biowissenschaften,

Institut für Technische Chemie und Polymerchemie

genehmigte

DISSERTATION

von

Dipl.-Chem. Nils David Wedler

geb. Jasinski aus

Heidelberg, Deutschland

Dekan: Prof. Dr. Willem Klopper

Referent: Prof. Dr. Christopher Barner-Kowollik

Koreferent: Prof. Dr. Hans-Achim Wagenknecht

Tag der mündlichen Prüfung: 10.02.2017

“Chemical synthesis is uniquely positioned at the heart of chemistry, the central science, and its impact on our lives and society is all pervasive.”

- Elias James Corey

Für

Nadin

ERKLÄRUNG

Ich erkläre hiermit, dass ich die vorliegende Arbeit im Rahmen der Betreuung durch Prof. Dr. Christopher Barner-Kowollik selbstständig verfasst und keine anderen als die angegebenen Quellen und Hilfsmittel verwendet habe. Wörtlich oder inhaltlich übernommene Stellen sind als solche kenntlich gemacht und die Satzung des Karlsruher Instituts für Technologie (KIT) zur Sicherung guter wissenschaftlicher Praxis wurde beachtet. Des Weiteren erkläre ich, dass ich mich derzeit in keinem weiteren laufenden Promotionsverfahren befinde und auch keine vorausgegangenen Promotionsversuche unternommen habe.

Karlsruhe, den

ZUSAMMENFASSUNG

Perlmutt, welches Muschelschalen maßgeblich ihre mechanischen Eigenschaften verleiht, ist ein Beispiel für Biokomposite mit hervorragender Festigkeit bei geringem Gewicht. Durch seine außergewöhnliche mechanische Leistungsfähigkeit, die nicht in seinen Einzelkomponenten, sondern vielmehr in deren Anordnung auf nanoskopischer Ebene beruht, ist es eine fortwährende Quelle der Inspiration für Materialwissenschaftler: 95 Vol% des Perlmutts bestehen aus nanometergroßen Aragonit-Plättchen ($CaCO_3$), die parallel in der sogenannten „brick-and-mortar“ (sinngemäß: „Backsteinwand“) Struktur angeordnet und mit 5 Vol% Biopolymer verklebt sind, was dazu führt, dass Perlmutt seine Komponenten in Zähigkeit um das 3000-fache übertrifft. Diese Doktorarbeit ist Teil einer größeren Kooperation, Perlmutts mikroskopische Struktur mit synthetischen Nanoclays (Natrium Fluorohectorit) und dynamisch (supramolekular und dynamisch kovalent) vernetzten Polymer-Matrices, deren Synthese Teil dieser Arbeit ist, in einem selbstorganisierenden Ansatz in Wasser nachzuahmen. Zusätzlich zu ihrem natürlichen Vorbild, sollen die entsprechenden Nanokomposite (durch ihre dynamischen Vernetzungspunkte) thermoreversibel vernetzen, was zur Verformbarkeit der Komposite bei erhöhter Temperatur führen soll. Im ersten Teil der vorliegenden Arbeit werden verschiedene synthetische Ansätze zu solchen dynamisch und reversibel vernetzten (wasserlöslichen) Polymeren beschrieben. Hierbei werden polymere Matrices, vernetzt durch selbst-komplementäre Wasserstoffbrückenbindung auf Basis von 2-Ureido-4-pyrimidonen (UPy), in Form von endgruppenfunktionalisierten Sternpolymeren, kurzen linearen Copolymeren und langen Copolymeren synthetisiert. Dabei werden Elektronentransfergenerierter Aktivator Atomtransfer Radikalpolymerisation (AGET ATRP), Reversible Additions-Fragmentierungs Kettentransfer (RAFT) und konventionelle Freie Radikalische Copolymerisation (FRP) als Polymerisationstechniken verwendet. Der Aufbau einer Bibliothek aus verschiedenen Polymerarchitekturen, Kettenlängen, Funktionalisierungsgraden mit UPy, einschließlich der Synthese neuer UPy-Monomere und der Entwicklung einer neuen elektrochemischen Methode zur Aufreinigung von wasserlöslichen Polymeren, wird detailliert ausgearbeitet. Jedes Polymer wird abschließend als Matrix in Nanokompositen verwendet und anschließend mechanischen Tests unterzogen, deren Ergebnisse im Hinblick auf die

molekularen Eigenschaften der Polymere diskutiert werden. In einem zweiten synthetischen Ansatz für thermoreversibel vernetzte Matrices wird das Hetero Diels-Alder Paar Cyanodithioester (CDTE) und Sorbinalkohol als dynamische und reversible Vernetzungschemie verwendet. Hierfür werden zwei entsprechend funktionalisierte Methacrylat-Monomere synthetisiert, mittels FRP copolymerisiert, als Matrixpolymer in Nanokompositen verwendet und abschließend in ihren mechanischen Eigenschaften in Kontext zur molekularen Beschaffenheit und zu vergleichbaren UPy-Matrices gesetzt. Im zweiten Teil dieser Dissertation werden, mit dem Ziel Einblicke in das Verhalten der Wasserstoffbrücken an den Matrix-Füllstoff-Grenzflächen der obigen Komposite zu gewinnen, makroskopische Siliziumwafer als Modelsubstrate verwendet. Mittels eines Tetrazol-Silans und Maleimid-funktionalisierten Wasserstoffbrückenbindungsmotiven werden die Wafer durch photochemische NITEC Reaktion mit örtlicher Auflösung funktionalisiert und Immobilisationsexperimente mit passenden Bindungspartnern aus Lösung durchgeführt. Hierbei wird das Immobilisationsverhalten mittels Flugzeit-Sekundärionen-Massenspektrometrie (ToF-SIMS) für selbstkomplementäre (UPy Dimere) und heterokomplementäre (a)symmetrische Oligoamide (SOA-AOA Dimere) untersucht, was in Kombination zu einem umfassenden Bild für Wasserstoffbrückenbindung an entsprechenden Grenzflächen führt. Zusätzlich hierzu wird im Fall der heterokomplementären Wasserstoffbrückenbindung die Wiederholbarkeit von Immobilisationszyklen demonstriert. Im dritten und letzten Teil der vorliegenden Dissertation wird die Fähigkeit des CDTE-Sorbinalkohol Hetero Diels-Alder Paares zur reversiblen Vernetzung polymerer Materialien in Form von Polymereinzelketten-Nanopartikeln gezeigt. In einem Ansatz, basierend auf einem externen Vernetzer, wird ein CDTE-funktionalisiertes Methacrylat mittels konventioneller FRP und RAFT copolymerisiert und die resultierenden polymeren Vorläufer werden durch einen Sorbinalkohol Bilinker zu Nanopartikeln kollabiert. Zusätzlich werden die Partikel unter Ausnutzung der reversiblen Natur von Diels-Alder Reaktionen mittels Sorbinalkohol wieder zu offenen Polymerketten entfaltet. Die Einflüsse von Kettenlänge, Vernetzungsgrad und kinetischen Effekten auf die Ketten(ent)faltung (gemessen mit Größenausschlusschromatographie (SEC), Protonen-Kernresonanzspektroskopie (^{1}H-NMR) und Dynamische Lichtstreuung (DLS)) werden im Zusammenhang mit thermodynamischen Voraussetzungen für Polymerkettenfaltung systematisch untersucht und diskutiert.

ABSTRACT

Nacre, which is part of the amour of seashells and one example of Nature´s lightweight, load-bearing bio-composites, constantly inspires material scientists, since its exceptional mechanic performance is based on in its precise structuring on nano-scale rather than its constituents. Composed of 95 vol% nano-meter sized aragonite ($CaCO_3$) platelets, parallelly aligned in a so-called “brick-and-mortar” structure and laminated with 5 vol% biopolymer, nacre excels the toughness of its components close to 3,000 times. The present thesis is embedded in a joint project with material scientists aiming at mimicking nacre´s microscopic structure with synthetic nanoclays (sodium fluorohectorite) and dynamically cross-linked (supramolecular and dynamic covalent) polymer matrices, whose fabrications are described herein, in a water-based self-assembly approach. Unlike the example by Nature, the final nano-composite (NC) is designed to be thermoreversibly cross-linked, capable to undergo several reshaping cycles at elevated temperature, based on the reversible nature of matrix cross-linking.

In the first of three parts of the present thesis, various routes towards such water-soluble, reversibly and dynamically cross-linked matrices are described. In a first approach, matrices, cross-linked *via* self-complementary hydrogen bonding of 2-ureido-4-pyrimidone (UPy), are prepared as endgroup-functionalized star polymers, short linear copolymers, fabricated by Reversible Addition-Fragmentation Chain Transfer (RAFT) copolymerization, and long copolymers, synthesized by conventional Free Radical Copolymerization (FRP). A library of different architectures, chain-lengths and degrees of UPy-functionalization is synthesized (including the synthesis of numerous new UPy monomers and the development of a new electrochemical purification method), employed in NC formation with nano-clays and subsequently tested mechanically. The mechanic performances of NCs are interpreted with regard to the molecular parameters of the matrices. In a second approach towards thermoreversibly cross-linked matrices, the cyanodithioester (CDTE)-sorbic alcohol hetero Diels-Alder (HDA) couple is employed as reversible cross-linker of the polymer matrix. Therefore, two methacrylate monomers with corresponding chemical moieties are synthesized, copolymerized *via* FRP and subsequently employed as matrices in NCs, which are investigated *via* tensile tests.

The mechanic performance of corresponding NCs is compared to similar UPy-matrices.

In the second part of the current thesis, seeking a deeper insight into hydrogen bonding at the interfaces of the prepared NCs, the surfaces of macroscopic silicon wafers are chosen as model system for the matrix-filler interface of the composites. Employing a tetrazole-silane agent and maleimide-functionalized hydrogen bonding motifs, the wafers are functionalized *via* the photochemically induced nitrile imine-mediated tetrazole-ene cycloaddition (NITEC) reaction in a spatially resolved manner and immobilization experiments from solution with suitable binding partners are performed. Adsorbents are monitored by Time-of-Flight Secondary Ion Mass Spectrometry (ToF-SIMS) and the behavior of self-complimentary hydrogen bonding (UPy dimers) and hetero-complementary hydrogen bonding of symmetrical and asymmetrical oligo amides (SOA-AOA dimers) are investigated systematically. The results of the studies are fused to a conclusive over-all picture. For hetero-complementary interfaces immobilization cycles were additionally investigated.

In order to demonstrate the capacity of hetero Diels-Alder chemistry to reversibly cross-link polymeric materials, in a third part of the thesis, single chain nano-particles (SCNPs) are fabricated employing reversible cross-links based on the Diels-Alder (DA) reaction of CDTE and sorbic alcohol. In a cross-linker mediated approach, a CDTE-functionalized monomer is synthesized and copolymerized *via* conventional FRP and RAFT polymerization to precursor polymers, which are subsequently folded with a new sorbic alcohol bis-linker. In addition, a SCNP is unfolded back to an open chain polymer exploiting the reversible Nature of DA chemistry by sorbic alcohol. The influences of chain-length and cross-linking density on the chain collapse, as well as kinetic effects are studied *via* Size Exclusion Chromatography (SEC), Proton Nuclear Magnetic Resonance (^{1}H-NMR) Spectroscopy and Dynamic Light Scattering (DLS) and discussed in the context of the thermodynamic requirements of a chain collapse.

TABLE OF CONTENTS

1 INTRODUCTION

The history of mankind was always closely intertwined with the discovery and utilization of new materials, since the availability and quality of tools, which form the basis for any form of human civilization, strongly depends on their constituents. Stones and wood were used already in the Stone Age, the first metal tools were used in the Bronze Age and in parallel to constant discovery of new materials, cities and cultures emerged – benefiting from new achievements in toolmaking and weapon manufacturing. Fully synthetic polymers were not discovered until the beginning of the 20th century and, although known just for a relatively short period, have undoubtedly had a massive impact on everyday life and human history. An impressive example for the historic importance of synthetic polymers is polyethylene, which nowadays is widely used in packaging. Its discovery in the ICI laboratories in England around 1930 lead to significant advances in radar technology, due to its good performance as electrical insulator, its mechanic strength and easy processability. Benefitting from the new light-weight insulator, mobile radars were decisive for turning back Germany´s submarine threat in World War II and, therefore, polyethylene significantly influenced the outcome of the war.[1] Without doubt also future dominance of cultures and progress in human development will depend on new technologies, tools and, therefore, eventually on new materials. Modern material scientists are constantly inspired by Nature´s materials, since they often consist of readily available constituents but frequently exceed in (mechanic) performance, due to their unique structuring (on microscopic scale). Nacre, as one important example for such a biomaterial, is part of the amour of sea-shells and, although consisting of brittle, nano-sized aragonite platelets, parallelly aligned and glued together with only 5 vol% biopolymer, nacre shows significantly increased energy dissipation compared to its single components. As many examples from Nature, nacre combines relatively weak single components in an exceptionally defined nanoscopic structure, resulting in remarkable increase in performance compared to its neat components (nacre excels aragonite single-crystals in toughness close to 3,000 times).[2]

The present thesis is part of a larger collaborative project aiming at mimicking nacre´s structuring on nano-scale with artificial materials, introducing thermoreversible reshapability as additional mechanic feature to the final nano-

composite for ready processability. The contribution to this overall aim of the present work is the fabrication of (thermo)reversibly cross-linked polymer matrices as soft component in the so-called brick-and-mortar structure, obtained in a aqueous self-assembly approach employing nano-clays as analogues for the aragonite platelets in nacre. For this purpose, reversibly and dynamically cross-linked, water-soluble polymer matrices are prepared, exhibiting different polymer architectures. As cross-linking within these matrices, self-complementary and thermolabile hydrogen bonding is employed, resulting in a rigid material at ambient temperature, which becomes flexible at elevated temperature. The hydrogen bonding polymer matrices are employed in nano-composite fabrication and mechanically tested in cooperation with material scientists (Chapter 3.1.1). Secondly, a less dynamic, covalent hetero Diels-Alder chemistry (HDA) is employed in a further approach towards reversibly cross-linked polymer matrices. (Chapter 3.1.2).

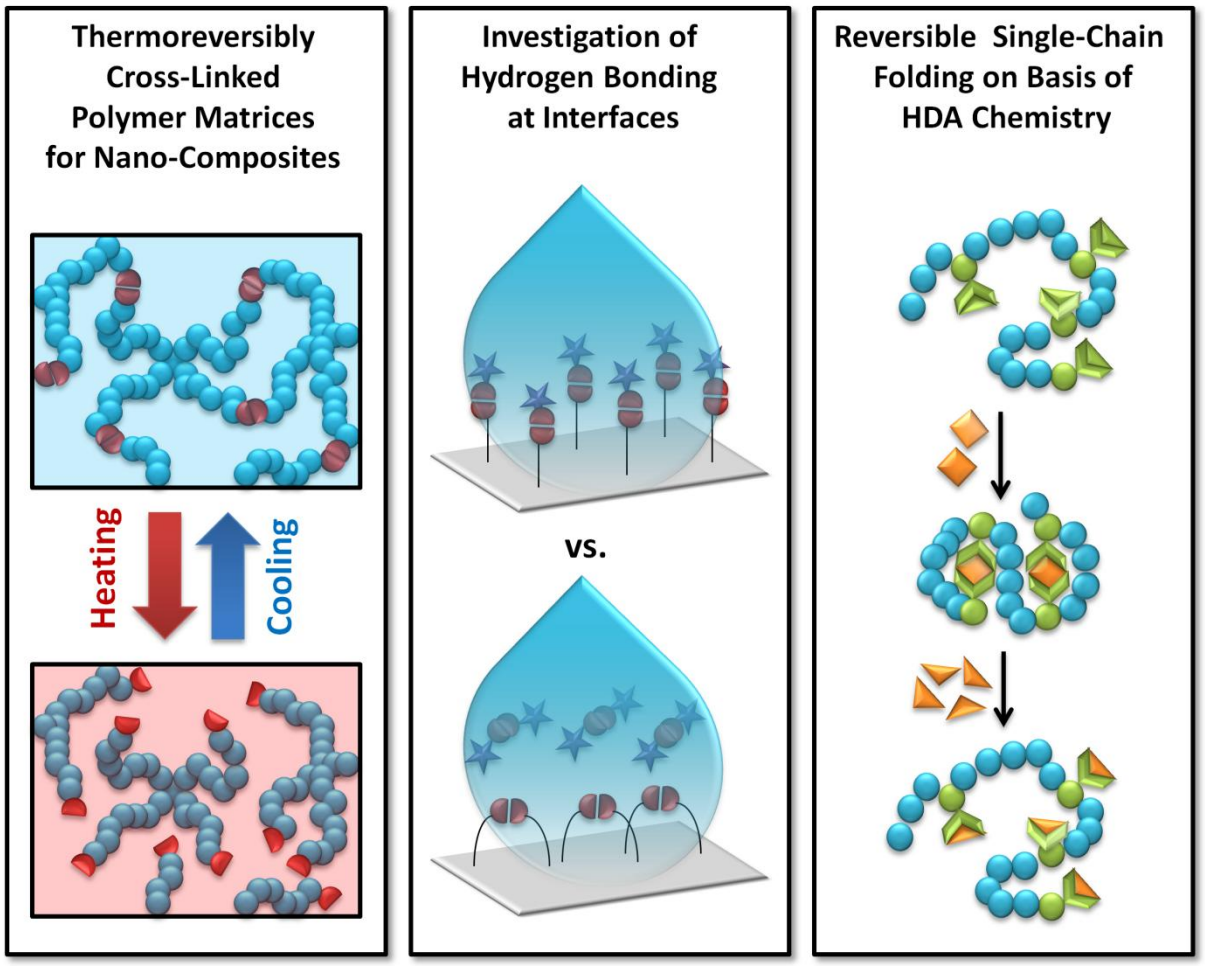

Figure 1: Overview over the projects of the present thesis.

Since nano-composites exhibit extraordinary large interfaces between filler and matrix, a reliable picture of hydrogen bonding processes at corresponding material interfaces is critically required in order to optimize performance. Therefore, in a second part of the thesis, hydrogen bonding capacity on macroscopic surfaces as model system for interfaces in prepared nano-composites is investigated in depth. Two fundamentally different scenarios of hydrogen bonding (self- and hetero-complementary dimerization) are investigated *via* immobilization of (marked) hydrogen bonding partners from solution onto a substrate, which is functionalized with spatial resolution with corresponding hydrogen bonding partners. The combination of the results of both systems provides a reliable and comprehensive picture of molecular processes at hydrogen bonding interfaces and critically expands the understanding of analogue systems (Chapter 3.2).

In order to demonstrate the capacity of hetero Diels-Alder chemistry to reversibly cross-link polymeric materials, in a third part of this thesis single chain nano-particles (SCNPs) are synthesized employing the identical Diels-Alder couple as employed for thermoreversibly cross-linked matrices in part one. Collapsed single polymer chains reverted back to an open chain state, exploiting the fully reversible potential of hetero Diels-Alder chemistry and kinetic and thermodynamic aspects of single chain folding with Diels-Alder chemistry are investigated (Chapter 3.3).

Herein, reversible (supramolecular and covalent) bonds are applied and systematically studied in depth in a broad context – including dynamically cross-linked polymer matrices for layered, biomimetic nano-composites, macroscopic surfaces as model system for interfaces in such nano-composites and reversible folding of polymer single chain nano-particles. Very critically, general trends in layered nano-composites, supramolecular surface chemistry and dynamic covalent chemistry in single chain folding are identified and literature-known trends are further verified, providing a valuable contribution to these fields of research.

2 BACKGROUND AND THEORETICAL CONSIDERATIONS

2.1 Modular Ligation

2.1.1 *(Hetero-)Diels-Alder Chemistry*

2.1.1.1 History and Characteristics

The first example of a Diels-Alder reaction was published in 1928 and, after intensive studies, led to the Nobel prize in 1950 for its pioneers.[3] Since then the reversible and highly selective [4+2] cycloaddition (CA) was, moreover, extended to hetero atoms containing π-systems (HDA). Diels-Alder (DA) reactions in general are thermodynamically favored, since π-bonds with lower binding-energy are transformed in σ-bonds with higher binding-energies and, belonging to the class of pericyclic reactions, can be predicted by the Woodward-Hoffmann rules (Section 2.1.1.2) and the Salem-Klopman-Equation.[4-6] Regular (H)DA reactions are frontier-controlled reactions and proceed between the Lowest Unoccupied Molecular Orbital (LUMO) of an electron deficient dienophile and the Highest Occupied Molecular Orbital (HOMO) of an electron rich diene *via* a six-membered transition state in a concerted reaction. Substituents (and hetero atoms) influence the energies and orbital coefficients of the Frontier Molecular Orbitals (FMO)s and therefore accelerate/decelerate the (H)DA reaction, while simultaneously influencing the regioselectivity of the product formation.[7] Photochemical (H)DA reactions are, according to the Woodward-Hoffmann rules, forbidden, because they proceed antarafacial, which is only possible in a high-energy transition state that is usually not accessible for [4+2] CAs. An important exception from this rule is the photoenol reaction, which forms its diene-form exclusively under irradiation and subsequently reacts in an thermal (and allowed) (H)DA reaction.[8]

An important feature of DA chemistry is the absence of byproducts (neglecting stereoisomers) and therefore the work-up usually is simple (if stereoisomers are

irrelevant, *e.g.* in polymer conjugation). DA reactions potentially result in high yields and exhibit good tolerance towards other functional groups, solvents, air and moisture. The most important feature for DA reactions regarding polymer chemistry is, however, the fully reversible nature of the adduct formation: At elevated temperatures the DA adduct decomposes into the starting diene and dienophile, often without degradation events. Therefore, due to its reversible and dynamic nature, (H)DA chemistry is extensively employed in self-healing materials and reversible polymers.[9] When a (H)DA reaction is conducted between two polymer chains, the equilibrium of the (H)DA reaction is influenced by the chain length: longer polymer chains tend to shift the equilibrium to the starting materials. Additionally, low chain stiffness and high molecular mass influence the equilibrium negatively.[10]

2.1.1.2 Frontier Molecular Orbitals and Woodward-Hoffmann rules

The Woodward-Hoffmann (WH) rules (by Robert Burns Woodward and Roald Hoffmann) predict, on basis of conservation of orbital symmetry during the reaction, whether a pericyclic reaction is symmetry allowed (low electronic energy barrier) or symmetry forbidden (high electronic energy barrier).[4] For his work Hoffmann was awarded in 1981 with a shared Nobel Prize with Kenichi Fukui (Woodward died two years before). Initially, the set of rules was applied to understand the stereospecificity of electrocyclizations (dis-/conrotatory) on basis of the number of involved π-electrons and how the reaction is conducted (thermally/ photochemically) *via* correlation diagram analysis.[4] This analysis (and the WH rules) can be extended to other pericyclic reactions, including cycloadditions including also (H)DA reactions (Figure 2).[11, 12]

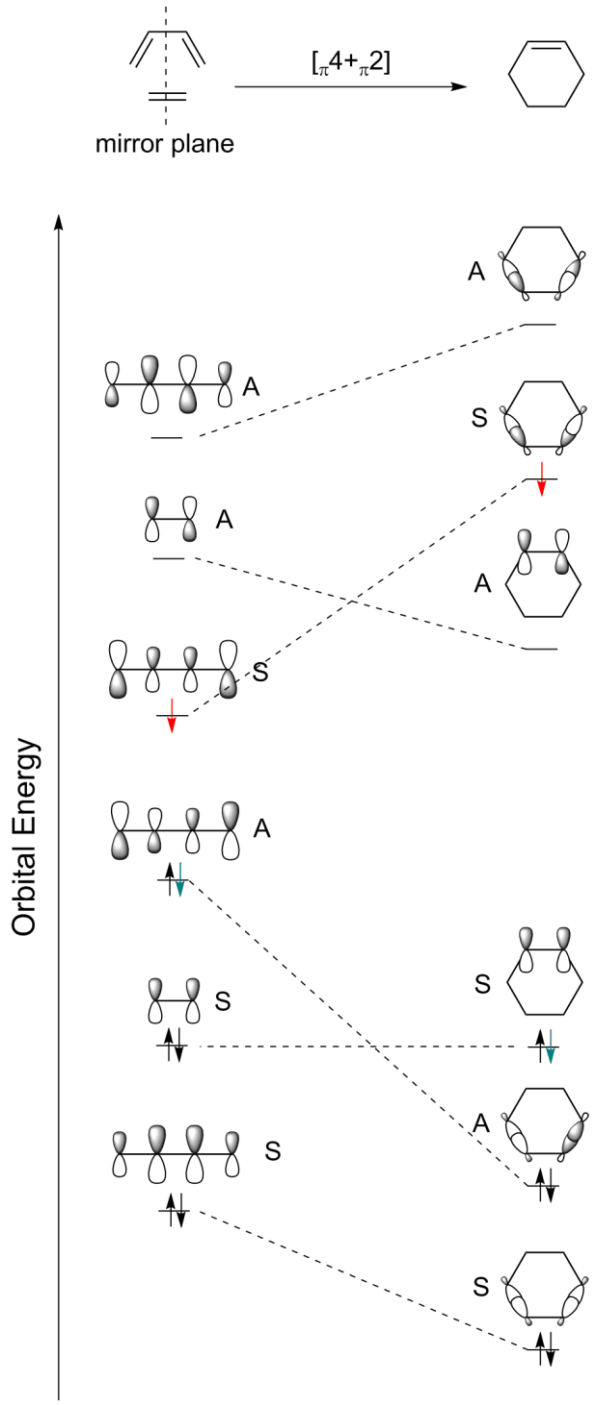

Figure 2: Correlation diagram of a [4+2] cycloaddition in the ground state (green) and the first excited state (red, S_1). Orbital symmetry (A/S) is labeled relative to the conserved mirror plane.

For construction of a correlation diagram the conserved symmetry elements have to be identified and the Molecular Orbitals (MOs) have to labeled symmetric (S) or asymmetric (A) with reference to the(se) element(s). MO symmetry is conserved throughout the (DA-)reaction and the MOs of the reactant(s) are correlated with MOs

of identical symmetry in the product(s), while lines of same symmetry must not cross (avoided crossing rule). The electronic states (excited state = red; ground state = green) can be constructed and correlated. Thermal reactions proceed out of the ground state, while photochemical reactions proceed out of the first excited state. For a (H)DA reaction, a thermal reaction (green) leads to a product in the ground state, while a photochemical reaction (red) leads to a product in an excited state and therefore (suprafacial-suprafacial) photochemical (H)DA reactions are symmetry forbidden and exhibit high kinetic barriers (Figure 2).[7] Further, the light-induced photoenol reaction (diene for UV-triggered DA reactions) is no exception from the WH rules: The DA reaction proceeds from an electronic ground state, and photons are not needed to lift the molecule to a reactive excited state, but to transfer it to its E-dienol form (*via* an path including excited states), from which the (H)DA-reaction proceeds.[13]

Focusing on the FMOs participating in the DA reaction and neglecting all other MOs (since their energetic contribution to the transition state is small compared with the FMOs) regioselectivity of the reaction can be predicted: DA reactions proceed *via* the HOMO-LUMO couple with the lowest energy gap (and can be accelerated by decrease of this gap), since they are frontier-controlled. Taking into account the polarization of these MOs and considering the Salem-Klopman Equation (combination of large-large and small-small orbital coefficients in the most favorable transition state) and the corresponding orbital polarizations, the lowest transition state can be identified and thus the regioselectivity of product formation can be predicted. FMO polarization and energies depend on the types of dienes/dienophiles and their substitution pattern. Some common examples are depicted in Figure 3.[5-7]

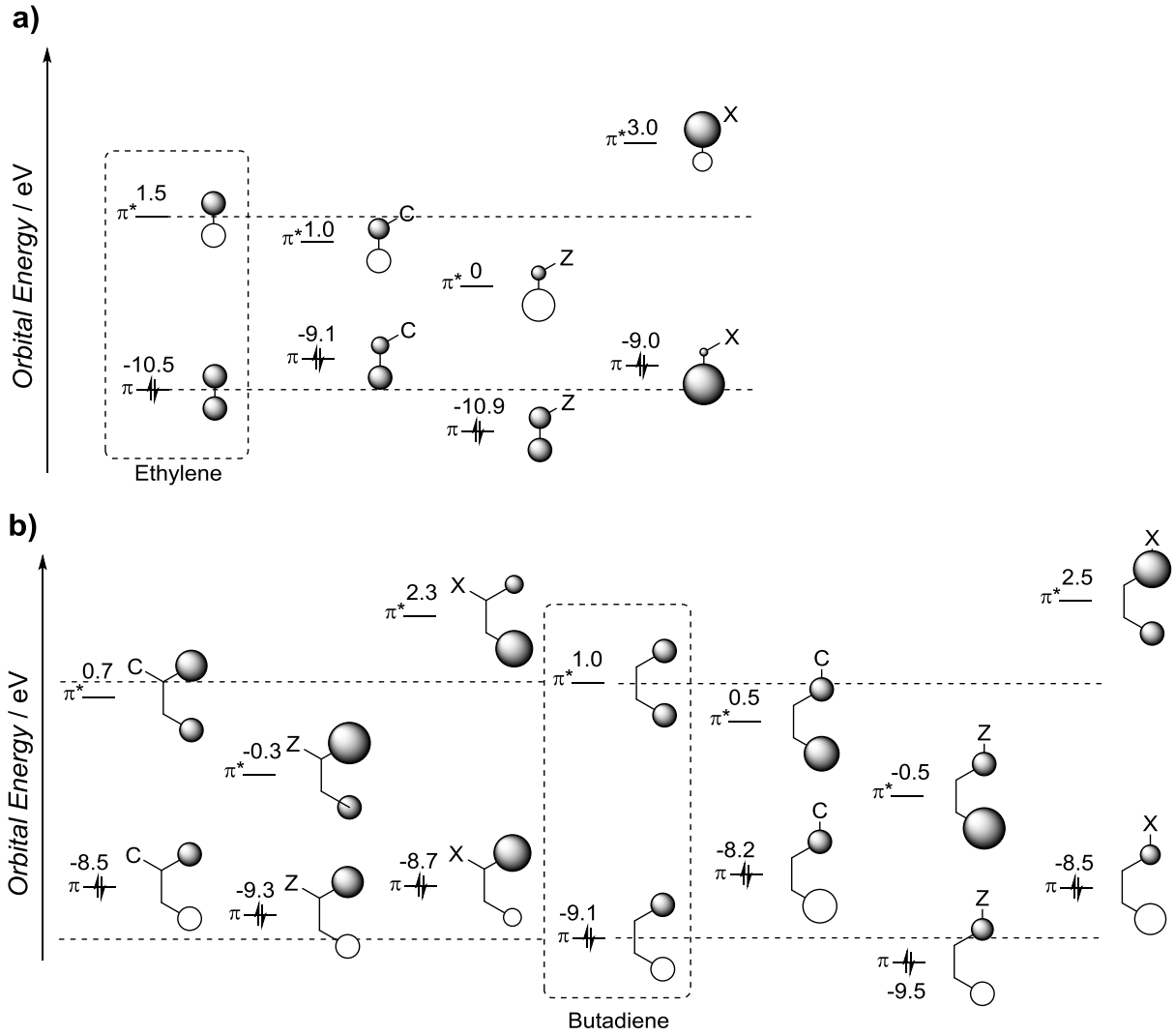

Figure 3: Quantitative FMO energies and qualitative orbital coefficients of substituted π-systems according to Houk *et al*.[14]

For all substitution patterns C-substituted (conjugating substituents) π-systems show a decrease in the HOMO-LUMO gap compared to the unsubstituted systems, however, C-substituents introduce only little polarization to the FMOs (due to similar electronegativities). Making them more reactive in DA reactions but leading to low regioselectivity. The FMOs of π-systems exhibiting Z-substituents (electron withdrawing) are shifted to lower orbital energies and show significant polarization, making especially Z-substituted ethylenes fast reaction partners in DA reactions with potentially high regioselectivity. Electron donating groups (X-substituents) increase the FMO energies of all π-systems and induce strong polarization.

Due to these substitution effects, in DA reactions with normal electron demand, globally, ortho- and para-products are favored over meta-products (Figure 4).

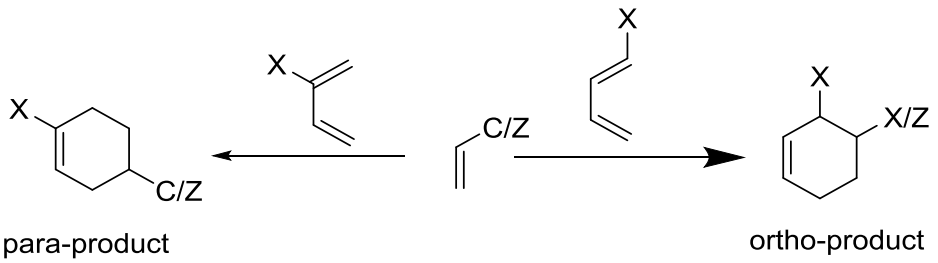

Figure 4: Regioselectivity of DA reactions based on the FMO theory, the Salem-Klopman equation and representative orbital coefficients.

2.1.1.3 Furan-Maleimide Couple

Furan (electron rich diene) and maleimide (electron deficient dienophile) represent an extensively studied and well-known DA couple, which was already discovered in 1952.[15-17]

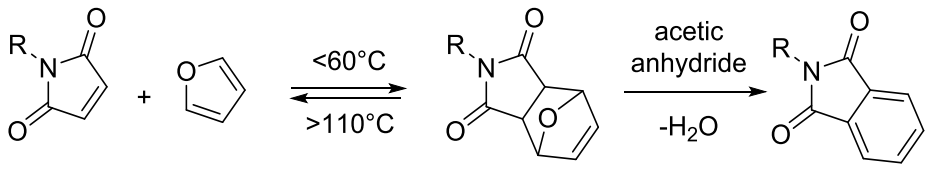

Scheme 1: The furan-maleimide DA couple. Decomposition can be suppressed by irreversible aromatization of the DA adduct.

Below 60°C the DA adduct formation is dominant, above 110°C the equilibrium shifted to furan and maleimide. Exploiting the high vapor pressure of furan with suitable reaction conditions (reduced pressure, high temperature) the retro-DA reaction can be forced back completely to a free maleimide. Therefore, furan is frequently employed as protective group for maleimides.[10, 11] The retro-DA reaction can be suppressed by aromatization of the CA adduct by acetic anhydride, if decomposition is undesired.[18]

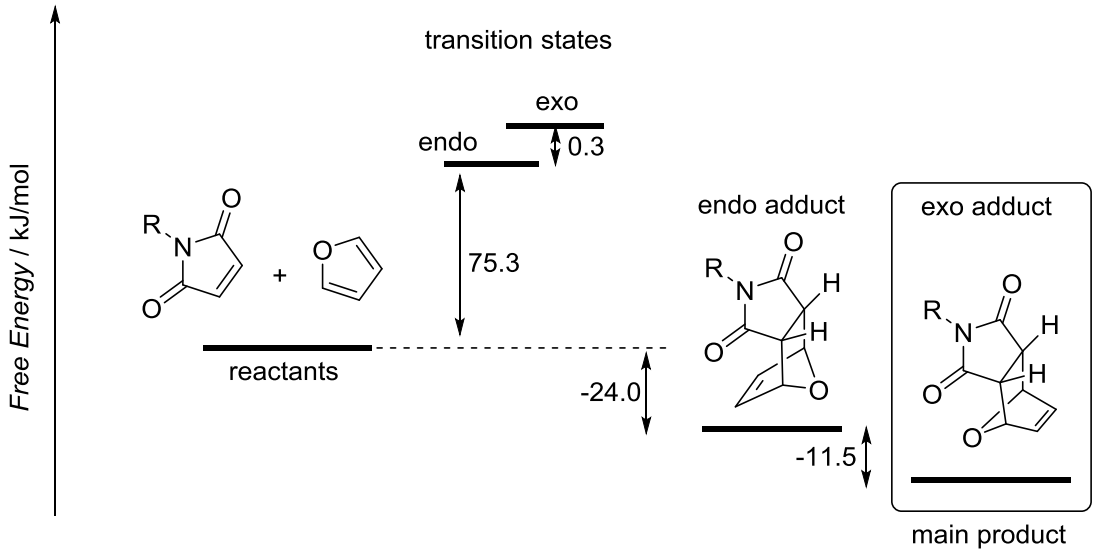

Figure 5: Free energy profile of the DA reaction between furan and maleimide. The thermodynamic exo adduct is preferred, due to the low energy difference in the transition states and the low retro temperature.[17]

Endo isomers are usually kinetically preferred (due to secondary orbital interactions), while exo isomers are thermodynamically more stable (due to steric effects). The relatively low retro temperature of the maleimide-furan adduct, however, overrules the kinetic preference of the endo adduct and leads to dominance of the exo isomer.[17]

2.1.1.4 Systems on Basis of Thiocarbonyls

Compared with (oxygen) carbonyls, the energy level of the C=S π-orbital is higher (because the binding energy of C and S is lower) and the π^*-orbital, which represents the LUMO, has less energy. Therefore, thiocarbonyls can be considered softer than their oxygen analogues. In addition, their electrophilic character is increased (due to the lower LUMO energy) compared with regular carbonyls, which makes them less stable towards nucleophilic attacks (*e.g.* by water), but on the other hand allows DA reactions to proceed under milder conditions. In addition, retro-DA temperatures of thiocarbonyls adducts, generally named 3,6-dihydro-*2H*-thiopyranes (DHTPs), are in general lower than for oxygen carbonyls.[19, 20] However, due to the similar electronegativities of sulfur and carbon, the π- (and σ-)MOs exhibit very little polarization and, therefore, the kinetic control over regioselectivity is poor. Still, substituents can shift the FMO energies introducing polarization and, thereby,

drastically influence the system´s kinetics and stereoselectivity.[21] Sulfur´s lone pair represents the system´s HOMO and has significantly higher energy than oxygen lone pairs (due to the lower electronegativity of sulfur), therefore, thiocarbonyls exhibit an increased nucleophilic character and, more importantly, often are sensitive towards oxidation (Figure 6).

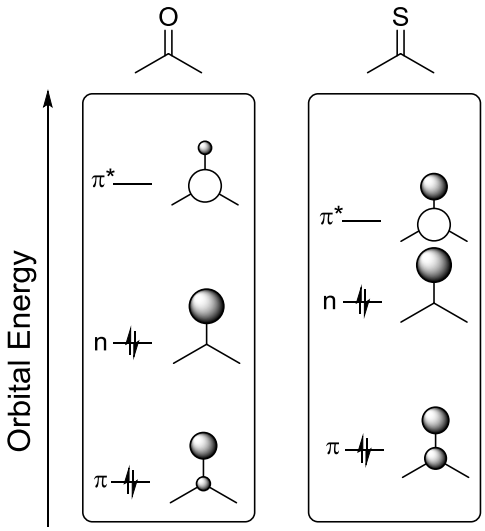

Figure 6: Qualitative depiction of FMO energies of (thio-)carbonyls and their polarization relative to the analogue oxygen carbonyls.

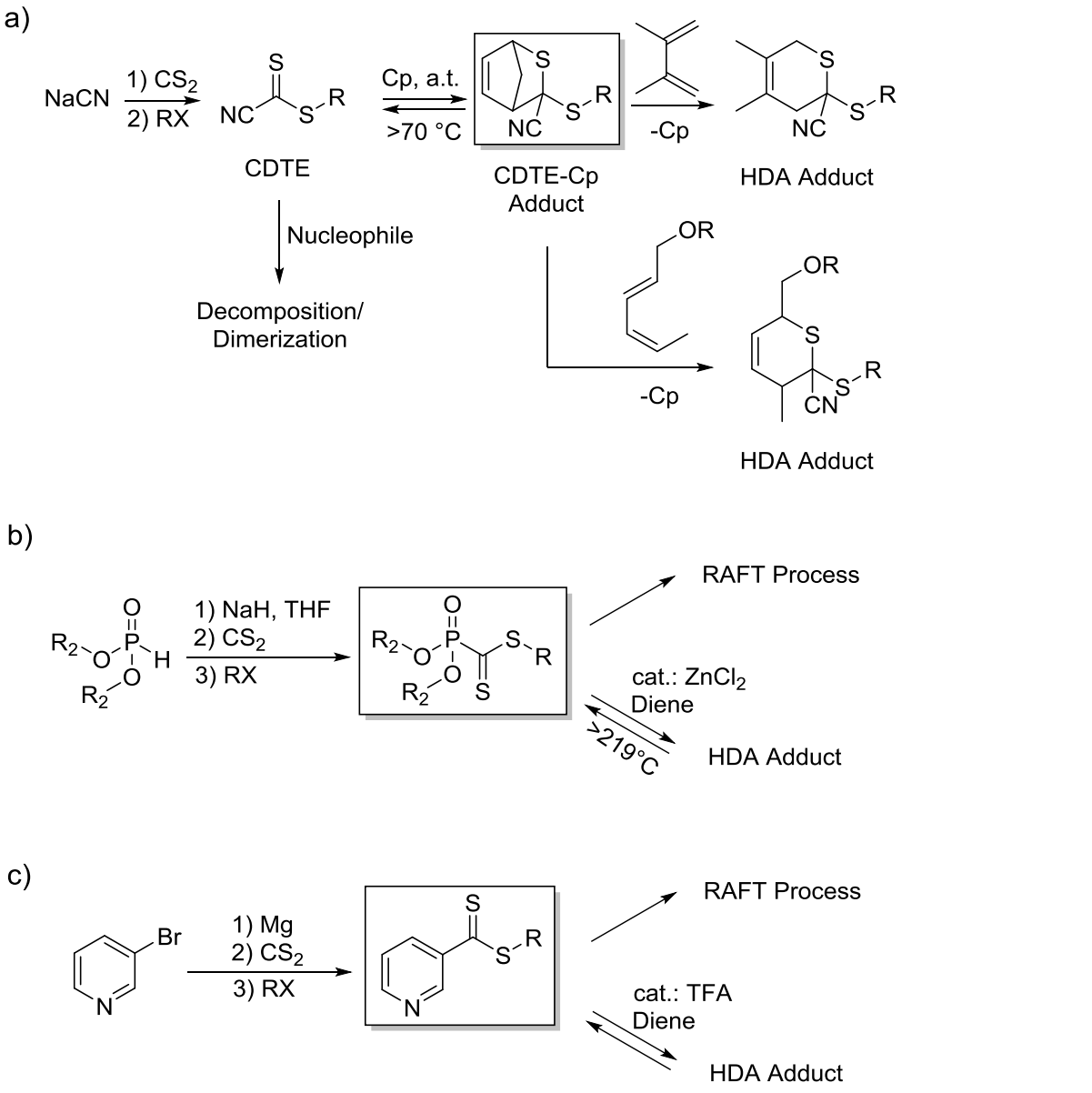

Scheme 2: Synthetic routes towards different dithioesters, which can be employed as dienophiles in reversible HDA chemistry.

Thioaldehydes (which are not stable under ambient conditions) and thioketones react very fast with dienes.[20-24] One strategy to overcome the difficulties associated with the general instability of thioaldehydes is to generate highly reactive thioaldehydes photochemically *via* the fragmentation of phenacylsulfide.[21, 23] Dithioesters, which are relatively stable towards hydrolysis (due to negative hyperconjugation of sulfur´s lone pair and $\pi^*_{C=S}$) and oxidation, need to be activated by electron withdrawing substituents (*e.g.* cyano in cyanodithioesters (CDTEs)) for HDA reactions.[25-27] Activation, however, simultaneously increases their sensitivity towards oxygen and moisture. CDTEs are highly unstable in their free form towards nucleophilic attacks

and need to be protected by an HDA reaction with cyclopentadiene (Cp) (Scheme 2a). The Cp adduct shows a relatively low retro-temperature (19% unprotected material at 130°C), and therefore can be easily substituted with other dienes, which form more stable DHTPs (*e.g.* sorbic alcohol and dimethylbutadiene).[28, 29]

Dithioesters can be substituted with electron donating groups (*e.g.* thiols, alcohols, aromatic compounds and phosphoryl-substituents). In these cases the energy of the LUMO ($\pi^*_{C=S}$) is increased and the electrophilic character (sensitivity towards hydrolysis), as well as, the reactivity as dienophile in DA reactions is decreased. Simultaneously, the system´s nucleophilic character increases and some of these reagents serve as RAFT agents (nucleophilic attack of the C=S double bond on the electron deficient monomer radicals).[7] Additionally pyridinyl- and phosphoryl-substituted thiocarbonyls (RAFT agents) can be transformed into reactive dienophiles for HDA reactions by activation *via* coordination of Lewis acids (trifluoroacetic acid, $ZnCl_2$) (Scheme 2b,c).[30-35]

2.1.2 *Copper-Catalyzed Azide-Alkyne Cycloaddition (CuAAc)*

2.1.2.1 CuAAc in the Context of Click-Chemistry

The thermal cycloaddition (CA) of azides with alkynes was first discovered by Huisgen in 1963 and further improved with regard to stereoselectivity and reaction rate by Sharpless by addition of catalytic amounts of Cu(I).[36] In 2001, when Sharpless introduced the concept of Click-Chemistry, he considered the Copper-Catalyzed Azide-Alkyne Cycloaddition (CuAAc) as the prototype of a Click-Reaction.[37]

Reactions labeled “Click-Reactions” have to fulfill a set of very restricting criteria, characterizing them as convenient, reliable and effective avenues for molecule construction. Moreover, since in polymer chemistry purification of reaction mixtures is demanding, if not impossible, even more criteria for the term “Click-Reactions” have been added the context of polymers.[38] In summary these extended click-criteria are: Absence of more than one reaction path (“single reaction trajectory”), “equimolarity”, “chemoselectivity” and stability of starting materials under ambient conditions. Moreover, Click-Reactions have to be “wide in scope”, “modular” and exhibit short reaction times. Further criteria are easy workup (“large scale purification”) and “high yield”.

Due to these very demanding characteristics, only the most efficient and reliable reactions are considered as tools in Click-Chemistry – with CuAAC being the best accepted one.

2.1.2.2 FMO Analysis and Mechanistic Details

Figure 7 provides an overview over the FMO energies and orbital coefficients of phenylazide, phenylacetylene (reactants in azide-alkyne cycloaddition) and styrene.**[7]** CAs proceed in general *via* the FMO couple with the smallest energy difference and the stereochemistry of product is predictable from the FMO coefficients (large coefficients interact with large coefficients and small ones with small ones). In the case of the CA of phenylazide and styrene, the reaction proceeds *via* the HOMO of phenylazide and the LUMO of styrene, resulting in the 1,4-CA adduct. In case of the (Cu-free) azide-alkyne CA, however, stereoselectivity is almost lost, since the both

FMOs of phenylacetylene are lower than for styrene and therefore the CA proceeds *via* both FMO couples, due to the almost identical FMO energy differences. Since both pathways lead to different stereoisomers (1,4- or 1,5- substituted triazole) but are almost equally preferred, a 1:1 mixture of products is obtained.[7, 39, 40] In a CuAAc (with catalytic amounts of Cu), however, the CA proceeds faster compared with the copper-free variant and stereoselectivity is significantly enhanced, forming the 1,4-adduct exclusively. The improved reaction rate and stereospecificity originates in the (complex) coordination of Cu(I)-ions with alkynes (and azides), influencing FMO energy differences and introducing preorientation simultaneously. The suggested coordination of Cu(I) with azide and alkyne during CuAAc is depicted in Scheme 3.[41]

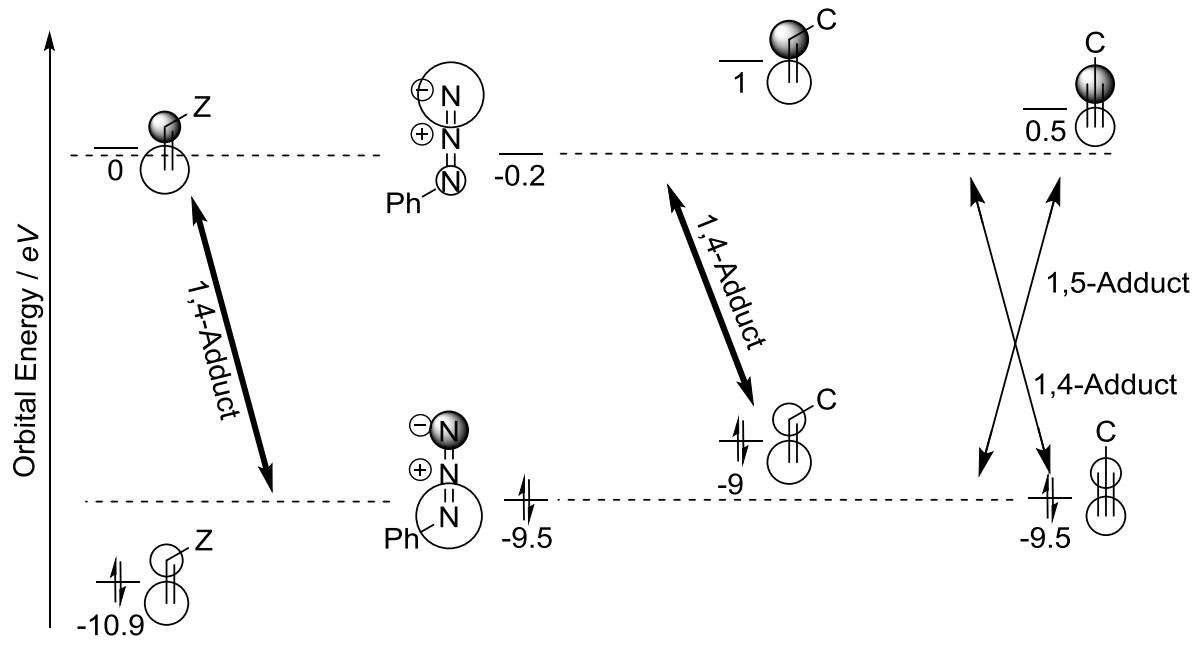

Figure 7: FMO couples of Z- and C-substituted alkenes in comparison with phenylazide and phenylacetylene. Preferred FMO couples are marked with a bold arrow and the corresponding CA adduct is given.[7, 39]

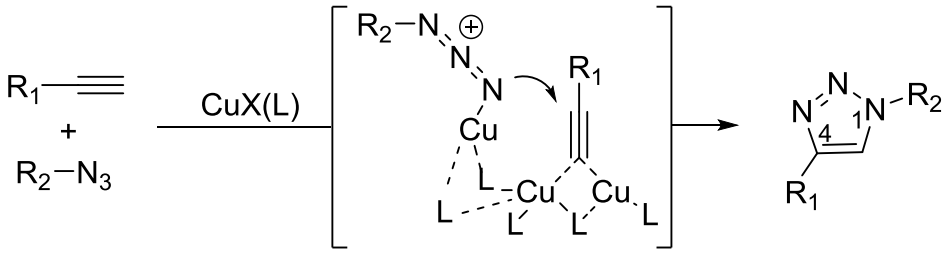

Scheme 3: General reaction scheme of a CuAAc with additional depiction of the most critical intermediate revealing the origin of stereoselectivity under Cu catalysis.[41]

2.1.2.3 Applications and Special Protocols

Due to its efficiency, orthogonality and convenient reaction protocol the CuAAc is widely employed in chemical science, *e.g.* in bioconjugation,[42-45] macrocyclization,[46, 47] dendrimeric architectures,[48] surface modification[49, 50] (including nano-particles[51, 52]) and especially in polymer chemistry[53] including both polymerization[54-56] and post-modification (*e.g.:* block-co-polymer[57-59] formation and endgroup/side-chain modification[57, 60, 61]).

Apart from side-chain modifications *via* CuAAc, which are a matter of (co)monomer functionalities, many polymers derived from CLRP protocols (*e.g.* RAFT, ATRP) can readily undergo endgroup modification by CuAAc. If suitable functional groups (azide, alkyne) are incorporated in the RAFT-agent or ATRP-initiator, these groups will be located at the *termini* of the polymers, due to the good endgroup fidelity of the corresponding polymerization techniques, opening the avenue for facile endgroup modifications. Moreover, for ATRP polymers a second approach is suitable: The initial bromine endgroup after polymerization can be substituted by an excess of sodium azide, resulting in a “click”able endgroup, as depicted in Scheme 4.

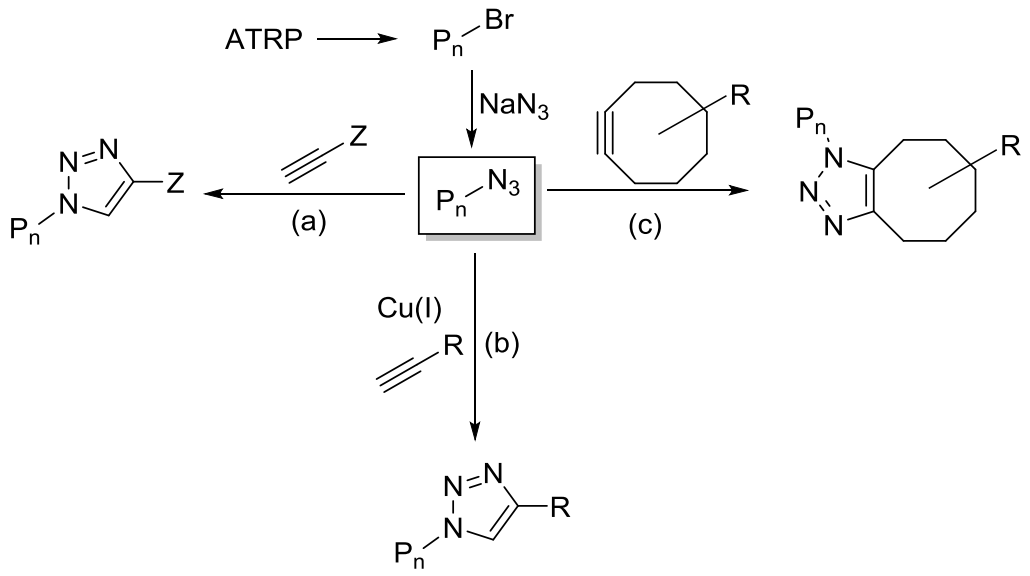

Scheme 4: Functionalization of ATRP polymers with azides opens three avenues for functionalization with alkynes: (a) non-catalyzed CA with electron deficient triple bonds, (b) conventional CuAAc and (c) strain promoted azide alkyne CA.

Typically 10 mol% Cu(I) is employed during CuAAc and subsequently removed from the reaction mixture by aqueous extraction of immobilization on aluminum oxide (AlOx). However, complete removal often remains challenging, especially when complexing groups are present in the product. To overcome the disadvantages of Cu(I) salts in the reaction mixture (cytotoxicity and lability towards oxidation by air) Cu-free alternatives have been developed employing either electron deficient alkynes (the impact on FMOs is depicted in Figure 7), resulting in a less orthogonal reaction path, due to the highly electrophilic triple bond (Scheme 4a), or strained triple bonds, which are on the other hand more difficult to prepare than conventional alkynes (Scheme 4c).[62, 63]

2.1.3 *Nitrile Imine-Maleimide Conjugation*

2.1.3.1 Basic Photochemical Considerations

Photochemical reactions, although crucial for many biologic processes and even essential for life on earth itself (photosynthesis), have to be selected carefully and employed economically in synthesis in general, since they are comparatively cost-intensive and difficult to conduct on large scales. However, photochemistry also offers some important advantages over conventional thermal chemistry, as irradiation (and therefore the area of chemical reaction) can be controlled spatially. Further, photochemical reactions can be highly orthogonal (to thermal reactions or even other photo-reactions) and can proceed under mild conditions regarding irradiation intensity and wavelength.

The first step in all photochemical processes is the absorption of photons, which is empirically described by Beer-Lambert´s law, (Figure 8a) stating that the absorbed intensity of light is depending on the concentration of absorbent (c), the length of the path of light (l) and, more importantly for the following considerations, the molar extinction coefficient (ε) of the absorbing species, which is a function of wavelength λ and is characteristic for each molecule. Molecules containing hetero atoms and therefore exhibiting electron lone pairs (or free electrons in general) electronic transitions involving these non-binding electrons ($n\rightarrow\pi^*/\sigma^*$) are of most importance (carbonyls, heterocycles), while for simple π-systems often $\pi\rightarrow\pi^*$ transitions are of interest (Figure 8b). Generally spoken, the molar extinction coefficient (ε) increases, if the MOs of the initial and final state of an electronic transition have good orbital overlap, since this increases the transition dipole moment.

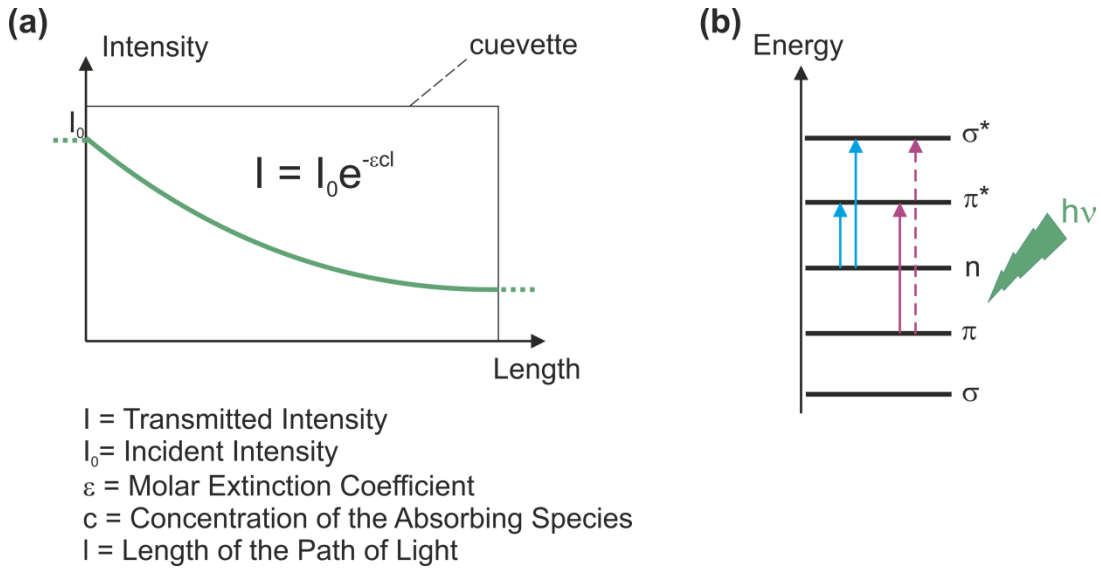

Figure 8: Absorption of light. (a) Beer-Lambert´s law describes absorption empirically, revealing that a wavelength dependent molar extinction coefficient (ε) exists for each compound. (b) UV/Vis irradiation induces electronic transitions in molecules. Depending on the electronic preconditions different transitions are of particular importance.

Photon absorption initially lifts molecules from the ground state (S_0) to an excited singlet state (S_n) in vibrational excitation (v_n), from which several other primary processes can occur. Absorption, internal conversion (IC), vibrational relaxation (VR), intersystem crossing (ISC) and luminescence (fluorescence and phosphorescence) are best described by the famous Jablonski diagram depicted in Figure 9a. Internal conversion (IC) is the transition between electronic states of same multiplicity ($S_1 \rightarrow S_0$) and can be followed by vibrational relaxation, which is a radiationless process in which the system reaches the vibrational ground state of the current electronic state ($v_n \rightarrow v_0$). Starting from the first excited singlet state after excitation (S_1,v_n) IC followed by VR is a radiationless path of relaxation into the ground state. A second path is VR into the (S_1,v_0) state followed by fluorescence to a vibrationally excited S_0 state or the ground state (S_0,v_0). The third monomolecular relaxation path is (the slow because quantum mechanically forbidden) intersystem crossing (ISC) from an excited singlet state into a triplet (T_n,v_n) state, followed by VR and phosphorescence into an vibrationally excited S_0 state or the ground state (S_0,v_0).

IC and ISC are accelerated, if the initial and final energy levels of states are close, which in general is the case if many vibrational levels exist (large molecules), the S_1-T_1 gap is small (*e.g.* carbonyls). Furthermore, in highly excited vibrational states,

which lie closer together than lower states (anharmonicity), crossing can occur easier. Luminescence (phosphorescence and fluorescence) occur from the vibrational ground state of an electronically excited state (T_1, S_1). However, since the transition from a triplet state to a singlet state is forbidden (and *vice versa*), T_1 has a significantly longer life time than S_1 and phosphorescence is observed on a longer time scale than fluorescence (half-times ≈ 30 s vs. 10^{-6} s). Additionally, since T_1 has less energy than S_1, phosphorescence is red-shifted compared with fluorescence (which is on the other hand red-shifted compared with the excitation wavelength).

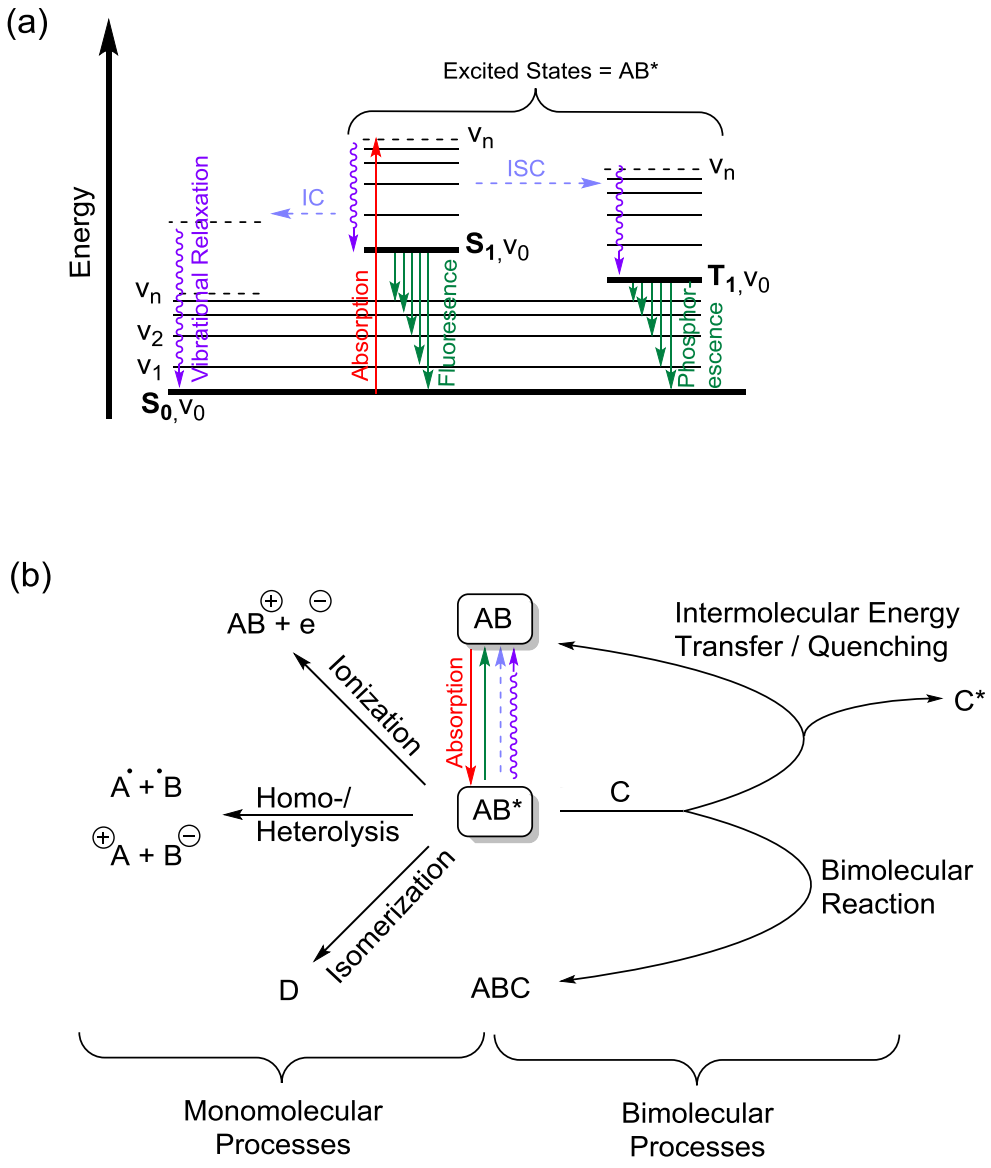

Figure 9: Primary processes after photon absorption and electronic excitation. (a) Important relaxation paths of electronically excited molecules summarized in the Jablonski diagram. (b) Conversion of electronic excitation of molecule AB* into chemical reactions *via* mono- and bimolecular events.

The Jablonski diagram focuses on processes that relax the excited molecule back to the ground state. However, in terms of chemical reactions, most of these processes are of little interest (or even undesired), since the energy of the absorbed photon is lost and not used to initiate a chemical reaction. If the photon energy of AB* is not lost due to luminescence or radiationless relaxation processes, it can be converted in mono- and bimolecular processes into a chemical reaction (Figure 9b): Photo-ionization can be achieved, if the MO energies are sufficiently high and the photon wavelength is short. Further, depending on the difference in electronegativities and charge stabilization, homo- or heterolysis can be induced by photon absorption, if a vibrational state is reached that lies above the dissociation energy (of the new electronic state). In complex molecules AB* electronically excited states can undergo isomerizations (*e.g.* electrocyclization). Moreover, in bimolecular events the photon energy can be transferred to a collision partner C (quenching or sensitizing), leaving the initially excited molecule AB* in an energetically lower state or, secondly, the photon energy can be converted in a chemical reaction (*e.g.* into ABC). In the later case triplet states are of particular interest, since their comparatively longer life-time facilitates collision events.

2.1.3.2 History, Synthesis and Photolysis Wavelengths of Tetrazoles

Tetrazoles were initially reported to decompose thermally in 1959 by Huisgen.[64] However, Huisgen later published a light-driven CA on basis of tetrazoles in 1967 and identified nitrile imines as reactive intermediates that are generated by photo-induced cycloreversion of the five-membered tetrazole ring with loss of N_2.[65-67] The [3+2] CA of nitrile imines (originating from photochemical decomposition of tetrazoles) with maleimide is the termed nitrile imine-mediated tetrazole-ene cycloaddition (NITEC) reaction and frequently considered as modular and bioorthogonal.[68-70] However, recently undesired side reactions of nitrile imines in biologic systems have been identified, indicating that full bioorthogonality cannot be achieved with NITEC reactions.[71]

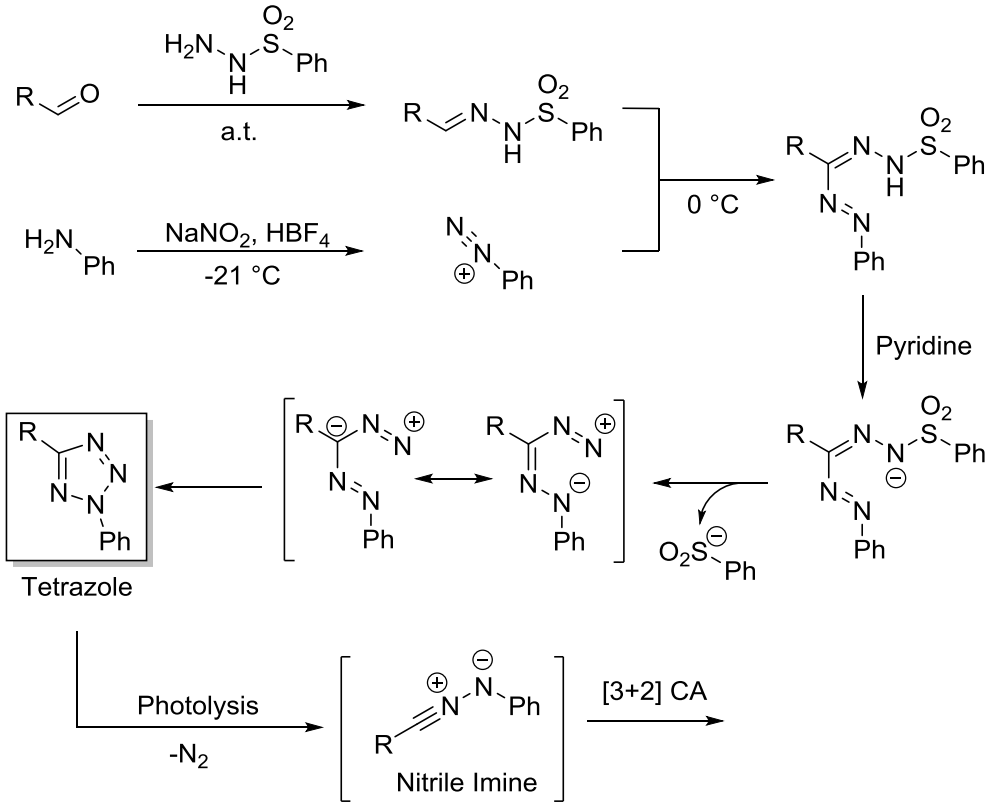

Scheme 5: General synthesis route to 2,5-disubstituted tetrazoles established by Kakehi and coworkers and its photolysis.[72]

Tetrazoles can be synthesized *via* various synthetic pathways.[73] The most important ones employ either aryl azide and *N*-phenylsulfonylbenzhydrazonoyl chloride (Dimroth-Merzbacher method)[74] or phenylsulfonylhydrazone and an arenediazonium salt (Kakehi and coworkers).[72] Since the method of Kakehi relies on stable starting materials, it is frequently employed for tetrazole synthesis and is depicted in detail in Scheme 5. Combination of cooled, basic solutions of the corresponding phenylsulfonylhydrazone and arenediazonium salt lead to formation of an unstable formazan that is deprotonated by the present base (pyridine) and subsequently eliminates benzenesulfinate followed by a 1,5-dipolar cyclization to tetrazole. In general, increased electrophilicity of the diazonium ion increases the yield.

Photolysis of tetrazoles is very efficient below 290 nm with a quantum yield of 0.5-0.9, which is almost not affected by substituents on the two aryl rings.[75, 76] However, to reduce the collateral photo damage from long time irradiation with short wavelengths of UV light, a significant amount of research was conducted to achieve bathochromic shifts in the absorption spectrum and photolysis wavelength of

tetrazoles, allowing milder reaction conditions *via* longer excitation wavelengths. Many tetrazoles with variable substitution patterns, diverse auxochromic groups and different absorption maxima were synthesized, still, a red-shift in the absorption maximum does not necessarily result in a longer excitation wavelength, since non-reactive electron transitions might be shifted.[77, 78] The most important tetrazoles with their corresponding experimental excitation wavelength are depicted in Figure 10.

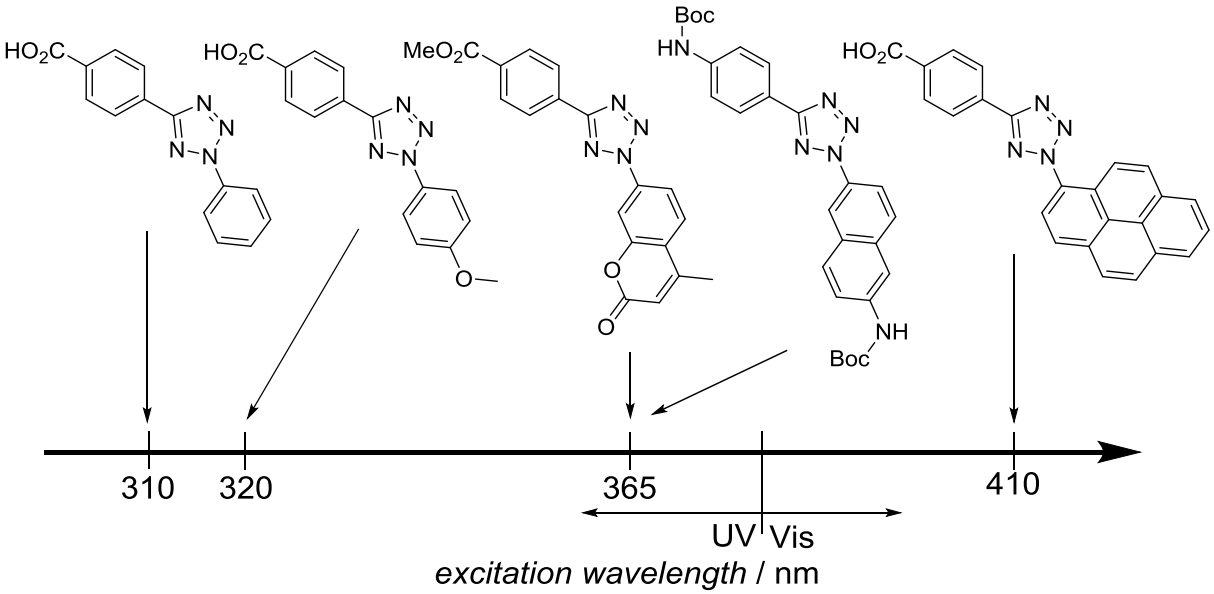

Figure 10: Structures and excitation wavelengths of selected tetrazoles.[79-82]

2.1.3.3 Nitrile Imines: [3+2] CAs and Competitive Reaction Paths

Upon irradiation with light, tetrazoles decompose irreversibly into N_2 and a highly reactive nitrile imine (1,3-dipole) that can undergo several reaction pathways – the most important one, however, is the [3+2] CA with electron deficient (Z-substituted) and conjugated (C-substituted) enes in a NITEC reaction. The resulting product, a 4,5-dihydro pyrazole, is potentially fluorescent (depending on the substituents), which can be in principle exploited for observation of reaction kinetics.[83, 84]

FMO analysis (Figure 11) reveals that exclusively taking into account electronic effects, 4-stubstituted 4,5-dihydro pyrazole is expected as main product for Z-substituted enes, but 5-substituted 4,5-dihydro pyrazole is expected for X-substituted enes. C-substitution introduces only very little polarization into the FMOs, consequently resulting in little regioselectivity. The fastest reaction rate is expected for Z-substituted enes, C- and X-substituted enes should react in similar but lower rates.

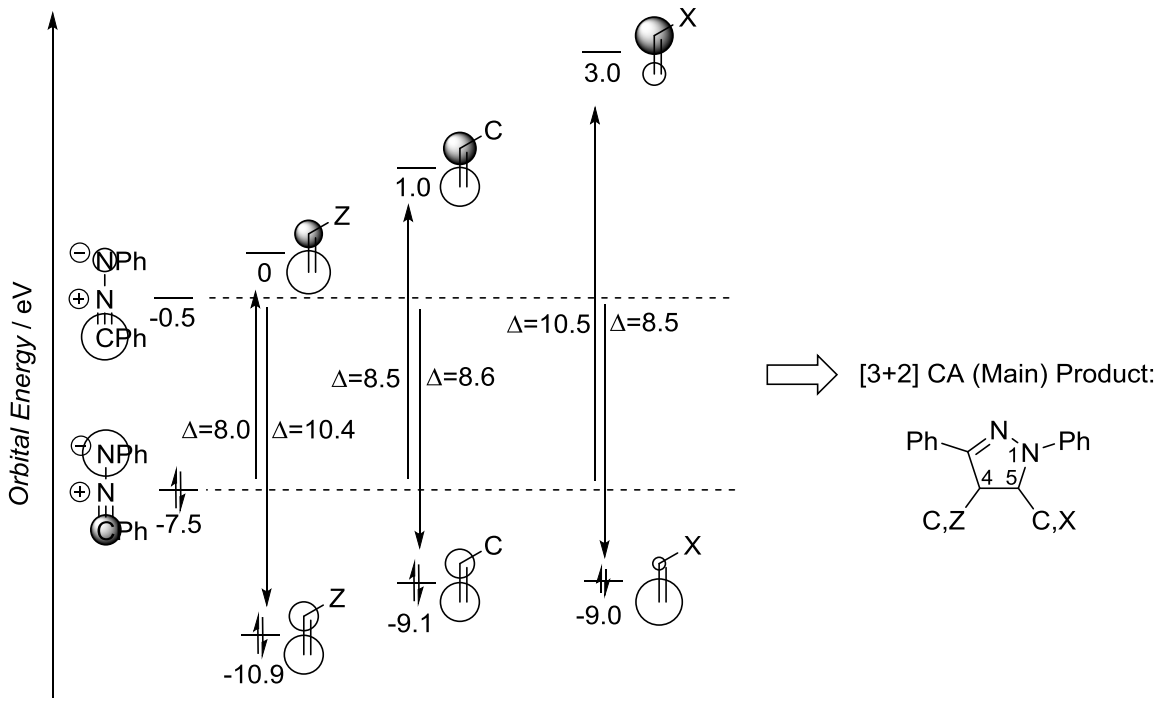

Figure 11: FMO energies and qualitative coefficients of an exemplary nitrile imine in comparison to enes with different substituents according to Houk *et al* and the corresponding kinetically preferred [3+2] CA adduct.[85]

The most important reaction paths of nitrile imines (generated by photolysis of tetrazoles) are reviewed in Scheme 6.[71] In the presence of acids (Scheme 6a), the protonation and subsequent nucleophilic attack of the corresponding base, followed by a 1,4-shift is favored over a [3+2]-CA. Moreover, in the presence of nucleophiles (Scheme 6c), *e.g.* amines and thiols, the nucleophilic addition on the C-terminus of the nitrile imine is favored over the [3+2] CA.[86, 87] In the presence of less nucleophilic alcohols, the NITEC reaction can be observed, however, the solvent has to be chosen carefully, since nitriles (*e.g.* MeCN) are also known to react as dipolarophiles in [3+2] CAs (Scheme 6b).

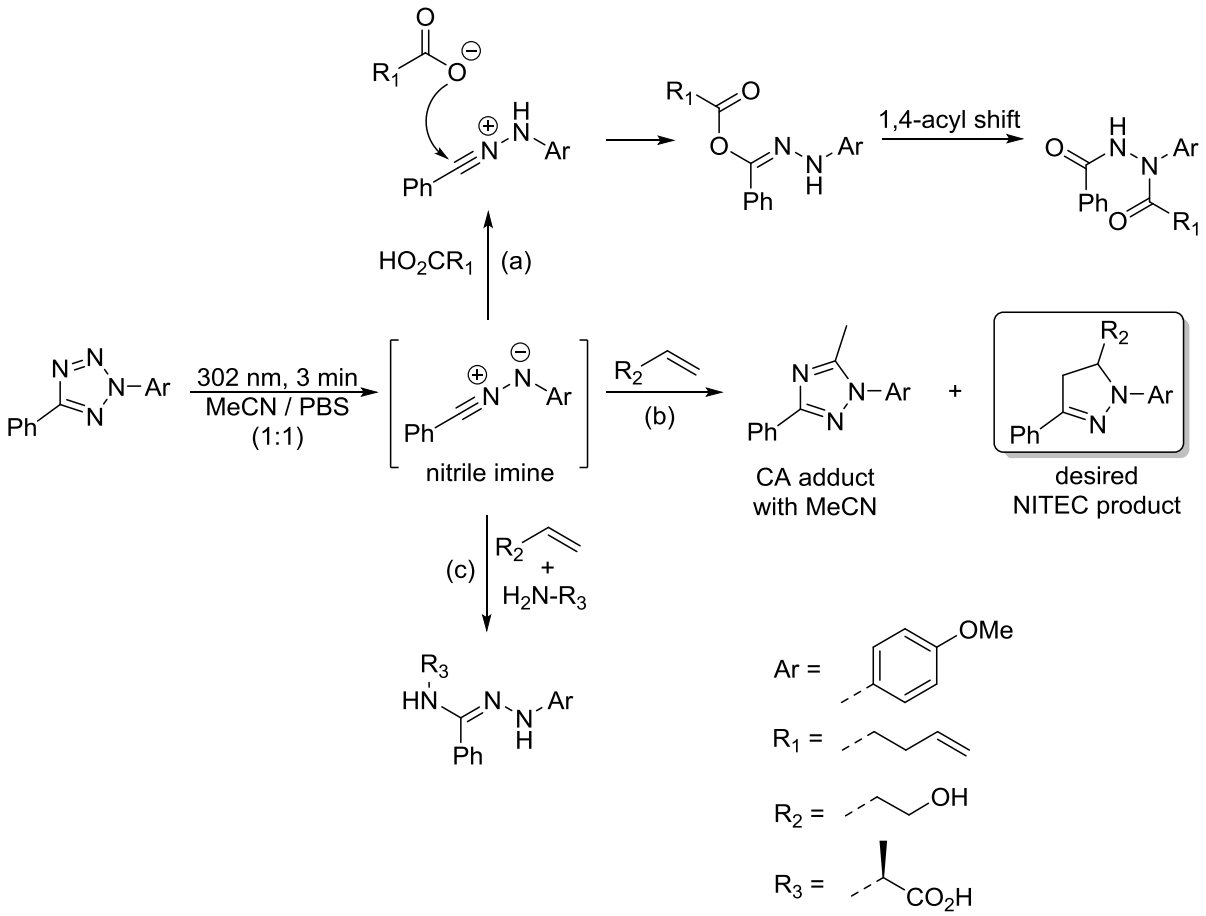

Scheme 6: Possible undesired reaction paths of nitrile imines.[71] (a) Acids protonate nitrile imines, activating them for nucleophilic attack of the corresponding base, followed by an 1,4-acyl shift. (b) Competing NITEC reactions with the desired ene and a badly chosen solvent (MeCN). (c) Nucleophilic attack of an amine on the C-terminus of the nitrile imine. The side reactions (a) and (c) proceed faster than competing NITEC reactions.

2.1.3.4 Applications of the NITEC Reaction

The NITEC reaction is widely employed in many fields of chemical science, due to the relatively good stability and orthogonality of non-irradiated tetrazoles and the good selectivity and high reactivity of nitrile imines towards π-systems (under well chosen conditions). Most importantly, NITEC is employed in bioconjugation (proteins,[69, 88] carbohydrates[89, 90] and nucleic acids[91, 92]), polymer chemistry (endgroup modification,[93] block formation,[79] cross-linking,[94] step growth polymerization[95] and SCNPs[83]) and – as in this present thesis – in spatially resolved surface functionalization.[80, 93, 96]

2.2 Hydrogen Bonding and Hydrogen Bonding Motifs

2.2.1 *Hydrogen Bonding*

Hydrogen bonding is crucial for many essential processes in living organisms: most importantly protein and DNA folding.[97-100] Although already discovered by Nernst in 1892, it was not termed “hydrogen bonding” before 1935. [101, 102]

Hydrogen bonding energy is the sum of electrostatic, polarization and charge transfer energy, as well as exchange repulsion and dispersion forces.[103, 104] It proceeds between a positively polarized hydrogen atom, covalently bound to a hetero atom with higher electronegativity (N, O, F, P, S) – so called proton donors (“D”) – and a hetero atom with a non-binding/free electron pair (proton acceptor “A”).[105] The binding energy depends on the solvent polarity and the dipole moment within D, thus energetically significant bonds (> 20 $kJ \cdot mol^{-1}$) are observed, if hetero atoms are N, O, or F. Charged atoms additionally increase the bonding strength.[106]

As all supramolecular forces, hydrogen bonding is much weaker (8-84 $kJ \cdot mol^{-1}$) than covalent (C-C 348 $kJ \cdot mol^{-1}$) or ionic (NaCl 788 $kJ \cdot mol^{-1}$) interactions, but it can be amplified by cooperative effects (meaning that the sum of two hydrogen bonds is stronger than two isolated hydrogen bonds).[97]

In general, hydrogen bonds exhibit linear geometry but if D interacts with an A having several available electron pairs or D exhibits several hydrogen atoms, derivations from this geometry can occur.[97, 103]

Depending on the sequence of D and A, attractive and repulsive secondary interactions vary (resulting in different binding strengths for an equal number of binding partners but different arrangements). Homo- and hetero-dimerization is possible depending on whether a hydrogen bonding array is self-complementary (only available for even numbers of D/A).[107] For a pair of complementary motifs molecular recognition is achievable, because the sequence of D/A predefines the preferred binding partner (orthogonality). All theoretically possible combination of D and A up to four binding sites per array and their theoretic binding constants are given in Figure 12.

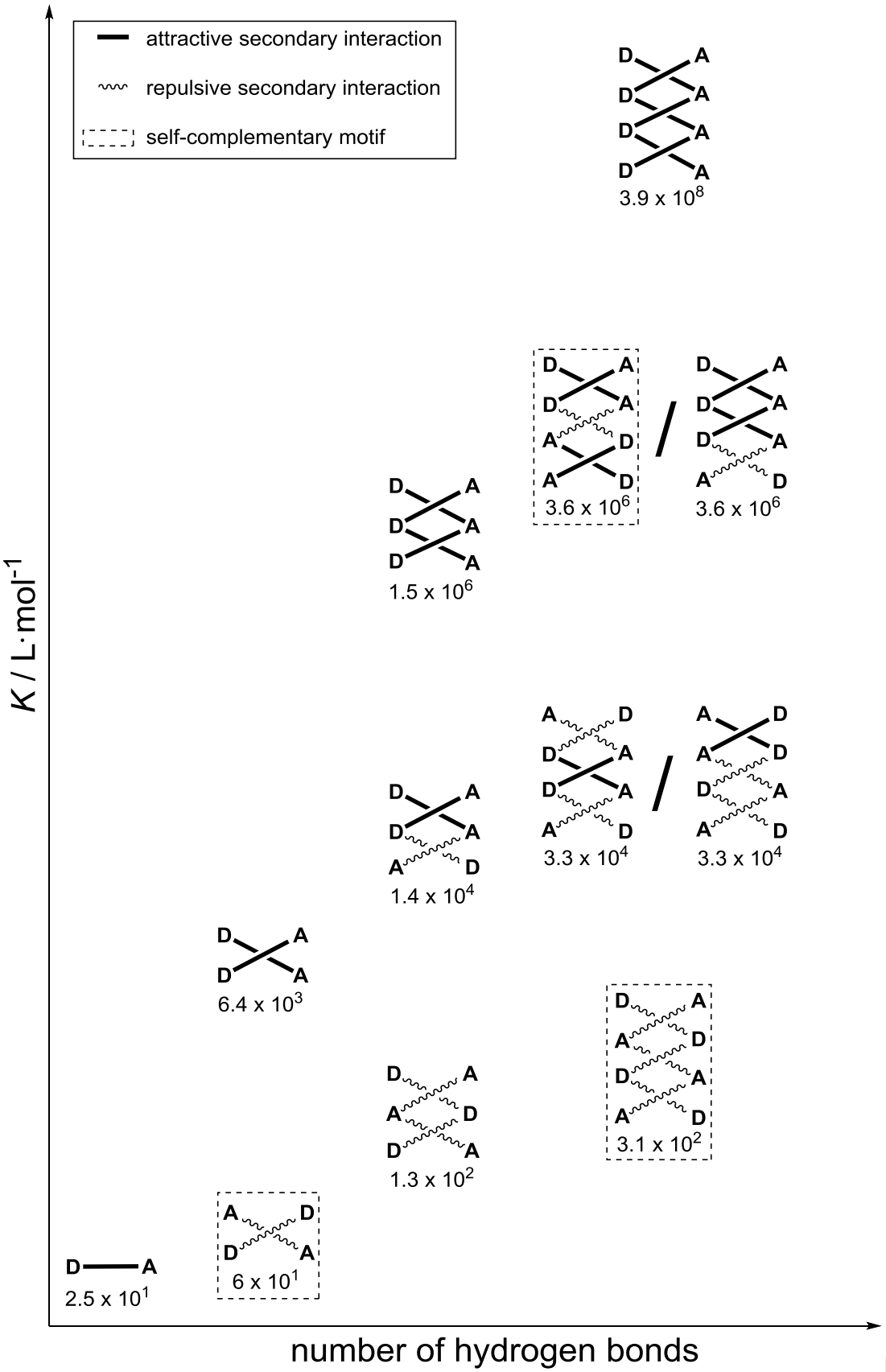

Figure 12: Schematic depiction of hydrogen bonding arrays and their binding constants according to Sartorius *et al.* ordered by the number of involved hydrogen bonds and dimerization constant.[107]

Figure 12 clearly indicates that for larger arrays of hydrogen bonding sites good binding strengths and orthogonality can be achieved, making these motifs valuable tools in supramolecular chemistry.

Hydrogen bonding is a fast process. Adducts show low kinetic stability and hydrogen bonding kinetics are usually diffusion controlled. [97, 108] Therefore, hydrogen bonds can be considered highly dynamic, orthogonal and reversible (regarding temperature, concentration and solvent polarity).

Telechelic molecules/polymer chains that are either able to form rings or polymeric aggregates tend to form rings at low concentrations. The concentration of cyclic adducts levels off quickly and stays constant starting at a critical concentration. Polymeric aggregates start to form as soon as a certain total concentration is exceeded and their concentration increases linearly with further increase in total concentration.[109, 110] An increase in temperature, however, leads to an entropy-driven polymerization (*e.g.* liquid sulfur) and the relative concentration of super-polymers increases linearly with temperature.[111]

In standard ^{1}H-NMR experiments, protons involved in hydrogen bonding exhibit higher chemical shifts than comparable non-binding protons, because their electron density is highly decreased. Therefore comparison of a ^{1}H-NMR in polar and apolar solvents can be a first step in identifying hydrogen bonding protons.[112]

Nowadays, modern synthetic chemists widely apply hydrogen bonding systematically in supramolecular containers and polymers, self-healing polymer networks, polymer composites, single chain folding and surface chemistry due to its orthogonality, reversibility and fast kinetics.[113-130]

2.2.2 *2-Ureido-4-pyrimidone (UPy)*

2-Ureido-4(*1H*)-pyrimidone (UPy) is a self-complimentary quadrupol hydrogen bonding motif based on an AADD array. For the synthesis of UPy, 2-amino-4-hydroxy-6-methylpyrimidine is either directly reacted with an appropriate isocyanate, or first activated by a phosgene analogue and then coupled to an appropriate amine. The ADD product tautomerizes towards the AADD array (UPy), which is able to undergo self-complementary homo-dimerization ($K = 10^7$-10^8 L·mol^{-1} in chloroform). Additionally, a second DADA tautomer exists, which is also capable of (yet much weaker) homo-dimerization ($K = 4.5 \times 10^5$ L·mol^{-1}), as depicted in Scheme 7. The DADA tautomer of UPy is slightly acidic and, therefore, can be deprotonated (to introduce electrostatic repulsion between UPy motifs and thus prevent dimerization) and subsequently modified with a protecting group.[131-133] Polar solvents (dimethyl sufloxide, tetrahydrofuran) weaken dimerization, as valid for all hydrogen bonds.[125, 129] Also, if R contains ethylene glycol units, the ADD tautomer which is incapable to dimerize is stabilized and, therefore, *K* is reduced. Yet, hydrophobic spacers ($C_{>6}$) can successfully shield UPy from these influences.[115, 130]

UPy is stable under elevated temperatures: In bulk UPy dimers dissociate (reversibly) at 80 °C and thermally degrade at 217 °C.[125]

Incorporated in polymers, UPy dimers form stacks and act as additional separated phase, which is further amplified by additional hydrogen bonding flanking groups (*e.g.* urethane, urea) increasing K and, simultaneously, decreasing over-all solubility.[113, 114, 134] The glass transition temperature increases linearly with the total concentration of UPy in bulk.[115, 125]

Additionally to homo-dimerization, UPy is able to hetero-dimerize *via* an ADDA tautomer with 2,7-diamido-1,8-naphthyridine (NaPy).[135] (Scheme 8)

Due to its convenient synthesis, its high dimerization constant and thermo-reversible dimerization UPy is widely employed in modern polymer and supramolecular chemistry: UPy is extensively employed in the field of supramolecular and self-healing polymers, networks and gels, as well as in composite preparation or modification of polymer miscibilities and single chain nano-particles (SCNP).[109-111, 126-128, 131, 132, 135-151]

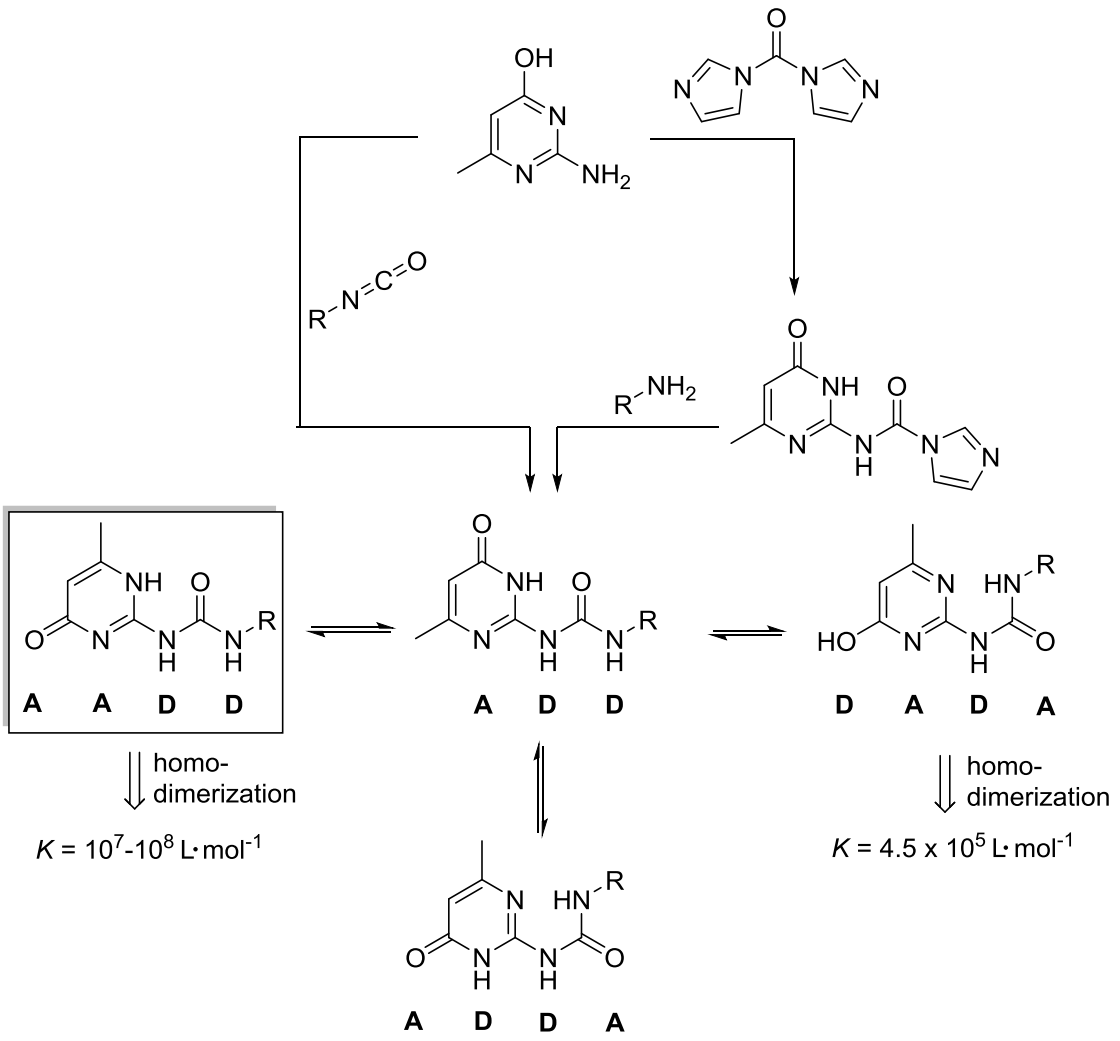

Scheme 7: Synthetic routes towards UPy. All tautomeric forms and the corresponding dimerization constants K are given.

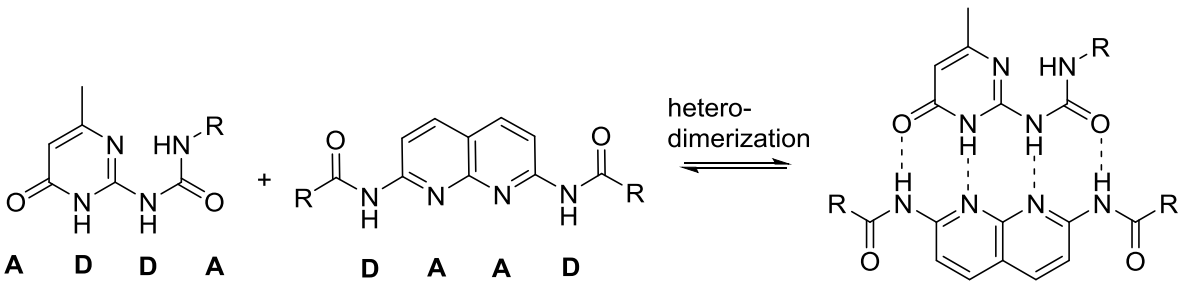

Scheme 8: Hetero-dimerization of the ADDA UPy tautomer with NaPy.

2.2.3 *Symmetrical Oligoamide (SOA) and Asymmetrical Oligoamide (AOA)*

The symmetrical oligoamide (SOA) and the asymmetrical oligoamide (AOA) represent a hetero-complementary hydrogen bonding couple with six complementary hydrogen bonding sites and were first synthesized by *Gong* and co-workers in 2000 (Scheme 9).[116]

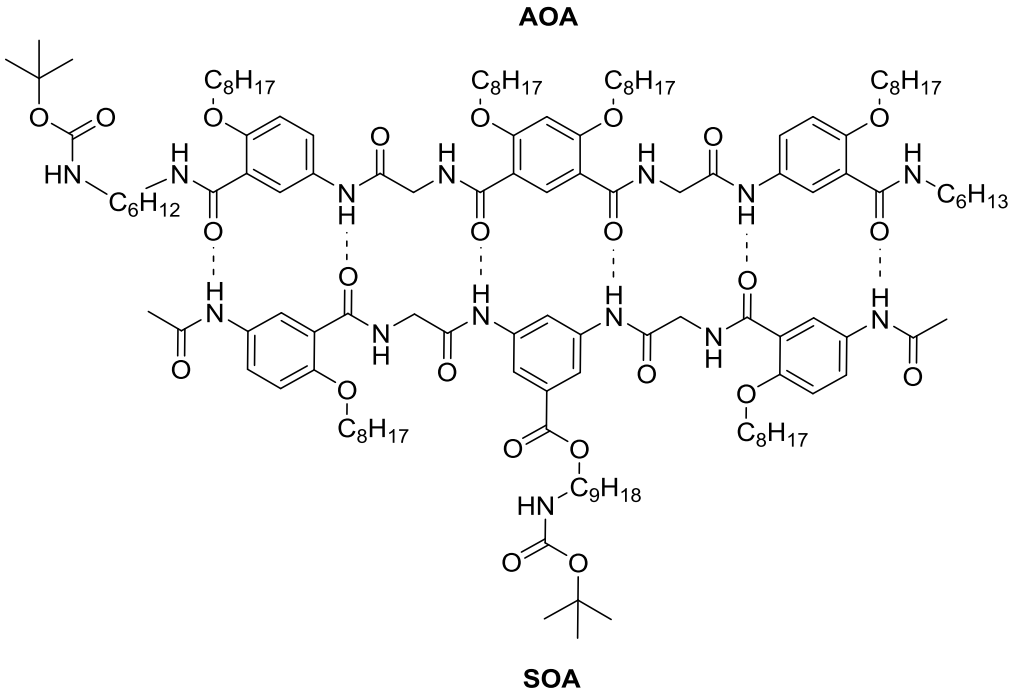

Scheme 9: Hydrogen bonding complex of SOA and AOA.

As expected from the generals trends of hydrogen bonding motifs (Figure 12) regarding binding constant and number of involved binding sites, the SOA-AOA couple exhibits a extremely high (hetero-)dimerization constant of $K = 1.3 \times 10^9$ L·mol^{-1} and is stable even under chromatographic conditions (high dilution, strong shear forces) in the presence of competing hydrogen bonding solvents (dimethylformamide).[116, 152, 153] The (hetero-)dimer is stable in bulk up to 150 °C.[152]

SOA is prepared in a convergent synthesis route with 11 steps, as depicted in Scheme 10. Methyl salicylate is reacted in a Williamson ether synthesis with octyl bromide, subsequently nitrated and saponified. The resulting benzoic acid (**1**)

derivate is transformed in the corresponding acid chloride and esterified with glycine ethyl ester. The aromatic nitro group is reduced employing hydrogen and palladium and subsequently amidated with acetyl chloride, followed by the saponification of the ethyl ester yielding the corresponding free acid (**2**). In parallel, 3,5-dinitrobenzoic acid is amidated with *t*-butyl (9-aminononyl)carbamate employing the coupling agent 2-(1*H*-benzotriazol-1-yl)-1,1,3,3-tetramethyluronium-hexafluorphosphat (HBTU) followed by the reduction of the aromatic nitro groups to amines, resulting in a *m*-aminoaniline core structure (**3**). Two equivalents acid **2** and one equivalent diamine **3** are coupled *via* amidation employing HBTU, finally resulting in the targeted *t*-butoxy carbonyl(Boc)-protected SOA.

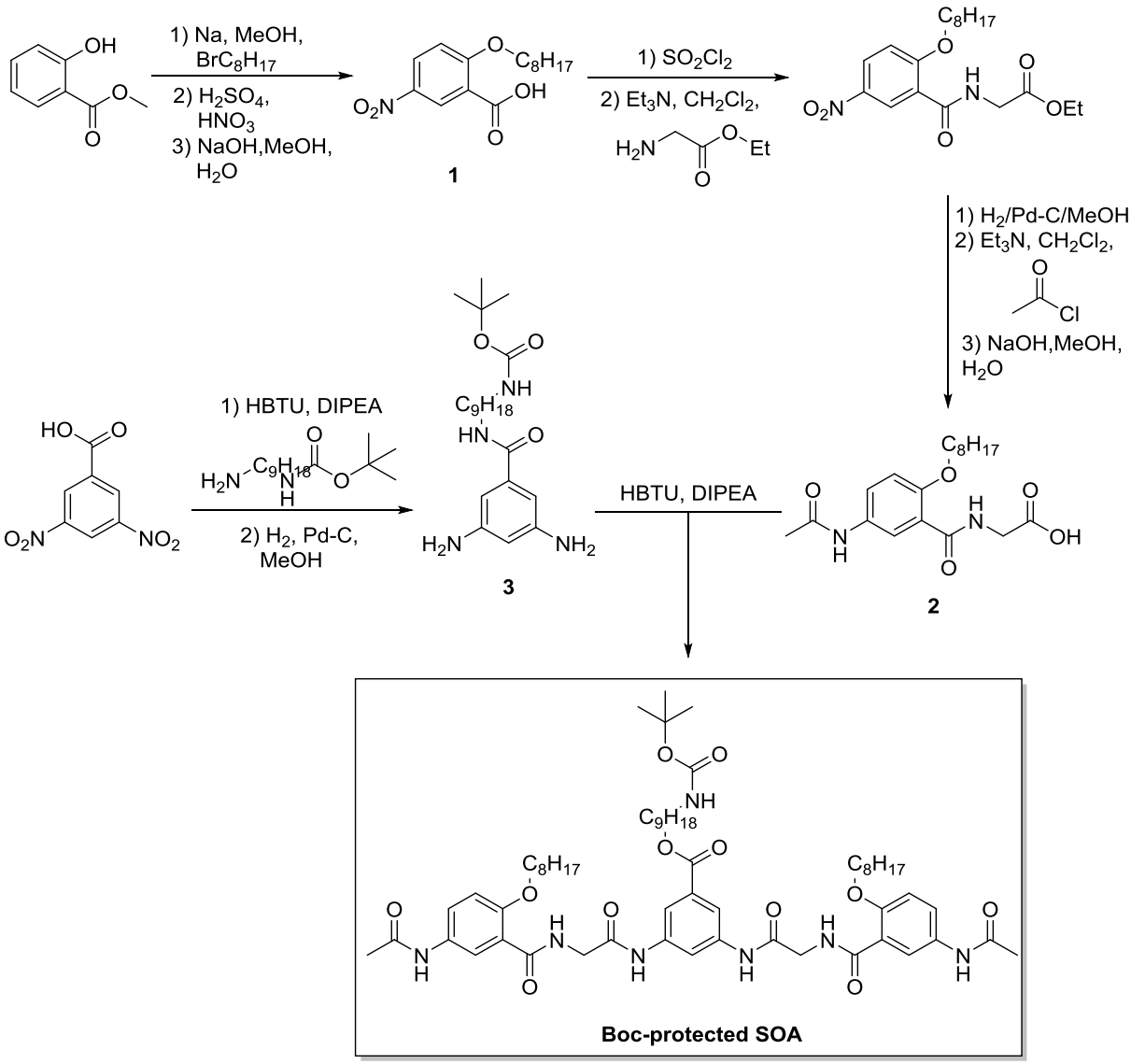

Scheme 10: Synthesis route towards Boc-protected SOA according to *Gong* and co-workers and *Bernard* and co-workers.[152, 153]

AOA is prepared in a convergent synthesis strategy with 20 steps, with the last step being a HBTU mediated coupling between two fragments of the final Boc-protected molecule. The detailed procedure is depicted in Scheme 11. For the first AOA fragment (**6**), methyl salicylate is subjected to a Williamson ether synthesis, followed by nitration and saponification (similar to the first steps in the SOA synthesis). The resulting aromatic acid (**1**) is converted to an acid chloride and amidated with hexyl amine. Subsequently, the aromatic nitro group is reduced, coupled to carboxybenzyl (Cbz)-protected glycine with HBTU and the Cbz group is removed *via* reduction, yielding the free amine **4**. In parallel, resorcinol is subject to two nucleophilic aromatic substitutions with potassium bicarbonate introducing two acid functionalities to the aromatic system. Both acid functionalities are protected as methyl esters, followed by two Williamson ether synthesis reactions with octyl bromide and subsequent deprotection of one of the two esters, resulting in an aromatic acid **5**. For the first fragment **6** in the convergent synthesis of Boc-protected AOA acid **5** and amine **4** are amidated *via* HBTU and the remaining methyl ester-protected aromatic acid functionality is deprotected by saponification resulting in **6**. The synthesis of the second fragment of Boc-protected AOA, the amine **7**, starts with the aromatic acid **1**, based on methyl salicylate (whose synthesis was described before). The benzoic acid derivate **1** is amidated *via* HBTU with Boc-protected hexyl diamine, which is prepared beforehand from di-*tert*-butyl dicarbonate (Boc_2O) and hexyl diamine. The amidation is followed by reduction of the aromatic nitro group and their amidation with Cbz-protected glycerin with subsequent reductive deprotection of the amine, resulting in the second fragment of Boc-protected AOA **7**. Both fragments **6** and **7** are finally combined by amidation *via* HBTU to the desired Boc-protected AOA.

In the literature, the hetero-complementary and very strong hydrogen bonding couple SOA-AOA is employed for supramolecular polymers and polymer precursors for nanoporous films (exploiting the reversibility of hydrogen bonding towards polar solvents).[153-155] Due to the time-consuming synthesis (11 + 22 steps), the hydrogen bonding pair is not widely used in supramolecular science, although its dimerization constant is extremely high.

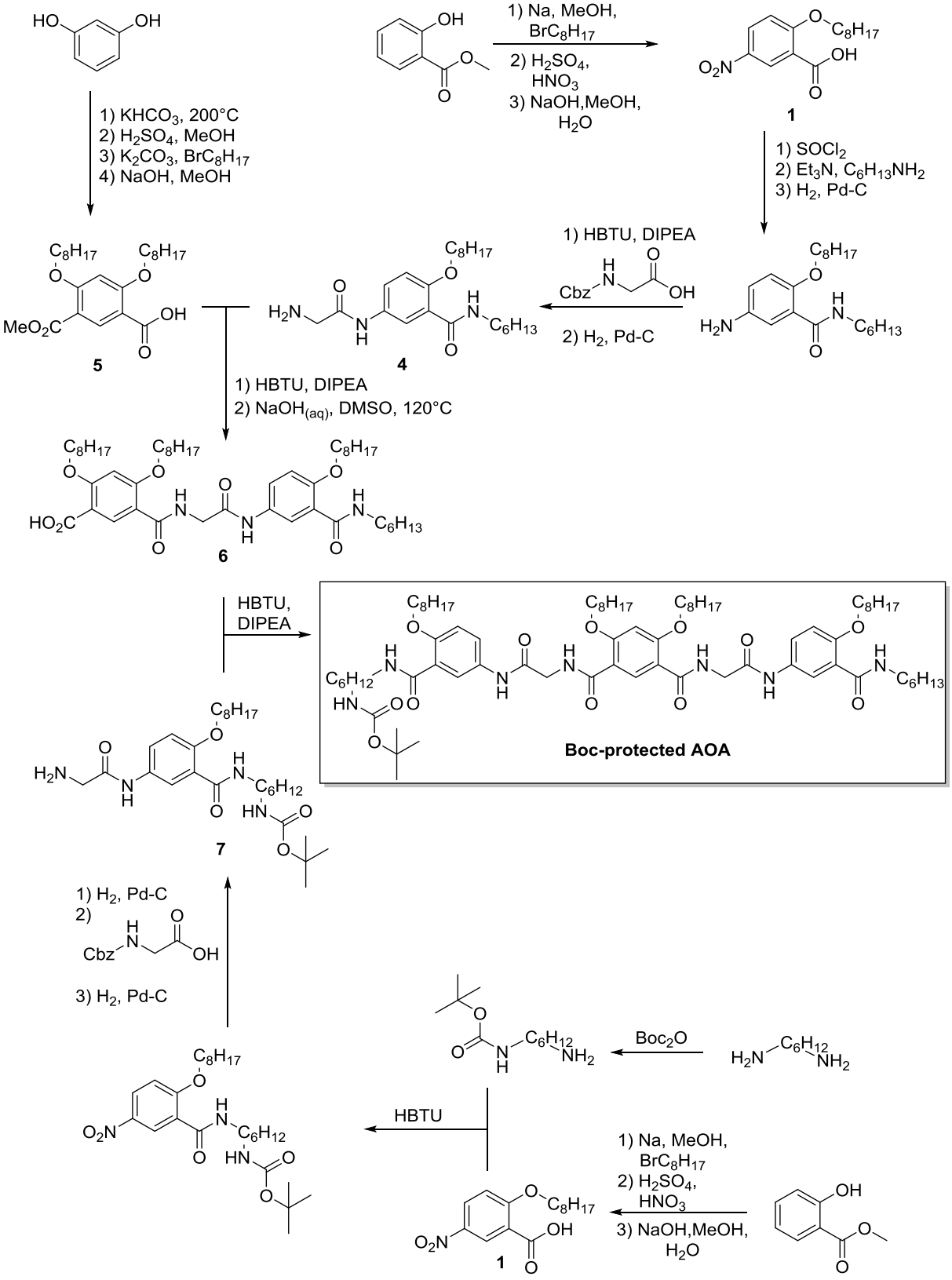

Scheme 11: Synthetic route towards Boc-protected AOA according to *Bernard et al*.[153]

2.3 Layered Nano-Composites (NCs) and Nacre

2.3.1 *Definitions and General Properties*

Composites are materials built-up from two or more single components with different physical (and chemical) properties that on one hand are blended but on the other hand still can be distinguished in the final (composite) material. Ideally, a composite exceeds its single components in a desired property (*e.g.* mechanic performance, flammability, barrier, membrane, electrical and magnetic properties).[156-159] Important composites taken from everyday life are cement, fiber-reinforced polymers or – even more crucial - bones.

Composites are termed “nano”-composites (NC) when the size of one component (often the hard/inorganic phase) becomes smaller than 100 nm and can be labeled according to the dimensions of the filler/hard phase as one-, two- or three-dimensional. NCs possess, compared to their microscopic analogues, larger number densities of filler-particles per matrix volume at comparable loadings (resulting in: increased particle-particle correlation, extensive interfacial area and short distances between particles)[160] and, therefore, exhibit additionally, potentially beneficial nano-effects:[161] Inorganic fillers can act as nuclei for crystallization,[162, 163] the increased viscosity at high filler loadings, however, retards diffusion and crystallization kinetics of polymer matrices.[164, 165] Depending on the quality of interfacial wetting, and chemistry of the filler surface, fillers can also disturb the packing of rigid polymer chains, thus creating free volume or act as plasticizers and decrease the glass-transition temperature.[166-168] Apart from the impact on crystallinity, numerous other nano-effects are known. (Figure 13)

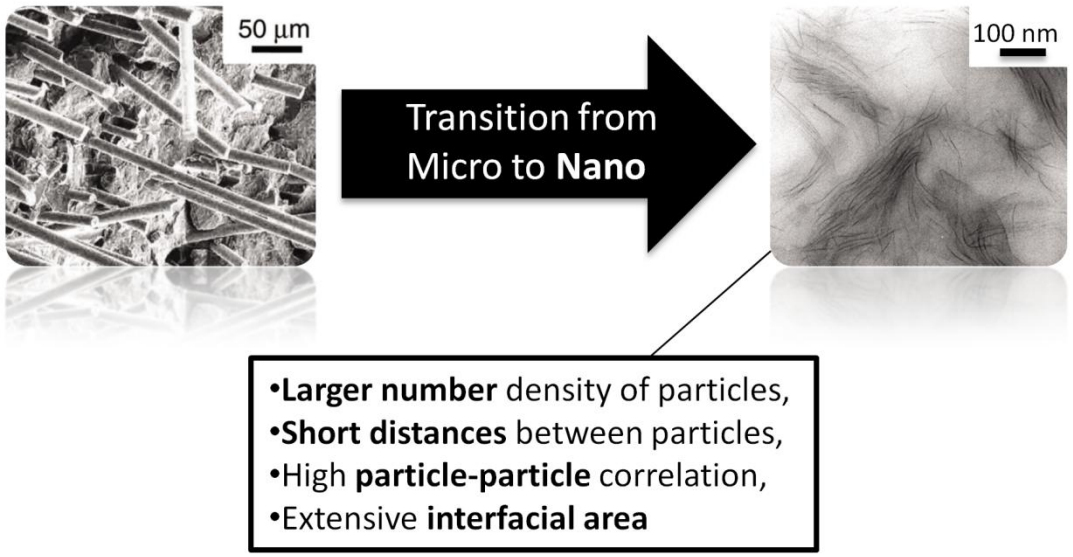

Figure 13: Most important features of NCs compared with "macroscopic" composite materials. TEM images adapted with permission.[160]

Organic/inorganic NC have been prepared combining soft polymer matrices (ductility, flexibility and processability) with rigid carbon nanotubes/nanofibers, graphene and other inorganic fillers, most importantly, clays (*e.g.* montmorillonite, hectorite and saponite), since they are readily available, cheap and environment-friendly.[169] These minerals consist of layered crystals exhibiting intercalated cations between the silicate layers or on the basal faces, which can, depending on the clay, be replaced with desired cations (*e.g.* ammonium functionalized surfactants), making the initially hydrophilic silicate layers miscible with hydrophobic polymers. [170, 171]

2.3.2 *Nacre – Natural Occurrence and Performance*

Nacre, which is the layer in the amour of sea-shell that generates mechanic resistance, consists of parallelly orientated 8 µm long and 0.4 µm thick aragonite platelets (95 vol%) laminated with a viscoelastic biopolymer (5 vol%) (Figure 14a). Since nacre exceeds its neat components in a remarkable manner (*i.e.* nacre is 3.000 times tougher than aragonite single-crystals), due to its brick-and-mortar structure on nano-scale, it is an important example for Nature´s ability to generate

exceptional materials regarding performance and structure and is frequently mimicked by material scientists.[2]

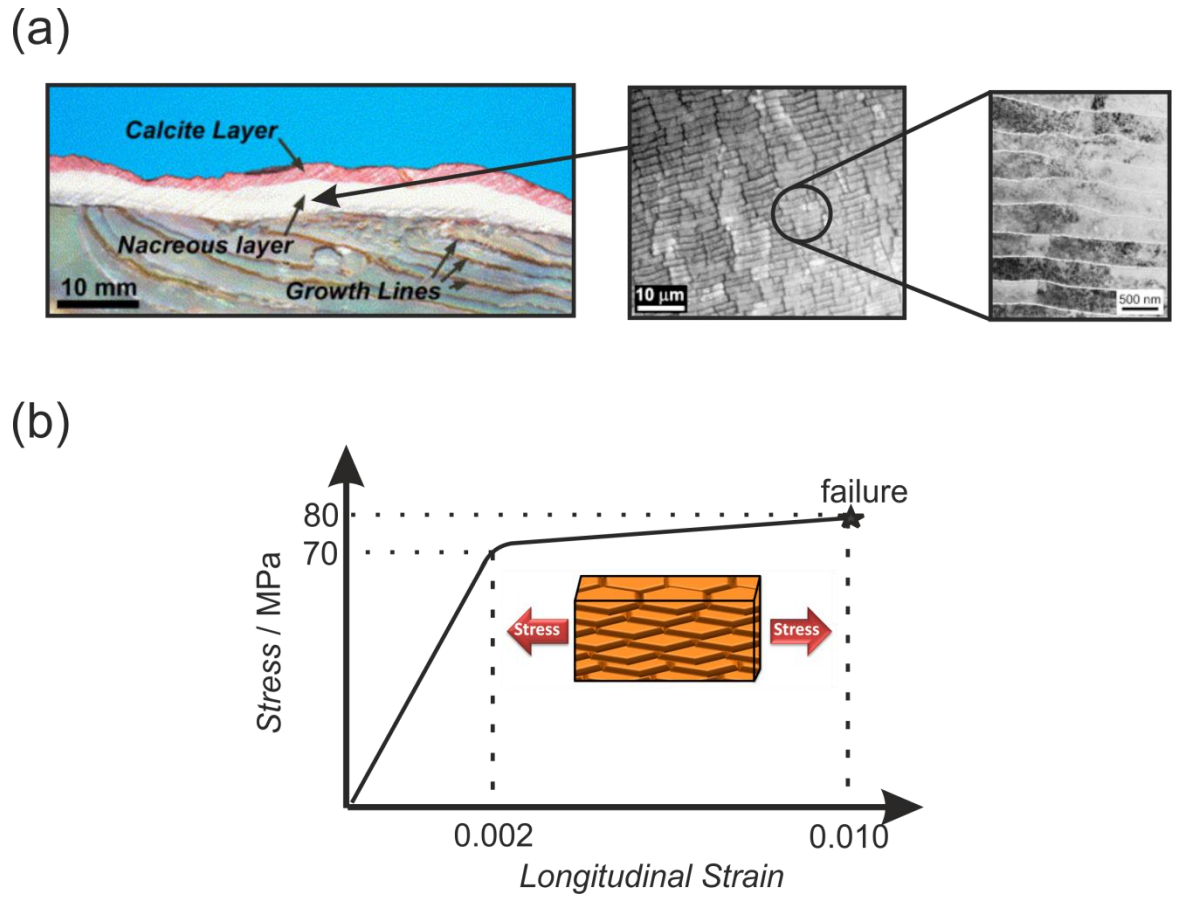

Figure 14: (a) Natural occurrence of nacre and structuring on nano-scale monitored by TEM: aragonite platelets (95 vol%) are orientated parallelly and laminated with biopolymer (5 vol%). Images taken from Barthelat *et al.* with permission.[172] (b) Stress-strain curve of nacre: Elastic regime up to 70 MPa, plastic deformation with strain-hardening up to 80 MPa. Adapted from Song *et al*.[173]

Nacre shows in tensile tests a linear elastic region up to a longitudinal strain of 0.002 and 70 MPa stress. Further increase of stress leads to a plateau of inelastic deformation during which the aragonite platelets slide on one another until macroscopically a longitudinal strain of 0.010 is observed (at a stress of 80 MPa) and the material finally breaks (Figure 14b) by pullout of tablets.[173] While ceramics are in general strong but brittle and elastomers are soft but ductile, nacre shows, due to synergetic effects based on its structure, strong and ductile behavior resulting in the material´s remarkable energy dissipation (which is proportional to the integral in the stress-strain curve).

In the literature, various strain-hardening mechanisms, occurring during interfacial sliding of aragonite platelets, forced by macroscopic, inelastic deformation, are discussed. Most probably all of them occur simultaneously with different contributions to the over-all effect: Sliding of platelets initially leads to breakage of aragonite bridges (Figure 15b)[174] and polymer unfolding (Figure 15a).[175] Further deformation induces breakage of sacrificial bonds in the biopolymer (Figure 15a), friction of nano-asperities on the interfaces (Figure 15c)[176, 177] and relocking of broken aragonite bridges (Figure 15b)[173] and wavy aragonite plates (Figure 15d).[172, 178]

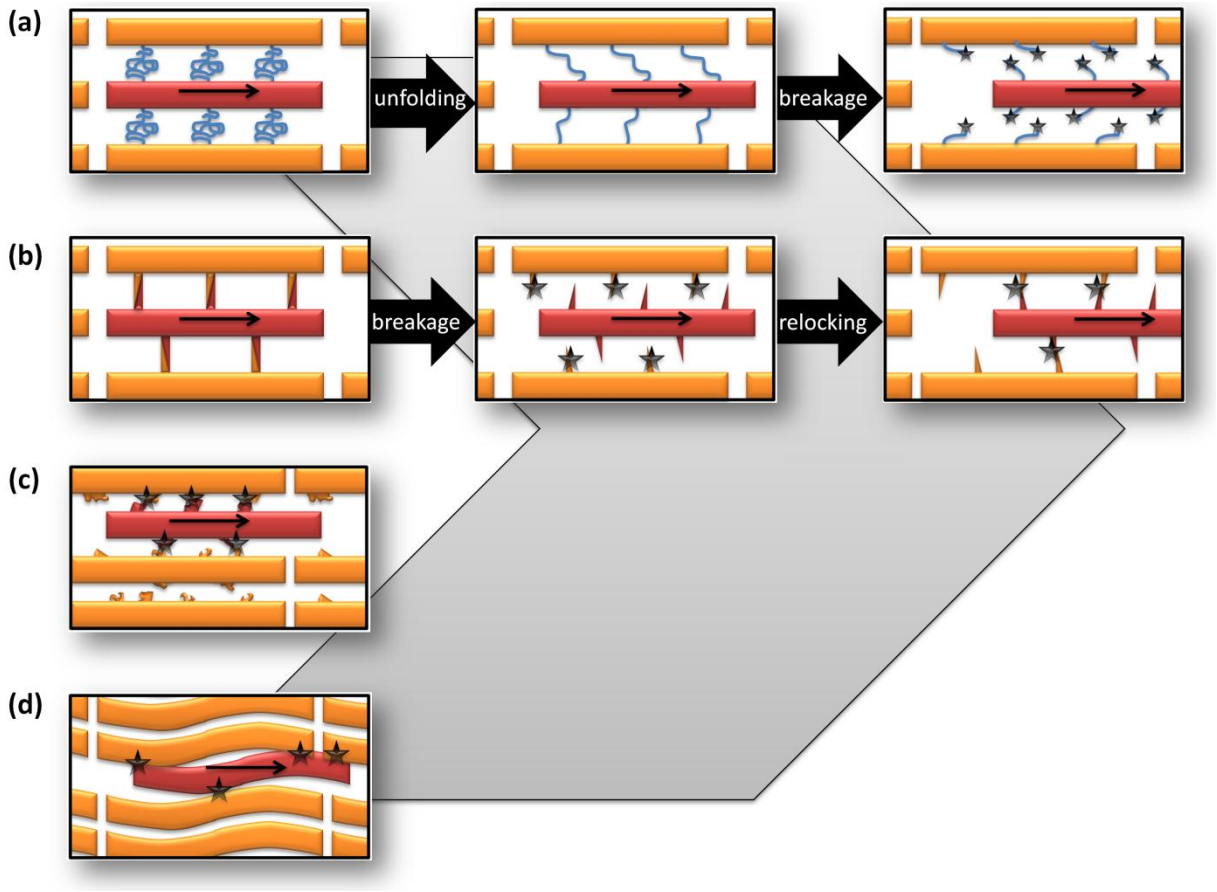

Figure 15: Strain hardening mechanisms discussed in the literature: (a) Unfolding of biopolymer and breakage of sacrificial bonds, (b) breakage and relocking of aragonite bridges, (c) friction induced by nano-asperities at the interfaces and (d) relocking of wavy platelets.[172-178]

2.3.3 *Preparation of Synthetic Layered Nano-Composites*

Exfoliation of platelets is a crucial requirement for optimal mechanic performance, which in general is further improved by parallel alignment of exfoliated platelets. However, complete disaggregation of platelets cannot be achieved by pure mechanic force alone but has to be additionally driven by energetic attraction, compensating the loss of conformational entropy of the matrix chains penetrating the clay galleries.[179, 180] Surface modification of clays (and nano-fillers in general) can reduce the clay-clay interactions simultaneously increasing clay-matrix affinity and, therefore, improve miscibility.[181] During the exfoliation process, clay tactoids (micron-sized clusters of clay aggregates) are broken by a sliding mechanism and each platelet is peeled off its platelet stack (aggregates) individually and sequentially in a very slow over-all process, while simultaneously polymer diffuses into the galleries.[179]

Clays can be either immiscible, intercalated (ordered and disordered), or exfoliated in a polymer matrix and the three equilibrium states of platelet exfoliation can be most conveniently identified by X-ray diffraction (XRD) and visualized by transmission electron microscopy (TEM) (Figure 16).

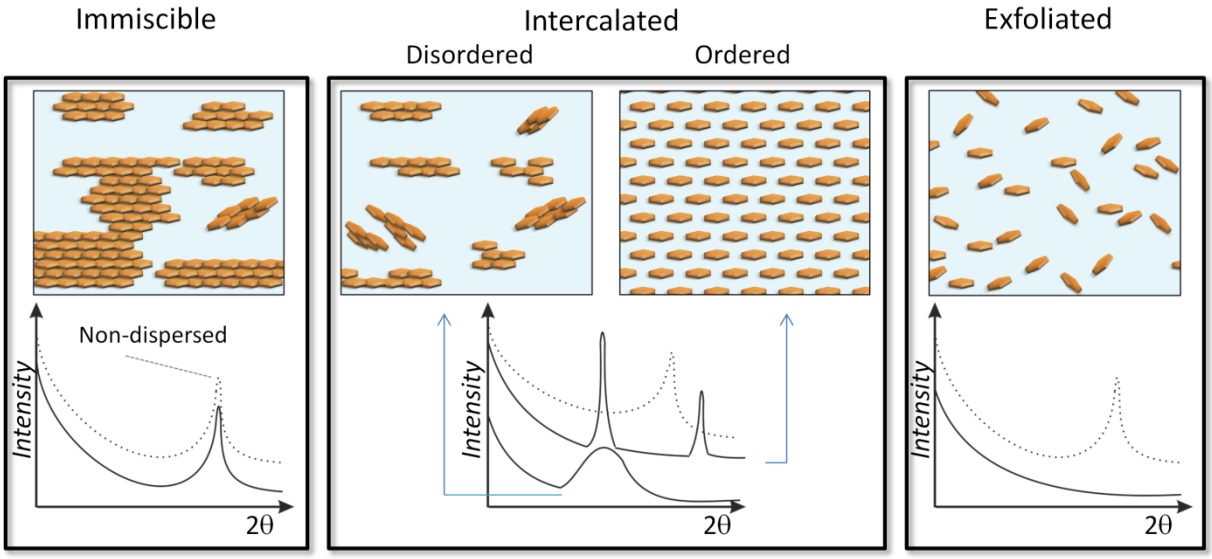

Figure 16: Immiscible, intercalated (disordered and ordered) and exfoliated nano-clay in a polymer matrix. Schematic XRD spectra are provided for each state of exfoliation. The dotted curve is the initial XRD before dispersion of the nano-particles in the matrix.[169, 179]

In the context of the fabrication of layered NCs only the most important techniques suitable for large scale fabrication will be briefly reviewed and are ordered by decreasing viscosity during the assembly process, thus increasing quality of exfoliation.

In melt intercalation clays are dispersed in a polymer melt. Since exfoliation is hindered by high viscosity, due to slow diffusion, the achieved exfoliation is poor. However, due to relative low costs and since the method can be scaled-up facilely, melt intercalation fits commercial needs best. Still, only little exfoliation is achieved.[182]

During solution casting the clay is dispersed in a polymer solution and because the viscosity in solution is generally lower than in melt, polymer chains can penetrate the clay´s galleries easier and better exfoliation is achieved.[182, 183]

A very critical technique for large scale fabrication of well exfoliated layered NCs is in-situ polymerization. Clay is dispersed in the monomer, penetrating galleries easier than polymer melts or solutions, allowing good exfoliation; subsequently the dispersion is polymerized. [156, 157]

In dense suspensions, nano platelets are forced into parallel orientation by shearing. Additional mechanic methods can further improve the alignment of layered NCs: Among others, centrifugation, sedimentation, dipping, vacuum filtration and slip casting have been employed to increase the structural order of thick NC films.[184]

2.4 Single Chain Nano-Particles (SCNPs)

2.4.1 *History and Motivation*

Single chain nano-particles (SCNPs) are formed *via* the collapse of individual polymer chains to denser coils (diameter 1.5-20 nm), leading to new properties and applications for these compact polymers.[123, 185-187] The earliest report for SCNP formation was published by Kuhn and Majer in 1955, who reported that under diluted conditions intramolecular cross-linking of polymers is favored over intermolecular cross-linking, thus resulting in SCNPs instead of networks.[188] However, due to the difficulties of the characterization of these particles and the lack of controlled polymerization techniques, only very few further contributions to this topic have been made in the following decades. Not till the availability of new precise polymerization techniques (*e.g.* ATRP and RAFT) new cross-linking chemistries and advanced characterization techniques (*e.g.* triple-detection SEC and DLS) SCNPs caught the attention of polymer chemists.

One of the most important aims of the single chain approach towards organic nano-particles is to mimic the precise structures and functions of natural proteins with fully synthetic polymers. Naturally occurring proteins are monodisperse poly-peptides folded by numerous orthogonal non-covalent and dynamic covalent interactions of precisely arranged functional groups along the peptide backbone. The folding process is controlled by enzymes inside the living cell and the final, delicate structure, which is critical for the proteins chemical function, can be divided into several substructures: The primary structure consists of the sequence of amino acids in the peptide backbone, which resembles the monomer repeating units of synthetic polymers. The secondary structure (α-helix and β-sheet) and tertiary structure (folding of secondary structure into compacter regimes) resemble the folding process of the single chain in general. The quaternary structure describes the arrangement of several peptide chains. The high level of control of natural proteins over the chain structure is not yet achieved with the SCNP approach. However, due to the numerous weak interactions that control their three-dimensional structure, proteins are very fragile (regarding pH, temperature and solvents) and their isolation is extremely expensive – drawbacks that might be overcome with synthetic proteins.

Probably one of the frequently employed methods to synthesize enzymes on a larger scale is the solid phase peptide synthesis by Merrifield, which is not exclusively limited to proteinogenic α-amino acids. Still, it is applicable only for relatively short sequences and limited to low amounts of material.[189] The approach of SCNPs towards synthetic proteins is fundamentally different to Merrifield's approach, trying to control the primary structure of synthetic proteins: A certain tertiary structure is realized *via* relatively few folding points along the backbone.[190] Therefore, the synthetic effort is significantly reduced (compared to methods that control the primary structure of synthetic proteins) and SCNPs are comfortably available protein mimetics.

2.4.2 *The Chain Collapse*

Single chain collapses can be classified in different categories.

Firstly, depending on the number of different types of functional groups introducing the folding, collapses can be labeled as hetero/homo-functional (Figure 17). Also, if several cross-linking chemistries are present that do not interfere with each other, collapses can be termed as (multi-)orthogonal.[191] If the cross-linking is triggered by an external cross-linker that has to be added to the dilute polymer solution SCNP formation is termed cross-linker-mediated.[192]

Secondly, if (orthogonal) folding units are introduced at distinct positions in the backbone, thus resulting in a precise folding, a chain is folded *via* the selective point folding approach. In the repeating unit approach the cross-links are randomly distributed along the polymer backbone.

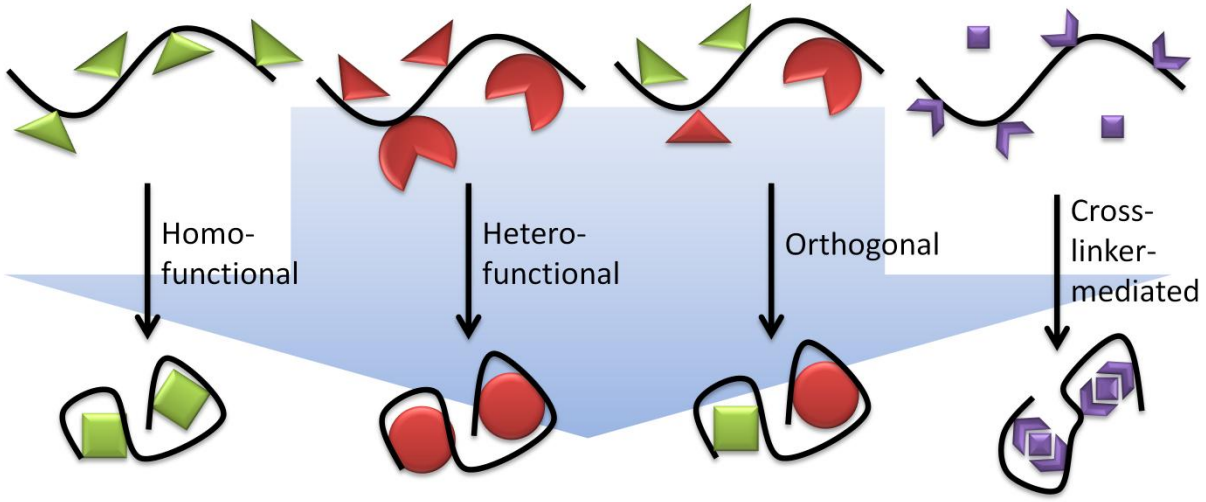

Figure 17: Classification of SCNP collapses according to the number and position of involved groups.

Furthermore, SCNP collapses can be classified with reference to the thermodynamic and kinetic stabilities of the cross-linking points:

Covalent SCNPs (with covalent cross-linking) represent the largest number of particles prepared by single chain collapse. These SCNPs in general are stable towards external stimuli. Due to the large number of covalently prepared particles, a broad chemical spectrum has been employed, including CuAAc (Section 2.1.2), thermal and photochemical cycloadditions, amine quaternization, Michael Addition and olefin metathesis.[185]

Dynamic covalent SCNPs are sensitive towards external stimuli *e.g.* pH or reduction/oxidation and respond structurally to them.[193, 194] Reversible cross-linking also allows incorporation and the triggered release of components form the particle, which makes these types of SCNPs interesting candidates for drug delivery systems. Some examples for dynamic covalent cross-linking are disulfides (redox stimulus), hydrazones and enamines (pH stimulus) and coumarin derivates (photochemical stimulus).[195-198]

The most labile SCNPs are based on non-covalent cross-linking and, due to the comparatively low energy barrier of these interactions, are extremely sensitive towards external triggers.[199] Some examples for this class of SCNPs are based on hydrogen bonding (Section 2.2), π-stacking, hydrophobic interactions and metal complexation.[199-202]

The current thesis introduces SCNPs based on dynamic covalent HDA chemistry (Section 2.1.1), employing a cross-linker-mediated collapse following the repeating unit approach (Section 3.3). Subsequently, the resulting SCNPs are converted back to an open-chain state by an external chemical stimulus.

Nano-particles based on single polymer chains feature controlled sizes (1.5-20 nm) and well defined functional groups, which can be arranged in a controlled manner, and, if desired, respond structurally to stimuli (solvent, pH, redox, temperature, light).[187, 192] Therefore, SCNPs can serve as rheologic agents, catalysts – in particular enzyme mimics in water, assist imaging *via* fluorescence, serve as contrast agents or, most importantly, serve as nano-medicine with designed release dynamics.[203-207]

3 RESULTS AND DISCUSSION

3.1 Preparation and Performance of Matrix Polymers

The polymer electrolysis was developed in cooperation with Andrea Lauer (macroarc group, KIT) in the context of her master thesis, corresponding AES measurements were performed by Silke Behrens and Sarah Essig (KIT). Nano-composites were cast and analyzed by Dr. Baolei Zhu and Saskia Gröer (RWTH Aachen). Thorsten Lückerath optimized the synthesis of CDTE-MA (**15**) during his master thesis.

A critical task in the fabrication of high performance NCs, apart from the assembly, is the choice of a suitable polymer matrix, in which the (inorganic) filler is dispersed. One aim of the current thesis is to provide a water-soluble polymer matrix capable of reversible and dynamic cross-linking for a clay based, layered NC inspired by nacre. A NC with such an employed polymer matrix is expected to result in a material that is cross-linked at ambient temperature but, more critically, can undergo thermoreversible reshaping processes at elevated temperature, due to the labile nature of cross-linking. For this purpose, two types of cross-linking chemistries have been under investigation.

First, different polymer architectures with varying positions and degree of functionalization with UPy as cross-linker have been synthesized and tested in NC fabrication. Therefore, end-group functionalized star polymers with different arm lengths and numbers have been synthesized *via* Activators Generated by Electron Transfer Atom Transfer Radical Polymerization (AGET ATRP) and, thereby, a new method of purification of strongly Cu-complexing polymers was established.[208] In addition, various RAFT copolymers bearing new UPy-monomers with distinct flanking units (which are reported to have an impact on the dimerization constant *K*) have been synthesized and employed in NCs. Moreover, long copolymer chains of a new UPy-monomer have been synthesized *via* conventional FRP and have also been utilized in NC fabrication. Second, the CDTE-sorbic alcohol HDA couple was chosen as dynamic covalent cross-linking system and a new CDTE containing monomer was synthesized for subsequent FRP. A long, water-soluble copolymer chain bearing both reactive sides, *i.e.* CDTE and sorbic alcohol, was synthesized. The HDA matrix was designed for higher dissociation temperatures and solvent independent cross-linking,

due to the more robust nature of dynamic covalent bonds (compared with hydrogen bonding UPys).

3.1.1 *UPy-Matrices*

3.1.1.1 Overview over the Synthesis Approaches

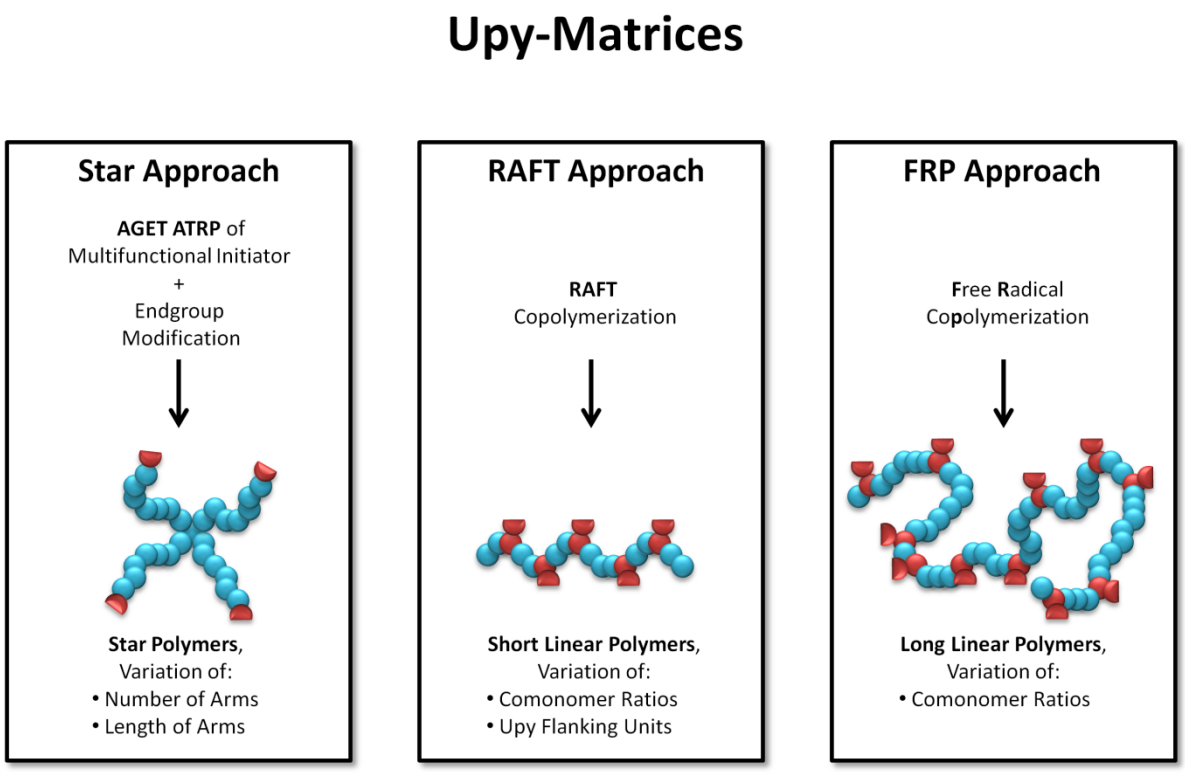

Figure 18: Overview over matrices prepared by the employed synthetic approaches towards UPy functionalized matrices and their varied structures.

Aiming for UPy functionalized water-soluble polymer matrices, three synthetic approaches were employed, resulting in distinct polymer architectures, degrees of UPy functionalization and chain lengths.

In the star approach, water-soluble polymer stars were synthesized utilizing AGET ATRP with commercial initiators containing four and six bromine atoms (4/6f-Bib), employing water-soluble poly(ethylene glycol) methyl ether methacrylate ($MeOEGMA_{300}$) as monomer, resulting in four and six armed bromine terminated star polymers. In a second step, the bromine endgroups were substituted with azides, allowing in a subsequent third step the introduction of alkyne functionalized UPys (synthesized in two steps) as endgroups *via* CuAAc. In total, five synthetic steps were fabricated *via* the star approach and polymers with varying numbers and lengths of arms were synthesized.

Increasing the functionalization with UPy compared to the star approach, the RAFT approach is based on the RAFT copolymerization of $MeOEGMA_{300}$ and two UPy bearing monomers. Both monomers exhibit additional flanking units (urea, urethane), which increase the dimerization constant but on the other hand decrease solubility. The flanked UPy monomers were synthesized in two and three steps. In total three or four synthetic steps were employed, fabricating a library of four short, linear RAFT copolymers with varying UPy ratios and flanking units.

The conventional FRP approach practically resembles the RAFT approach, however, a new UPy monomer was synthesized in two steps, exhibiting an ethylene glycol chain thus increasing the solubility and, thereby, improving drastically the copolymerization behavior. A library of four long chains, with varying molecular weight and copolymer composition was synthesized in three synthetic steps.

3.1.1.2 UPys for Polymer Matrices

Depending on the employed strategy, UPys were either introduced as endgroups *via* CuAAc to an azide terminated star polymer (star approach) or different UPy-functionalized methacrylate comonomers (RAFT and conventional FRP approach). Although these syntheses are essentially different, all UPys are based on a shared synthesis concept starting with 2-amino-4-hydroxy-6-methylpyrimidine (Scheme 12).

UPy-Urethane-Alkyne (**9**), employed in the endgroup modification of water-soluble, azide terminated star polymers **P2** (star approach), was readily synthesized in two synthetic steps without further purification *via* column chromatography. Thus for the synthesis of UPy-Urethane-Alkyne (**9**) 2-amino-4-hydroxy-6-methylpyrimidine was reacted with 1,6-diisocyanato hexane at 100 °C for 24 h resulting in UPy-NCO (**8**), which precipitates from the reaction solution, making the synthesis of this crucial intermediate in UPy synthesis very efficient. (UPy-NCO (**8**) also represents the first step in synthesis of UPys employed in Chapter 3.2.) Subsequently, intermediate **8** underwent an addition reaction with propargyl alcohol in bulk at 60 °C for 24 h, resulting in the alkyne functionalized UPy **9** that was also purified *via* precipitation and was isolated in excellent purity (total yield: 43%).

Meanwhile, for the RAFT and conventional FRP approach various UPy containing monomers with different flanking units, influencing both dimerization constant *K* and solubility, have been synthesized.

Initially, in a simple approach, an 2-amino-4-hydroxy-6-methylpyrimidine was coupled to 2-isocyanatoethylmethacrylate *via* addition reaction in dimethyl sulfoxide (DMSO) at ambient temperature for 2 h. The corresponding product **10** was readily precipitated from the reaction solution (yield 92%). To further increase the dimerization constant *K* of the monomer and, therefore, strengthen the cross-linking in the polymer matrices at constant degrees of functionalization of UPy, a second and third monomer were designed with additional hydrogen bonding flanking units (urea, urethane).

For synthesis of UPy-Urethane-MA (**11**), hydroxyethylmethacrylate (HEMA) was reacted with the free isocyanate of **8** resulting in the addition product **11** after heating the reaction in dichloromethane (DCM) overnight. The monomer **11** could be isolated by precipitation (total yield: 77%).

A third UPy monomer **12** was synthesized exhibiting urea flanking, which led to a further increase in the dimerization constant *K* but a significant decrease in solubility (compared to **11**). In a first step 2-amino-4-hydroxy-6-methylpyrimidine was activated with 1,1'-carbonyldiimidazole (CDI) in DMSO at 80 °C for 2 h and the activated product isolated by precipitation. Subsequently, the intermediate was coupled to diamino hexane in a suspension in DMF. The product of the addition reaction was isolated *via* filtration after a reaction time of 2 h at ambient temperature. The resulting amino functionalized UPy was suspended in DMSO and reacted with 2-isocyanatoethylmethacrylate for 2 h at ambient temperature thus resulting in the urea flanking unit of UPy-Urea-MA (**12**) in three synthetic steps (total yield: 52%, new molecule).

To overcome the disadvantage of low solubility of **11** and **12**, which affects the copolymerization behavior negatively and, therefore, limits the maximal incorporation into the final copolymer, a fourth UPy monomer **13** was designed, which bears ethylene glycol units for increased solubility. On the other hand, the negative impact on the dimerization constant was reduced with a hydrophobic spacer between the ethylene glycol units and the UPy. Starting from UPy-NCO (**8**), in a second step poly(ethylene glycol) methacrylate ($OEGMA_{360}$) was coupled to the residual isocyanate moiety in a suspension in DCM for 21 h, which was refluxed. The final product UPy-EG-MA (**13**) was isolated by precipitation in cold cyclohexane and subsequent washing until excellent purity was achieved (total yield: 14%, first synthesis).

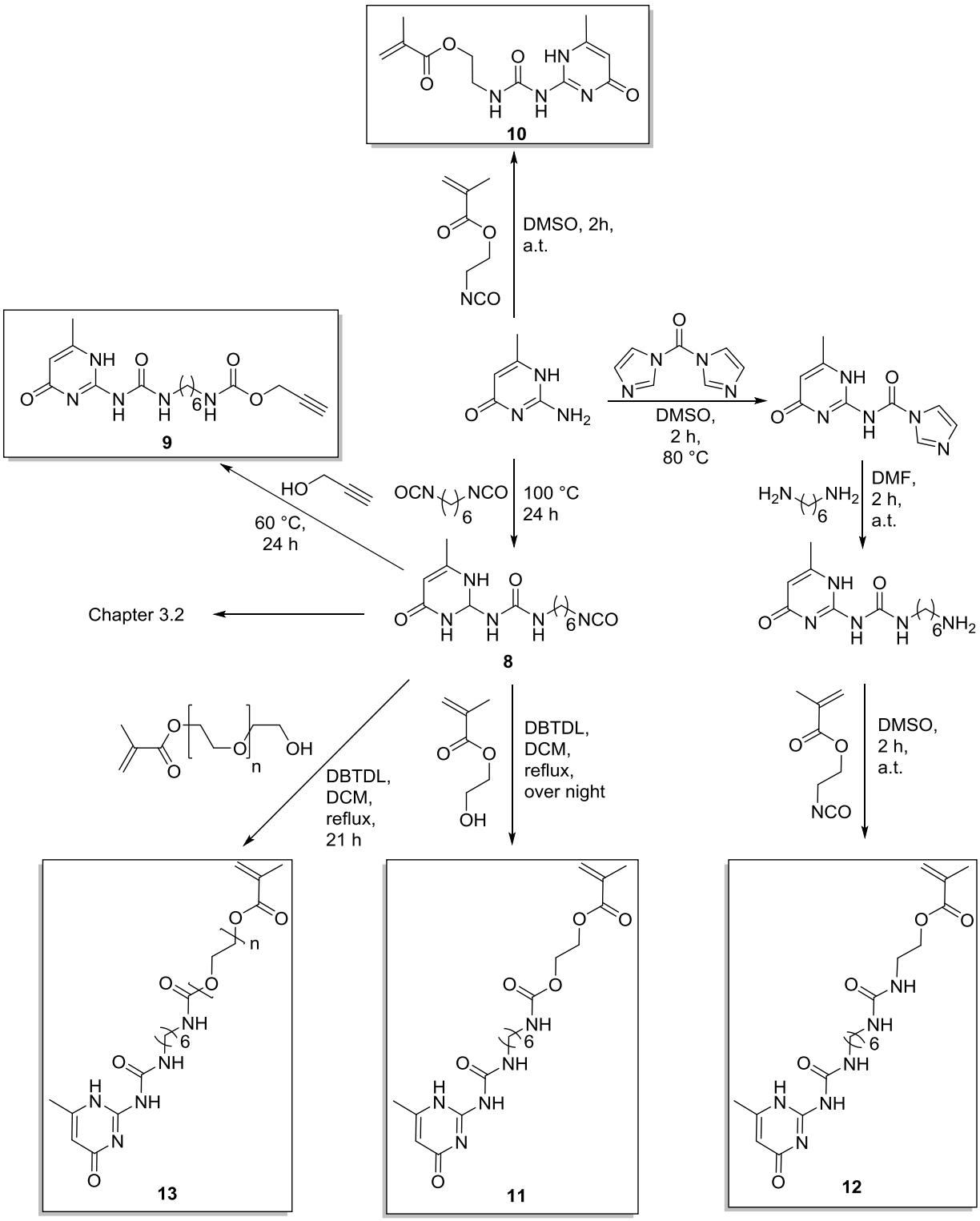

Scheme 12 Synthesis routes towards UPy monomers and UPys for endgroup modification employed in chapter 3.1.

3.1.1.3 Star Approach

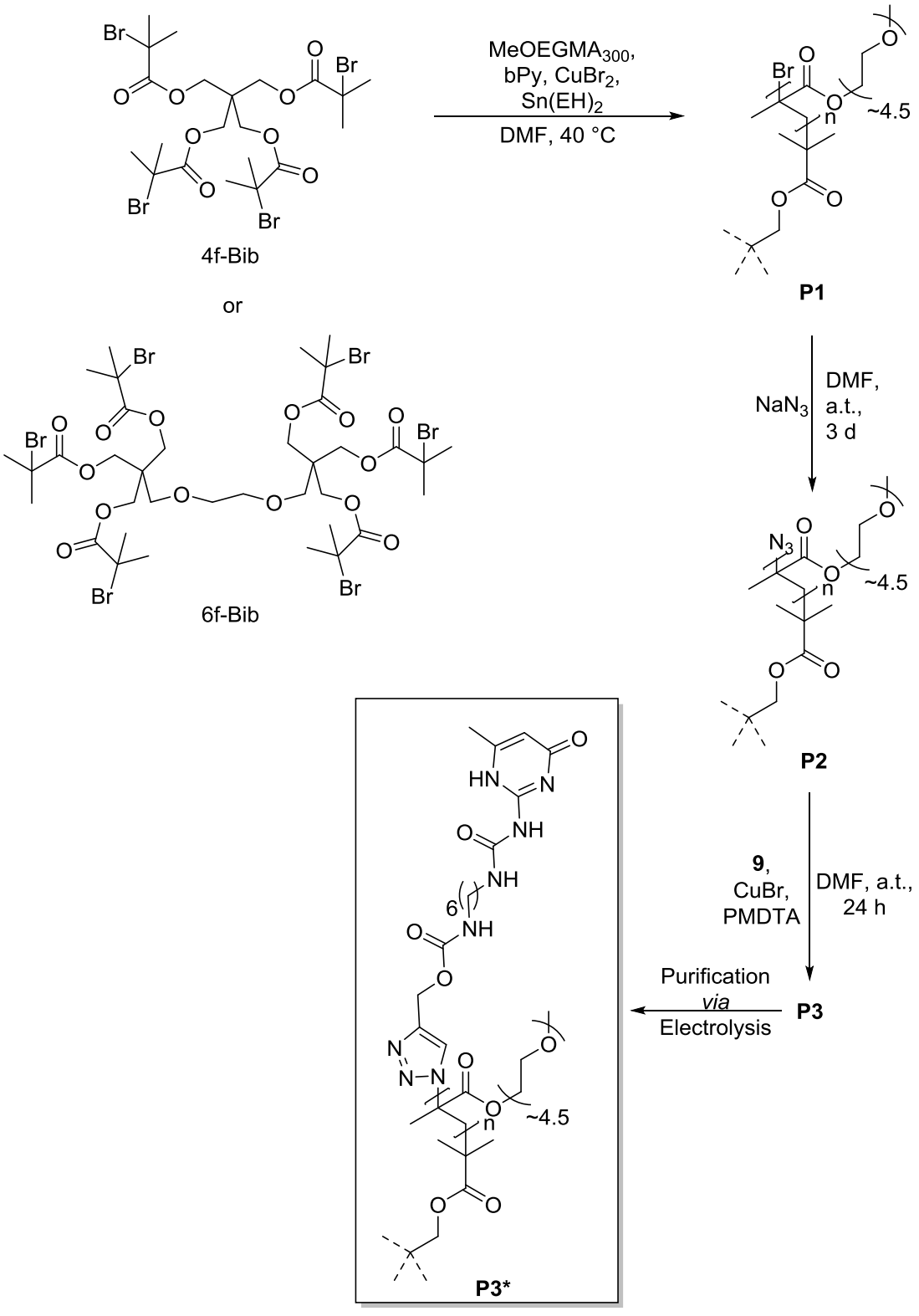

Scheme 13: Overview over synthetic steps employed in the star approach towards an UPy bearing, water-soluble polymer matrix based on the star polymer **P3***.

The star approach is based on three synthetic steps (excluding UPy synthesis) starting with the AGET ATRP polymerization of $MeOEGMA_{300}$ in the presence of the four and six armed initiators pentaerythritol tetrakis(2-bromoisobutyrate) (4f-Bib) and dipentaerythritol hexakis(2-bromoisobutyrate) (6f-Bib). In a subsequent second step, the ATRP star polymers **P1** underwent a post-polymerization functionalization with sodium azide (resulting in **P2**), which were employed in a third step in the CuAAc reaction with UPy-Urea-Alkyne (**9**) yielding the UPy terminated star polymers **P3**. As a result of the strong complex formation between the UPy moieties and the Cu ions, the final polymers remained contaminated with Cu (originating from the CuAAc reaction) after conventional polymer purification procedures. Therefore, the aqueous electrolysis of a polymer solution was established as new method of choice to remove the residual Cu ions nondestructively from an ion complexing polymer, thus resulting in the purified UPy terminated stars **P3***.[208]

In the first step, an AGET ATRP towards the synthesis of **P1**, four (4f-Bib) or six (6f-Bib) armed ATRP initiators were employed. The polymerizations were carried out with 2,2′-bipyridine (bPy) as ligand in dimethylformamide (DMF) as solvent at 40 °C. In order to suppress any radical coupling occurring during the polymerization, low conversions and, thus, short reaction times were targeted (max. 3 h). After the polymerization the final polymers (**P1**) were purified *via* dialysis in water and isolated as colorless, highly viscous liquids after subsequent lyophilization.

In total, a library of two short armed polymers (**$P1A_4$**, **$P1B_4$**), one polymer with medium arm size (**$P1C_4$**) and one with longer arms (**$P1D_4$**) was prepared utilizing 4f-Bib as initiator. Additionally, a six armed polymer with short arms was prepared (**$P1_6$**), employing 6f-Bib, and one short, four armed star polymer(**$P1_{el}$**) was prepared for the electrolysis experiments.

The resulting polymers were analyzed *via* SEC (Figure 19) and ^{1}H-NMR (Figure 20). The corresponding data indicates the presence of all expected magnetic resonances (^{1}H-NMR). Moreover, the SEC demonstrated the good control over radical polymerization of the conducted AGET ATRPs at low molecular weights.

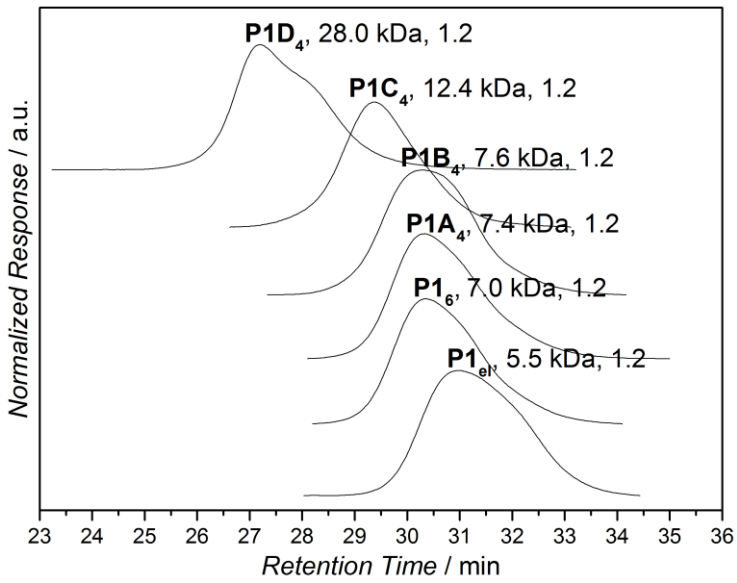

Figure 19: SEC elugrams of polymers **P1** with corresponding M_n and $Đ$ values based on a polystyrene calibration.

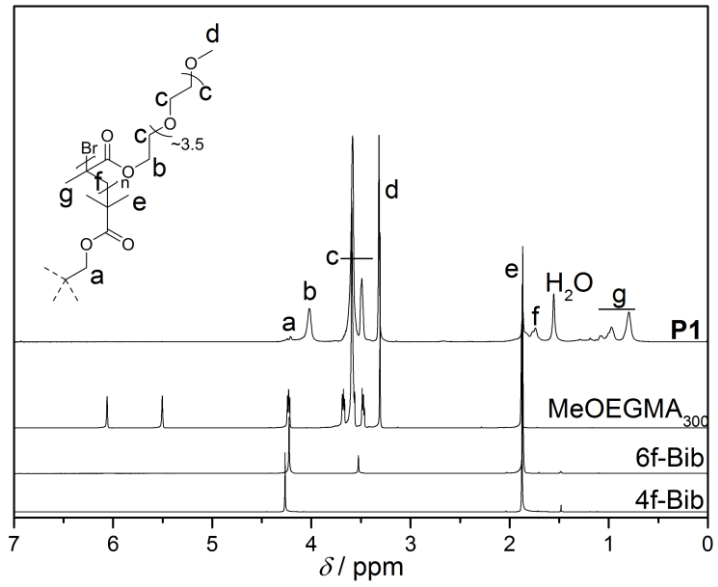

Figure 20: Representative ^{1}H-NMR spectrum of **P1** in $CDCl_3$ in direct comparison with its reactants.

In the second synthetic step the bromine endgroups of polymers **P1** were substituted with azides in a nucleophilic substitution, resulting in **P2**. Since endgroup conversion from Br to N_3 is extremely difficult to verify *via* ^{1}H-NMR, due integral overlap with backbone protons, and SEC, due to the insignificant shift in molecular weight, the

introduction of the azides was monitored *via* Infrared (IR) spectroscopy in direct comparison with the corresponding precursor **P1**. Nevertheless, none of these characterization techniques can verify complete endgroup conversion, since an appearance of a N_3-vibrations does not exclude presence of remaining bromines – therefore, harsh reaction conditions were adapted (> 70 eq. NaN_3, 3 d, low reaction volumes). Consequently, conversions had to be assumed to be complete. SEC, ^{1}H-NMR and IR analysis were performed with all prepared polymers **P2** and are discussed in the context of the third synthetic step towards **P3**.

In the last synthetic step, the azide endgroups of polymers **P2** were reacted in a CuAAc with UPy-Urea-Alkyne (**9**) resulting in UPy terminated, water-soluble star polymers **P3**. Therefore, precursors **P2**, **9**, *N*,*N*,*N*′,*N*″,*N*″-pentamethyldiethylenetriamine (PMDTA) and (equimolar amounts of) Cu(I)Br were reacted for 24 h under inert conditions at ambient temperature. The final polymers **P3** were purified *via* aqueous dialysis, isolated by freeze drying and analyzed with SEC, ^{1}H-NMR and IR. The SEC analysis (Figure 21) of the polymers **P3** in comparison with the corresponding precursors **P2** verifies that none of the two post-polymerization steps affected the shape of the molecular weight distributions of the initial polymers **P1**. Moreover, the SEC elution trace of **P3** is shifted to higher M_n values, as expected with regard to the introduction of the bulky UPy-Urea-Alkyne (**9**). ^{1}H-NMR analysis (Figure 22) reveals new resonances a, b, c, e and n for **P3** compared to the initial polymers **P1**, associated to the UPy motifs, verifying the successful introduction of UPys to the azide precursors **P2**. Furthermore, the new magnetic resonance signal d, arising from the newly formed triazole-linkage demonstrates the successful CuAAc reaction. The comparison of the IR spectra of **P1**, **P2**, **P3** and **9** (Figure 23) shows that a new vibration band (2120 cm^{-1}) arises upon introduction of N_3 as endgroups (**P2**), which disappear completely in the third synthetic step towards **P3**. Additionally, the alkyne vibration band of **9** (2120 cm^{-1}) disappears, indicating (in combination with the ^{1}H-NMR analysis) that **9** is covalently attached to the endgroups of **P3** *via* a triazole and, thus proving the success of the CuAAc.

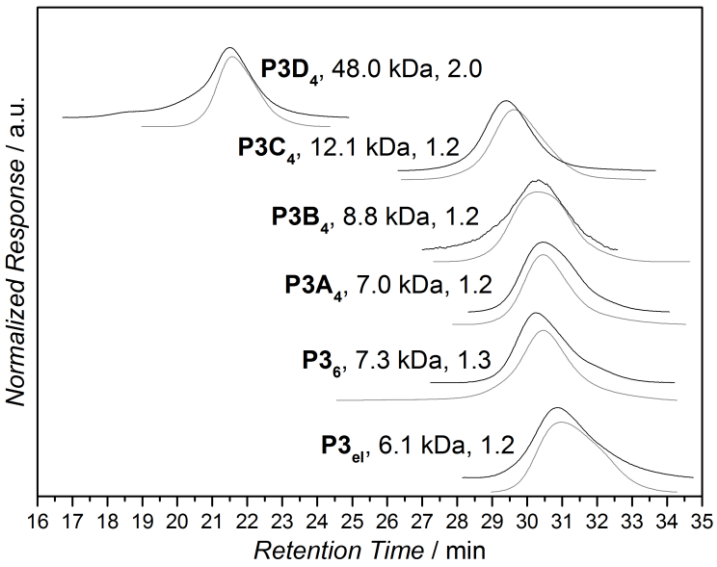

Figure 21: SEC elugrams of polymers **P3** (black) compared with their precursors **P2** (grey). M_n and $Đ$ values for **P3** are included and were obtained with a polystyrene calibration.

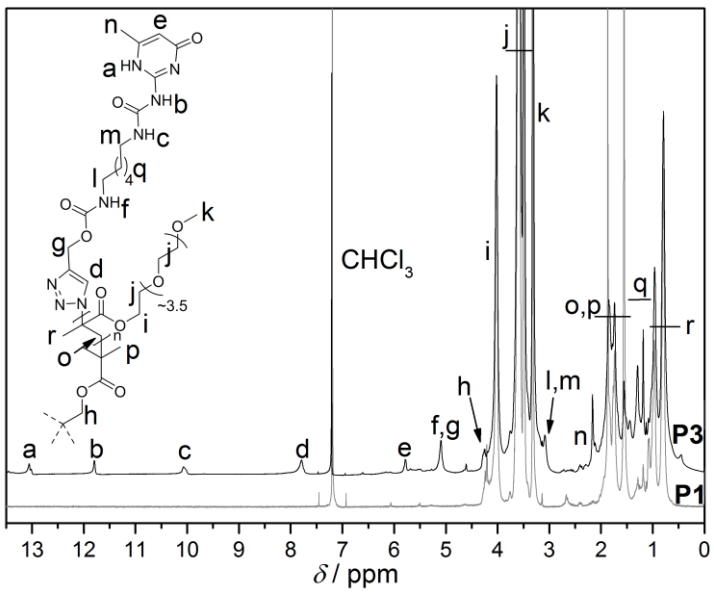

Figure 22: Representative and comparative ^{1}H-NMR spectrum of **P3** and **P1** in $CDCl_3$.

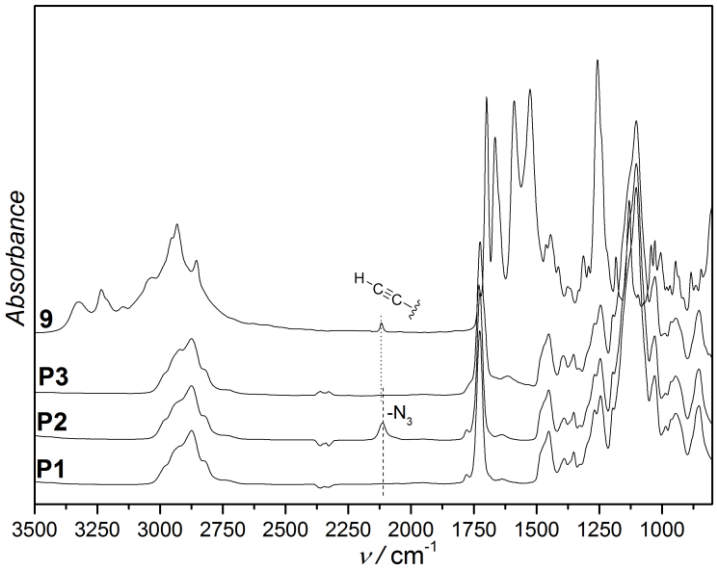

Figure 23: Representative IR spectra of polymers **P1**, **P2**, **P3**, and UPy-Urea-Alkyne (**9**). The azide vibration band of **P2** is located at 2120 cm^{-1}, the alkyne vibration band of **9** is located at 2120 cm^{-1}.

Quite unusually, in the last synthetic step equimolar amounts of Cu(I) relative to **9** had to be employed during CuAAc of **P2** towards **P3**, since the reaction did not proceed with catalytic amounts as initially expected. The requirement of such high amounts of catalyst indicates strong interactions (potentially based on the UPy moiety) shielding the catalytic ions from the CuAAc reaction partners. More remarkably, the polymer **P3** was obtained as a dark green liquid, which cannot be understood with regard to the involved functional groups (**P2**, **9** and triazoles are supposed to be colorless). The color could not be removed by conventional polymer purification protocols (*i.e.* dialysis, precipitation and filtration over aluminum oxide (AlOx)), alternative protocols could not be employed due to the water solubility of the polymer **P3** (*e.g.* extraction with ethylenediaminetetraacetic acid (EDTA)) solution). Therefore, electrolysis of a solution of $\mathbf{P3_{el}}$ was performed resulting in a deposition of red metal at the cathode and discoloration of the green polymer solution.

Various parameters *i.e.* electrolysis time (5.5-44 h), polymer concentration (9-18 $g \cdot L^{-1}$) and voltage (7.5-12 V) have been investigated systematically with regard to the remaining amount of Cu, monitored by Atomic Emission Spectrometry (AES) (Table 1). The representative study of electrolysis conditions was carried out with $\mathbf{P3_{el}}$.

Sample	*polymer concentration* ($g \cdot L^{-1}$)	*Voltage* (V)	*Time* (h)	residual Cu (wt%)	removed Cu (%)
$P3_{el}$	-	-	-	2.895	-
$P3_{el}$*A	9.0	9	5.5	1.726	40.4
$P3_{el}$*B	9.0	12	5.5	1.315	54.6
$P3_{el}$*C	9.0	12	24	0.096	96.7
$P3_{el}$*D	9.0	7.5	24	2.854	1.4
$P3_{el}$*E	4.8	12	24	0.042	98.6
$P3_{el}$*F	9.0	12	44	0.047	98.4
$P3_{el}$*G	18.1	12	24	0.060	97.9

Table 1: Summary of the results of the electrolysis of **$P3_{el}$**. wt% of Cu was determined *via* AES.

As a result of the electrolysis investigation, a voltage of 7.5 V was insufficient to remove significant amounts of Cu from the polymer (**$P3_{el}$*D**), and higher voltages up to 12 V generally accelerated electrolysis (**$P3_{el}$A** vs. **B**). Long electrolysis times (up to 44 h) resulted in the almost complete removal of Cu from the UPy functionalized polymer (**$P3_{el}$*F**) (Figure 24a), while concentration effects have not been observed in the investigated regime (Figure 24b).

The integrity of the electrolyzed polymers **P3*** was individually verified *via* SEC and ^{1}H-NMR and in the following the stability of **$P3_{el}$*G** is discussed. Comparative SEC measurements (Figure 25) reveal that the molecular weight distribution is stable under the employed electrolysis conditions and, moreover, ^{1}H-NMR analysis (Figure 26) proves that none of the present functional groups in the polymer are subject to degradation (*e.g.* oxidation). Therefore, electrolysis was employed for the purification of polymers **P3** to the water-soluble, UPy endgroup functionalized, star polymers **P3*** that were studied as polymer matrices in NC formation. Employing electrolysis as new tool for polymer purification was successfully published.[208]

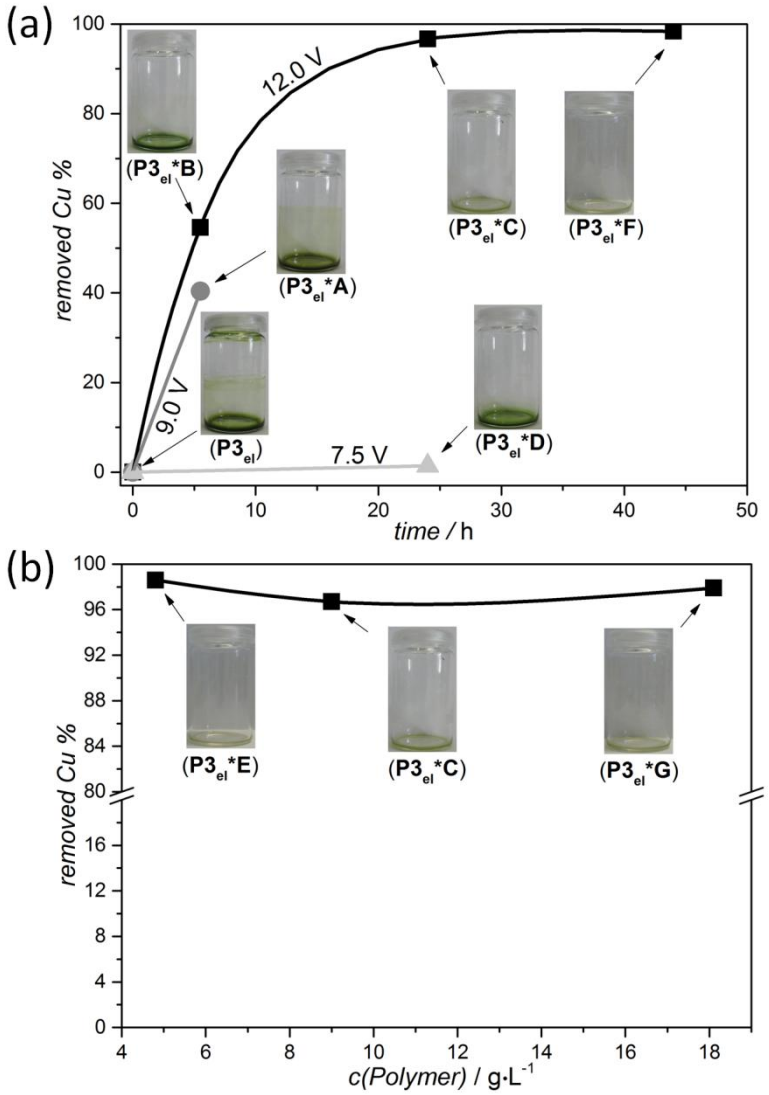

Figure 24: (a) Removed Cu % for different electrolysis times and voltages at a constant concentration of 9.0 g·L^{-1}. (b) Removed Cu % for different polymer concentrations at constant voltage (12 V) and electrolysis times (24 h).

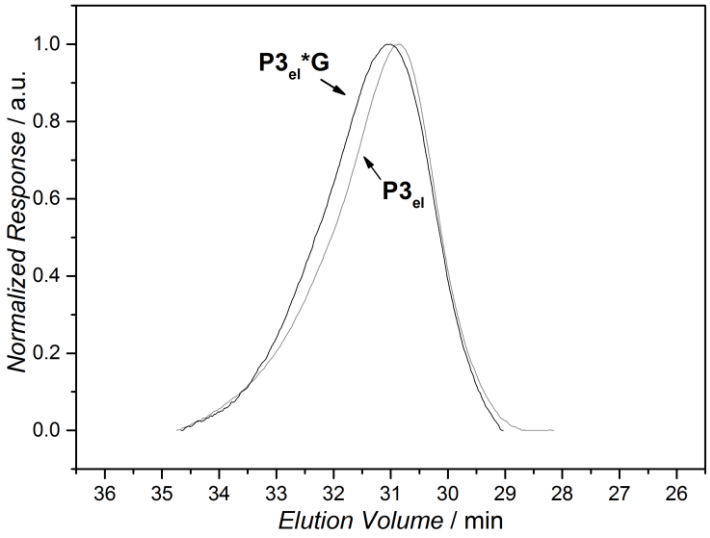

Figure 25: Representative SEC elugrams before (**$P3_{el}$**) and after (**$P3_{el}$*G**) electrolysis.

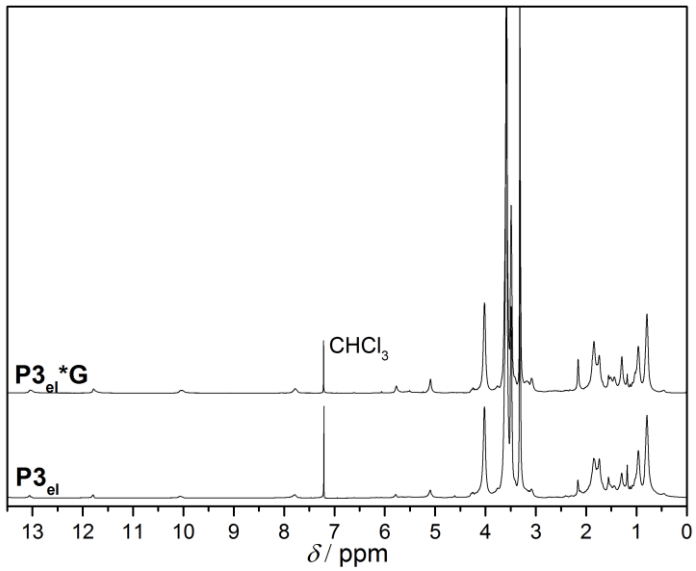

Figure 26: Representative ^{1}H-NMR spectrum before (**$P3_{el}$**) and after (**$P3_{el}$*G**) electrolysis.

3.1.1.4 RAFT Approach

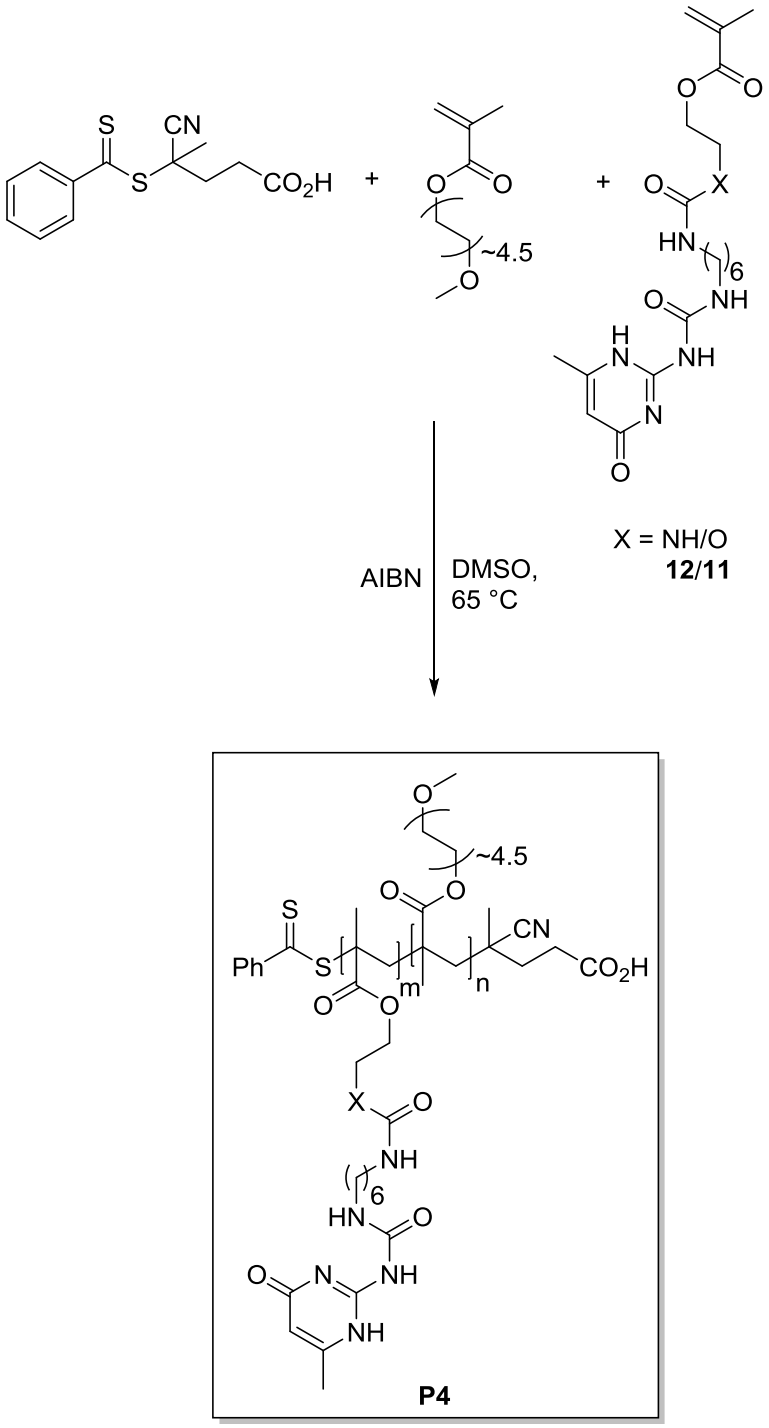

Scheme 14: Synthetic route towards MeOEGMA$_{300}$-**11**/**12** copolymers **P4** fabricated in the RAFT approach and employed as UPy matrices in NC formation.

Following the RAFT approach, MeOEGMA$_{300}$ and UPy-Urea-MA (**12**) or UPy-Urethane-MA (**11**) underwent copolymerization *via a* RAFT process controlled by 4-Cyano-4-(phenylcarbonothioylthio)pentanoic acid, yielding copolymers with varying

ratios of UPy units, varying chain lengths and different types of flanking units (Scheme 14). The comonomer **11**/**12**, $MeOEGMA_{300}$, 4-cyano-4-(phenylcarbonothioylthio)pentanoic acid and azobisisobutyronitrile (AIBN) were dissolved in DMSO, degassed and copolymerized at 65 °C, resulting in copolymers **P4** with varying flanking units (urethane, urea), comonomer ratios and molecular weights. All polymers were purified by aqueous dialysis and isolated employing a freeze dryer. Due to the strong dimerization of flanked UPys, the monomer solubility proved to be challenging and even DMSO (as very polar solvent) could only dissolve the monomers **11**/**12** to a limited extent at elevated temperatures (65 °C). In comparison, non-flanked UPy **10** is readily soluble under similar conditions. Due to the poor solubility, the polymerizations remained turbid and copolymerization was negatively affected – 7 mol% UPy comonomer in the polymerization mixture resulted in 5/3 mol% UPy in the copolymer. Higher concentrated initial comonomer mixtures (13%) were only dissolved incompletely, leading to low incorporation (10%) and a large amount of wasted UPy comonomers. The molecular weight distributions of the final polymers **P4** were obtained by SEC analysis and verify good control in the employed RAFT process (Figure 27), indicated by monomodal individual distributions with reasonable dispersities. Copolymer compositions were calculated by ^{1}H-NMR spectroscopy and indicated incorporation of UPys **11**/**12** in the $MeOEGMA_{300}$ polymer backbone (Figure 28). Due to the poor solubility of the copolymer, owing to the strong UPy dimerization, spectra were recorded in DMSO-d_6.

In summary, four copolymers were prepared: Two polymers with high amounts of UPy (10 mol%), high molecular weights (38.8 kDa, 34.2 kDa) and urea/urethane flanking groups were synthesized (**P4**$^{\mathbf{NH}}_{\mathbf{10}}$, **P4**$^{\mathbf{O}}_{\mathbf{10}}$). Additionally, two shorter chains (28.5 kDa, 23.8 kDa) with lower UPy ratios (3 mol%, 5 mol%) have been prepared with urea and urethane groups (**P4**$^{\mathbf{NH}}_{\mathbf{3}}$, **P4**$^{\mathbf{O}}_{\mathbf{5}}$). All fabricated polymers **P4** have been used in NC fabrication, revealing the influence of flanking groups and copolymer composition on the UPy based nacre mimetics.

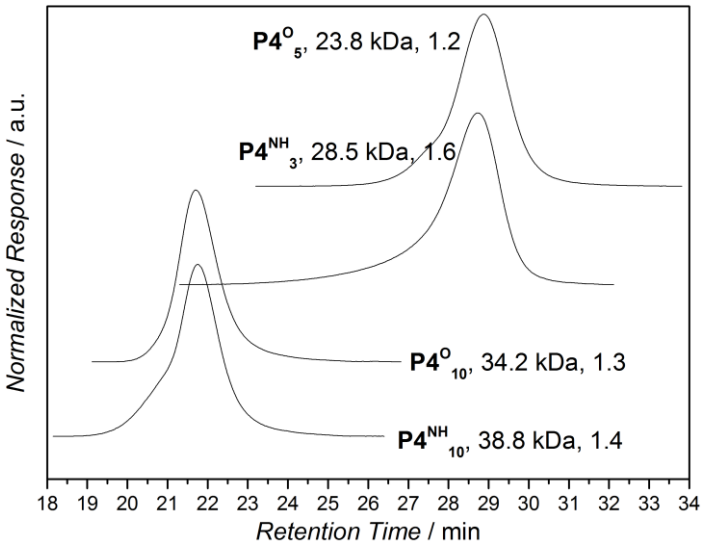

Figure 27: SEC elugrams of the polymers **P4** with calculated values for M_n and $Đ$ based on a polystyrene calibration.

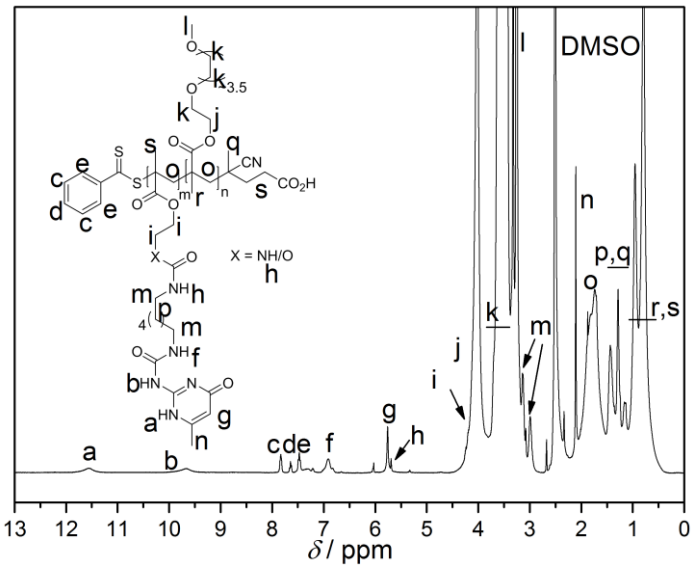

Figure 28: Representative ^{1}H-NMR spectrum of **P4** in DMSO-d_6. Copolymer compositions were calculated with the integral values of the magnetic resonance resonances g and r.

3.1.1.5 Conventional FRP Approach

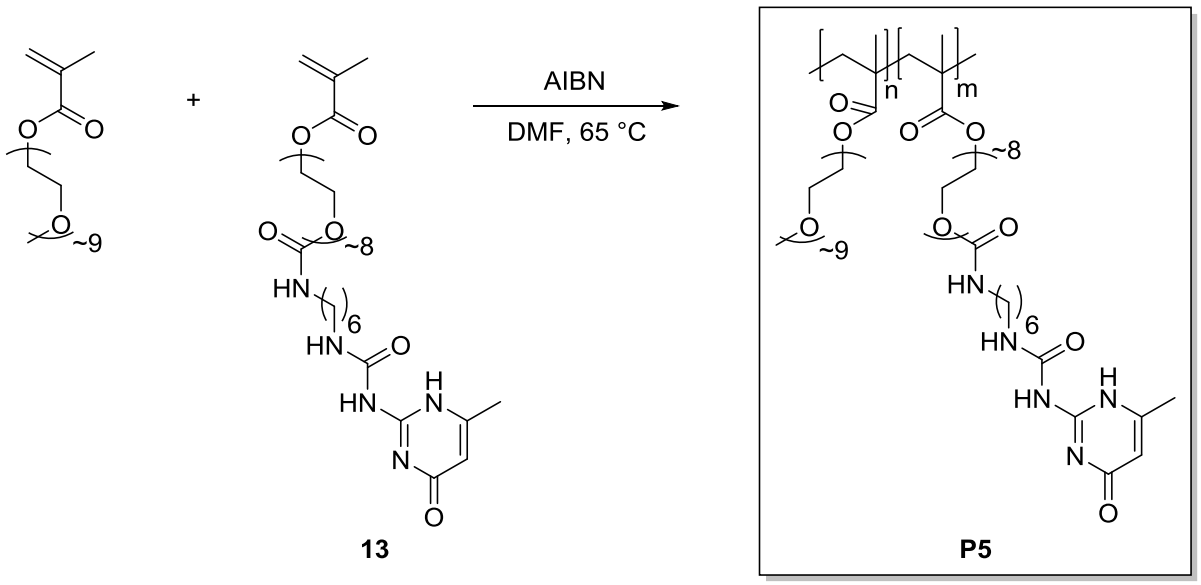

Scheme 15: Synthetic route towards MeOEGMA$_{500}$-**13** copolymers **P5** in the conventional FRP approach, employed in fabrication of nacre mimetics

In order to overcome the disadvantages of the RAFT approach (low M_n, low degree of functionalization with UPy), in the conventional FRP approach the PEGylated UPy comonomer **13**, which exhibits improved solubility compared with **11** and **12** was employed in a FRP with MeOEGMA$_{500}$ (Scheme 15). The comonomers and AIBN were dispersed in DMF, degassed, copolymerized at 65 °C, dialyzed against water and isolated by freeze drying. Due to better solubility of **13** (compared with **11** and **12**), higher UPy ratios (up to 20 mol%) in the final polymer could be achieved and, owing to FRP, high molecular weights (M_n = 414.0 kDa) have been obtained. However, these advantages were achieved on the expense of dispersity. Although broad, the obtained molecular weight distributions were still monomodal (Figure 29) and ^{1}H-NMR analysis verifies the successful copolymerization of MeOEGMA$_{500}$ and **13** (Figure 30). Four (co)polymers have been synthesized *via* the conventional FRP approach: A long reference polymer without UPys (**P5$_0$**, M_n = 365.0 kDa), two large copolymers with high UPy ratios (**P5$_{14}$**, M_n = 339.0 kDa; **P5$_{20}$**, M_n = 414.0 kDa) and a short copolymer (**P5$_{10}$**, M_n = 161.0 kDa), which have been employed in nacre mimetic fabrication.

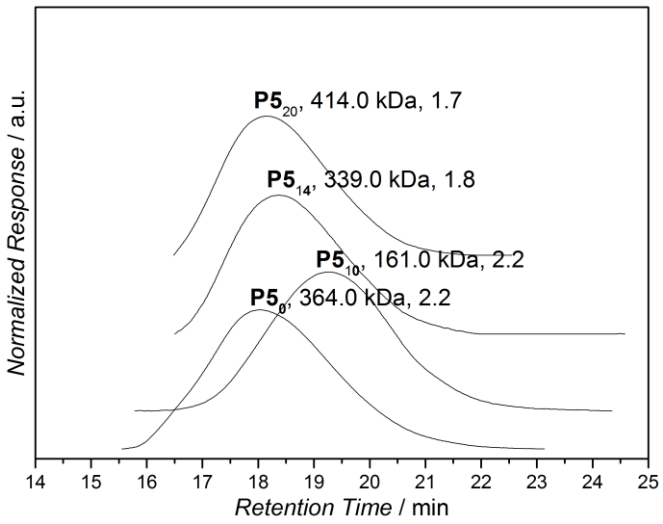

Figure 29: SEC elugrams of the polymers **P5** with calculated values for M_n and $Đ$.

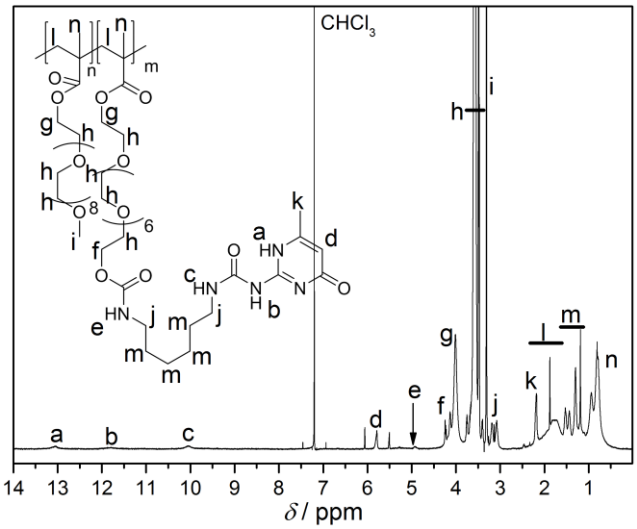

Figure 30: Representative ^{1}H-NMR spectrum of the copolymer **P5** of MeOEGMA$_{500}$ and UPy-OEG-MA (**13**) in $CDCl_3$. Copolymer compositions (mol% UPy) were calculated employing integral values of the magnetic resonance signals d and i.

3.1.1.6 Performance in Nano-Composites

Three routes towards UPy functionalized matrices have been investigated, employing different architectures and a multitude of matrix polymers for each approach (Table 2). Films were cast by combination of a dispersion of sodium fluorohectorite (NHT) nano-clay (1 nm thick sheets, aspect ratio of 750, chemical formula: $Na_{0.46}(Mg_{2.6}Li_{0.46})Si_4O_{10}F_2$) in water and an aqueous polymer solution, adjusting the desired weight ratio of the composite components. The polymer-NHT dispersions were stirred overnight, concentrated *in vacuo* and films were cast in a petri dish resulting in the final nano-composites (NC). These NCs mimic the microscopic structuring of nacre with the overall goal to result in a comparable stress-strain behavior. Therefore, a steep slope in the linear elastic region of deformation and a subsequent plateau of inelastic deformation at higher stresses are targeted for the NCs to maximize absorbed mechanic energy.

Approach	Polymer	UPy	SEC data: M_n (kDa), $Đ$	^{1}H-NMR data: mol% UPy	Comment	Film NHT:Polymer = 50:50	
						Tensile Strength (MPa)	Strain
Star	**P3A$_4$**	**9**	7.0, 1.2			65	0.28
Star	**P3B$_4$**	‖	8.8, 1.2			85	0.62
Star	**P3C$_4$**	‖	12.1, 1.2			60	0.76
Star	**P3D$_4$**	‖	48.0, 2.0			72	1.05
Star	**P3$_6$**	‖	7.3, 1.2		6 arms	84	0.64
RAFT	**P4$^{O}_{10}$**	**11**	34.2, 1.3	10	Urethane	148	0.69
RAFT	**P4$^{O}_{5}$**	‖	23.8, 1.2	5	‖	51	1.71
RAFT	**P4$^{NH}_{10}$**	**12**	38.8, 1.4	10	Urea	118	0.73
RAFT	**P4$^{NH}_{3}$**	‖	28.5, 1.6	3	‖	92	1.78
FRP	**P5$_0$**	**13**	364.0, 2.2	0		14	1.78
FRP	**P5$_{10}$**	‖	161.0, 2.2	10		5.3 (plateau)	
FRP	**P5$_{14}$**	‖	339.0, 1.8	14		14 (plateau)	
FRP	**P5$_{20}$**	‖	414.0, 1.7	20		21	0.62

Table 2: Employed polymers in NC formation with their tensile strength and corresponding strain of 50 wt% NCs.

The stress-strain curves for 50 wt% composites of four armed **P3** clearly demonstrate that longer arms result in softer and more ductile materials (Figure 31), in total agreement with tensile tests performed on UPy functionalized polymers in the literature. According to the results of tensile tests of **P3$_6$**, **P3A$_4$** and **P3B$_4$** (Figure 32) the influence of the number of arms (four or six) is almost insignificant, as neither tensile stress, nor strain increases significantly with more arms in the investigated regime. The increase of the weight percentage (wt%) of NHT results in stronger materials, while a decrease results in softer films, demonstrated for long (**P3D$_4$**) and short (**P3A$_4$**) arms and in complete agreement to general trends in literature (Figure 33).

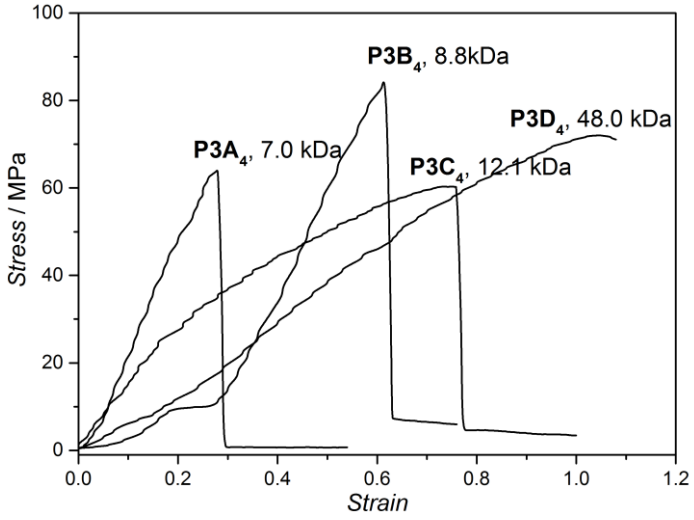

Figure 31: Stress-strain curves of NCs (50 wt% NHT) employing the four armed UPy star polymers demonstrating the influence of the arm length on the mechanic performance. M_n values of the employed polymers based on SEC measurements are provided.

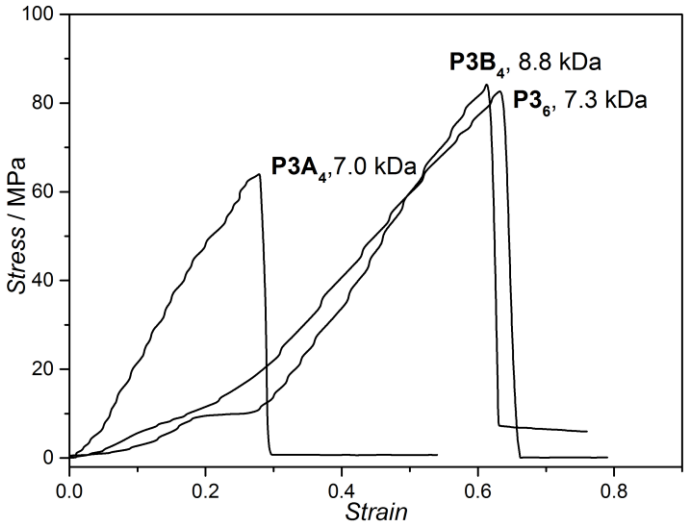

Figure 32: Stress-strain curves of NCs (50 wt% NHT) of short four and six armed UPy star polymers, demonstrating the influence of the number of arms on the mechanic performance. M_n values of the employed polymers based on SEC measurements are provided.

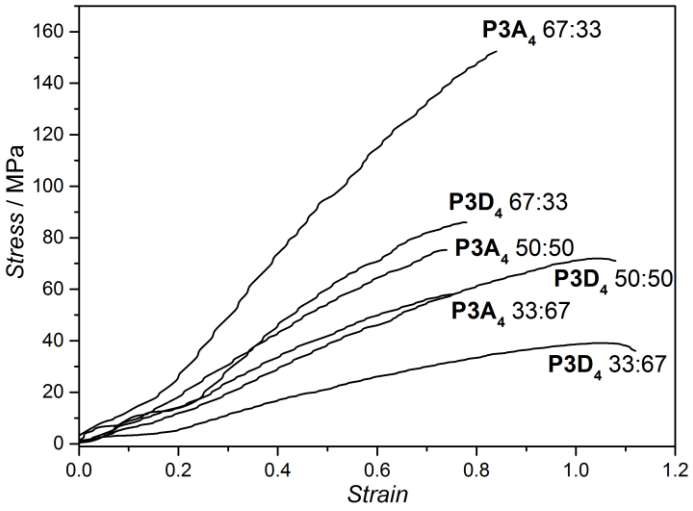

Figure 33: Stress-strain curves of NCs with varying compositions (wt% NHT:polymer) employing a short and a long UPy star polymer, demonstrating the influence of composition on the mechanic performance.

Tensile tests of NCs employing the copolymers **P4** further underpin the general trend that higher amounts of UPy (corresponding to shorter arms in the star approach) result in stiffer and stronger materials, while low UPy ratios led to softer materials

with increased ductility (Figure 34). The influence of flanking units on the mechanic performance, however, is not clear from the measurements.

The results obtained by 50 wt% NCs with **P5** show similar trends of increased stiffness but decreased ductility for higher UPy ratios (Figure 35). More interestingly however, $\mathbf{P5_{10}}$ and $\mathbf{P5_{14}}$ (which differ in molecular weight and UPy ratio) show plateaus of inelastic deformation, similarly to nacre but at lower stresses. An increase of molecular weight and UPy content increases the height of the plateau. When, however, the UPy ratio increases further ($\mathbf{P5_{20}}$) the film becomes stiffer but the plateau is lost.

The comparison of molecular weights with similar ratios of UPy ($\mathbf{P5_{10}}$, $\mathbf{P4^{NH}_{10}}$, $\mathbf{P4^{O}_{10}}$) but strongly differing molecular weights reveals that shorter chains result in a significant increase in strength in expense of the material´s ductility (Figure 36).

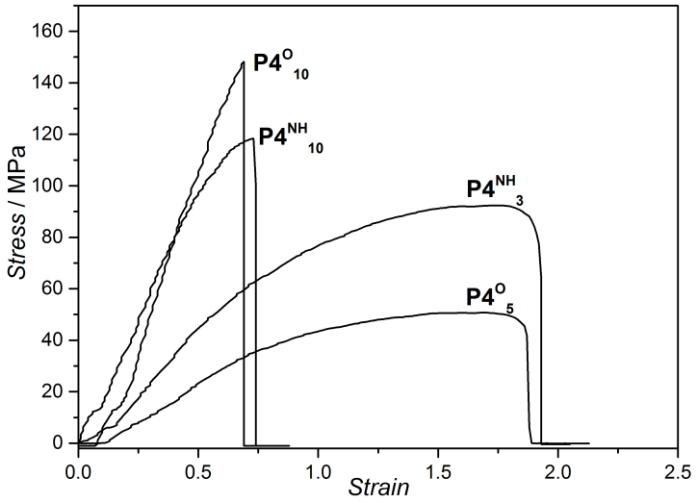

Figure 34: Stress-strain curves of NCs (50 wt% NHT) with polymers **P4** exhibiting high and low degrees of UPy functionalization (indicated by the subscripts) and varying flanking groups (indicated by the superscripts).

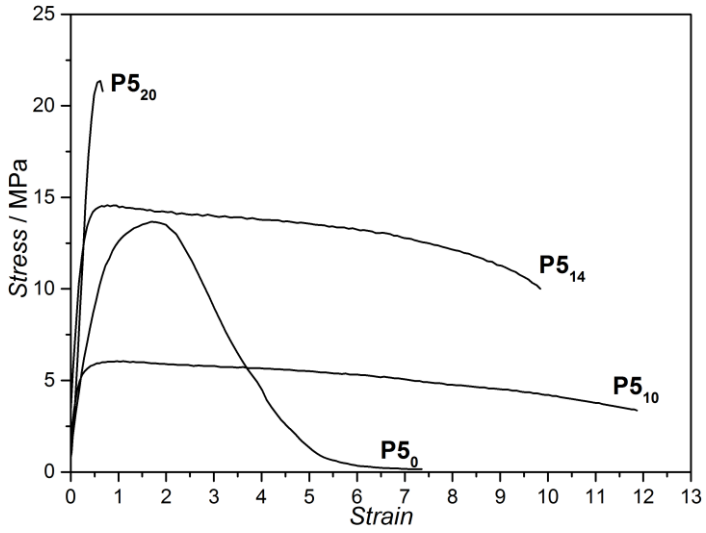

Figure 35: Stress-Strain curves for of NCs (50 wt% NHT) with polymers **P5** with varying comonomer ratios, indicated by the subscripts

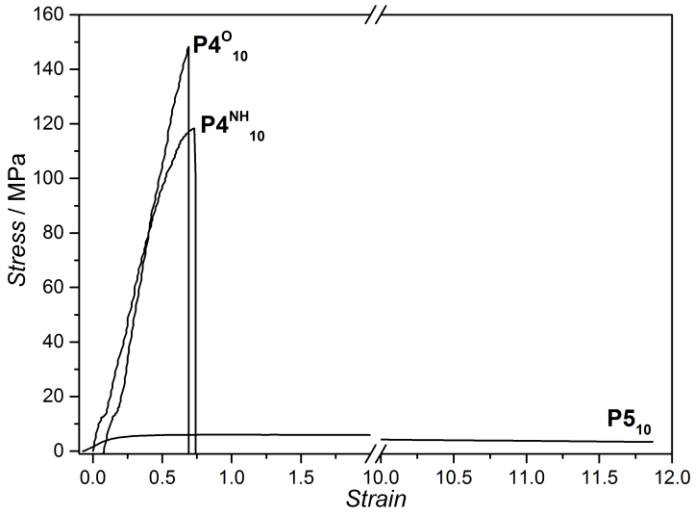

Figure 36: Stress-strain curves for of NCs (50 wt% NHT) with polymers **P5$_{10}$**, **P4$^{O}_{10}$** and **P4$^{NH}_{10}$**.

Summarizing the results of the tensile tests of NCs with UPy matrices fabricated by the three different synthetic approaches (*i.e.* star, RAFT, conventional FRP), less functionalization with UPy results in softer and more ductile materials in complete agreement with literature. Likewise, in agreement with literature results, higher filler loadings increase material´s strength and decreases ductility. The influence of flanking groups shows no clear trend and seems negligible compared with other effects, according to the conducted experiments. At constant UPy ratios higher molecular weights increase NC ductility at the expense of strength. Very interestingly,

under conditions with beneficial interplay of chain length, and UPy ratio plateaus of inelastic deformation in the stress-strain curve can be observed. These stress-strain curves resemble qualitatively the behavior of nacre and were initially desired for the NCs. However, these plateaus have been observed at lower stresses compared with nacre and, therefore, absorbed mechanic energy is smaller. In principle, increased chain length introduces entanglement, which is beneficial for mechanic performance, yet on the downside widens the NHT galleries in the composite, potentially resulting in softer materials. UPy is responsible for cross-linking, increasing material´s strength, but also disadvantageously decreasing chain dynamics. Presumably, there are optima for both critical matrix parameters (UPy ratio, chain length), which have to be balanced in order to obtain maximal slip-stick interactions of UPys, chain unfolding and nano sheet relocking during film deformation, potentially resulting in high performance NCs.

3.1.2 *Hetero-Diels-Alder (HDA-)Matrices*

3.1.2.1 HDA vs. UPy Matrices

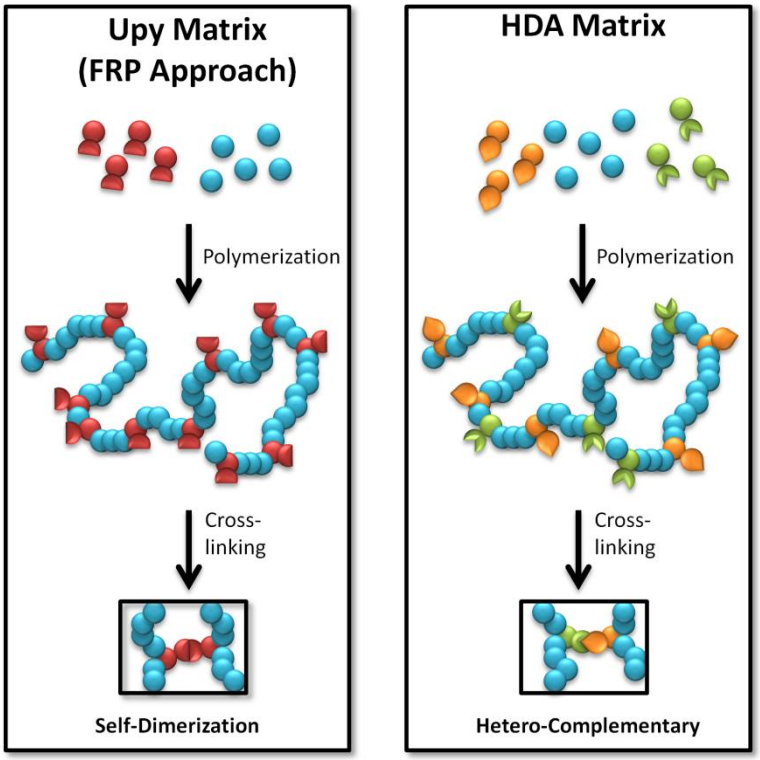

Figure 37: HDA and UPy matrices are directly compared with regard to cross-linking and synthesis.

Although sharing the function as thermoreversibly cross-linked polymer matrix, the concepts of HDA and UPy matrices differ significantly in synthetic effort (in comparable approaches), kinetic and thermodynamic stability, due to the complementarity and chemical nature of the cross-linking (Figure 37).

Cross-linking in UPy matrices is based on the self-complementary dimerization of UPys *via* hydrogen bonds. While hydrogen bonding is in general a rather weak and dynamic (since supramolecular) interaction, UPy´s self-dimerization results in little synthetic effort to introduce cross-linking, because only one type of function has to be included in the polymer.

In HDA matrices, cross-linking proceeds covalently *via* two complementary motifs (diene and dienophile). As a consequence, the synthetic effort to generate such matrices is approximately doubled compared to self-complimentary cross-linking,

since two functionalities have to be introduced into the polymer (instead of just one). Moreover, due to the hetero-complementarity of HDA cross-linking, a functional moiety cannot simply react with all available other surrounding cross-linking motives (as it is the case for self-complementary UPy), but exclusively with corresponding complimentary moieties, which reduce the number of potential binding partners at comparable degrees of functionalization by half. On the other hand, covalent interactions are in general kinetically and thermodynamically much more stable (than supramolecular interactions). Therefore, dissociation temperatures are potentially higher and cross-linking is solvent-independent and less dynamic – resulting a polymer matrix showing conceivably less creep behavior.

3.1.2.2 HDA Monomer Synthesis

The HDA matrix, synthesized and studied in the present thesis, is based on the CDTE-sorbic alcohol HDA couple, which was introduced to the water-soluble polymer chain. The polymer was fabricated *via* non-controlled FRP, employing comonomers with suitable HDA moieties. Consequently, a (Cp-protected) CDTE containing monomer **15** and a monomer containing sorbic alcohol **16** had to be synthesized (Scheme 16).

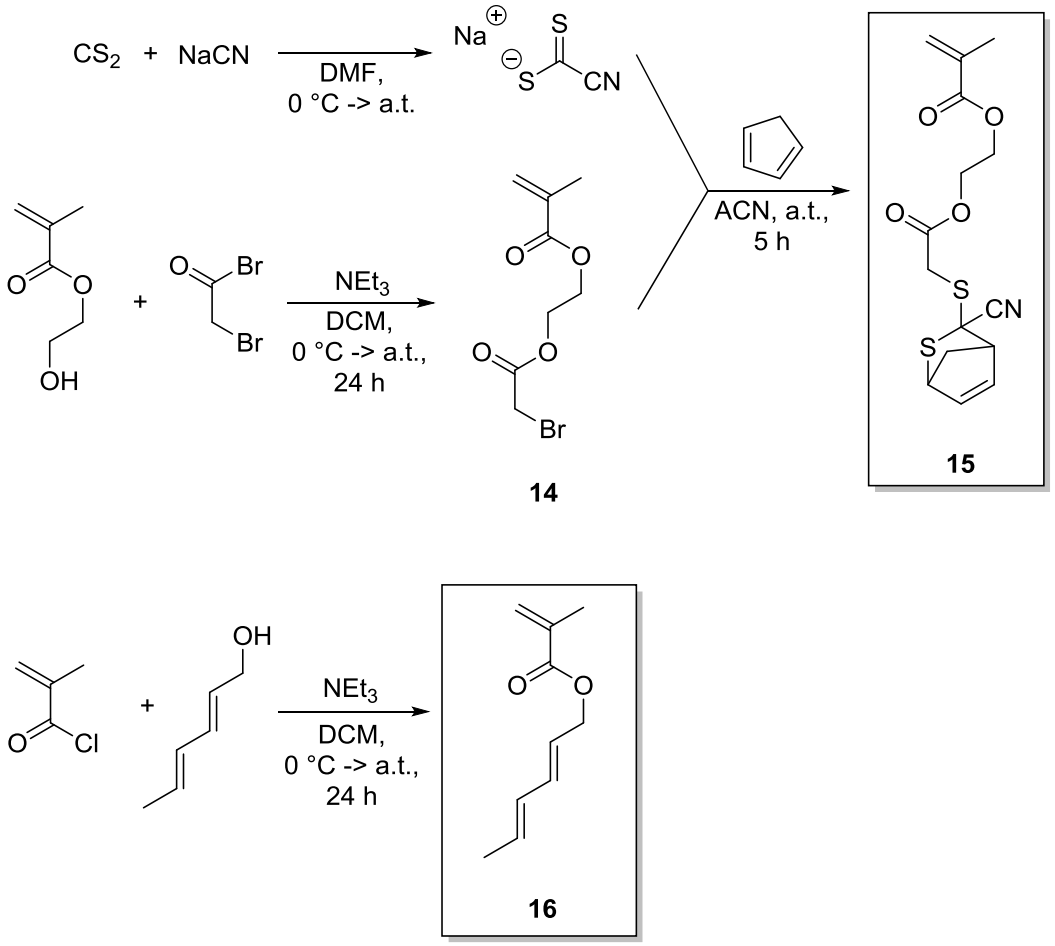

Scheme 16 Synthesis route towards CDTE-MA (**15**) and Sorb-MA (**16**) employed in HDA matrix synthesis.

The three step synthesis of the new CDTE-MA (**15**) starts with the straightforward esterification of HEMA with bromoacetyl bromide in DCM in the presence of an amino base (TEA). The reaction was conducted starting with the slow, dropwise combination of the reaction partners at 0 °C and stirring overnight reaching ambient temperature. Finally, the obtained α-bromo functionalized HEMA ester **14** can be further employed in synthesis after purification *via* aqueous extractions; column chromatography is not necessarily needed (yield: 44%).

Sodium carbonocyanidodithioate that was employed as nucleophile in the third step, was synthesized according to a modified literature protocol.[28] Carbon disulfide in DMF was carefully added to a cooled suspension of sodium cyanide, the mixture was allowed to reach ambient temperature and stirred until complete solidification, due to precipitation of the product of the nucleophilic addition of NaCN to CS_2 (which results in an insoluble salt). To remove residual sodium cyanide, the product was dissolved

in hot isopropyl alcohol and the residual solids were filtered off from the heated solution. Sodium carbonocyanidodithioate was subsequently obtained by precipitation from the cooled solution, filtration and washing with Et_2O. The product was obtained as a brown powder (yield: 58%).

In the third synthetic step towards the new molecule CDTE-MA (**15**) the α-bromine of **14** underwent a nucleophilic substitution with carbonocyanidodithioate, which is known to react only with highly activated substrates (*e.g.* C-, Z-substituted electrophiles) and, therefore, initially demanded **14** as intermediate in the employed synthetic strategy. The product of nucleophilic addition (a cyanodithioester), however, decomposes/dimerizes in the presence of nucleophiles (*i.e.* the bromide resulting from the nucleophilic substitution) and, consequently, had to be protected *e.g.* in a Diels-Alder reaction with Cp resulting in CDTE-MA (**15**). Exploiting the reversible nature of DA reactions, the protective Cp can be substituted by dienes that form more stable DA adducts with CDTE in a subsequent step, if desired. Synthesizing CDTA-MA (**15**) bromide **14**, Cp and sodium carbonocyanidodithioate were stirred in acetonitrile (ACN) at ambient temperature for 5 h, allowing the nucleophilic substitution of bromine with carbonocyanidodithioate and subsequent DA reaction of the intermediate with Cp. After column chromatography the product was obtained as colorless liquid (total yield: 19%).

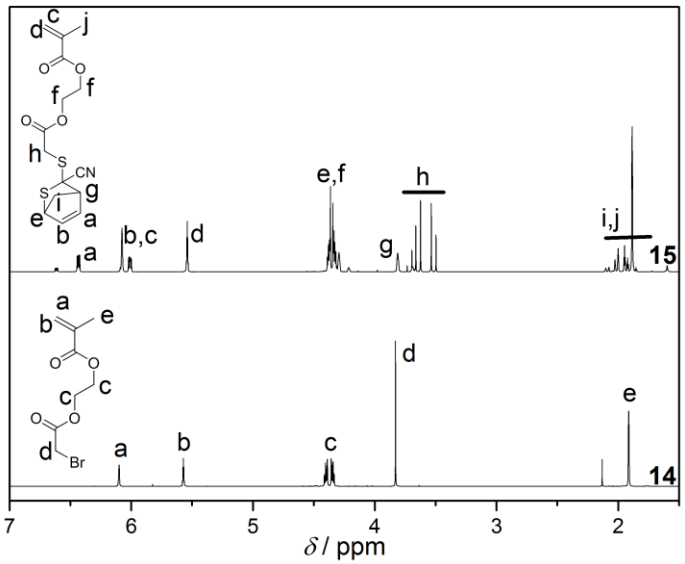

Figure 38: Comparative ^{1}H-NMR spectra of Br-MA (**14**) and CDTE-MA (**15**) in $CDCl_3$.

^{1}H-NMR analysis of the reaction sequence of **14** to **15** demonstrates the shift of the initial α-protons (resonance d; **14**) of Br-MA to lower ppm in the final CDTE-MA (resonance h; **15**) and additionally the appearance of new resonances (a. b. g. e and i, **15**) corresponding to the protective Cp (Figure 38), thereby verifying the successful conversion.

Synthesizing the sorbic alcohol functionalized methacrylate **16**, a solution of sorbic alcohol was carefully combined with methacryloyl chloride and NEt_3 in DCM at 0 °C and allowed to reach ambient temperature overnight. The product of esterification Sorb-MA (**16**) was purified *via* column chromatography and received as yellow oil (yield: 45%).

3.1.2.3 HDA Matrix

Fabricating a thermoreversibly cross-linked, water-soluble polymer matrix, based on DA chemistry instead of multiple hydrogen bonding (*i.e.* UPy), the two HDA monomers CDTE-MA (**15**) and Sorb-MA (**16**) have been copolymerized with $MeOEGMA_{500}$ *via* FRP, resulting in **P6** (Scheme 17). Both monomers have been prepared beforehand (Section 3.1.2.2).

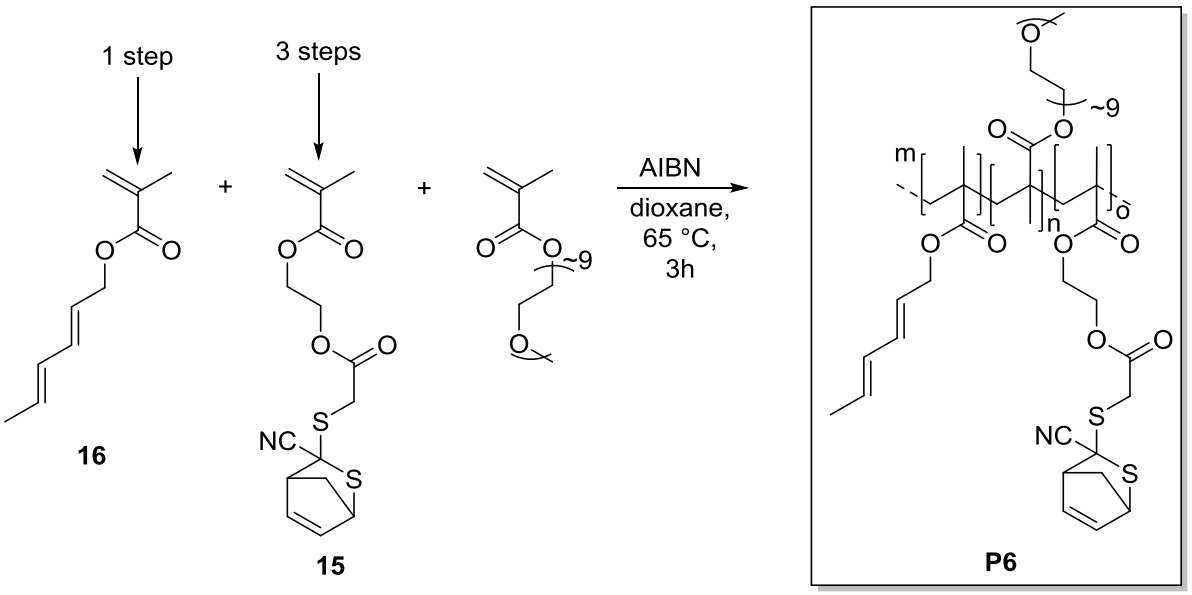

Scheme 17: Synthetic route to **P6**

For the synthesis of **P6**, the three monomers **15**, **16** and $MeOEGMA_{500}$ and the radical initiator AIBN were dissolved in dioxane, degassed and heated to 65 °C for 3 h. The resulting polymer **P6** was purified *via* aqueous dialysis and isolated employing a freeze dryer, yielding a yellow viscous liquid. The successful polymerization was monitored *via* SEC and ^{1}H-NMR spectroscopy.

^{1}H-NMR analysis of **P6** reveals the smooth copolymerization of both HDA monomers **15** and **16** with $MeOEGMA_{500}$ (Figure 39). The composition of the copolymer **P6** (6 mol% **15**, 4 mol% **16**) was almost identical with the comonomer ratios in the initial copolymerization mixture (5 mol% **15**, 5 mol% **16**). For composition calculations, ^{1}H-NMR resonances a, b and k have been employed. The corresponding SEC elugram reveals a monomodal molecular weight distribution of long polymer chains (Figure 40). Demonstrating the reactivity of the HDA system, the polymer **P6** (M_n = 127.2 kDa, $Đ$ = 2.3, 6 mol% **15**, 4 mol% **16**) was accidentally cross-linked

during storage at ambient temperature for few days, however, aqueous and cooled solutions were stable for several weeks.

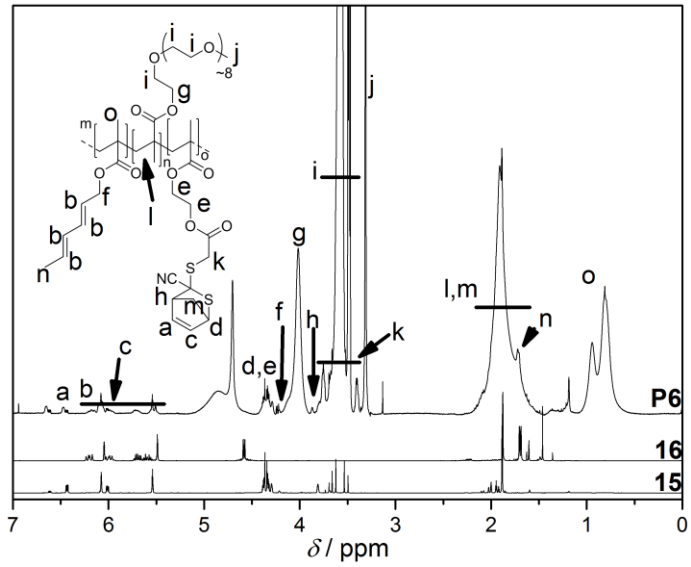

Figure 39: ^{1}H-NMR spectra of HDA matrix **P6** and the HDA monomers **15** and **16** in $CDCl_3$.

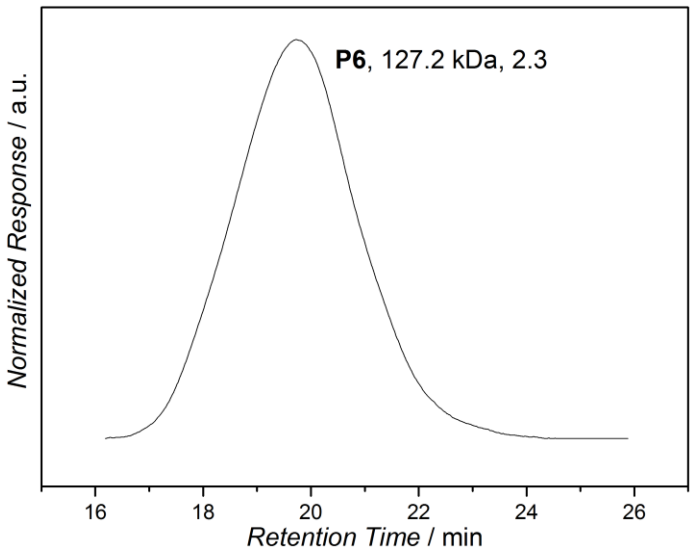

Figure 40: SEC elugram of **P6** with calculated values for M_n and $Đ$ based on a polystyrene calibration.

3.1.2.4 Performance in Nano-Composites

In analogy to NCs employing UPy matrices, films were cast by combination of a dispersion of sodium fluorohectorite (NHT) nano-clay in water and an aqueous polymer solution, adjusting the desired ratio of composite components (50 wt%). The polymer-NHT dispersions were stirred overnight, concentrated *in vacuo* and films were cast in a petri dish. Additionally, in order to increase cross-linking, thermal activation was provided *via* heating to 100 °C in an oven and in a heated press, potentially resulting in cross-linking of sorbic alcohol moieties and CDTE. The three films (cast, oven, press) were eventually compared mechanically.

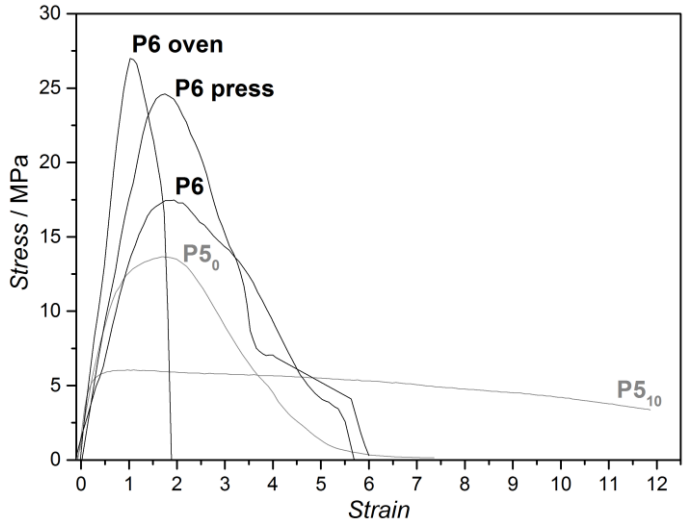

Figure 41: Stress-strain curves of NCs (50 wt% NHT) employing the HDA matrix **P6** after casting, heating in an oven to 100 °C and heating to 100 °C in a press in direct comparison with the analogue UPy matrix **P5$_{10}$** and non-functionalized matrix **P5$_0$**.

Unfortunately, the mechanic performance of cast NC films was low (as indicated by the low maximal stress and the lack of a plateau of inelastic deformation) and could not be further increased by a heating step after casting. The lack of increased performance after heating indicates that the cross-linking has either no significant influence on the performance (which is very unlikely), or cross-linking density is low, due to little comonomer-functionalization of the matrix **P6**. Compared to the UPy matrix **P5$_{10}$**, the HDA matrix results in stronger films at the expense of ductility, potentially due to the lack of slip-stick interactions but stronger cross-linking (covalent vs. supramolecular) on a molecular scale. However, globally, the mechanic performance resembles the completely unfunctionalized matrix **P5$_0$**, indicating that

cross-linking is insufficient, potentially due to the hetero-complementary cross-linking situation, which reduces the amount of available binding partners per HDA moiety compared to the analogue UPy polymer.

3.2 Hydrogen Bonding at Interfaces

ToF-SIMS measurements were performed by Dr. Alexander Welle (KIT). Kilian Wüst (macroarc group, KIT) kindly provided **25**, SOA-PMMA and AOA-NHBoc were provided by Dr. Julien Bernard (INSA-Lyon) and coworkers.

Due to the large surface-to-volume ratio in NCs, processes at interfaces between the polymer matrix and the filler are essential for the performance of the final material, as discussed in the context of strain hardening of nacre. In contrast to the example by Nature, the NCs consisting of NHT nano sheets and UPy-functionalized polymers fabricated in this thesis, cannot achieve strain hardening by mechanisms based on mineral bridges between platelets. Instead they must rely on polymer chain unfolding, friction based on platelet waviness and, more important in the context of this chapter, slip-stick interactions based on dynamic UPy dimers (between physisorbed UPys on the clay surface and UPys in the polymer matrix).

In order to gain a deeper understanding of the UPy dimerization and hydrogen bonding at interfaces in general, the second task of the present thesis was to investigate the dimerization behavior of hydrogen bonding motifs on macroscopic surfaces, as a model system for the polymer-filler interfaces.

In the mentioned macroscopic model system, three distinct scenarios are feasible for self-complimentary motifs (UPy): (i) no hydrogen bonding, due to low concentrations, (ii) hydrogen bonding within each phase but without interfacial bonding and (iii) hydrogen bonding at the interface (Figure 42). For hetero-complimentary motifs (SOA/AOA) only non-bonding and interfacial bonding are possible. Very critically, the non-binding state is highly unlikely in NCs, since concentrations in bulk are high.

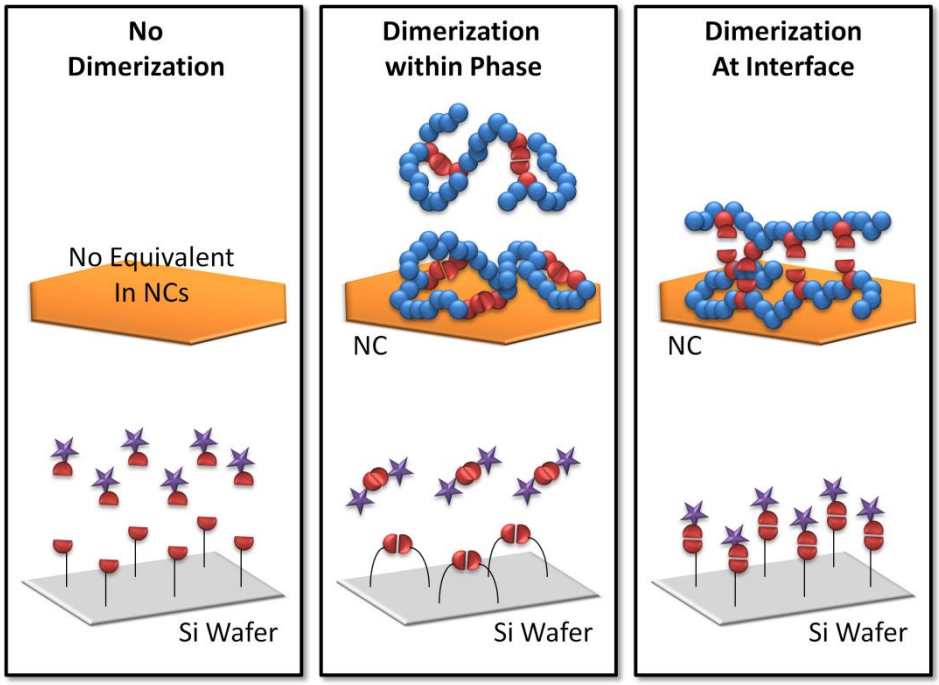

Figure 42: Schematic representation of possible scenarios in self-complementary hydrogen bonding at interfaces in nano-composites (NCs) and the macroscopic model system, in which binding partners from the solution carry a chemical marker.

From an analytical point of view, detection of the chemical marker (purple) of binding partners from solution on the surface indicates that interfacial hydrogen bonding is dominant (Figure 43). However, missing marker signals on the surface can result from either the non-binding scenario, or binding within each phase. Since for hetero-complementary motifs (*i.e.* SOA/AOA) the second scenario is inaccessible, the combination of the analytic results for both model systems (UPy, SOA/AOA) aids to identify the dominant hydrogen bonding state on surfaces and, therefore, at interfaces in NCs. Consequently, both self-complimentary UPy-dimerization and the hetero-complementary SOA-AOA couple, were studied on macroscopic silicon wafers.

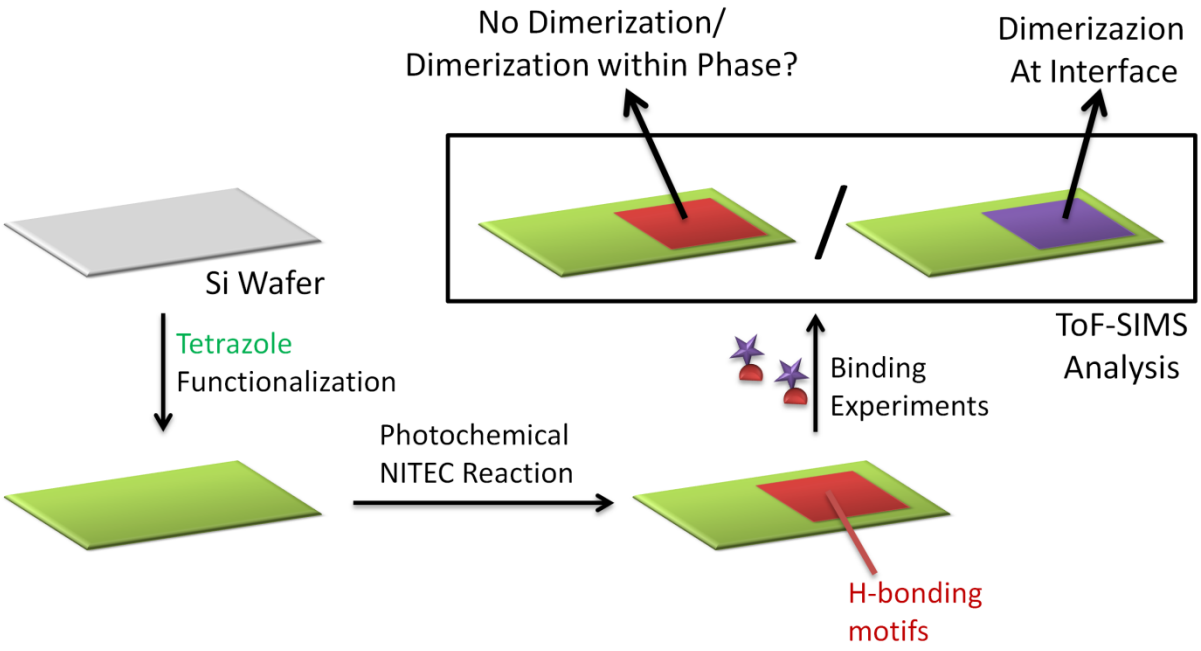

Figure 43: General synthetic approach for hydrogen bonding at surfaces as model systems for interfacial bonding in NCs. Si wafers are activated and globally coated with tetrazole moieties, allowing in a second step to covalently attach hydrogen bonding motifs onto the wafer surface (in a spatially resolved manner). Possible outcomes of ToF-SIMS analysis after binding experiments with marked, complementary bonding motifs and their microscopic interpretation are depicted.

To construct model systems for hydrogen bonding at interfaces, silicon wafers were functionalized with tetrazoles allowing the wafer to be functionalized in a spatially resolved manner *via* the NITEC reaction in a next step.

For the self-complementary UPy model system maleimide-functionalized UPy was covalently immobilized (photochemical NITEC reaction) onto distinct areas on the wafer and adsorption experiments with halogen labeled UPys from solution were performed. Hydrogen bonding at the interface was monitored *via* ToF-SIMS, imaging the labeled binding partners from solution on the surface.

To study hydrogen bonding at a macroscopic surface for hetero-complementary systems, the SOA-AOA couple was employed and tetrazole functionalized silicon wafers were functionalized with spatial resolution *via* a NITEC reaction with the new maleimide-functionalized AOA. Subsequently, immobilization experiments with SOA-PMMA from solutions were carried out.

3.2.1 *Investigation of UPy Dimers*

3.2.1.1 UPys for Surface Attachment

In both model systems (for the investigation of interfacial hydrogen bonding) macroscopic Si wafer were employed as substrates for immobilization of hydrogen bonding motifs. The wafers were initially coated with the tetrazole-functionalized silane **18** and subsequently employed in a NITEC reaction to attach hydrogen bonding motifs in a spatially resolved manner to the surface. The synthesis of the tetrazole silane agent **18** was conducted according to literature procedures (Scheme 18).[69, 209]

In a first step, 4-formylbenzoic acid was transformed to the corresponding benzenesulfonylhydrazone employing benzenesulfonohydrazide, subsequently precipitated and combined with benzenediazonium salt in basic solution at 0 °C. Under these conditions the highly reactive formazan intermediate is *in-situ* deprotonated, resulting in the elimination of benzenesulfinate and electrocyclization to tetrazole **17**, which was obtained as pink powder after extraction and precipitation (yield: 34%). Finally, **17** was subject to a Steglich esterification with (3-aminopropyl)triethoxysilane (APTES) employing *N,N'*-dicyclohexylcarbodiimide (DCC) and 4-dimethylaminopyridine (DMAP) in DCM under inert conditions. After column chromatography and recrystallization, the desired product **18** was obtained as pale red powder in excellent purity, which could be stored in the fridge (4 °C) over three months (total yield: 5%).

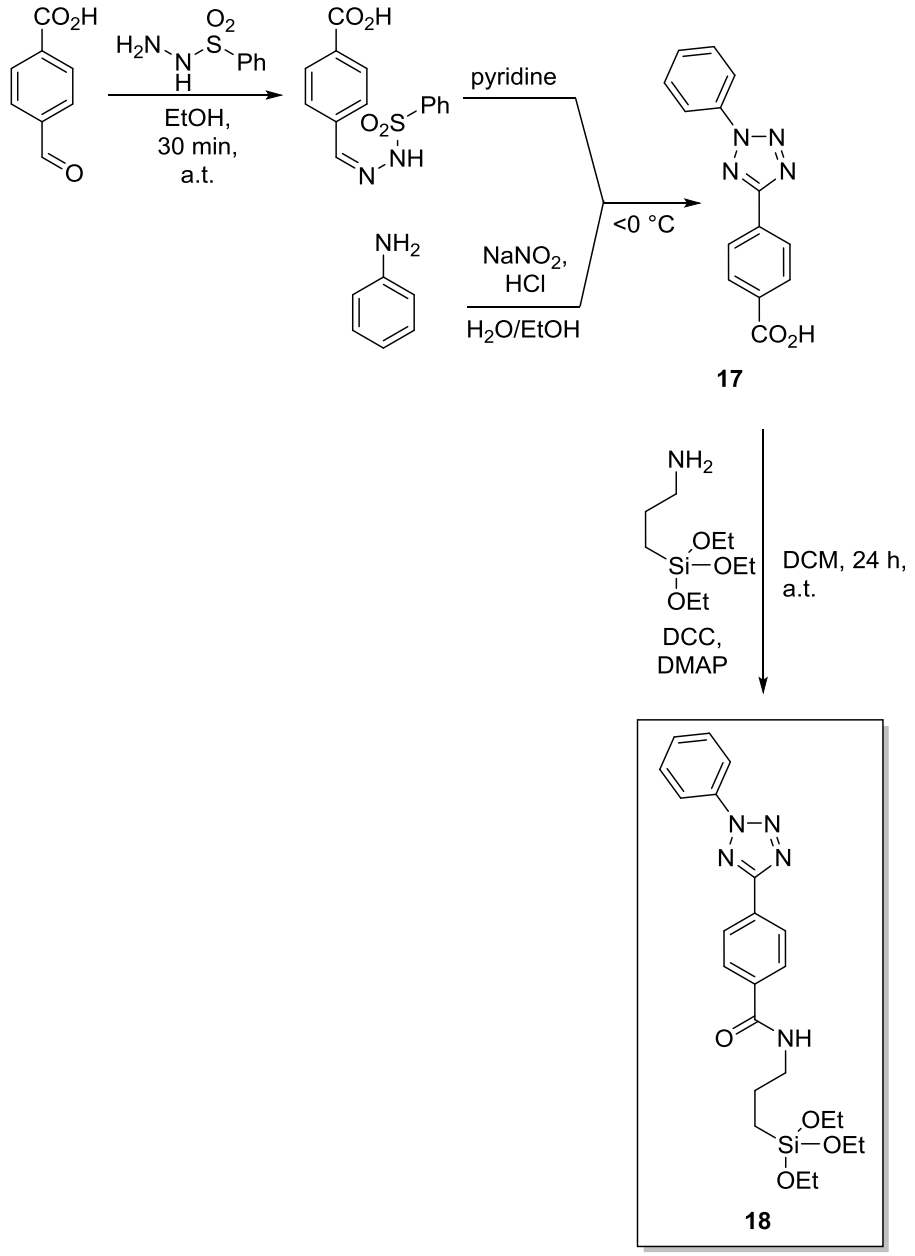

Scheme 18: Synthetic strategy for the preparation of tetrazole silane agent Tet-Silane (**18**).

In order to fabricate the UPy model system, UPy-Mal (**22**) (for covalent immobilization on tetrazole functionalized silicon wafers *via* NITEC reaction) was prepared in a convergent synthesis strategy with five steps, including the two new molecules **21** and **22** (Scheme 19). Starting with the DA reaction of maleic anhydride and furan in toluene for 6 h at 80°C, the crystallized product **19** (yield: 72%) was further reacted with ethanolamine resulting in MalPG-OH (**20**) after crystallization (yield: 50%), according to a procedure reported by Mantovani *et al*.[210] UPy-NCO (**8**) was prepared as described before and coupled to **20** *via* urethane formation in DCM during reflux

overnight in the presence of a Sn(II)-catalyst, resulting in **21** (yield: 70%). The ^{1}H-NMR spectrum of the new molecule **21** exhibits all proton resonances, expected with regard to its reactants and demonstrates the successful formation of **21** (Figure 44). Resonances a, b and c arise from hydrogen bonding protons associated with the UPy moiety, while the characteristic resonance d corresponds to a furan-protected maleimide. Subsequently, in the last synthetic step towards UPy-Mal (**22**), **21** was heated to 130 °C for 15 h in Schlenk vacuum, promoting the retro-Diels-Alder (rDA) reaction and removing the protective furan from the target molecule (total yield: 65%). ^{1}H-NMR analysis of the reaction sequence reveals that resonances associated with the protons l, m and n, corresponding to protected maleimide in the reactant **21**, disappear, while the new resonance d, associated with unprotected maleimide, arose, demonstrating the successful deprotection to **22** (Figure 45).

To facilitate the analysis of the hydrogen bonding situation on the surface, UPys for adsorption from solution were tagged with halogen atoms (Br, F), which can be easily and unambiguously detected *via* ToF-SIMS. In particular, two small molecule UPys with different halogen labels and one labeled UPy copolymer were prepared. In small molecule synthesis, UPy-NCO (**8**) was either coupled to trifluoroethanol, resulting in UPy-CF_3 (**23**) (total yield: 65%), which was synthesized for the first time, or coupled to bromoethanol, yielding UPy-Br (**24**) (total yield: 62%) after reflux in DCM in the presence of a catalyst in two synthetic steps. ^{1}H-NMR analysis of the new molecule **23** demonstrates the successful introduction of CF_3 (Figure 46).

Additionally to **23** and **24**, a polymeric F-labeled UPy was synthesized, enhancing solubility and aiming for better signal-to-noise ratios in ToF-SIMS analysis. Therefore, UPy-MA (**10**), 2,2,2-trifluoroethyl methacrylate (TFEMA) and butyl methacrylate (BMA) were dissolved in DMSO, degassed and copolymerized *via* FRP at 60 °C for 24 h, resulting in **P7** after precipitation (M_n = 63.0 kDa, $Đ$ = 1.4, 4 mol% **10**, 8 mol% TFEMA).

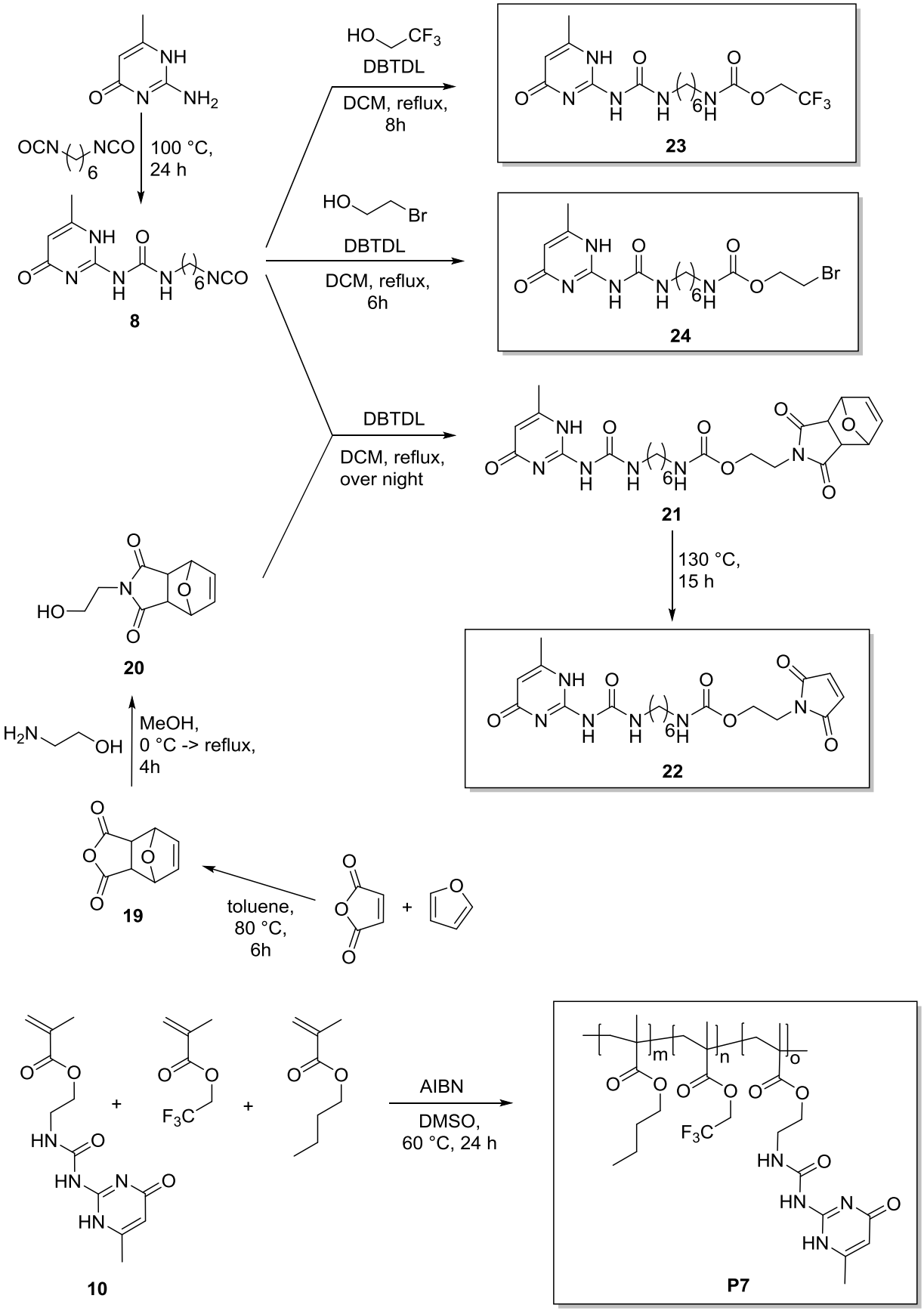

Scheme 19: Synthetic pathways for the preparation of UPy derivates employed in surface attachment.

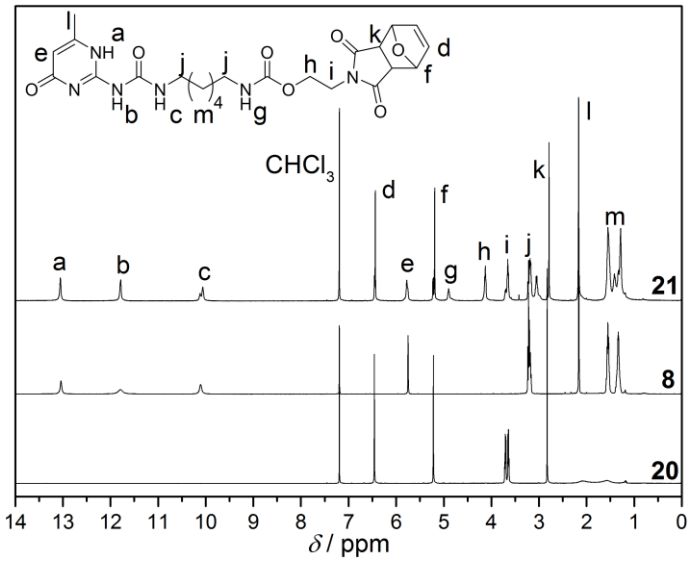

Figure 44: ^{1}H-NMR spectra of UPy-MalPG (**21**) and its reactants UPy-NCO (**8**) and MalPG-OH (**20**) in $CDCl_3$.

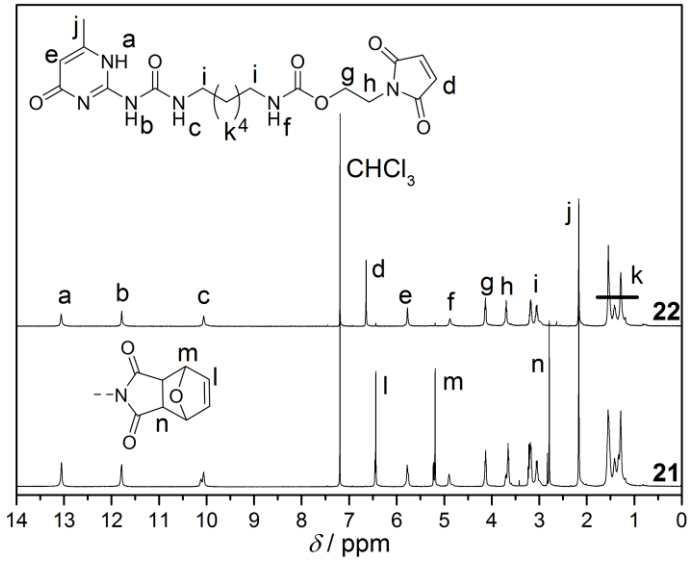

Figure 45: ^{1}H-NMR spectra of UPy-Mal (**22**) and its reactant UPy-MalPG (**21**)) in $CDCl_3$. Disappearance of resonances l, m and n in from **21** to **22** and appearance of the new resonance d verify the successful deprotection.

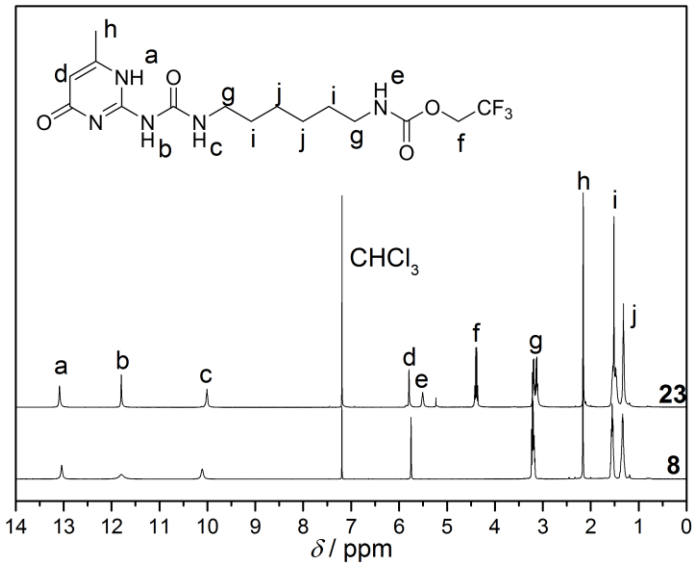

Figure 46: ^{1}H-NMR spectra of UPy-CF_3 (**23**) and precursor **8** in $CDCl_3$. The resonance f indicates the successful introduction of the fluorine label.

3.2.1.2 Surface Functionalization and Immobilization

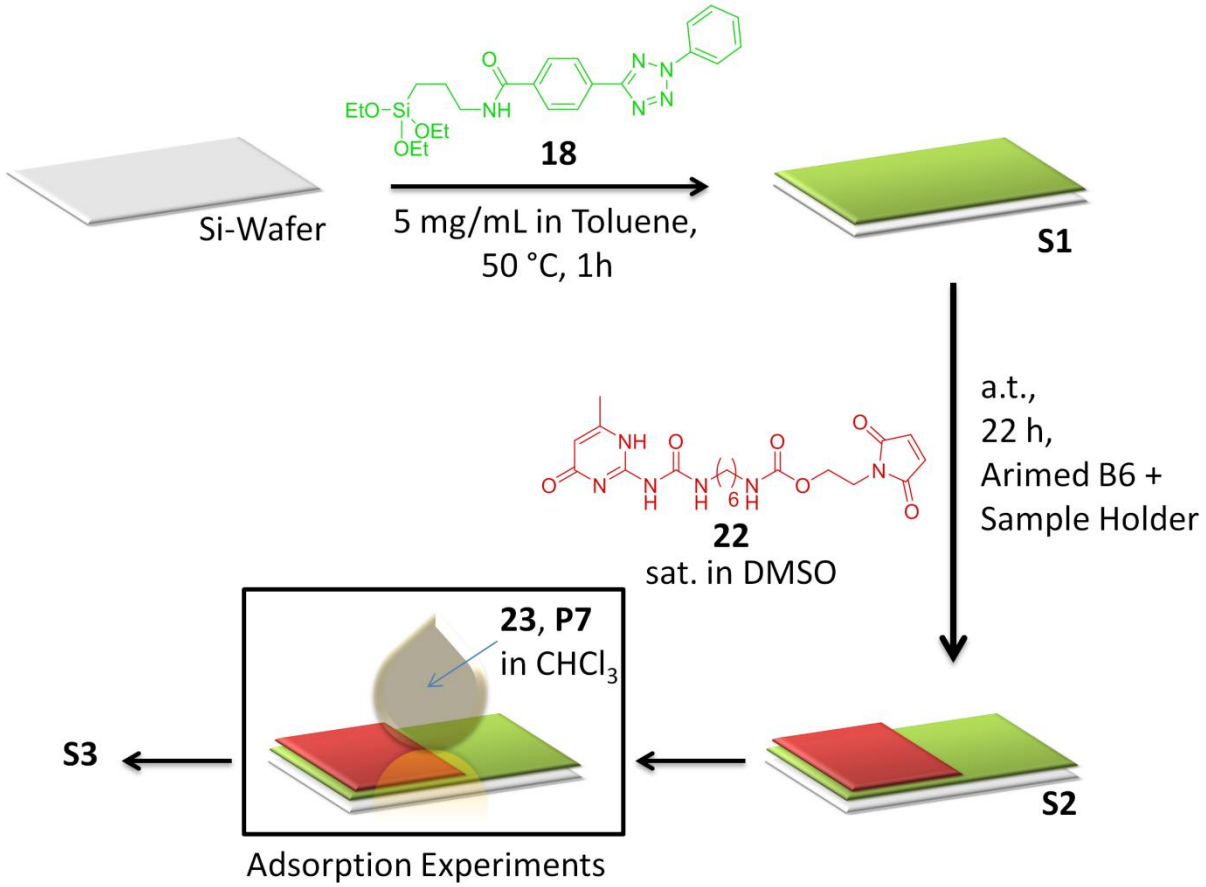

Scheme 20: Synthetic scheme for the fabrication of spatially UPy-functionalized Si wafers **S2** and for adsorption experiments with UPys (**23**, **P7**) from solution, resulting in surfaces **S3** for ToF-SIMS analysis.

Fabricating a macroscopic model system for UPy dimerization at NC interfaces, silicon wafers were covalently functionalized with UPy (in two steps) and adsorption experiments from solutions were performed (Scheme 20).

In a first synthetic step of the synthesis (shared with the model system for SOA/AOA) a silicon wafer was activated in a mixture of H_2O_2/conc. H_2SO_4 (1/2) for 2 h at 100 °C, resulting in a clean and oxidized surface for the functionalization with silanes. Subsequently, the treated surface was rinsed with MilliQ water, dried (N_2 stream) and immersed in a solution of Tet-Silane (**18**) in dry toluene for 1 h at 50 °C and stored overnight at ambient temperature. The obtained globally tetrazole-functionalized silicon wafer (**S1**) was rinsed with toluene to remove physisorbed **18**, dried in a N_2 stream and used as a substrate in NITEC reactions with maleimide-functionalized hydrogen motifs without further characterization.

Subsequently, UPy 22 was immobilized covalently and in a spatially resolved manner on the tetrazole-functionalized wafer **S1**. Therefore, **S1** was mounted in a sample holder, which shielded parts of the surface from UV irradiation and thus the NITEC reaction. The loaded sample holder was immersed in a saturated solution of UPy-Mal (**22**) in dry DMSO and irradiated for 22 h, promoting the NITEC reaction between tetrazole **18** on the wafer surface and maleimide **22** in solution, thereby introducing UPy motifs on a distinct area of the wafer (**S2**). Finally, the wafer **S2** was extensively washed (THF, acetone, MeOH and DCM) and dried in a N_2 stream. Subsequent ToF-SIMS analysis convincingly demonstrates the spatially resolved immobilization of **22** onto the wafer (Figure 47), as a clear edge of functionalization is readily visible. The mapped $C_5H_6N_3O^-$-ion was identified as characteristic fragment of **22** in spin coating experiments before.

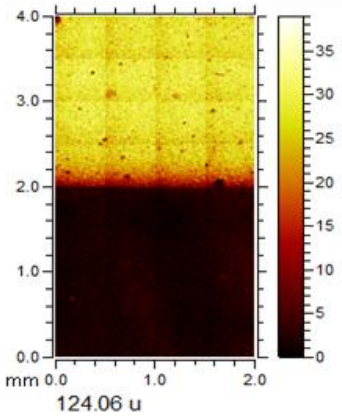

Figure 47: ToF-SIMS map of the $C_5H_6N_3O^-$-ion (m/z = 124.06), assigned to UPys for surface **S2**.

For adsorption experiments of UPys from solution onto UPy-functionalized **S2**, the wafers were immersed in filtered solutions of UPy (**23**, **P7**) in $CHCl_3$, heated to 50 °C for 15 min to increase trans-dimerization dynamics and kept at ambient temperature for 1 h, allowing the system to equilibrate. To remove physisorbed UPy from the surfaces **S3**, the wafers were gently washed with a defined procedure (employing solvents that do not interfere with hydrogen bonds), summarized in Table 3. Numerous adsorption experiments (10) with varying washing procedures were conducted and the corresponding ToF-SIMS analysis is provided in detail.

Surface	Adsorption: UPy, conc.	Washing: (solvent, volume, time, procedure)	TOF-SIMS Analysis	
			m/z[a] = 69.00	m/z[b] = 124.06
S3A	**23**, saturated	$CHCl_3$, 2 mL, 10 sec., immersed	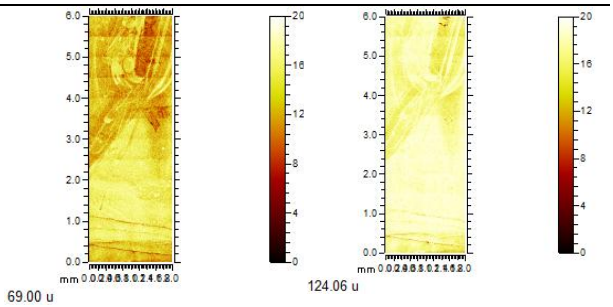	
S3B	Ⅱ	$CHCl_3$, 2 mL, 60 sec., immersed	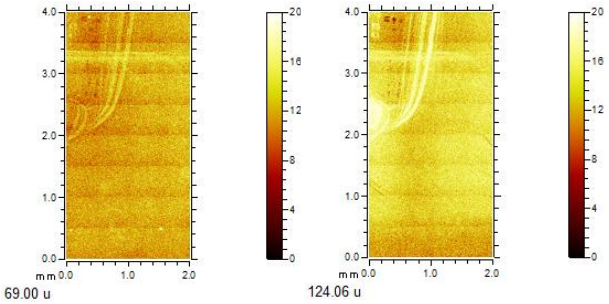	
S3C	Ⅱ	Toluene, 2 mL, rinsed	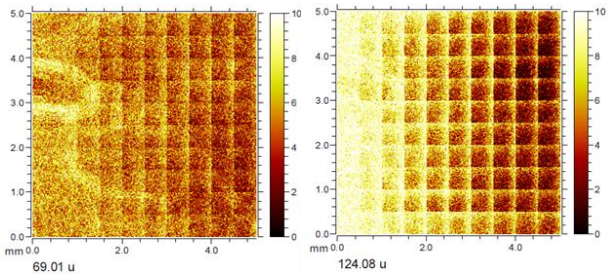	
S3D	Ⅱ	$CHCl_3$, 2 mL, rinsed	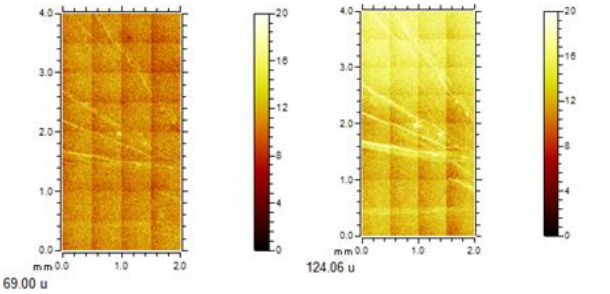	
S3E	Ⅱ	$CHCl_3$, 6 mL, rinsed	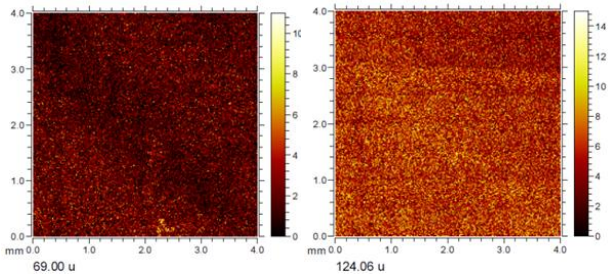	

S3F	Ⅱ	$CHCl_3$, 10 mL, rinsed	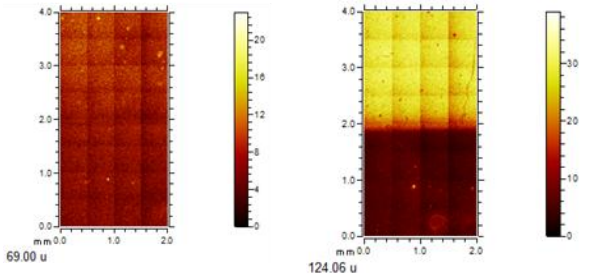
S3G	Ⅱ	Toluene, 10 mL, rinsed	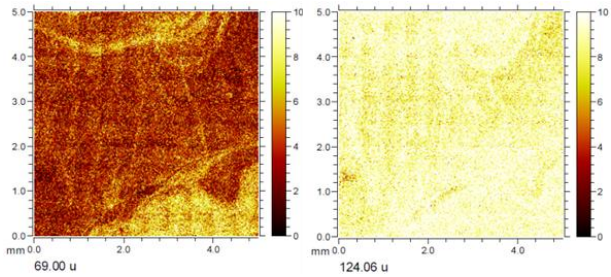
S3H	Ⅱ	DCM, 12 mL, rinsed	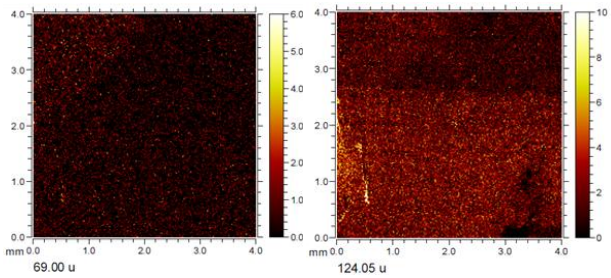
S3I	**P7**, 8 g·L^{-1}	$CHCl_3$, 6 mL, rinsed	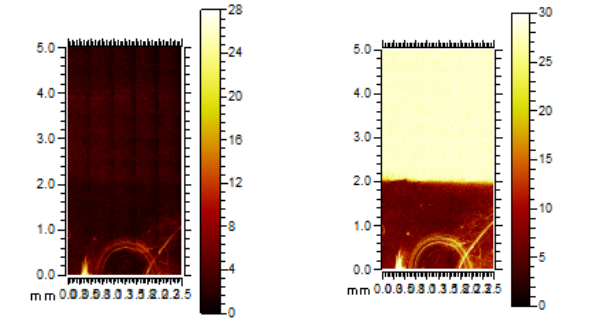
S3J	Ⅱ	$CHCl_3$, 12 mL, rinsed	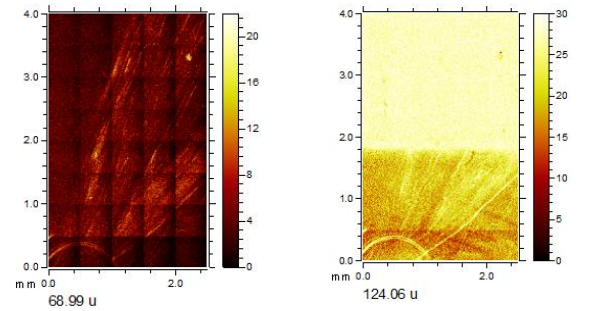

Table 3: Detailed washing conditions for **S3** and the corresponding ToF-SIMS ion maps. Masses correspond to (a) CF_3^--fragments and (b) $C_5H_6N_3O^-$–fragments.

The signal m/z = 69.00 (CF_3, left column) arises solely from UPys from solution (**23**, **P7**), which were labeled with fluorine. The ion m/z = 124.06 ($C_5H_6N_3O$, right column)

corresponds to the overall UPy signal and depicts the sum of covalently bound **22** plus UPys from the adsorption solution. In case of adsorption of UPy-CF_3 (**23**) immersion of the wafer in $CHCl_3$ resulted in insufficient removal of physisorbed **23**, independently of the immersion time (**S3A**, **B**). An increase of the $CHCl_3$ volume (2-10 mL) in the washing procedures based on rinsing decreased the amount of immobilized **23** on the surface without significant residual **23** in the UPy-functionalized part of the surface (**S3D**, **E**, **F**). Employing 2 mL solvent, **23** was found globally on the surface, while 10 mL resulted in complete removal of **23** from the surface with only covalently bound UPy remaining. In contrast to $CHCl_3$, toluene was unsuitable to remove physisorbed **23** from the surface (**S3C, G**) and DCM entirely washed off **23** (**S3H**). Due to the enhanced solubility of **P7** compared with **23**, identical washing procedures led to less remaining signal arising from **P7** on the surface (**S3E**, **I**). Similarly to the adsorption experiments employing **23**, **P7** was either globally found on the surface, or completely washed off – without any evidence of preferential binding into the UPy-functionalized part of the silicon wafer.

After taking into account all the absorption experiments and washing procedures, it can be concluded that the dominant process of immobilization of UPys from solution onto an UPy-functionalized silicon wafer is unspecific physisorption. Independent of the washing procedure, no contrast in immobilization between UPy-functionalized and unfunctionalized areas of the surface could be achieved, indicating that hydrogen bonding motifs at the surface have no influence on immobilization from solution. This observation implies that either no hydrogen bonding occurs at all, or hydrogen bonding occurs within the same phase and not at the surface-solution interface. Since hydrogen bonding within the same phase is impossible in hetero-complementary motifs (in contrast to homo-complementary UPys), a similar study, employing SOA/AOA, was conducted to further identify dominant the processes at hydrogen bonding surfaces.

3.2.2 *Investigation of SOA-AOA Dimers*

3.2.2.1 Synthesis of SOA and AOA Compounds

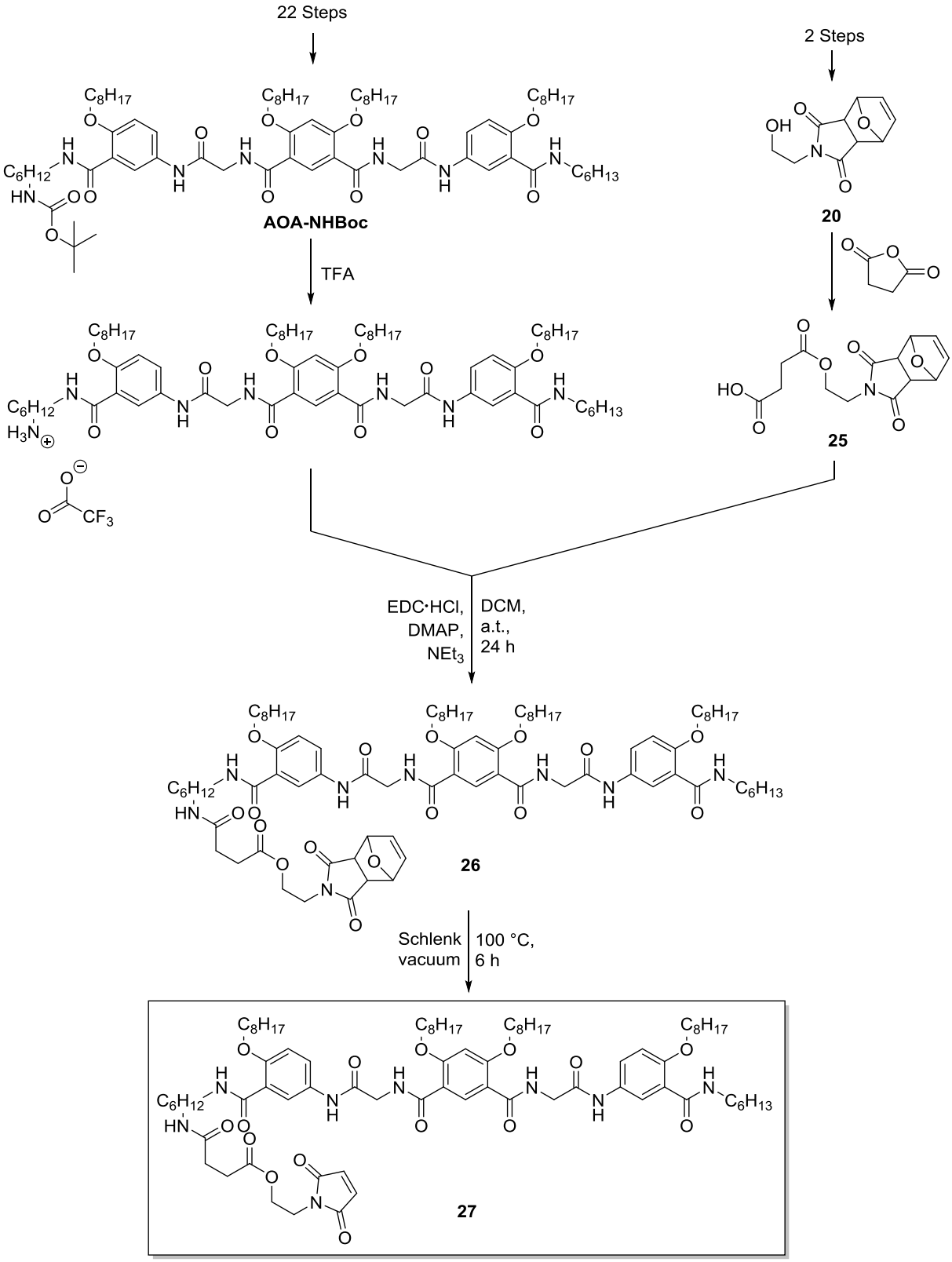

Scheme 21: Synthesis route to AOA-Mal (**27**).

In order to improve the hydrogen bonding recognition and study a model system with hetero-complementary hydrogen bonding, the SOA-AOA couple was employed. Functionalized AOA was spatially resolved immobilized on silicon wafers *via* the NITEC process and adsorption experiments with an SOA endgroup-functionalized PMMA (SOA-PMMA) were performed. The reactants AOA-NHBoc and SOA-PMMA were provided by Dr. Julien Bernard and coworkers (INSA-Lyon) (Scheme 22),[153] **25** was kindly provided by Kilian Wüst (macroarc group, KIT)

Synthesizing the maleimide-functionalized AOA-Mal (**27**) for surface immobilization, AOA-NHBoc that was prepared in 22 steps, as described before, was deprotected in a solution in trifluoroacetic acid (TFA) and subsequently isolated. The corresponding TFA-salt was employed in a further step without purification and analysis. The reaction conversion was monitored *via* thin-layer chromatography (TLC). In a second synthetic step the ammonium salt was esterified with MalPG-CO_2H (**25**), prepared in three synthetic steps, employing 1-ethyl-3-(3-dimethylaminopropyl)carbodiimide (EDC·HCl), DMAP and additionally 1 eq. NEt_3 (to deprotonate the AOA-ammonium salt to the corresponding free amine, thus enabling further Steglich esterification) in dry DCM under inert gas. The reaction mixture was stirred for 24 h at ambient temperature. Afterwards, the solvent was removed *in vacuo* and the new molecule AOA-MalPG (**26**) was purified *via* column chromatography (yield: 40%).

AOA-Mal (**27**) was obtained by deprotection (*via* rDA reaction) of **26** in Schlenk vacuum at 100 °C for 6 h, resulting in a yellow solid that was used without further purification (total yield, last three steps: 40%). Very remarkably, dissolution of **27** in $CDCl_3$ resulted in gelation overnight. The reaction sequence of AOA-NHBoc to AOA-Mal (**27**) was monitored with ^{1}H-NMR spectroscopy and the sequence of spectra convincingly proves the conversion to the target molecule (Figure 48). The new resonances k and r verify the successful esterification with **25** and in the last deprotection step, the disappearance of resonances r and j and the additional new resonance h corresponding to deprotected maleimide evidence complete deprotection and first successful synthesis of **27**.

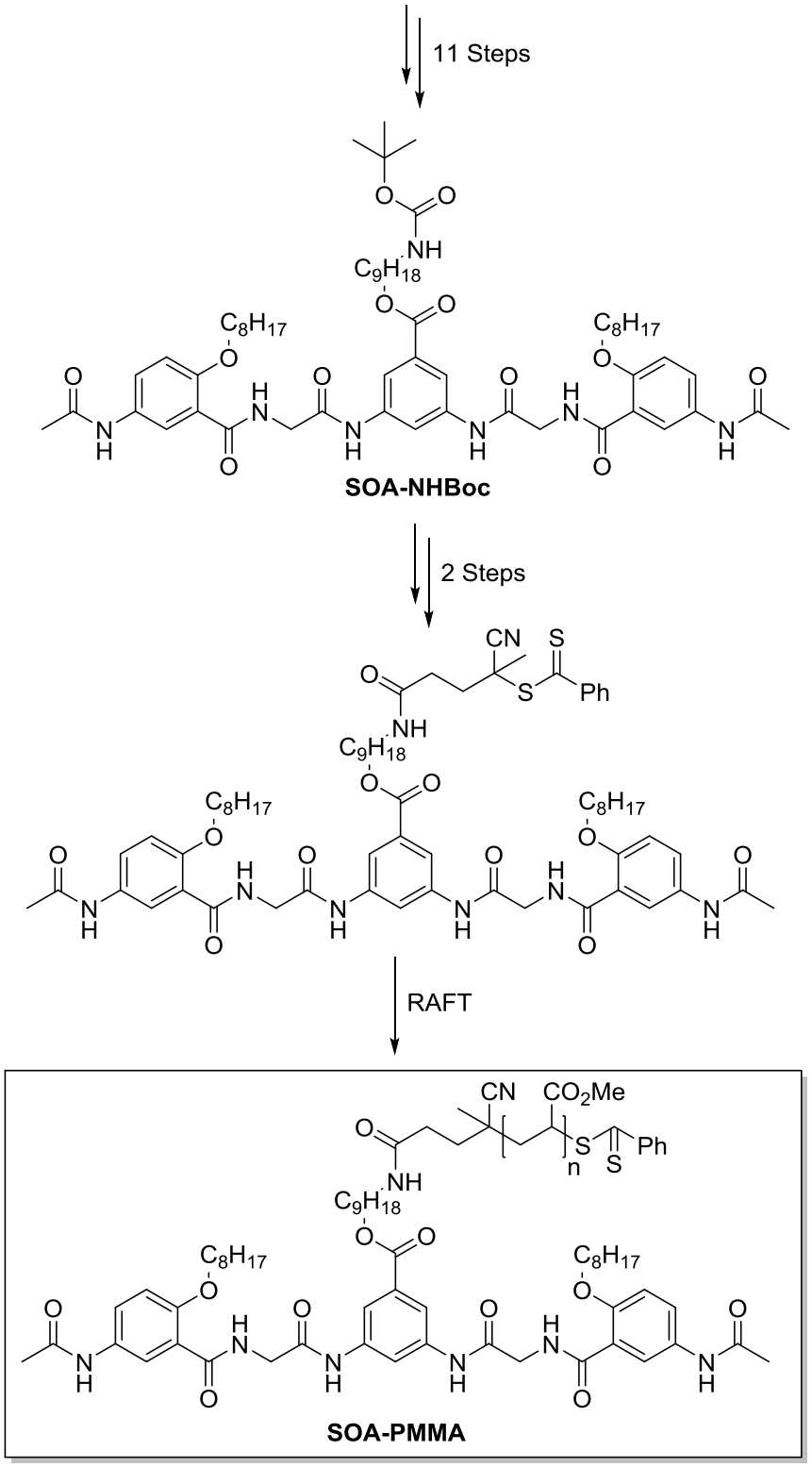

Scheme 22: Synthesis route to SOA-PMMA carried out by Bernard and Coworkers.[153]

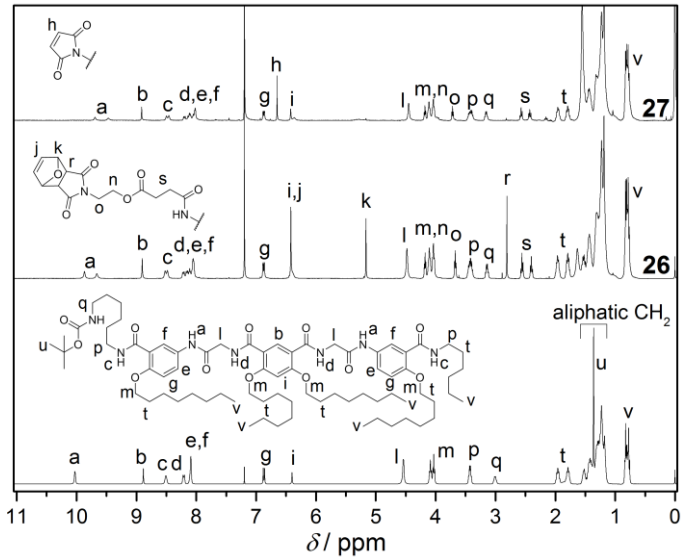

Figure 48: Comparative ^{1}H-NMR spectra of AOA-NHBoc, AOA-MalPG (**26**) and AOA-Mal (**27**) in $CDCl_3$.

3.2.2.2 Surface Functionalization and Immobilization

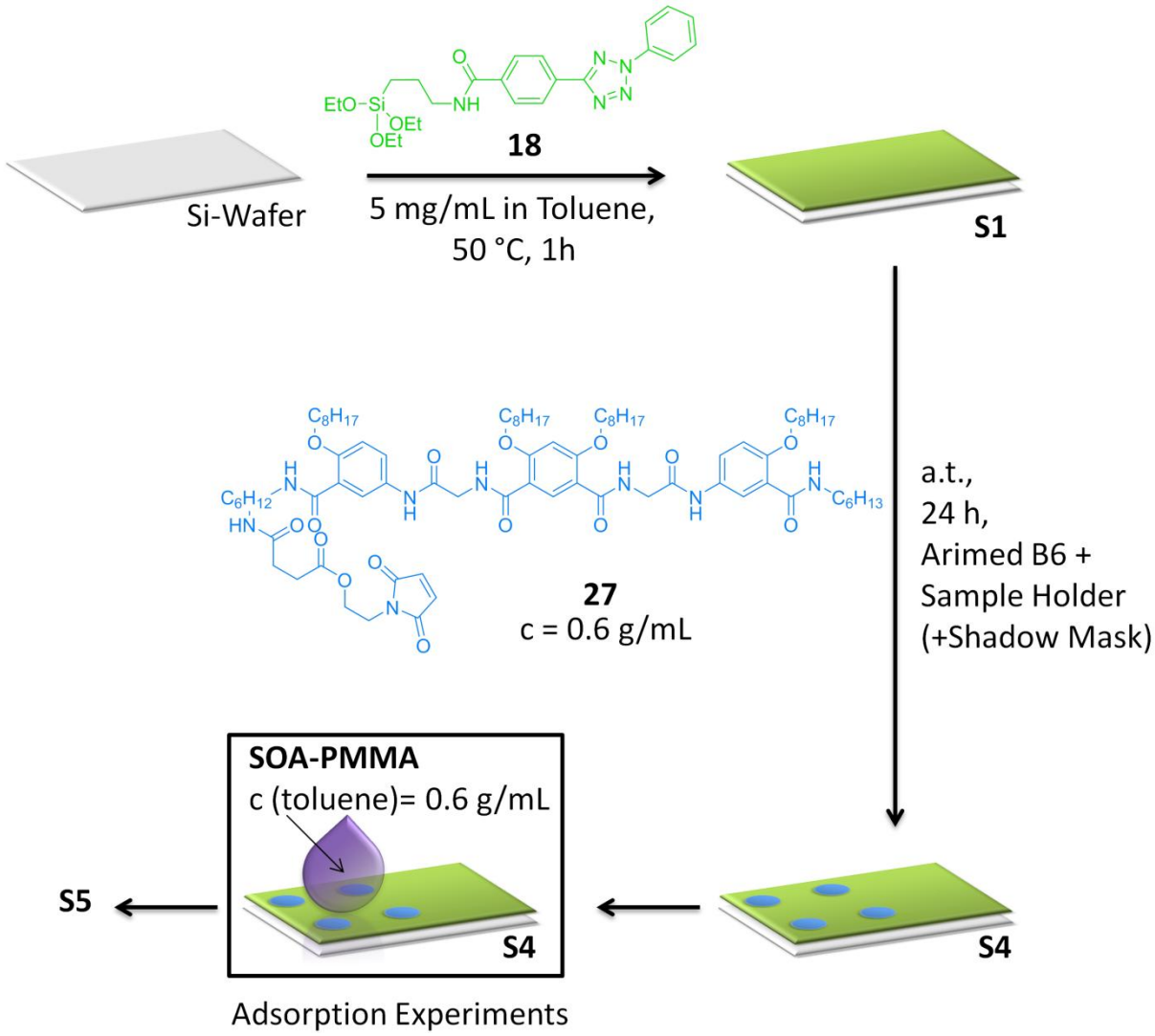

Scheme 23: Fabrication of silicon wafers with spatially resolved AOA-functionalization (**S4**) for adsorption experiments with SOA-PMMA from solution.

Expanding the study of hydrogen bonding at macroscopic surfaces as model system for interfaces in polymer-based NCs, the hetero-complementary hydrogen bonding on a silicon wafer surfaces was studied by employing the SOA-AOA couple.

Firstly, silicon wafers were activated and functionalized with Tet-Silane (**18**), in an analogue approach to the case of UPy-functionalized wafers, yielding (the identical) surface **S1**. Secondly, **S1** was mounted in a sample holder with a dotted shadow mask and immersed in a solution of AOA-Mal (**27**) in dry DCM, which was subsequently degassed in an ice bath and irradiated for 24 h with an Arimed B6 lamp (Figure 56). The UV-irradiation induced the NITEC reaction between the surface

immobilized tetrazole **18** and the maleimide moiety of **27** and, thereby, introduced AOA in a spatially resolved manner to the non-shielded areas of the wafer (in circular shape). The sample was removed from the sample holder and the shadow mask, washed extensively with DCM and dried in an inert gas stream. The AOA-functionalized wafer **S4** was used (without further surface analysis) for immobilization of SOA-PMMA based on hetero-complementary hydrogen bonding in a further step. For the immobilization experiment, **S4** was immersed in a filtered solution of SOA-PMMA in dry toluene (c = 0.6 g·mL^{-1}) for 10 min. The obtained surface **S5** with immobilized SOA-PMMA was washed extensively with toluene to remove any traces of physisorbed PMMA and dried in an inert gas stream. The obtained surface **S5** was analyzed *via* ToF-SIMS and characteristic fragments corresponding to PMMA (which were identified in a spin-coating experiment before) were detected exclusively in the circles, were AOA-functionalization was expected (Figure 49c).

In contrast to self-complementary hydrogen bonding (UPy) on surfaces, where no binding partners from solution could be detected on the surface, in the hetero-complementary model system (SOA-AOA) binding partners from solution could be readily immobilized onto areas with complementary functionalization. The results from the hetero-complementary system demonstrate that hydrogen bonding on surfaces with relative few binding sites (compared with *e.g.* DNA) is in fact possible and, therefore, in case of self-complementary motifs dimerization within the same phase (surface-surface, solution-solution) must be dominant over dimerization at the interface. Absence of hydrogen bonding in self-complementary system as source of the lack of adsorption of molecules from solutions can be consequently excluded.

Further pushing the limits of hetero-complementary hydrogen bonding on surfaces, the surface **S5** was washed with a MeOH/$CHCl_3$ mixtures, to break SOA-AOA dimers and wash off PMMA from the surface entirely, resulting in the cleaned surface **S4*** (Figure 49a,c). Several adsorption-washing cycles were conducted with surfaces, prepared without shadow mask but sample holder exclusively and the ion count for a distinct fragment ($C_4H_5O_2^-$) associated with PMMA was normalized to the applied primary ion dose for comparability (Figure 49b). The comparison of the normalized ion intensity for the characteristic PMMA fragment demonstrates the good stability of the surface during the immobilization-washing cycles with a minimal decrease of signal after 4 immobilization steps of 34%.

The fabrication of the AOA-functionalized surfaces **S4**, including the synthesis of the two new molecules **26**, **27**, and the adsorption experiments studying reversibility and spatial resolution of SOA-PMMA immobilization were successfully published.[96]

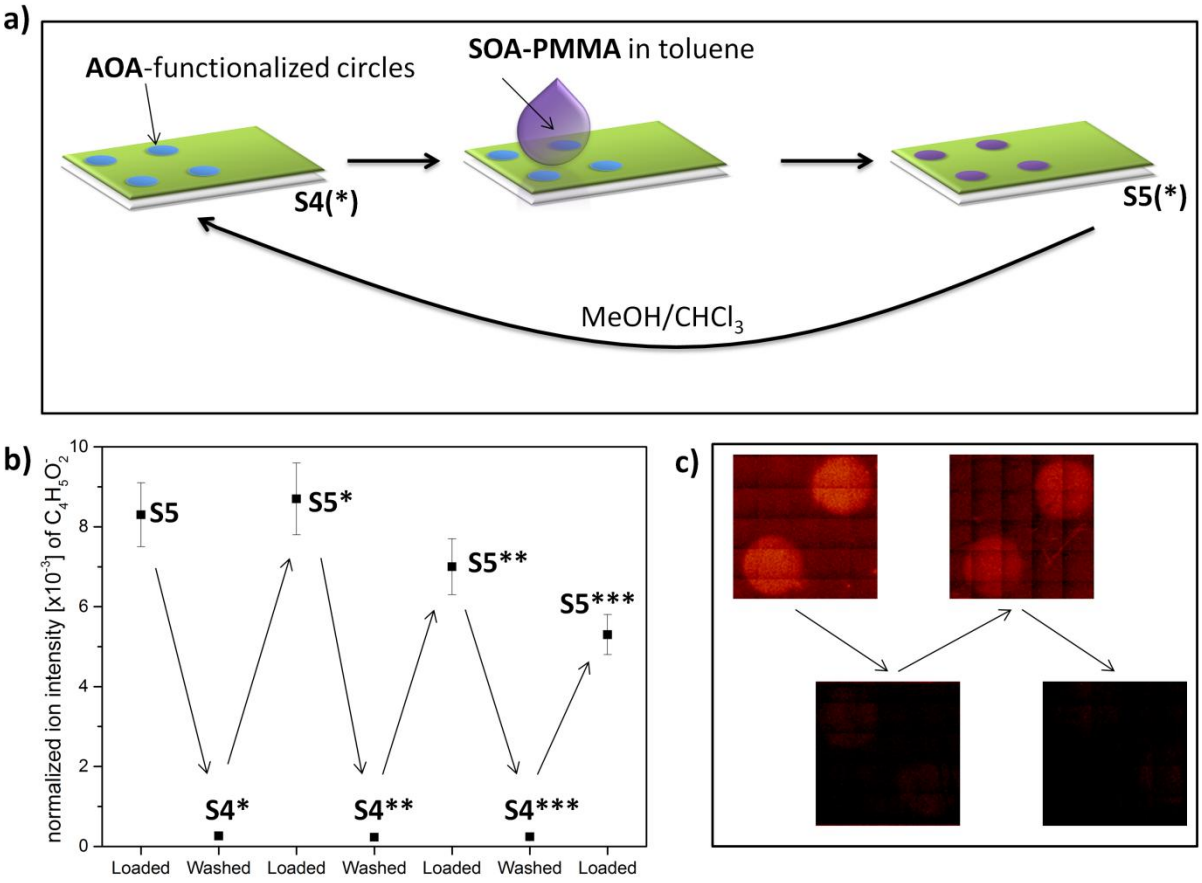

Figure 49: (a) Schematic depiction of performed immobilization-washing cycles of SOA-PMMA and the surfaces **P4**/**P5**. (b) Normalized ion intensities for fragment $C_4H_5O_2^-$ corresponding to PMMA depicting the surface´s stability during immobilization-washing cycles. (c) ToF-SIMS images for the $C_4H_5O_2^-$ ion of different stages of immobilization, employing surfaces that were fabricated with a shadow mask, demonstrating the reversible and spatially resolved immobilization of SOA-PMMA into the AOA-functionalized circles.

3.3 Reversible, Cross-Linker Mediated Single Chain Folding based on Hetero-Diels-Alder Chemistry

SCNPs on the basis of HDA Chemistry were synthesized in collaboration with Thorsten Lückerath, who was supervised by NW in the context of his master thesis “Dynamic Covalent Single-Chain Nanoparticles (SCNPs) Based on Hetero Diels-Alder Chemistry”. The experiments were designed by NW and conducted by NW and TL equally. SCNP unfolding was designed and conducted by NW, exclusively. DLS measurements were conducted by Dr. Hatice Mutlu (macroarc group, KIT) and the corresponding instrument was kindly provided by Dr. Pavel Levkin (KIT). Alexander Schenzel (macroarc group, KIT) is acknowledged for kindly providing Bis-Cp.

To demonstrate that the CDTE-sorbic alcohol HDA couple is capable to form cross-links in polymeric materials, it was not only employed as thermo-reversible cross-linking chemistry in HDA matrices in NC formation, but moreover utilized as cross-linker in single chain nano-particles synthesis, described in the current chapter (Figure 50).

The CDTE-functionalized methacrylate CDTE-MA (**15**) was copolymerized *via* RAFT and conventional FRP with MMA in distinct ratios, yielding a library of precursor copolymers with defined composition, architecture and narrow chain length distribution (fabricated by RAFT). Moreover, a high molecular weight precursor copolymer was prepared by conventional FRP. The precursor polymers were heated individually in dilute solution in the presence of a external cross-linker exhibiting two sorbic alcohol moieties (new molecule) resulting in intra-chain cross-linking *via* the CDTE-sorbic alcohol HDA couple (SCNP formation). single chain folding was monitored by SEC and ^{1}H-NMR analysis.

Exploiting the full potential of the reversible nature of HDA chemistry, one selected SCNP was unfolded back to an open chain state, by heating the nano-particle in the presence of sorbic alcohol, which expelled the external cross-linker and, thereby, restored the unfolded polymer chain. The success of the polymerization-folding-unfolding sequence was demonstrated *via* ^{1}H-NMR spectroscopy, SEC and DLS. Additionally, data on the kinetic and thermodynamic stability of each chain state is presented and discussed, confirming fundamental principles in single chain folding.

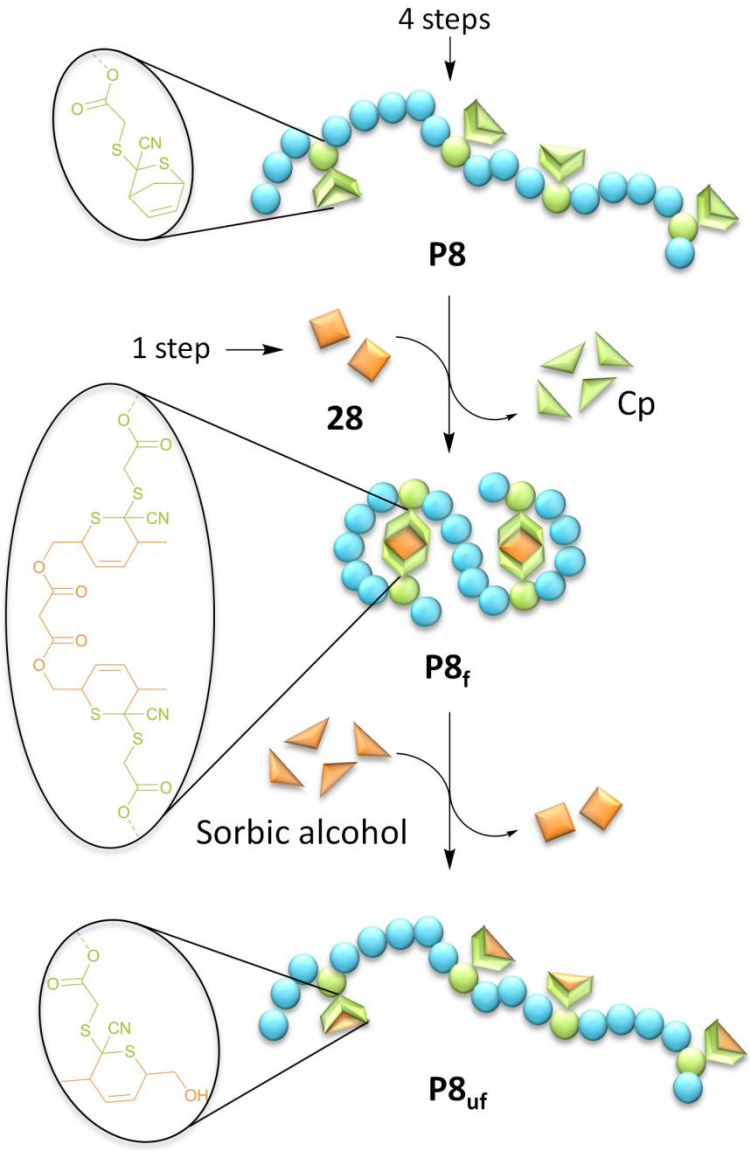

Figure 50: Schematic representation of the single chain folding and unfolding process. Precursor copolymers **P8** of MMA and CDTE-MA (**15**) were folded with an external cross-linking agent $Sorb_2$ (**28**) to SCNPs $\mathbf{P8_f}$. In a subsequent step, a selected SCNP was unfolded to an open polymer chain $\mathbf{P8_{uf}}$.

The fabrication and unfolding of SCNPs on basis of CDTE-sorbic alcohol HDA chemistry was successfully published.[211]

3.3.1 *Cross-Linker Synthesis and RAFT/FRP Copolymerizations of MAA and **15**.*

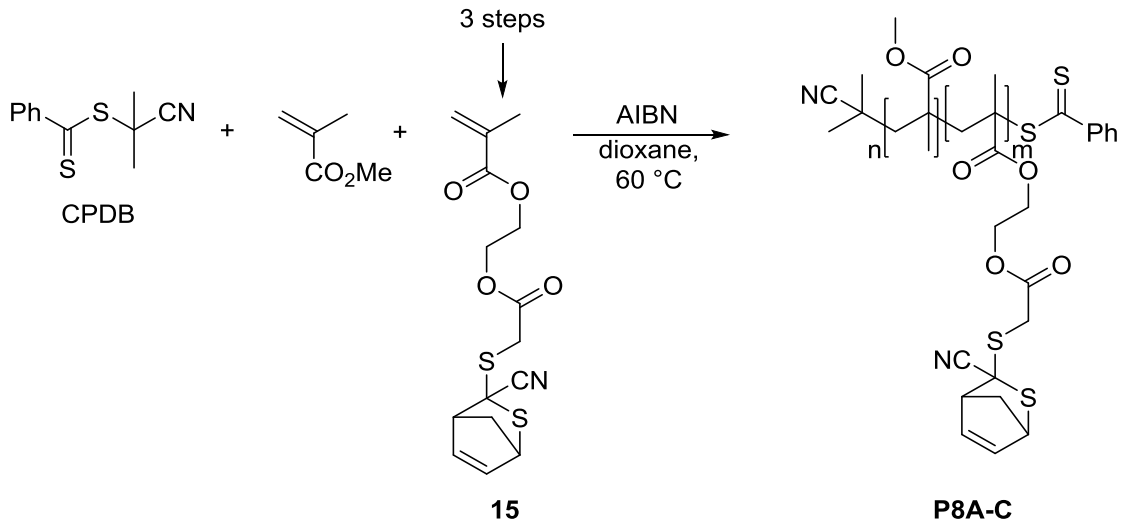

Scheme 24: Synthesis of copolymer precursors **P8A-C** *via* RAFT polymerization.

To fabricate copolymer precursors exhibiting CDTE moieties in distinct ratios in the polymeric backbone, the monomer CDTE-MA (**15**), initially prepared for thermoreversible cross-linking in matrices for NCs, was copolymerized *via* RAFT with MMA moderated by 2-cyano-2-propyl benzodithioate (CPDB) (Scheme 24). Therefore, MMA, **15**, CPDB and AIBN were dissolved in dioxane, degassed and subsequently polymerized at 60 °C, varying comonomer ratios and reaction times. The corresponding RAFT copolymers **P8A-C** were isolated and purified by repeated precipitation in cold cyclohexane and characterized *via* SEC (Figure 53, Figure 54) and ^{1}H-NMR analysis (Figure 51). The initial comonomer ratios of the polymerization mixture were retrieved in the final polymer backbones (Table 11).

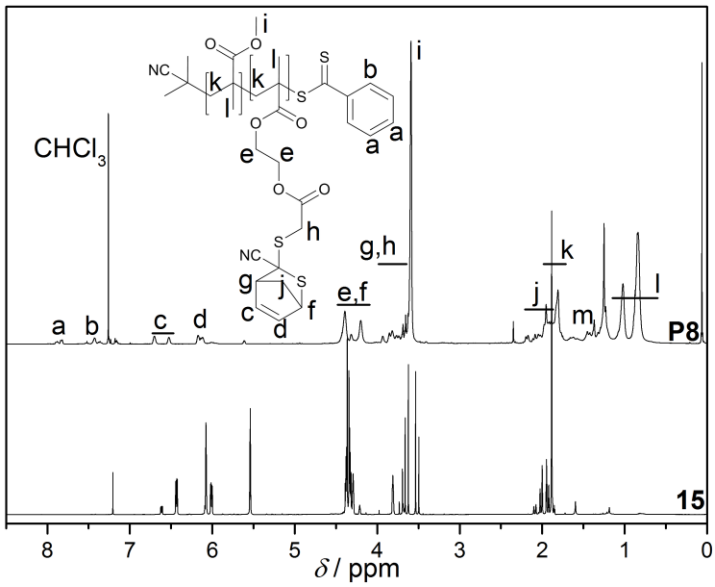

Figure 51: Representative ^{1}H-NMR spectrum of **P8** in comparison with CDTE-MA (**15**) in $CDCl_3$. For estimating the of copolymer composition resonances c and i have been employed.

In a second synthetic approach, aiming for high molecular weights, **15** and MMA were copolymerized *via* conventional FRP in an analogue procedure to RAFT (yet without the CPDB control agent), yielding the large copolymer precursor **P8FRP** (M_p = 47.8 kDa).

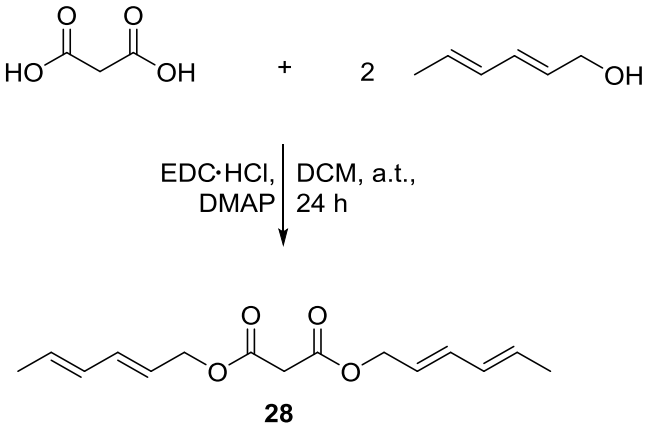

Scheme 25: Synthesis of $Sorb_2$ (**28**), which was employed as external cross-linking agent in SCNP formation.

In addition to the polymer precursors, the external cross-linker $Sorb_2$ (**28**), containing two sorbic alcohol moieties was prepared for the first time in one synthetic step. Malonic acid was esterified with two equivalents of sorbic alcohol in a Steglich

esterification, employing EDC·HCl and DMAP in dry DCM under inert conditions (yield: 48%) (Scheme 25).

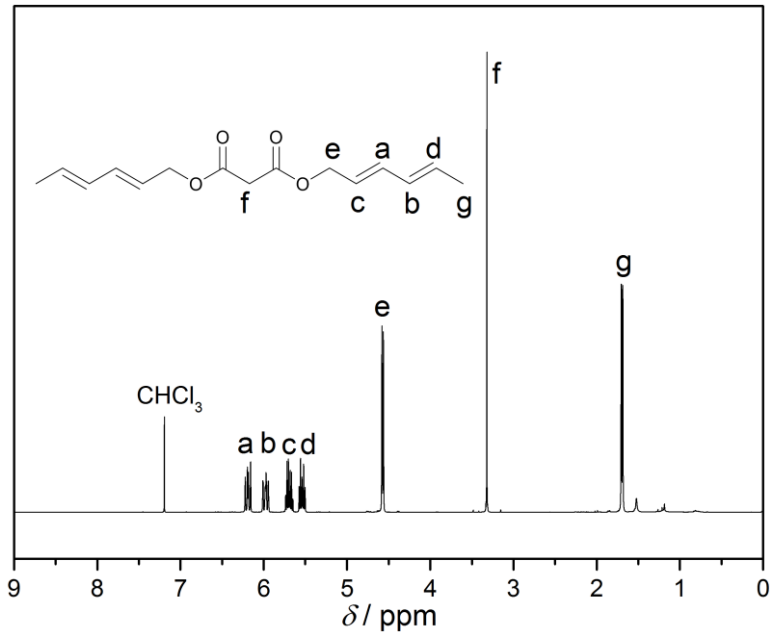

Figure 52: ^{1}H-NMR spectrum of $Sorb_2$ (**28**) in $CDCl_3$.

3.3.2 *Chain Collapse and SCNP unfolding*

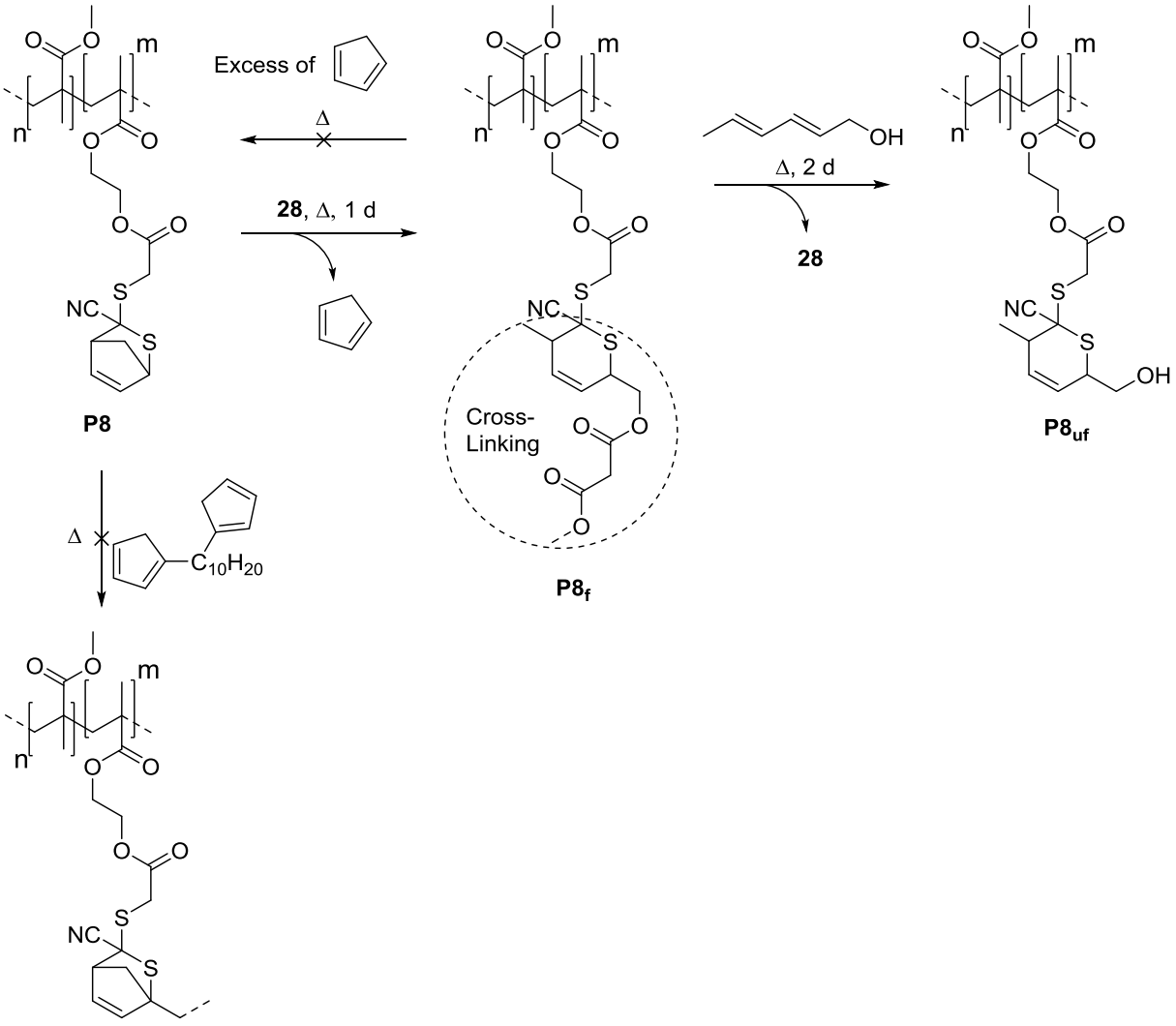

Scheme 26: Synthetic steps in folding of polymer precursors and unfolding of corresponding SCNPs and additional experiments investigating the thermodynamic requirements for single chain folding

To demonstrate the CDTE-sorbic alcohol HDA couple´s capability to cross-link polymeric materials (intramolecularly to SCNPs), each polymer precursor **P8** was transformed into a collapsed chain employing the external cross-linker $Sorb_2$ (**28**). Therefore, highly diluted solutions of **P8** in toluene ($c_{polymer}$ = 0.2 g·L^{-1}) with 0.5 eq. (per CDTE moiety) **28** were stirred for 1 d at 90°C, allowing the sorbic alcohol moieties to substitute the protective Cp from the CDTE groups in the polymer backbone and, thus, cross-link two CDTEs *via* the corresponding DA adduct – resulting in SCNP **P8$_f$** (Scheme 26). To isolate the final SCNPs, the solution was

concentrated *in vacuo* and finally precipitated in cold cyclohexane, yielding the folded single chains as a grayish powder. Comparative SEC analysis of SCNPs **P8$_f$** and their corresponding precursors **P8** reveals that the retention times were shifted to higher values, thus the hydrodynamic volumes of the chains contracted and SCNPs were successfully formed (Figure 53, Figure 54a). With regard to the obtained shifts in apparent molecular weight for the library of four precursor polymers certain general trends in SCNP formation can be confirmed (Table 4). Firstly, collapsed chains exhibit slightly reduced dispersity of (apparent) molecular weight distributions compared to their starting materials. Secondly, higher CDTE ratios in the precursor backbone led to higher relative shifts (**P8B** vs. **P8C**), since the cross-linking density increases likewise. Further, longer precursor chains result in stronger absolute and relative (apparent) decreases in the peak molecular weight at comparable cross-linking densities (**P8C** vs. **P8A** vs. **P8FRP**). The HDA reaction between CDTE and **28** as the molecular mechanism for SCNP folding was verified *via* ^{1}H-NMR spectroscopy of the representative SCNP **P8A$_f$** (Figure 54b). ^{1}H-NMR analysis reveals that the resonances a and b corresponding to Cp-protected CDTE decrease significantly during the folding process and the new resonances c and d can be assigned to the adduct with **28**, hence verifying the successful cross-linking *via HDA* chemistry. The residual 14% of initial Cp-protected CDTE was attributed to shielding effects in the collapsed chain, preventing further reaction with **28**, due to steric hindrance. This hypothesis is supported by the lack of further shift in SEC after 1 d reaction time (thus no further chain contraction), which indicates that the single chain folding has reached its maximum.

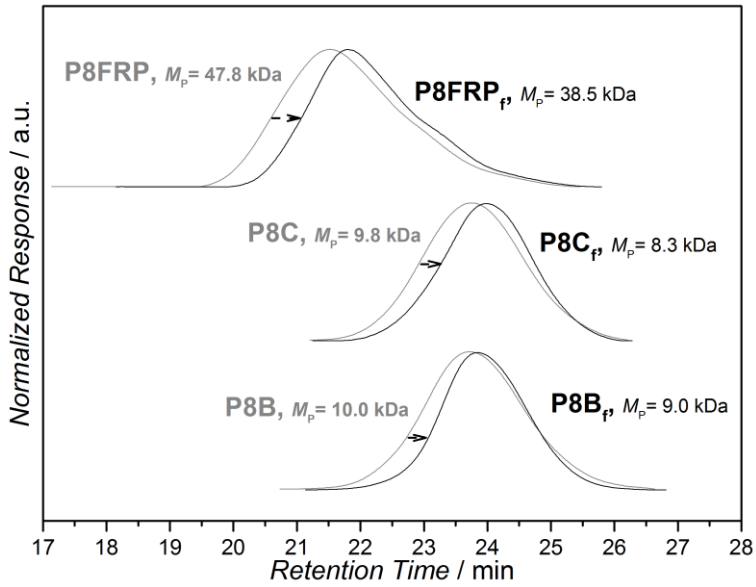

Figure 53: Comparative SEC analysis of single chain folding of the precursors **P8B**, **P8C**, **P8FRP** with calculated M_P values of open chain polymers and corresponding SCNPs

Precursor (M_P, $Đ$, mol% **15**)	SCNP (M_P, $Đ$, ΔM_P, $\Delta\%M_P$)	Unfolded SCNP (M_P, $Đ$)
P8A, 13.8 kDa, 1.3, 17%	**P8A$_f$**, 11.7 kDa, 1.2, -2.1 kDa, -15%	**P8A$_{uf}$**, 14.0 kDa, 1.2
P8B, 10.0 kDa, 1.3, 10%	**P8B$_f$**, 9.0 kDa, 1.2, -1.0 kDa, -10%	-
P8C, 9.8 kDa, 1.3, 17%	**P8C$_f$**, 8.3 kDa, 1.2, -1.5 kDa, -15%	-
P8FRP, 47.8 kDa, 1.6, 15%	**P8FRP$_f$**, 38.5 kDa, 1.5, -9.3 kDa, -19%	-

Table 4: Summarized SEC data on folding and unfolding sequences

SCNP unfolding was demonstrated with the representative SCNP **P8A$_f$**, which was heated in a solution with 5 eq. sorbic alcohol in toluene ($c_{polymer}$ = 0.2 g·L^{-1}) to 90 °C for 2 d, allowing **28** to be expelled by sorbic alcohol from the CDTEs in the polymer backbone, thus opening cross-links and unfolding the SCNP to an open chain **P8A$_{uf}$** (Scheme 26). The entire folding-unfolding sequence of **P8A** was monitored by ^{1}H-NMR spectroscopy, SEC and DLS (Figure 54). SEC (a) and DLS (c) data

consistently demonstrate the decrease in hydrodynamic volume in the first folding step to **P8A$_f$** (- 15% apparent peak molecular weight) and a subsequent increase back to the initial value of the precursor **P8A** for the unfolded SCNP **P8A$_{uf}$**. As already alluded to above, the comparative ^{1}H-NMR spectra (b) of the sequence reveal that folding exhibits shielding effects, allowing only 86% of the CDTEs to form cross-links with **28** and keeping residual 14% of the Cp-protected CDTEs unreacted, possibly due to steric hindrance. Longer reaction times for the folding process do not result in any shifts in SEC and DLS, further supporting the assumption of shielding processes, drawn from ^{1}H-NMR analysis. Moreover, unfolding of **P8A$_f$** allows sorbic alcohol to access each CDTE in the backbone, as residual Cp-protection is decreased to 0% during unfolding.

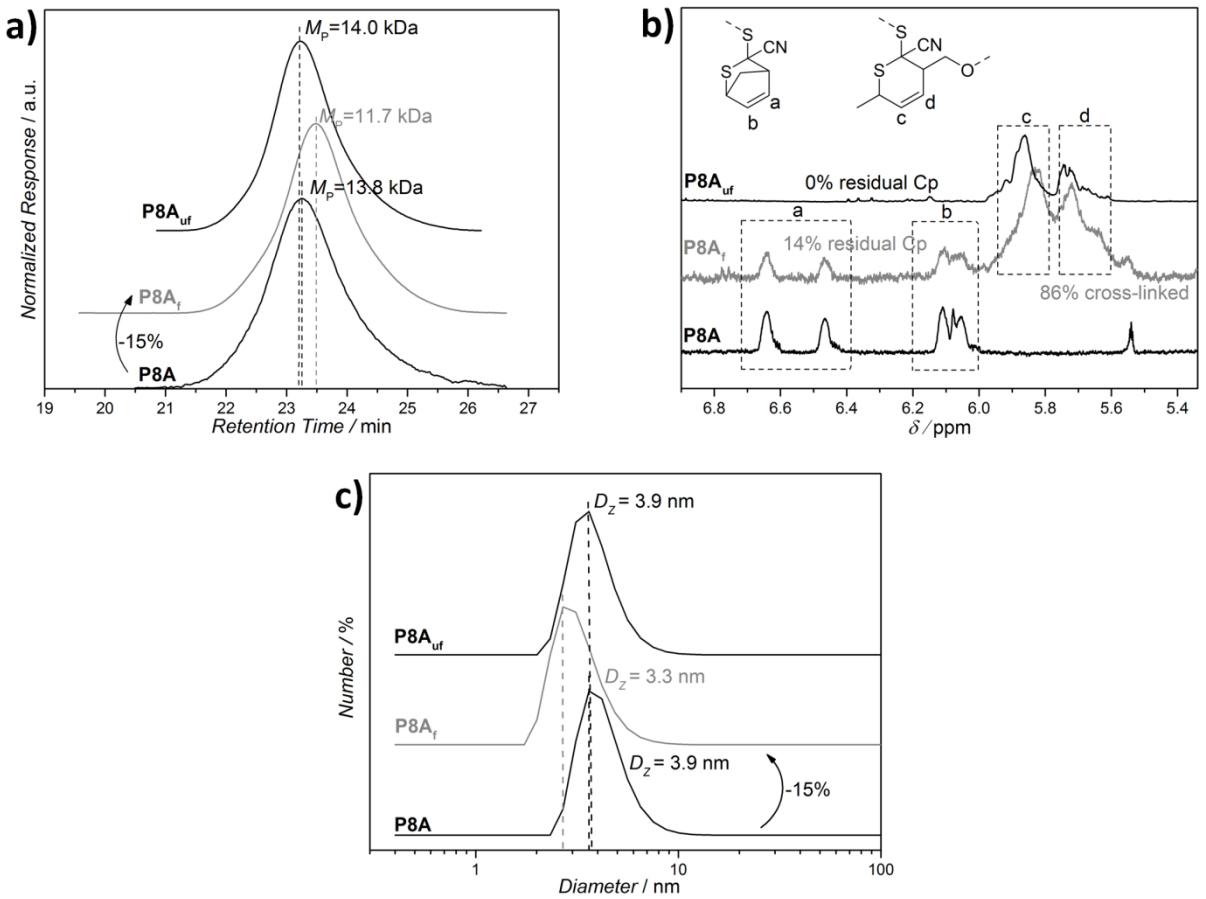

Figure 54: Collated analytic data on folding and subsequent unfolding of precursor **P8A**. (a) Sequential SEC analysis demonstrates excellent folding and complete unfolding of the polymer chain to the open chain **P8A$_{uf}$**. (b) Comparison of ^{1}H-NMR spectra reveals 14% residual Cp in the folded single chain **P8A$_f$**, which react entirely in the sequential unfolding step towards **P8A$_{uf}$**. (c) DLS analysis verifies single chain folding and unfolding.

Kinetic analysis of the folding-unfolding sequence of **P8A** (Figure 55) reveals that folding is faster (1 d) than unfolding (2 d) under comparable conditions (neglecting the five times higher concentration of sorbic alcohol moieties in the unfolding step, which is expected to accelerate unfolding). Two possible explanations for the comparably slower unfolding are presented and supposably both are valid to a certain extent. From a thermodynamic point of view, the adduct of CDTE with **28** is more stable than the Cp-adduct. Therefore, at constant temperature the concentration of free CDTE required for reaction with sorbic alcohol is smaller and the subsequent reaction step becomes slower. Secondly, steric hindrance of the CDTEs inside the collapsed polymer coils, which was hypothesized before with regard to ^{1}H-NMR analysis, delays the unfolding kinetics.

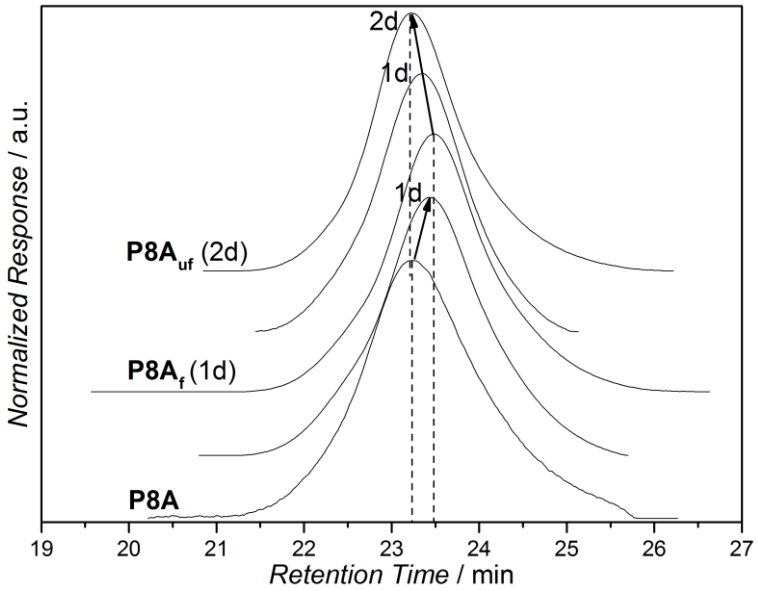

Figure 55: Kinetic data on folding of **P8A** and unfolding of **P8A$_f$** derived *via* sequential SEC analysis.

In addition, the general requirement for a thermodynamic driving force for the collapse of a polymeric precursor to a SCNP was confirmed in additional experiments (Scheme 26). Attempts to fold **P8A** to a SCNP employing a Bis-Cp linker, instead of $Sorb_2$ (**28**) were unsuccessful and no shifts in the SEC elugrams were observed. As expected from theory a more stable HDA adduct (compared with the Cp-protected CDTE) has to be formed in order to force the polymer chain in a collapsed SCNP. For unfolding of a SCNP, which is a thermodynamically unfavored chain state, however, a path *via* a less stable adducts (back to a Cp-protected CDTE) is not followed by the

system, even if an excess of reaction partner is provided. Allowing the SCNP to relax into an open chain by an HDA adduct of the same thermodynamic stability (sorbic alcohol), yields unfolded polymer chains **P8A$_{uf}$**. These results further confirm that the loss in conformational entropy of an open polymer chain has to be thermodynamically compensated by the cross-linking reaction in order to obtain an SCNP. Consequently, if the system lacks a thermodynamic driving force, an open chain state is preferred.

4 CONCLUSIONS

Within the current thesis thermoreversibly cross-linkable polymer matrices for nano-composites (NCs), inspired by nacre, were prepared, adapting two different cross-linking mechanisms. The first mechanism is based on the dimerization of 2-ureido-4-pyrimidone (UPy) *via* hydrogen bonding. Employing UPy as cross-linker, three synthetic approaches (star, RAFT, conventional FRP) towards matrices have been implemented, including the synthesis of two new UPy monomers (**12**, **13**) and synthesis of a library of UPy functionalized polymer architectures (**P3**, **P4**, **P5**).

In the star approach five star polymers **P3** (M_n = 7.0-48.0 kDa) with varying numbers of arms (four and six), endgroup functionalized with UPys, were prepared in five synthetic steps, starting with an AGET ATRP of $MeOEGMA_{300}$ and commercially available 4/6f-Bib. In the second step the bromine endgroups were substituted with NaN_3 and subsequently employed in a CuAAc, introducing alkyne functionalized UPy **9** as endgroups. Characterization was carried out *via* ^{1}H-NMR spectroscopy, SEC and IR spectroscopy, revealing the excellent control of the AGET ATRP over the molecular weight distribution, as well as complete endgroup functionalization. Since UPys complex Cu ions, preventing removal of residual Cu after CuAAc employing standard polymer purification protocols (*e.g.* dialysis, precipitation, extraction), non-destructive electrolysis of aqueous polymer solutions was pioneered and systematically studied with regard to residual Cu contamination remaining as a function of electrolysis time, voltage and concentration. Electrolysis times of 44 h and voltages of 12 V (at c(UPy) = 0.0134 mmol·mL^{-1}) were identified as optimal conditions to remove 98% of the Cu contamination. The non-destructive polymer electrolysis was monitored *via* AES, ^{1}H-NMR spectroscopy, SEC and successfully published as new tool for purification of ion complexing, water-soluble polymers.[208]

In the second (RAFT) approach, allowing higher degrees of UPy functionalization compared with the star approach, two UPy monomers were synthesized in two and three synthetic steps (including synthesis of the new UPy monomer **12**) and copolymerized with $MeOEGMA_{300}$ in a RAFT process controlled by 4-Cyano-4-(phenylcarbonothioylthio)pentanoic acid. A library of four short, linear polymers **P4** varying in chain lengths (M_n = 23.8-38.8 kDa), UPy flanking units (urea, urethane) and UPy ratios (3-10 mol%) was prepared. The polymers **P4** were characterized *via*

SEC and ^{1}H-NMR spectroscopy. Due to the limited solubility of the flanked UPy monomers **11** and **12**, even in polar solvents at elevated temperature, high UPy ratios in the final copolymers **P4** were synthetically demanding.

Following the third (FRP) approach, the new UPy monomer UPy-EG-MA (**13**) was synthesized within two synthetic steps, resulting in a urethane flanked UPy motif with ethylene glycol units for enhanced solubility and improved copolymerization behavior with methacrylate monomers. Monomer **13** was copolymerized in a FRP with $MeOEGMA_{500}$ in distinct ratios resulting in a library of four long polymer chains **P5** varying in molecular weights (M_n = 161.0-414.0 kDa) and UPy ratios (0-20 mol%), which were characterized by ^{1}H-NMR spectroscopy and SEC.

The three UPy polymer libraries (including 13 polymers in total) were employed in layered nano-composites, inspired by the structuring of nacre, and fabricated with sodium fluorohectorite (NHT) nano sheets *via* film casting, based on aqueous solutions/dispersions. Distinct wt% ratios (37:66, 50:50 and 66:37) of NHT filler and polymer matrix were employed and the mechanic performances of the NC films were investigated *via* tensile testing. The influence of the arm length, the number of arms in the star approach (**P3**), the filler-matrix ratio, the UPy ratios in copolymers, the type of UPy flanking unit and the impact of molecular weight on the mechanic performance of the layered NC films were systematically studied. In agreement with literature low UPy functionalizations (resembling long arms in the star approach), result in soft and ductile films, while high UPy functionalization (resembling short arms in the star approach) increases tensile strength at expense of ductility. The influence of flanking ureas and urethanes, which are known to increase the dimerization strength of UPy, follows no clear trend with respect to the mechanic performance of NCs. Higher molecular weights at constant UPy ratios apparently lead to a decrease in tensile strength but an increase in ductility, however, the number of arms has no influence on mechanic performance in the investigated regime. Moreover, in agreement with literature, increased NHT loadings yield strong but brittle films. For two matrices (**$P5_{14}$**, **$P5_{10}$**), plateaus of inelastic deformation in tensile testing of the NC, similar to nacre, were observed. The plateau heights, however, were significantly lower but increased with the UPy ratio and chain length to a certain point of drastic decrease in mechanic performance (**$P5_{20}$**). It was hypothesized that the optima of chain length (entanglement vs. gallery widening) and

UPy ratio (cross-linking vs. decreased chain dynamics) have to be balanced carefully to obtain high performance matrices.

The second mechanism of thermoreversible cross-linking in a polymer matrix was based on the CDTE-sorbic alcohol HDA couple. The two corresponding HDA monomers, each bearing one of the complementary HDA functions, were synthesized in one and three synthetic steps, including the first synthesis of CDTE-MA (**15**). Subsequently, the HDA monomers were copolymerized with $MeOEGMA_{500}$ *via* FRP resulting in the water-soluble copolymer **P6** (M_n = 127.2 kDa, 10 mol% HDA comonomers) within five synthetic steps, resulting in an HDA matrix for reversibly cross-linked NCs. The HDA matrix was employed in NC film casting and films were additionally heated after casting to induce HDA cross-linking. Tensile tests, however, indicated that the HDA matrix resembles in performance rather a non-functionalized polymer, than an UPy matrix with comparable cross-linking capacity. Furthermore, mechanic performance of HDA NCs was not increased by heating steps, which should in principle result in firmer cross-linking. In conclusion, the results indicate that cross-linking at the presented copolymer composition is insufficient and comparably lower than for similar UPy-matrices, potentially due to the reduced amount of binding partners per HDA moiety compared to UPys (based on the hetero-complementary cross-linking situation in HDA chemistry).

The second aim of the current thesis was the study of hydrogen bonding at the interface between physisorbed polymers on the clay surfaces and the polymer matrix. Employing macroscopic silicon wafers as model systems for clay surfaces, wafers were activated and functionalized with the tetrazole-functionalized silane **18** that was prepared in two steps before, resulting in the surfaces **S1** as substrates for further functionalizations with hydrogen bonding motifs *via* photochemical NITEC reaction. From a microscopic point of view, the lack of immobilized hydrogen bonding partners form solution on the surface potentially originates from (i) the lack of hydrogen bonding at the wafer-solution interface at all or (ii) hydrogen bonding within each phase (surface-surface, solution-solution) independently from the interface. Therefore, the self-complementary (UPy) and hetero-complementary (SOA-AOA) system, in which the later situation is inaccessible, were studied, clearly identifying the dominant binding situation at the interfaces.

In order to investigate the self-complementary situation for UPy dimers, maleimide-functionalized UPy **22** was synthesized in a convergent strategy within five steps, including two new molecules (**21**, **22**). In a next step, **22** was covalently bound to a distinct area on the wafer **S1** *via* photochemical NITEC reaction between surface-immobilized tetrazoles **18** and the maleimide **22**. During photochemical immobilization a sample holder was employed to shield parts of the surface from UV-irradiation, resulting in spatially resolved, UPy-functionalized wafers **S2** upon reaction. The successful functionalization of **S2** with UPy **22** was demonstrated *via* ToF-SIMS analysis. UPys with halogen labels as chemical markers for ready detection in ToF-SIMS analysis of the wafer surface were synthesized starting with UPy-NCO (**8**) as platform that was functionalized with CF_3 and Br moieties in a single synthetic step. Thereby, the new molecule UPy-CF_3 (**23**) was synthesized in two synthetic steps in total. In addition, enhancing adsorbent solubility and potential numbers of UPy-UPy interactions per molecule, a third, polymeric, fluorine labeled UPy was prepared employing conventional FRP of TFEMA, BMA and UPy-MA (**10**), which was prepared in one synthetic step, resulting in the polymeric adsorbent **P7** (M_n = 63.0 kDa, $Đ$ = 1.4, 4 mol% **10**, 8 mol% TFEMA). A library of ten immobilization experiments, employing **23** and **P7** as adsorbents onto **S2**, was investigated, systematically varying the solvent type ($CHCl_3$, toluene, DCM), the solvent volume (2-12 mL) and the procedure (immersion, rinsing) of the washing step after exposure of **S2** to a solution of adsorbent. For each sample **S3**, ToF-SIMS analysis was performed, comparing a fragment corresponding to the halogen label (depicting binding UPys from solution) and a characteristic UPy fragment (corresponding to the sum of UPys bound covalently and adsorbed from solution). Washing *via* immersion of **S3** proved to be insufficient to remove physisorbed adsorbent from non-UPy-functionalized areas of the wafer, independently from the time of exposure. In the case of washing of the surface with $CHCl_3$, a larger solvent volume reduced the amount of physisorbed adsorbent outside of the UPy-functionalized area of the surface significantly, making it a suitable tool to remove undesired, physisorbed UPys. However, the identical effect was observed for adsorbents in UPy-functionalized zones of the wafer surface and, very critically, no significantly higher affinity of adsorbent to UPy-functionalized substrate was observed. Toluene, as less polar solvent, was unable to remove physisorbed UPys from any parts of the surface, while DCM yielded comparable results to $CHCl_3$. For both, small molecule **23** and

polymeric adsorbent **P7**, no contrast in immobilization behavior towards UPy-functionalized or non-functionalized substrate was observed. Consequently, in the studied self-complementary situation of UPy dimerization at a surface, hydrogen bonding motifs at the interface of solution and substrate cannot have any influence on immobilization and, therefore, hydrogen bonding with partners from solution must be absent in such systems. Otherwise a higher affinity of adsorbents (**23**, **P7**) to UPy-functionalized areas of the wafer compared to non-functionalized parts would have been observed. Therefore, in such a system two microscopic scenarios are possible: (i) absence of any type of dimerization, based on hydrogen bonding and (ii) dimers, formed from binding partners in the same phase (surface-surface, solution-solution), exhibit higher stability than dimers based on interfacial hydrogen bonding (surface-solution). With the employed analytic methods, the two scenarios could not be distinguished further and, therefore, a second, hetero-complementary model system based on the SOA-AOA couple was investigated, in which the latter scenario (ii) was inaccessible, giving the opportunity for an in depth study of the microscopic behavior.

Fabricating the hetero-complementary model system, AOA-NHBoc was deprotected and coupled to a maleimide in three additional synthetic steps, resulting in AOA-Mal (**27**), including the synthesis of two the new molecules **26** and **27**. A globally tetrazole-functionalized silicon wafer **S1** was functionalized with AOA **27** *via* NITEC reaction. Spatial resolution was achieved by combination of a sample holder and a shadow mask, shielding parts of the surface **S1** from UV-irradiation. Thereby, the surfaces **S4**, with different shapes of AOA-functionalization (large quadrangular area or circles) were obtained and could be employed in subsequent immobilization experiments. Further investigating the microscopic picture of dimerization at interfaces, based on hydrogen bonding, a PMMA that was endgroup-functionalized with SOA was employed as adsorbent from solution onto **S4**. Very interestingly, after a washing step, a good contrast of immobilization between AOA-functionalized substrate and unfunctionalized wafer was obtained (**S5**), as visualized *via* ToF-SIMS analysis of a fragment corresponding to PMMA. Even more critically, employing a polar solvent mixture, immobilized material could be washed off entirely and could subsequently be immobilized again exclusively on a substrate with complementary hydrogen bonding partners. Within four immobilization-washing cycles only little decrease in loading capacity of the surface **S4** was observed and qualitative ToF-SIMS images, moreover, demonstrated stability of the shape of the area of

immobilization. The reversible immobilization, based on the SOA-AOA couple, was consequently published as a new benchmark for the fewest number of hydrogen bonding sites for surface encoding.[96] Since the hetero-complementary model systems exhibits interfacial hydrogen bonding, in the self-complementary system (based on UPy dimers) hydrogen bonding cannot be absent entirely (scenario i). Therefore, the lack of immobilization partners from solution on an UPy-functionalized substrate was attributed to the competing dimers in the same phase (solution-solution, surface-surface), which consequently have to be favored over mixed dimers (ii). Transferring the results of the model systems to the level of NCs with reversibly cross-linked matrices based on self-complementary UPy dimerization, it can be expected that a significant amount of UPys are inaccessible for cross-linking at the interface of physisorbed matrix on the clay particles and surrounding matrix, due to competing, dynamic cross-linking events. However, taking into account the results of the mechanic testing of the NCs derived from the first project in this thesis, the remaining (accessible) UPys still exhibit a significant impact on material properties.

In a third project, examined in this thesis, the CDTE-sorbic alcohol HDA couple, which was initially employed in thermoreversibly cross-linked polymer matrices for nano-composite fabrication, was demonstrated as reversible cross-linking chemistry in SCNPs.

Therefore, CDTE-MA (**15**), which was prepared as a new molecule within three synthetic steps and used before in the HDA matrix in the first project, was employed in several copolymerizations with MMA (RAFT and conventional FRP). Thereby, a library of copolymers with varying chain lengths (M_p = 9.8-47.8 kDa) and comonomer ratios (10-17 mol% **15**), which were characterized *via* ^{1}H-NMR spectroscopy and SEC, was built-up. The initial comonomer composition of the polymerization mixture was retrieved in the final polymer precursors **P8** and molecular weight distributions were monomodal (and narrow for RAFT polymers).

Following a cross-linker mediated approach towards intramolecular cross-linking, the external cross-linker $Sorb_2$ (**28**), including two sorbic alcohol moieties, was synthesized in one synthetic step for the first time (yield: 48%).

Employing the entire library of SCNP precursors, in total four polymers **P8** were collapsed to SCNPs using equimolar amounts (with regard to CDTEs) of HDA cross-

linker **28** at elevated temperature in highly dilute solutions, thus allowing the protective Cp-CDTE adduct to be substituted by the corresponding adduct of sorbic alcohol moieties of the linker. The SCNP formations to **P8$_f$** were monitored *via* sequential SEC, revealing an apparent shift to lower molecular weights, due to the decreased hydrodynamic volumes of collapsed chains compared with their precursors, for each polymer. Since the library of four polymers enabled studying influences of molecular weight and copolymer composition on the molecular folding, distinct trends of SCNPs could be confirmed: (i) The dispersity of the molecular weight distribution of an SCNP is less than the dispersity of its open chain precursor. (ii) The absolute and relative apparent decrease in peak molecular weight of a SCNP in comparison to its precursor is increased, when the chain length of the precursor is increased. (iii) Precursor polymers with similar chain lengths but increased potential cross-linking density (resembling mol% of **15** in the polymer precursor) show higher absolute and relative apparent decrease of molecular weight. ^{1}H-NMR analysis of the representative SCNP **P8A$_f$** verifies the CDTE-Sorb$_2$ adduct as source of SCNP formation and, very interestingly, indicated that even after reaching the maximum of chain collapse in SEC, 14% residual Cp-protected CDTE remained in the polymer backbone. The unreacted Cp-protected CDTE was attributed to shielding effects, preventing reaction with **28**, due to steric hindrance in the collapsed polymer coil.

Demonstrating the reversibility of the CDTE-sorbic alcohol HDA couple in SCNP formation, the representative SCNP **P8A$_f$** was unfolded back to an open chain state **P8A$_{uf}$** by substitution of cross-linker **28** with neat sorbic alcohol. The entire folding-unfolding sequence was monitored *via* ^{1}H-NMR spectroscopy, SEC and DLS. The latter two methods successfully verify the effective folding to a SCNP and complete unfolding towards an open chain state, exhibiting the initial hydrodynamic volume of the polymer precursor **P8A** in excellent quantitative agreement. Shielding effects, observed in the step of SCNP formation were further confirmed by ^{1}H-NMR analysis of the unfolded polymer **P8$_{uf}$**, in which all CDTEs react completely to the corresponding HDA adduct with sorbic alcohol, since such effects are absent in the targeted open chain state. In addition, the kinetic aspects of single chain (un)folding were studied: SEC samples were drawn from the (un)folding reaction mixtures and analyzed, revealing that maximal folding occurs within 1 d but unfolding takes 2 d (under similar reaction conditions). Two explanations for the kinetic stability of each chain states were discussed: (i) Since the Cp-CDTE adduct is thermodynamically

less stable than the $Sorb_2$-CDTE adduct, the equilibrium concentration of free CDTE at similar temperature is increased and, therefore, the corresponding reaction (folding) is faster. (ii) Due to shielding effects in the collapsed chain state, CDTEs are less accessible for unfolding, than in the precursor state for folding.

Confirming the general requirement of a thermodynamic driving force for a single chain collapse, additional experiments were conducted, which demonstrate the lack of (un)folding, if unsuitable reaction partners are chosen. Precursor polymers **P8** could not be forced into an unfavorable, collapsed chain state by a bisCp-linker with similar thermodynamic stability (compared to the protective Cp), since the loss in conformational entropy of the polymer chain is not compensated under these conditions. On the other hand, the collapsed chain $\mathbf{P8_f}$ could not be unfolded by even employing an excess of Cp, which would result in a less stable CDTE adduct, but a more favorable chain state. Therefore, in general, at similar adduct stability open chains are preferred, while collapses are achieved only with increased adduct stabilities. The reversible SCNP formation on the basis of HDA chemistry was successfully published.[211]

In summary, in the present thesis, which has to be understood in context of a larger collaboration aiming for thermoreversibly cross-linked nacre mimetics, dynamic covalent and supramolecular bonds were employed in a broad spectrum of interfaces. Libraries of different polymer architectures and bonding motifs were applied as polymer matrices in NC formation and the results of mechanic testing were evaluated systematically with respect to the matrix properties. Model studies of macroscopic hydrogen bonding surfaces provided insight in homo- and hetero-complementary binding situations on interfaces in general, revealing that most homo-complementary motifs are unavailable for interfacial binding. In context of cross-linking capacity, an HDA couple, which was utilized in matrices before, was demonstrated as reversible cross-linking chemistry in SCNPs. Therefore, a valuable contribution to the understanding of dynamically cross-linked layered NCs was provided. General trends and aspects of such biomimetic materials were identified, conclusively interpreted and, moreover, cross-linking capacities of the chosen chemistry was demonstrated.

5 EXPERIMENTAL PART

5.1 Materials

Acetone (p.a., VWR), acetonitrile (ACN) (Normapur, VWR). 2-amino-4-hydroxy-6-methylpyrimidine (2-Amino-6-methyl 4(3H)-pyrimidone) (98 %, Alfa Aesar), (3-aminopropyl)triethoxysilane (APTES) (99 %, Sigma), ammonium hydroxide (p.a., Acros), ascorbic acid (99 %, Acros), 2,2'-Azobis(isobutylonitrile) (AIBN) (VWR) was recrystallized twice from methanol, bis(hydroxymethyl)propionic acid (98 %, Sigma), 2,2´-bipyridine (bpy) (99 %, ABCR), bromoacetyl bromide (98 %, Alfa Aesar), bromisobutylbromide (97 %, ABCR), 2-bromoethyl isocyanate (97 %, Sigma), butyl methacrylate (BMA) (99%, Sigma), carbon disulfide (99.9 %, Sigma), chloroform-d1 (99.8 %, EURISO-TOP), copper(I) bromide (98 %, Fluka), copper(II)bromide (99 %, Fluka), 2-cyano-2-propyl benzodithioate (CPDB, 97 %, Sigma-Aldrich), 4-Cyano-4-(phenylcarbonothioylthio)pentanoic acid (Sigma), cyclopentadiene (Cp) was freshly distilled from dicyclopentadiene (>95%, Sigma), dialysis membranes (MWCO 2.000 , Roth), dibutyltin dilaurate (DBTDL) (95 %, Sigma), dichloromethane (DCM) (p.a., VWR), anhydrous dichloromethane (DCM) (99.8 %, AcroSeal®, Acros), *N,N'*-dicyclohexylcarbodiimide (DCC) (99 %, Acros), 1,6-diisocyanato hexane (98%, Sigma), 2,2-dimethoxypropane (98 %, ABCR), 1-(3-dimethylaminopropyl)-3-ethylcarbodiimide hydrochloride (EDC·HCl) (98 %, Alfa Aesar), 4-dimethylaminopyridine (DMAP) (99 %, Acros), dimethylformamide (DMF) (99.8 %, Acros), anhydrous dimethyl sulfoxide (DMSO) (99.7 %, Acros), dimethyl sulfoxide-d_6 (DMSO-d_6, 99.8 %, EURISO-TOP), ethanol (p.a., VWR), ethanolamine (98 %, Sigma), ethyl acetate (EE) (p.a., VWR), 4-formyl benzoic acid (96%, Acros), furan (>99 %, Sigma), *n*-hexane (p.a., VWR), hydrochloric acid (p.a., Roth), hydrogen peroxide (35%, Roth), hydroxyethyl methacrylate (HEMA) (97%, Sigma), 2-isocyanatoethylmethacrylate (98 %, Sigma), maleic andydride (>99 %, Sigma), methacryloyl chloride (>97 %, Sigma), malonic acid (99%, Alfa Aesar), methanol (MeOH) (p.a., VWR), Pentaerythritol tetrakis(2-bromoisobutyrate) (4f-Bib) (97%, Sigma-Aldrich), *N,N,N´,N´,N´´*-penta-methyldiethylentriamine (PMDTA) (for synthesis, Merck), poly(ethylene glycol) methyl ether methacrylate ($MOEGMA_{300}$) (Sigma), poly(ethylene glycol) methacrylate ($OEGMA_{360}$) (Sigma), propargyl alcohol (99 %, Alfa Aesar), propargylamine (98%, Sigma), anhydrous pyridine (99.5 %, Acros),

sodium azide (99.5 %, Sigma), sodium bicarbonate (99 %, Roth), sodium cyanide (97%, Sigma), sodium hydroxide (99 %, Roth), sodium nitrite (98 %, Alfa Aesar), sodium sulfate (99 %, Roth), sorbic alcohol (98 %, Alfa Aesar), sulfuric acid (96%, roth), tetrahydrofuran (THF) (p.a., VWR), trifluoroethanol (>99 %, Sigma), 2,2,2-trifluoroethyl methacrylate (TFEMA) (99%, Sigma), triethylamine (NEt_3) (99 %, Acros), trifluoracetic acid (TFA) (99 %, ABCR), toluene (p.a., VWR), *p*-toluenesulfonic acid monohydrate (98 %, Sigma), *p*-toluene sulfonyl hydrazide (98 %, Alfa Aesar),

5.2 Instrumental Data

^{1}H NMR Spectroscopy was performed using a Bruker Ascend 400 spectrometer (^{1}H, 400 MHz; ^{13}C, 100 MHz). All samples were dissolved in chloroform-d^1. The δ-scale is referenced to the internal standard tetramethylsilane (TMS, δ = 0.00 ppm).

ESI-MS (Electrospray Ionization Mass Spectrometry) was performed on a Q Exactive (Orbitrap) mass spectrometer (Thermo Fisher Scientific, San Jose, CA, USA) equipped with a HESI II probe. The instrument calibration was carried out in the *m/z* range 74 – 1822 using calibration solutions from Thermo Scientific. A constant spray voltage of 4.7 kV and a dimensionless sheath gas of 5 were applied. The capillary temperature and the S-lens RF level were set to 320 °C and 62.0, respectively. The samples were dissolved on a THF:MeOH micture (3:2) containing 100 μmol of sodium triflate and injected with a flow of 5 $\mu L \cdot min^{-1}$.

Alternative measurements were performed on a LXQ mass spectrometer (ThermoFisher Scientific) exhibiting an atmospheric pressure ionization source. The calibration was carried out employing standards of caffeine, Met-Arg-Phe-Ala acetate (MRFA) and a fluorinated phosphazenes (Ultramark 1621) received from Sigma-Aldrich. The samples were prepared in a THF/MeOH solution (3 : 2) with sodium trifluoroacetate (14.0 $mg \cdot L^{-1}$) and were measured *via* direct injection.

SEC (Size Exclusion Chromatography) measurements were performed on a Polymer Laboratories PL-GPC 50 Plus Integrated System, comprising an autosampler, a PLgel 5 µm bead-size guard column (50 × 7.5 mm) followed by three PLgel 5 µm Mixed-C and one PLgel 3 µm Mixed-E columns (300 × 7.5 mm) and a differential refractive index detector using DMAc as the eluent at 50 °C with a flow rate of 1 $mL \cdot min^{-1}$. Calibration was carried out employing linear poly(styrene) standards ranging from 476 to 2.5×10^6 $g \cdot mol^{-1}$.The injected polymers were dissolved in DMAc (HPLC-grade) with a concentration of 2 $mg \cdot mL^{-1}$.

***DLS* (*Dynamic Light Scattering*)** was performed on a Zetasizer Nano ZS light scattering apparatus (Malvern Instruments, UK) equipped with He-Ne laser (at a wavelength of 633 nm, 4 mW). The Nano ZS instrument incorporates a non-invasive backscattering (NIBS) optic with a detection angle of 173°. The polymer solutions were prepared in DMSO ($c_{Polymer}$ = 2 $g \cdot L^{-1}$) and were subsequently filtered into quartz

cuvettes. The prepared samples were stabilized prior to DLS analysis at ambient temperature (20 °C) for 120 seconds. All values of the apparent hydrodynamic diameter for each polymer mixture were averaged over six measurements (average of 20 runs/measurement), and were automatically provided by the instrument using a cumulative analysis.

ToF-SIMS (Time-of-Flight Secondary Ion Mass Spectrometry) was performed on a TOF.SIMS5 instrument (ION-TOF GmbH, Münster, Germany), equipped with a Bi cluster liquid metal primary ion source and a non-linear time-of-flight analyzer. The Bi source was operated in the "high current bunched" mode providing 0.9 ns Bi_3^+ ion pulses at 25 keV energy and a lateral resolution of approx. 4 µm. The short pulse length allowed for high mass resolution to analyze the complex mass spectra of the immobilized organic layers. Images larger than the maximum deflection range of the primary ion gun of 500 × 500 μm^2 were obtained using the manipulator stage scan mode with a pixel distance of 10 µm. Spectra were calibrated on the C^+, CH^+, CH_2^+, CH_3^+; or on C^-, CH^-, CH_2^- and C_2^-, respectively. Primary ion doses were kept below 10^{11} ions/cm^2 (static SIMS limit). Measurements have been carried out by Dr. Alexander Welle (KIT).

AES (Atom Emission Spectroscopy) The Cu content was determined by atomic emission spectroscopy with inductively coupled plasma using an Agilent 725-ES ICP-OES spectrometer, Agilent Technologies. Before measurement, the samples were dissolved in 5 mL 0.2 M HNO_3. The instrument was calibrated in the range of 10 to 100 µg mL^{-1} using Cu standards from SPC SCIENCE. Before measurement, these standards were dissolved in distilled water, acidified with HNO_3, and diluted according to the calibration range. Measurements were performed by Silke Behrens and Sarah Essig (Institut für Katalyseforschung und –technologie,KIT).

FT-IR (ATR IR) (Attenuated Total Reflection Infrared) spectroscopy was conducted employing a VERTEX 80 research spectrometer with a PIKE MIRacle ATR unit and a DTGS detector. The spectra were recorded with a resolution of 4 cm^{-1} and 128 scans and underwent baseline correction as well as atmospheric compensation.

Electrolysis was performed on a custom-built device, comprising a laboratory power supply unit EA-PS 3016-10 B (Elektro-Automatik GmbH&CO KG), platinum electrodes and a magnetic stirrer (Heidolph MR Hei-Mix L).

Mechanical tensile tests were carried out on a DEBEN minitester equipped with a 20N load cell. All measurements were conducted at room temperature and specimens were conditioned at 60% relative humidity for a minimum of 2 days. The specimen sizes used were in the range of 2 cm ×1.25 mm ×35 µm. A nominal strain rate of 0.5 mm/min was used. Experiments were conducted by Dr. Baolei Zhu and Saskia Groer.

For **UV irradiation** an Arimed B6 lamp was employed. The corresponding emission spectrum is provided below (Figure 56).

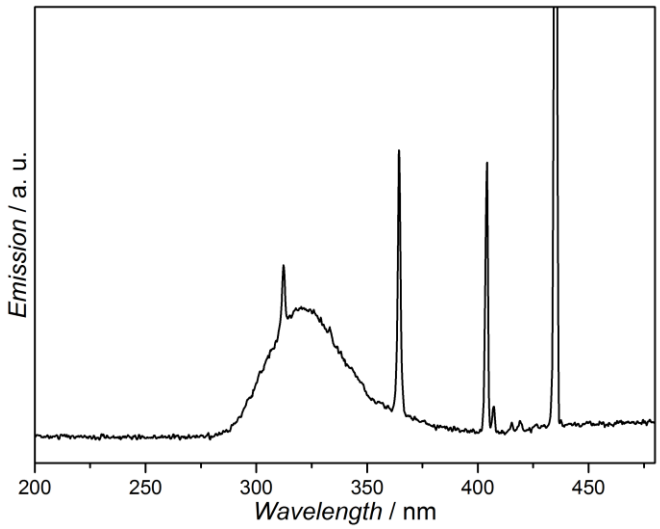

Figure 56: Emission spectrum of an Arimed B6 lamp.

5.3 Small Molecule Synthesis

5.3.1 *UPy-NCO (**8**)*

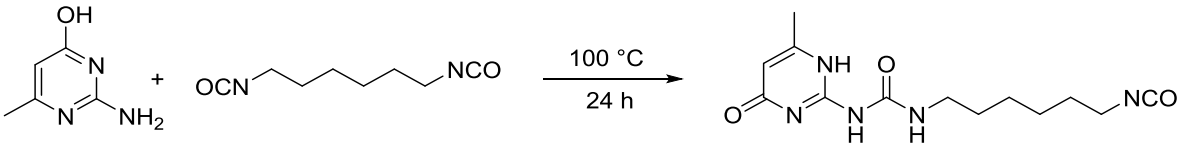

The synthesis procedure is adapted from Mansfeld *et al*.[212] 2.30 g (0.02 mol, 1 eq.) 2-Amino-4-hydroxy-6-methylpyrimidine was suspended in 20 mL (21.00 g, 0.12 mol, 6.0 eq) 1,6-diisocyanato hexane and heated to 100 °C for 24 h. The white solid was filtered off, washed with EE and DCM and dried under reduced pressure at 40 °C to yield the product in excellent purity (5.50 g, 0.019 mol ,95% yield). A ^{1}H-NMR spectrum is provided in Figure 57.

^{1}H-NMR (400 MHz, $CDCl_3$): δ(ppm) = 13.07 (s, 1H), 11.82 (s, 1H), 10.10 (s, 1H), 5.79 (s, 1H), 3.27 (m, 4H), 2.21 (s, 3H), 1.61 (m, 4H), 1.41 (m, 4H).

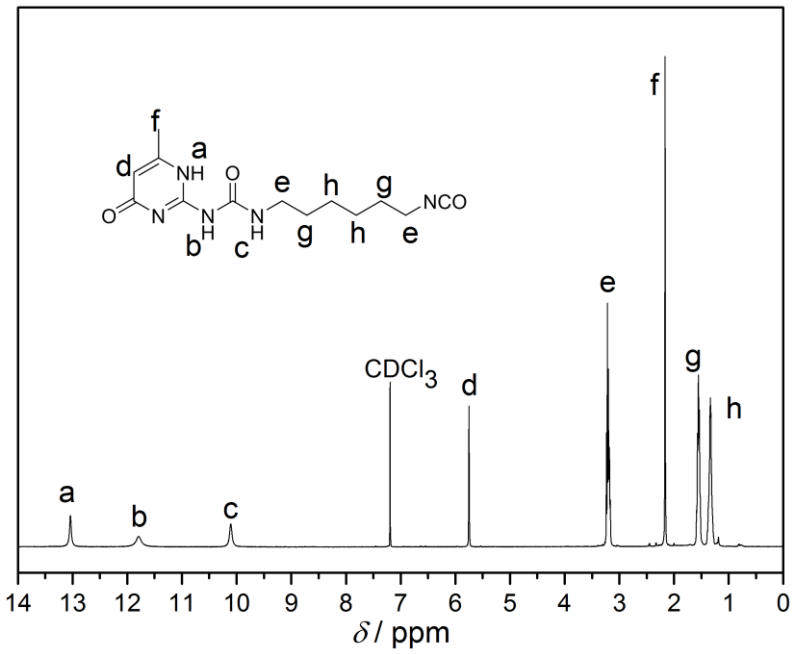

Figure 57: ^{1}H-NMR spectrum of UPy-NCO (**8**) in $CDCl_3$.

5.3.2 *UPy-Urethane-Alkyne (**9**)*

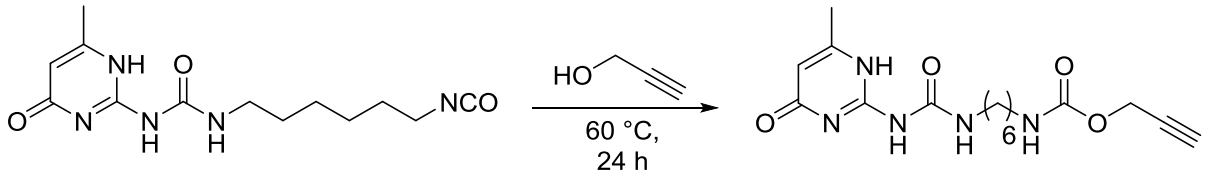

5.368 g (18.3 mmol, 1 eq.) UPy-NCO (**8**) and one drop DBTDL are suspended in 20.00 mL (19.40 g, 346.1 mmol, 19 eq.) dry propargyl alcohol and heated to 60 °C for 24 h. The white solid is filtered off, washed with cyclohexane and DCM and dried resulting in product **9** (3.050 g, 8.3 mmol, 45% yield).

^{1}H-NMR (400 MHz, $CDCl_3$): δ(ppm) = 13.05 (s, 1H), 11.80 (s, 1H), 10.13 (s, 1H), 5.75 (s, 1H), 4.61 (m, 2H), 3.20 (m, 4H), 2.21 (s, 1H), 2.16 (s, 3H), 1.61 (m, 4H), 1.41 (m, 4H).

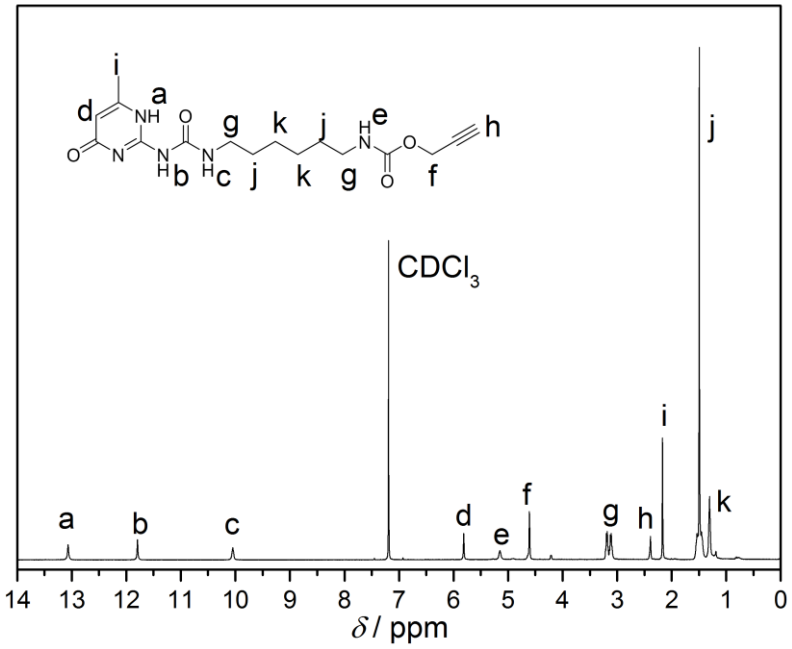

Figure 58: ^{1}H-NMR spectrum of UPy-Urethane-Alkyne (**9**) in $CDCl_3$

5.3.3 *Upy-Urea-Alkyne*

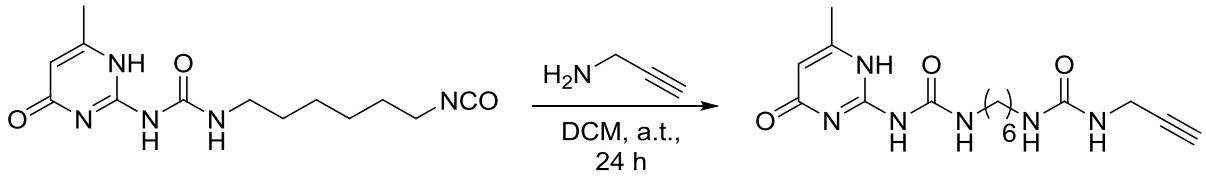

500 mg (1.7 mmol, 1 eq.) UPy-NCO (**8**) and 2.50 mL (2.15 g, 39.0 mmol, 23. eq.) propargylamine were suspended in 8 mL dry DCM and were stirred for 24 h at ambient temperature. The solid was filtered off, washed with acetone and dried (292 mg, 8.4 mmol, 49% yield).

^{1}H-NMR (400 MHz, $CDCl_3$): δ(ppm) = 13.05 (s, 1H), 11.83 (s, 1H), 10.08 (s, 1H), 5.77 (s, 1H), 5.24 (s, 2H), 3.28-3.08 (m, 4H), 2.27 (s, 1H), 2.10 (s, 3H), 1.61-1.38 (m, 4H), 1.38-1.14 (m, 4H).

m/z $([M+Na]^+)_{exp}$ = 371.33, $([M+Na]^+)_{theo}$ = 371.18, $([M_2+Na]^+)_{exp}$ = 719.08, $([M_2+Na]^+)_{theo}$ = 719.37. Values obtained with a LXQ mass spectrometer.

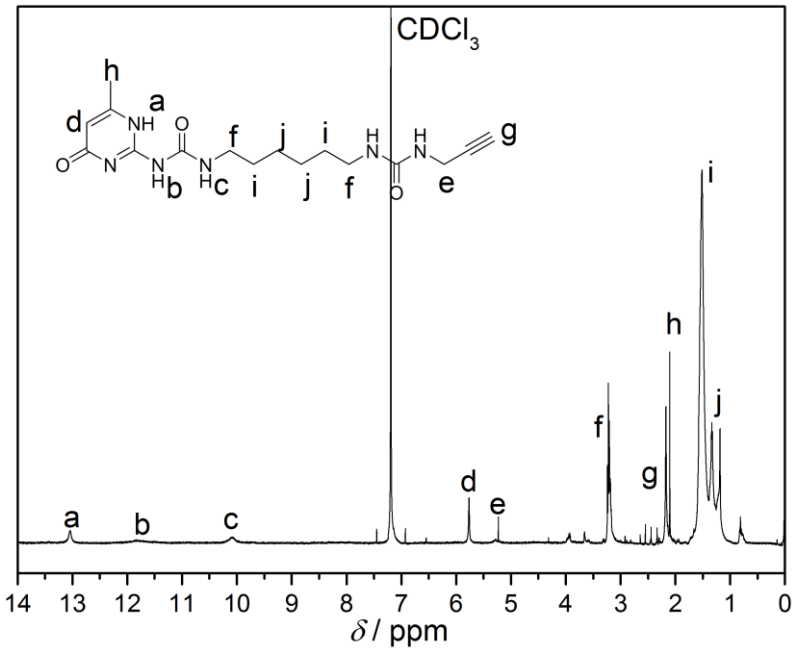

Figure 59: ^{1}H-NMR spectrum of Upy-Urea-Alkyne in $CDCl_3$.

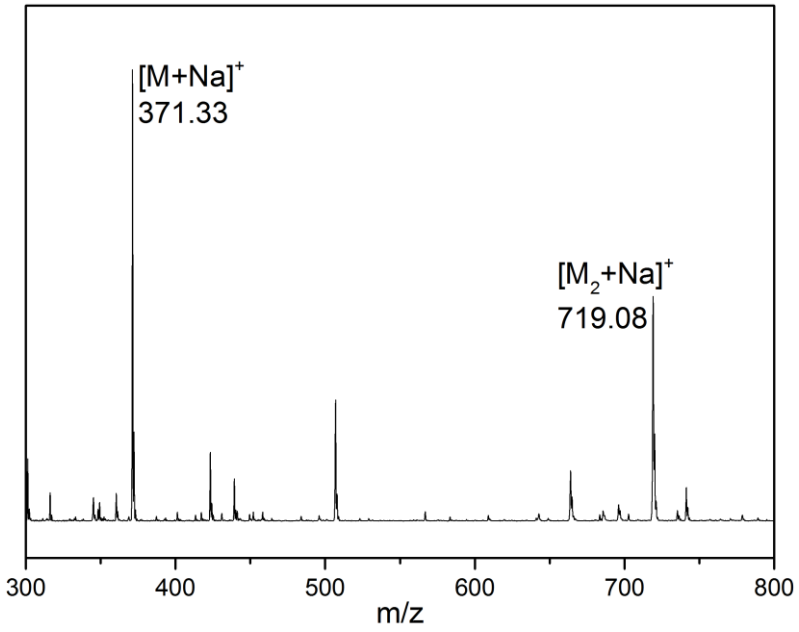

Figure 60: Mass spectrum of UPy-Urea-Alkyne.

5.3.4 *UPy-MA (**10**)*

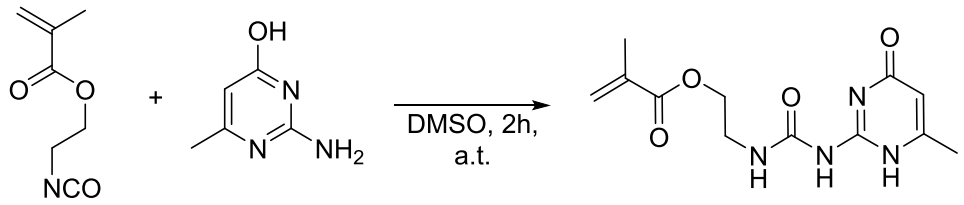

1.5 g (12.0 mmol, 1 eq.) 2-Amino-4-hydroxy-6-methylpyrimidine was dissolved in 20 mL hot (150 °C) DMSO and subsequently cooled to a.t., 2.0 g (13.0 mmol, 1.1 eq.) 2-isocyanatoethylmethacrylate was added and the reaction mixture was stirred for 2 h until the product forms as white precipitate. Acetone is added and the product is filtered off and dried (3.1 g, 11 mmol, 92% yield). The protocol was adapted from Park *et al*.[141]

^{1}H-NMR (400 MHz, $CDCl_3$): δ(ppm) =13.00 (s, 1H), 11.81 (s, 1H), 10.50 (s, 1H), 6.21 (s. 1H), 5.80 (s, 1H), 5.52 (s, 1H), 4.28 (t, *J* = 6.2 Hz, 2H), 3.56 (q, 2H, *J* = 6.2, 11.5 Hz, 2H), 2.21 (s, 3H), 1.91 (s, 3H).

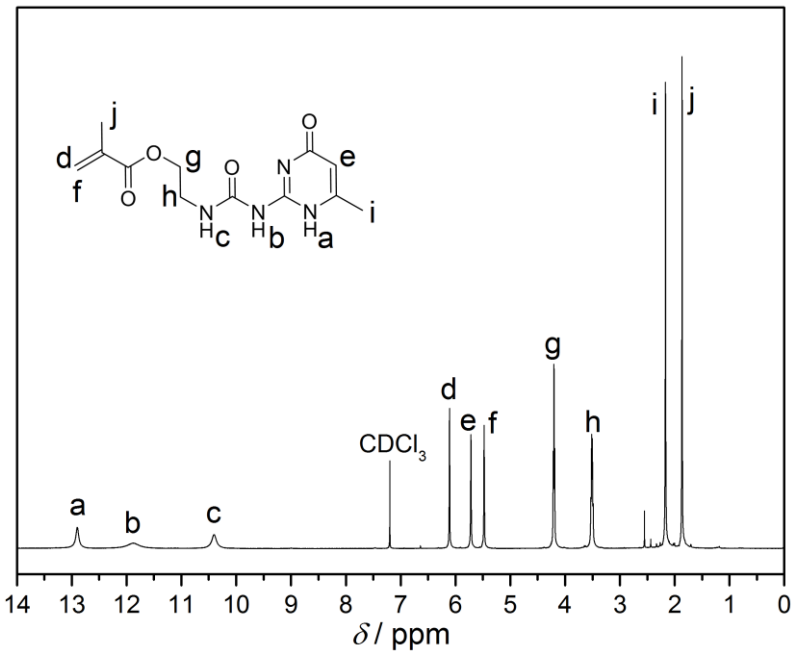

Figure 61: ^{1}H-NMR spectrum of UPy-MA (**10**) in $CDCl_3$.

5.3.5 *UPy-Urethane-MA (**11**)*

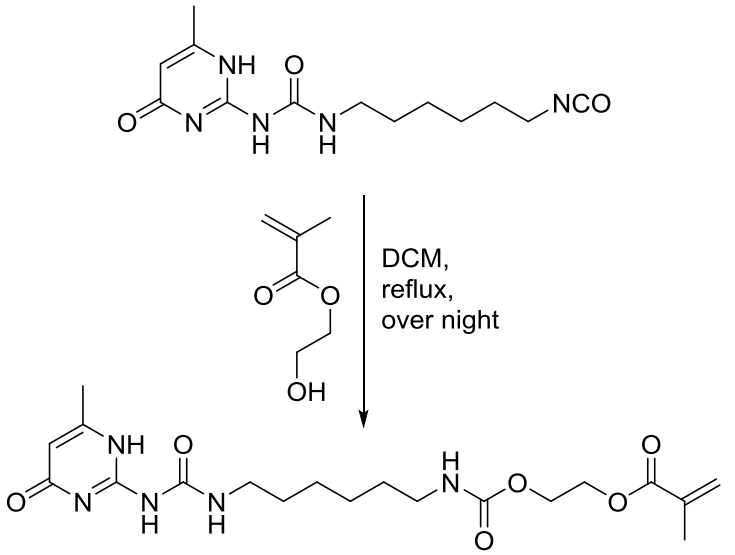

5.00 g (17.0 mmol, 1 eq.) UPy-NCO (**8**), 2.44 g (18.7 mmol, 1.1 eq) HEMA and one drop of DBTDL were dissolved in dry DCM and refluxed overnight. The product was isolated by precipitation of the reaction mixture in cyclohexane, filtered off and dried in vacuum (5.84 g, 13.8 mmol, 81% yield). The procedure was adapted from Berda *et al.*[132]

^{1}H-NMR (400 MHz, $CDCl_3$): δ(ppm) = 13.03 (s, 1H), 11.82 (s, 1H), 10.05 (s, 1H), 6.06 (s, 1H), 5.78 (s, 1H), 5.51 (m, 1H), 4.94 (s, 1H), 4.25 (m, 2H), 3.23-3.01 (m, 4H), 2.16 (s, 3H), 1.87 (s, 3H), 1.56-1.37 (m, 4H), 1.33-1.23 (m, 4H).

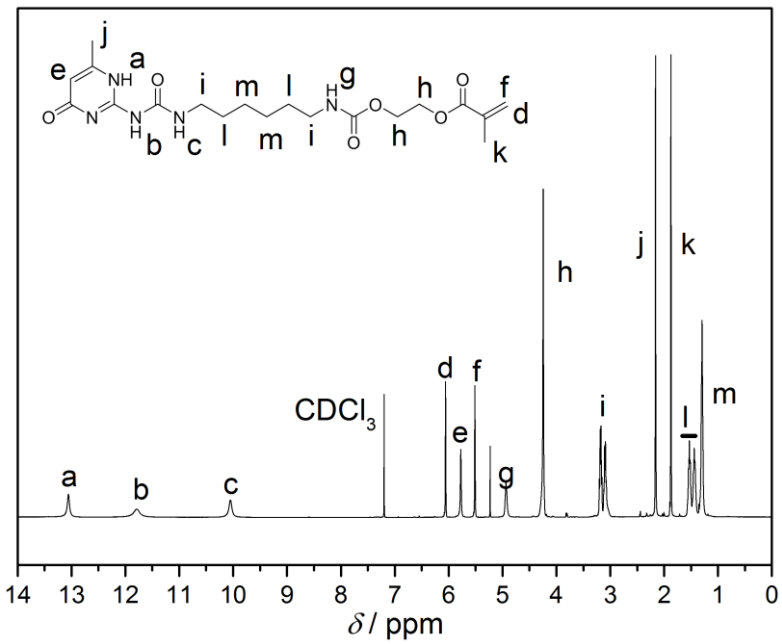

Figure 62: ^{1}H-NMR spectrum of UPy-Urethane-MA (**11**) in $CDCl_3$.

5.3.6 *UPy-Urea-MA (**12**)*

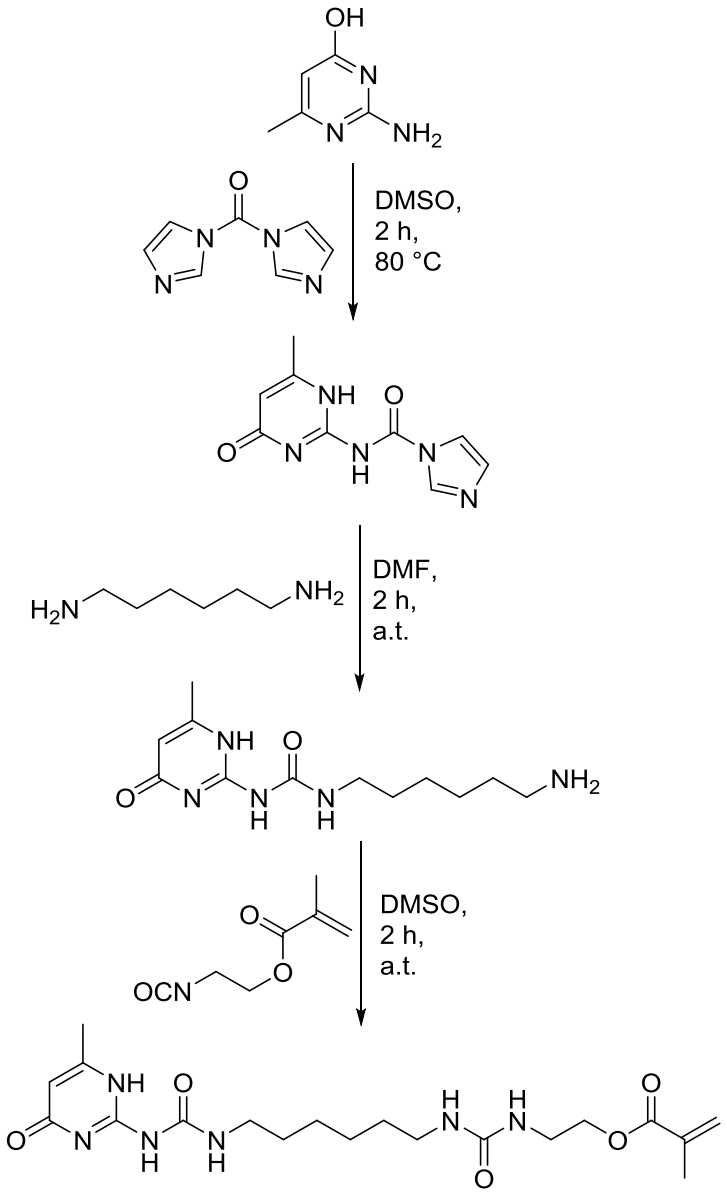

4.00 g (32.0 mmol, 1 eq.) 2-Amino-4-hydroxy-6-methylpyrimidine, 7.30 g (45.0 mmol, 1.4 eq.) CDI were suspended in dry DMSO and heated to 80 °C for 2h, subsequently cooled to ambient temperature. The precipitate was filtered off, washed with ethanol, dried and used without further purification or characterization.

The CDI-activated 2-amino-4-hydroxy-6-methylpyrimidine and 15.1 g (130 mmol, 4.1 eq.) 1,6-diaminohexane were suspended in 50 mL dry DMF and stirred for 2 h at ambient temperature. The solid was filtered off and washed with EE, acetone, ethanol and DCM and subsequently dried. The amin-functionalized UPy was used without further purification or characterization.

Amino-UPy was heated in 20 mL dry DMSO to 150 °C until dissolved and cooled to ambient temperature. 4.20 mL (4.62 g, 27.1 mmol, 0.85 eq.) 2-isocyanatoethylmethacrylate was added and the mixture was stirred 2 h at ambient temperature. The solid was filtered off, washed with 1M HCl, THF and chloroform and subsequently dried (6.96 g, 16.5 mmol, 52% yield).

^{1}H-NMR (400 MHz, DMSO-d_6): δ(ppm) =11.54 (s, 1H), 9.64 (s, 1H), 7.31 (s, 1H), 6.06 (s, 1H), 5.96-5.88 (m, 2H), 5.77 (s, 1H), 5.71-5.64 (m, 1Hz), 4.05 (t, *J* = 5.6 Hz, 2H), 3.29-3.23 (m, 2H), 3.13 (dd, *J* = 12.6, 6.5 Hz, 2H), 2.97 (dd, *J* = 12.6, 6.5 Hz, 2H), 2.11 (s, 3H), 1.89 (s, 3H), 1.50-1.32 (m,. 4H), 1.31-1.21 (m, 4H).

m/z $([M-C_4O_2H_5+Na]^+)_{exp}$ = 360.39, $([M-C_4O_2H_5+Na]^+)_{theo}$ = 360.19, $([M+H]^+)_{exp}$ =423.32, $([M+H]^+)_{theo}$ = 423.24, $([M+Na]^+)_{exp}$ = 445.28, $([M+Na]^+)_{theo}$ = 445.22, $([M_2+Na]^+)_{exp}$ = 867.33, $([M_2+Na]^+)_{theo}$ = 867.45.

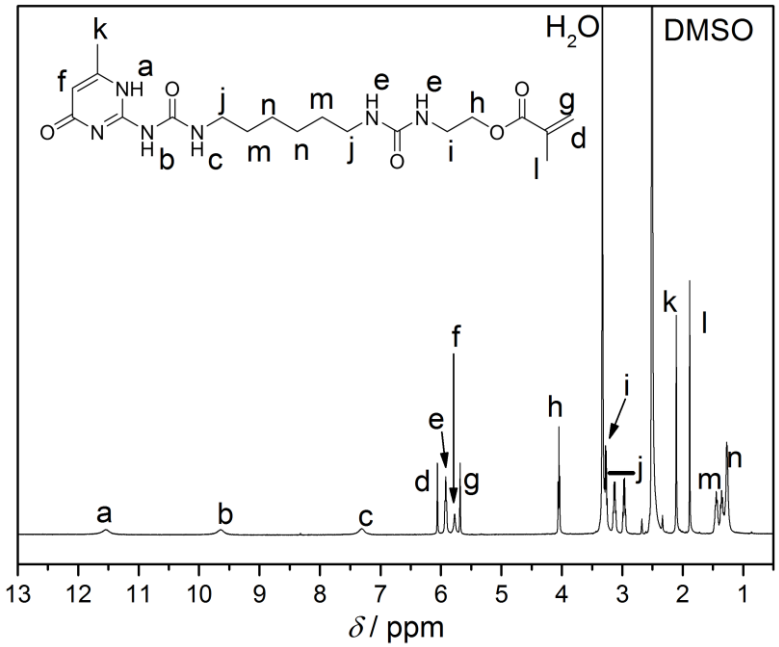

Figure 63: ^{1}H-NMR spectrum of UPy-Urea-MA (**12**) in DMSO-d_6.

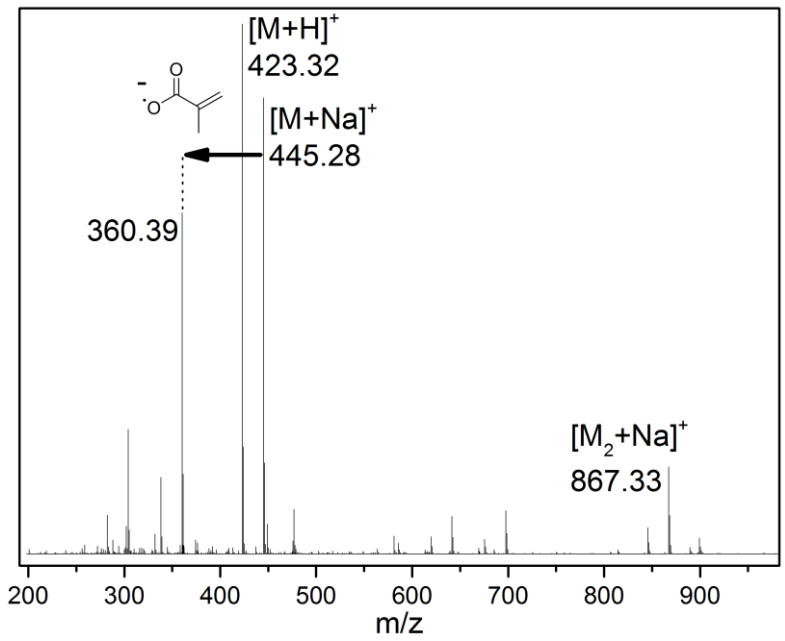

Figure 64: Mass spectrum of UPy-Urea-MA (**12**).

5.3.7 *UPy-OEG-MA (**13**)*

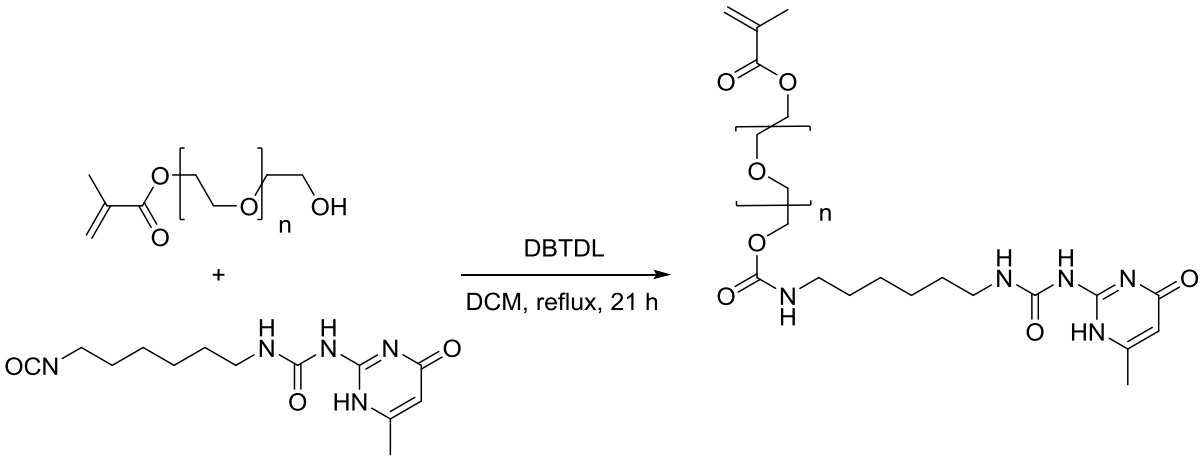

1.0 g (3.4 mmol, 1 eq.) UPy-NCO (**8**), 5.0 g $OEGMA_{360}$ (14 mmol) and 1 drop DBTDL were dissolved in 25 mL dry DCM. The slurry was refluxed for 21 h, concentrated *in vacuo* and precipitated in cold cyclohexane. Precipitation was repeated twice and the product was dried overnight, resulting in a white powder with excellent purity (0.34 g, 0.50 mmol, 15 % yield).

^{1}H-NMR (400 MHz, $CDCl_3$): δ(ppm) =13.04 (s, 1H), 11.80 (s, 1H), 10.04 (s, 1H), 6.06 (s, 1H), 5.78 (s, 1H), 5.51 (m, 1H), 4.92 (s, 1H), 4.24 (m, 2H),4.14 (m, 2H), 3.58 (m, 4nH), 3.13 (m, 4H) 2.17 (s, 3H), 1.87 (s, 3H), 1.47 (m, 4H), 1.36 (s, 4H).

5.3.8 *Br-MA (**14**)*

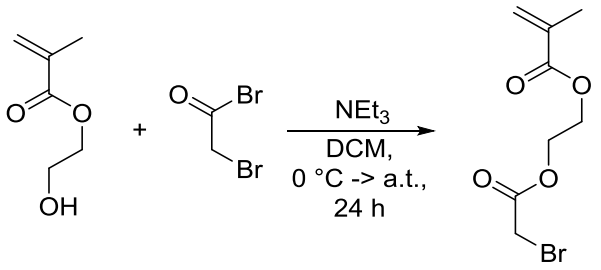

2.34 mL (2.50 g, 19.2 mmol, 1 eq.) HEMA and 3.99 mL (2.91 g, 28.8 mmol, 1.5 eq.) NEt_3 were dissolved in 25 mL dry DCM under inert gas and cooled to 0 °C. 2.01 mL (4.66 g, 23.1 mmol, 1.2 eq) Bromoacetyl bromide diluted in 10 mL dry DCM was added carefully over a period of 30 minutes. The reaction was allowed to warm to ambient temperature and stirred overnight. The reaction mixture was extracted twice with saturated $NaHCO_{3(aq.)}$, once with 1M $HCl_{(aq.)}$ and dried over $MgSO_4$. The crude product was isolated by removal of the solvent under reduced pressure and purified *via* column chromatography with (cyHex /EE 5/1) as eluent, yielding a slightly yellowish liquid (2.10 g, 8.36 mmol, 44% yield).

^{1}H-NMR ($CDCl_3$, 400 MHz), δ(ppm) = 6.1 (m, 1H), 5.5 (m, 1H), 4.3 (m, 4H), 3.8 (s, 2), 1.9 (dd, J = 1.6, 1.0 Hz, 3H). ^{13}C-NMR ($CDCl_3$, 400 MHz), δ(ppm) = 167.1, 167.0, 135.8, 126.3, 63.8, 62.0, 25.5, 18.2.

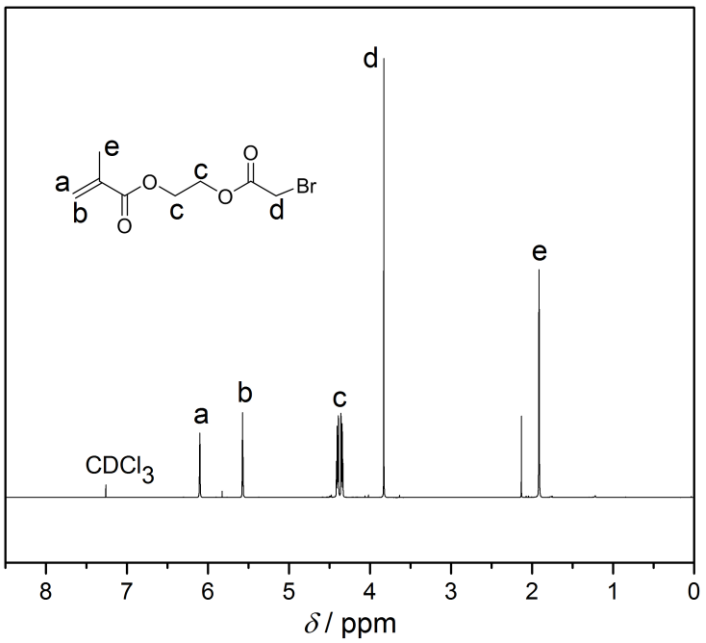

Figure 65: ^{1}H-NMR spectrum of Br-MA (**14**) in $CDCl_3$.

5.3.9 *Sodium Carbonocyanidodithioate*

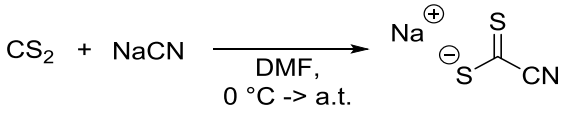

5.46 g (111 mmol, 1.1 eq) NaCN were suspended in 20 mL DMF, cooled to 0 °C and a solution of 7.75 g (102 mmol, 1 eq) CS_2 in 13 mL DMF was added dropwise. The reaction mixture was allowed to warm to ambient temperature and stirred until complete solidification. 150 mL isopropyl alcohol were added, and the precipitate was dissolved by heating to 90 °C. The residual NaCN was filtered off the warm suspension and the clear solution was cooled in liquid nitrogen to precipitate the product, which was subsequently filtered off and washed with Et_2O. The product was purified by recrystallization in isopropyl alcohol/Et_2O (1/1) and used without further characterization (7.38 g, 59.0 mmol, 58% yield). The procedure was adapted from Öhlenschläger *et al*.[28]

5.3.10 *CDTE-MA (**15**)*

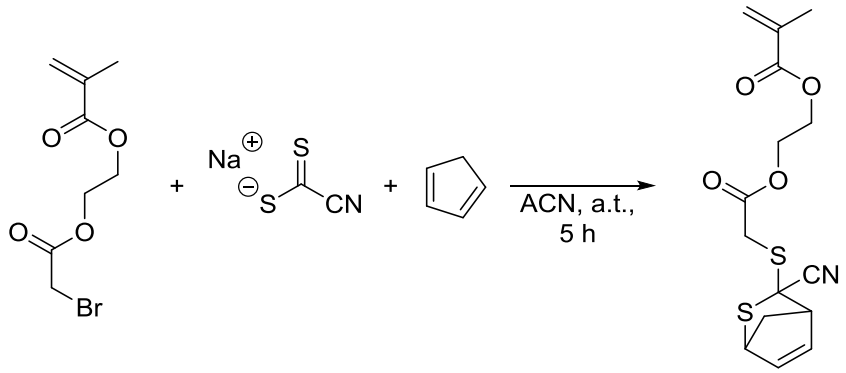

1.80 g (7.17 mmol, 1 eq.) Br-MA (**14**) and 1.60 mL (1.28 g, 19.4 mmol, 2.7 eq.) Cp were dissolved in 25 mL ACN and combined at ambient temperature with 2.02 g (16.1 mmol, 2.25 eq.) sodium carbonocyanidodithioate in 25 mL ACN. After 5 h the brown color of the reaction mixture disappeared and NaBr had precipitated, resulting in a turbid, yellow solution. ACN was removed *in vacuo*, the residue was dispersed in EE and filtered over a short column with silica to remove solids. Subsequently, the crude product was isolated again under reduced pressure and purified *via* column chromatography in (cyHex /EE 5/1). The product was obtained as colorless liquid (1.01 g, 2.98 mmol, 42% yield).

^{1}H-NMR ($CDCl_3$, 400 MHz), δ(ppm) = 6.7-6.3 (m, 1H), 6.1-6.0 (m, 2H), 5.6-5.5 (m, 1H), 4.4-4.2 (m, 6H), 3.9-3.4 (m, 3H), 2.2-1.8 (m, 5H).

^{13}C-NMR ($CDCl_3$, 400 MHz), δ(ppm) = 169.0, 167.1, 141.7, 138.5, 135.8, 131.3, 130.2, 126.3, 119.6, 63.6, 62.1, 56.5, 55.4, 51.6, 48.9, 35.8, 18.3.

m/z $([M\text{-}Cp+Na]^+)_{exp}$ = 296.00, $([M\text{-}Cp+Na]^+)_{theo}$ = 296.00, $([M+Na]^+)_{exp}$ = 362.05, $([M+Na]^+)_{theo}$ = 362.05, $([M_2+Na]^+)_{exp}$ = 701.10, $([M_2+Na]^+)_{theo}$ = 701.10.

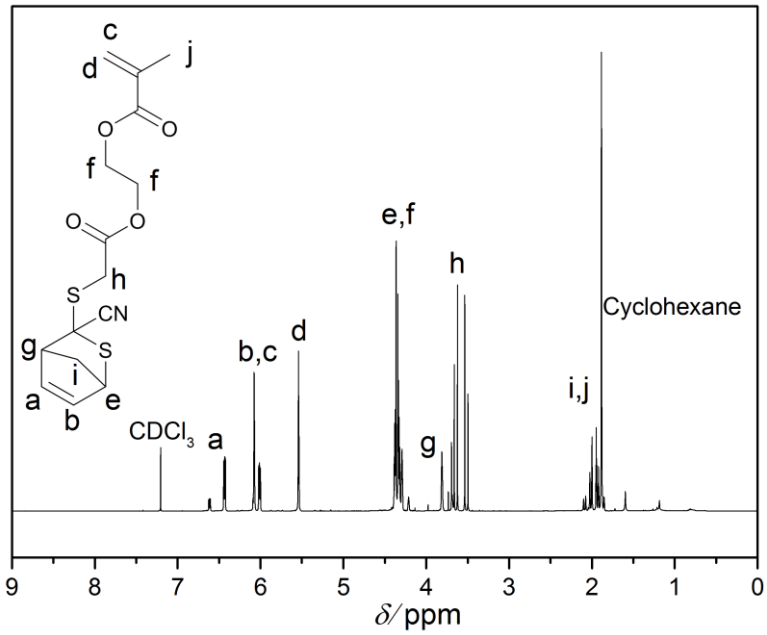

Figure 66: ^{1}H-NMR of CDTE-MA (**15**) in $CDCl_3$.

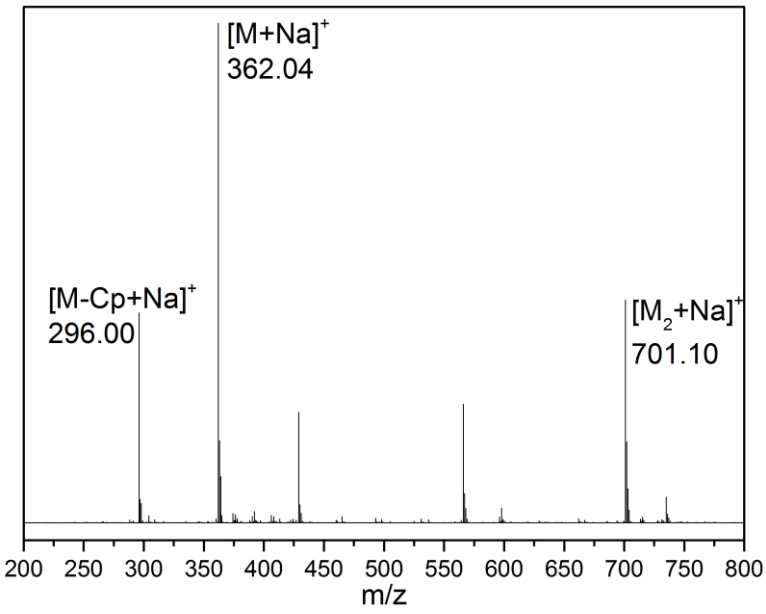

Figure 67: Mass spectrum of CDTE-MA (**15**).

5.3.11 *Sorb-MA (**16**)*

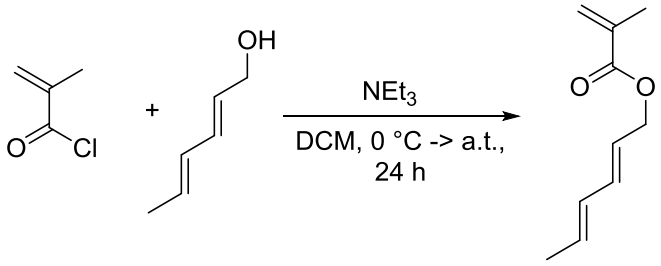

1.161 mL (1.254 g, 12.0 mmol, 1.2 eq.) Methacryloyl chloride and 1.660 mL (1.210 g, 12 mmol, 1.2 eq.) triethylamine were dissolved in 20 mL dry DCM and cooled to 0°C. A solution of 1.00 g (10.2 mmol, 1 eq.) sorbic alcohol in 10 mL dry DCM was added dropwise. The reaction was stirred overnight allowing to reach ambient temperature. The reaction was diluted with DCM and extracted once with 1M HCl and twice with brine, dried over $MgSO_4$ and the solvent was removed *in vacuo*. The crude product was purified *via* column chromatography (R_f = 0.67, cyclohexane/EE 5/1) and received as yellow oil (913 mg, 5.49 mmol, 45% yield).

^{1}H-NMR (400 MHz, $CDCl_3$): δ(ppm) = 6.20-5.45 (6H), 4.58 (d, *J* = 6.6 Hz, 2H), 1.95 (dd, *J* = 1.6, 1.0 Hz, 3H), 1.79-1.74 (m, 3H).

^{13}C-NMR (400 MHz, $CDCl_3$): δ(ppm) = 167.20, 136.38, 134.70, 131.17, 130.47, 125.46, 123.84, 65.14, 26.92, 18.33, 18.11.

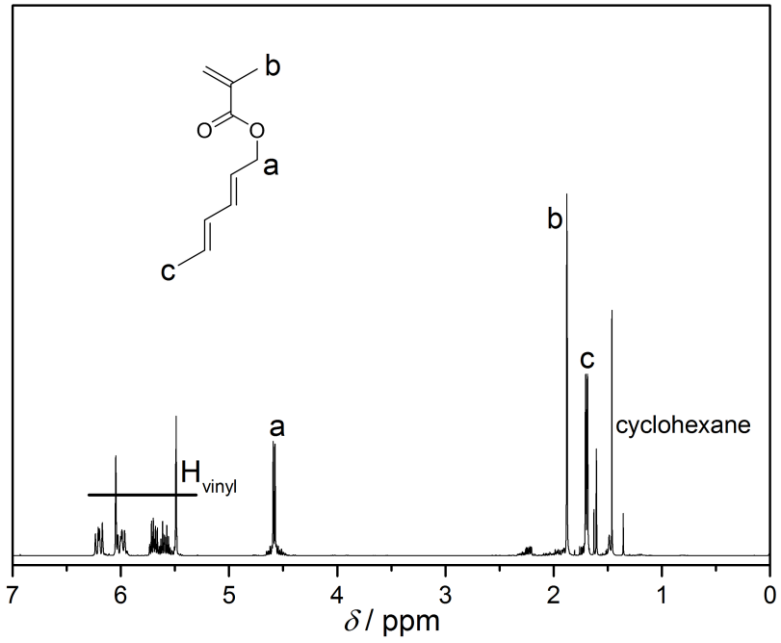

Figure 68: ^{1}H-NMR spectrum of Sorb-MA (**16**) in $CDCl_3$.

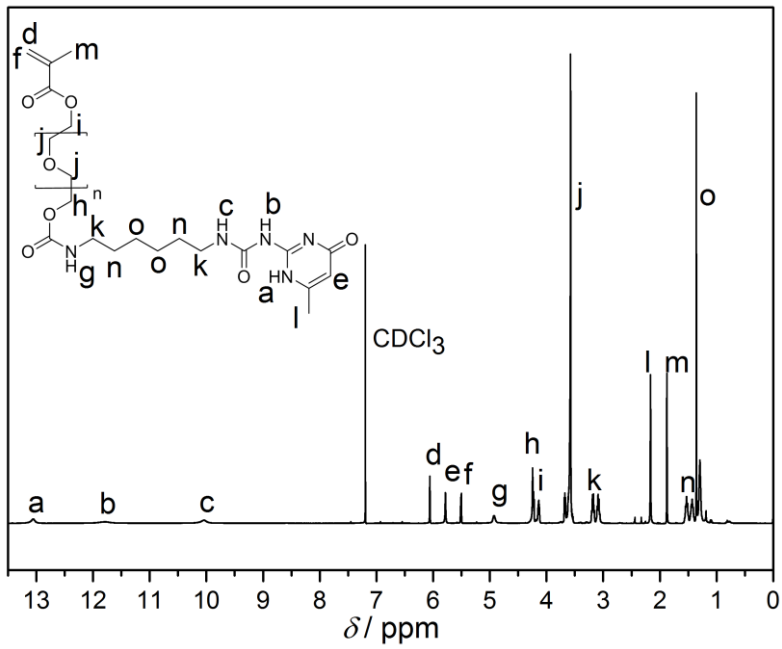

Figure 69: ^{1}H-NMR spectrum of UPy-OEG-MA (**13**) in $CDCl_3$.

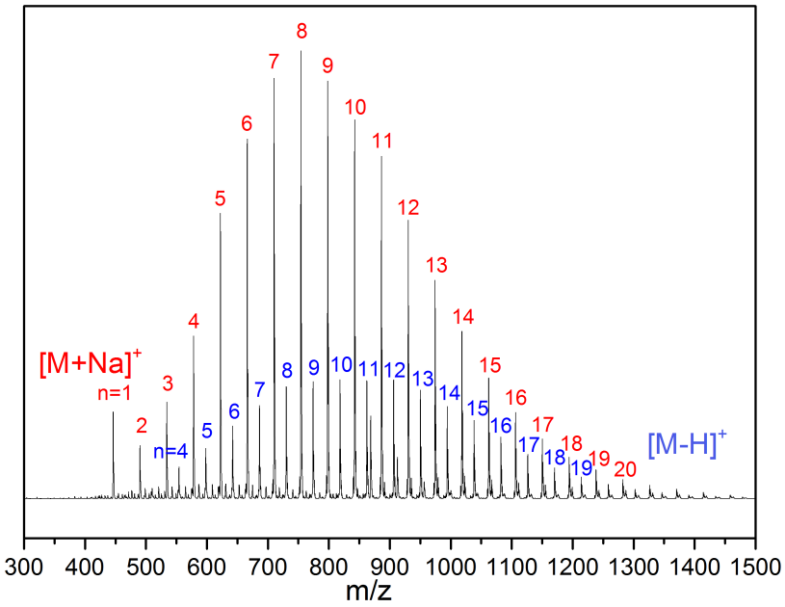

Figure 70: MS spectrum of UPy-OEG-MA (**13**) measured on a LXQ mass spectrometer.

n	$[M+Na]^+$ m/z_{theo}	$[M+Na]^+$ m/z_{exp}	$[M-H]^+$ m/z_{theo}	$[M-H]^+$ m/z_{exp}
2	490.23	490.33	466.25	-
3	534.26	534.33	510.28	-
4	578.29	578.33	554.31	554.33
5	622.32	622.33	598.34	598.33
6	666.35	666.33	642.37	642.33
7	710.38	710.42	686.40	686.42
8	754.41	754.42	730.43	730.33
9	798.44	798.42	774.46	774.33
10	842.47	842.42	818.49	818.33
11	886.50	886.42	862.52	862.42
12	930.53	930.42	906.55	906.42
13	974.56	974.42	950.58	950.50
14	1018.59	1018.42	994.61	994.42
15	1062.62	1062.42	1038.64	1038.42
16	1106.65	1106.42	1082.67	1082.50
17	1150.68	1150.50	1126.70	1126.50
18	1194.71	1194.50	1170.73	1170.58
19	1238.74	1238.50	1214.76	1214.50
20	1282.77	1282.50	1258.79	-

Table 5: Theoretical and experimental m/z values of the MS spectrum of UPy-OEG-MA (**13**). Colors refer to the ion in Figure 70. Measurement was performed on a LXQ mass spectrometer.

5.3.12 *TetCO$_2$H (**17**)*

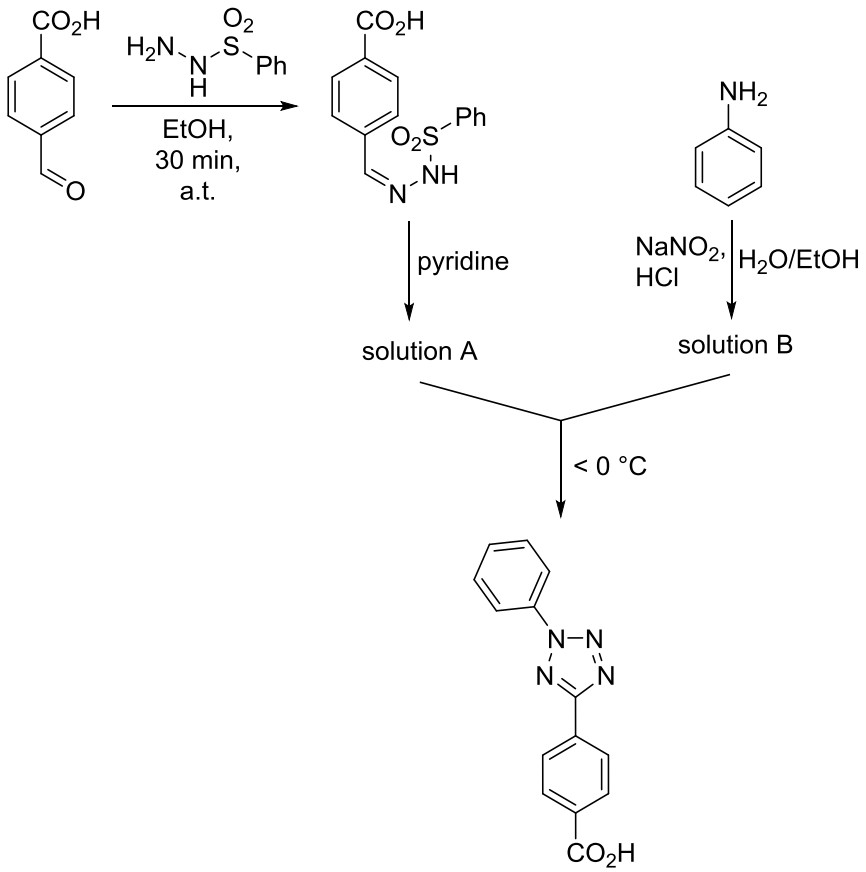

0.75 g (5.0 mmol, 1 eq.) 4-Formylbenzoic acid and 0.86 g (25 mmol, 5 eq.) benzenesulfonohydrazide were dissolved in 50 mL ethanol and stirred for 30 min at a.t. to result in the corresponding benzenesulfonylhydrazone, which was precipitated as white solid *via* addition of 100 mL water and filtered off. The hydrazone is dissolved in 30 mL pyridine (= solution A).

0.345 g (5.0 mmol, 1 eq.) sodium nitrite in 2 mL water was added dropwise to a solution of 1.3 mL concentrated HCl and 0.465 g (5.0 mmol, 1 eq.) aniline in 8 mL water/ethanol (1/1) (=solution B).

Solution A was cooled to -10-0 °C and solution B was added slowly. The reaction mixture was extracted with EE trice and to the combined organic layers 250 mL of 3M HCl were added to precipitate the target molecule, which was filtered off and dried (0.45 g, 1.7 mmol, 34%)

The synthesis procedure was conducted as described by Song *et al*.[69]

^{1}H-NMR (400 MHz, DMSO-d_6): δ(ppm) = 12.30 (s, 1H), 8.32 (d, *J* = 8.0 Hz, 2H), 8.19 (t, *J* = 8.5 Hz, 4H), 7.73 (t, *J* = 7.5 Hz, 2H), 7.66 (t, *J* = 7.5 Hz, 1H).

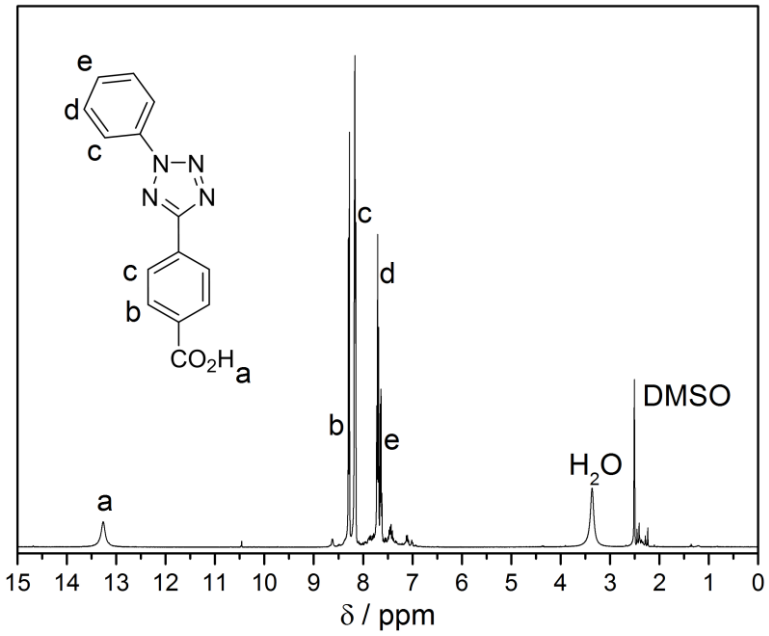

Figure 71: ^{1}H-NMR spectrum of TetCO_2H (**17**) in DMSO-d_6.

5.3.13 *Tet-Silane (**18**)*

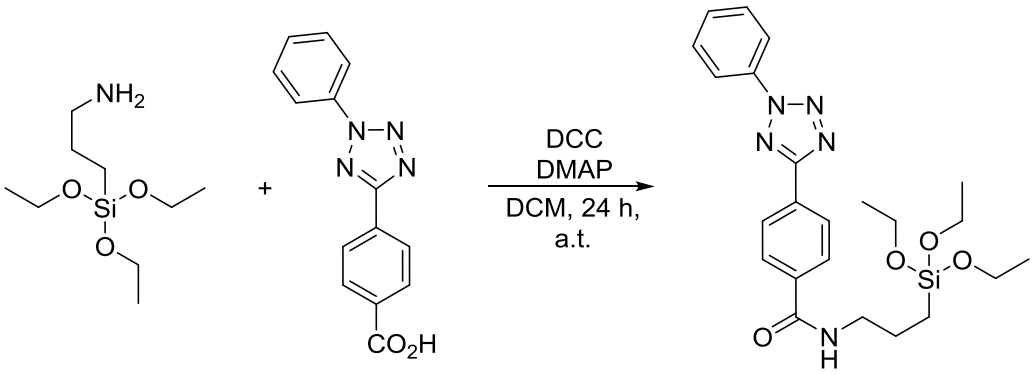

1.2 g (4,5 mmol, 1 eq.) TetCO_2H (**17**), 1.225 mL (1.295 g, 5.9 mmol, 1.3 eq.) APTES, 1.393 g (6.8 mmol, 1.5 eq.) DCC and 220 mg (1.8 mmol, 0.4 eq.) DMAP were dissolved in 50 mL dry DCM under inert gas and stirred at ambient temperature for 24 h. The solvent was removed *in* vacuo and the crude product was purified by column chromatography (R_f = 0.27, DCM/EE 1/1) and recrystallized from n-hexane resulting in a slightly red powder (300 mg, 0.6 mmol, 14 % yield). Synthesis was adapted from Dietrich *et al*.[209]

^{1}H-NMR (400 MHz, DMSO-d_6): δ(ppm) = 8.80-8.59 (m, 1H), 8.37-8.03 (m, 5H), 7.83-7.60 (m, 3H), 3.88-3.68 (q, J = 7.0 Hz, 6H), 3.43-3.23 (m, 2H), 1.70-1.54 (m, 2H), 1.28-1.09 (t, J = 7.0 Hz, 9H), 0.71-0.53 (m, 2H).

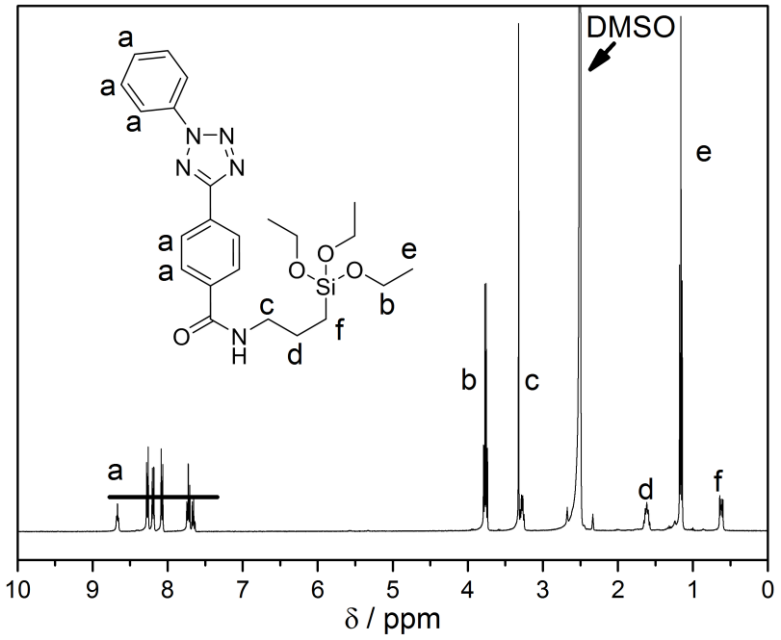

Figure 72: ^{1}H-NMR spectrum of Tet-Silane (**18**) in DMSO-d_6.

5.3.14 *MalPG (**19**)*

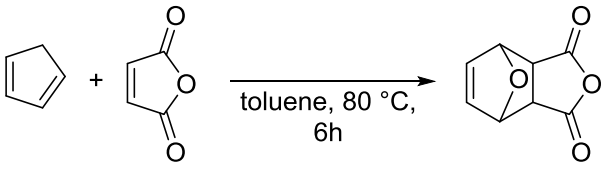

30.6 g (312 mmol, 1 eq.) Maleic anhydride was suspended in 150 mL toluene and heated to 80 °C. 35 mL (32.9 g, 483 mmol, 1.5 eq.) furan were added dropwise and the reaction was stirred for 6 h at 80 °C. Subsequently, the solution is cooled to ambient temperature, resulting in the crystallization of product overnight, which was then filtered off (28.4 g, 171 mmol, 72% yield). The procedure was adapted from Mantovani *et al.*[210]

^{1}H-NMR (400 MHz, $CDCl_3$): δ(ppm) = 6.51 (s, 2H), 5.39 (s, 2H), 3.11 (s, 2H).

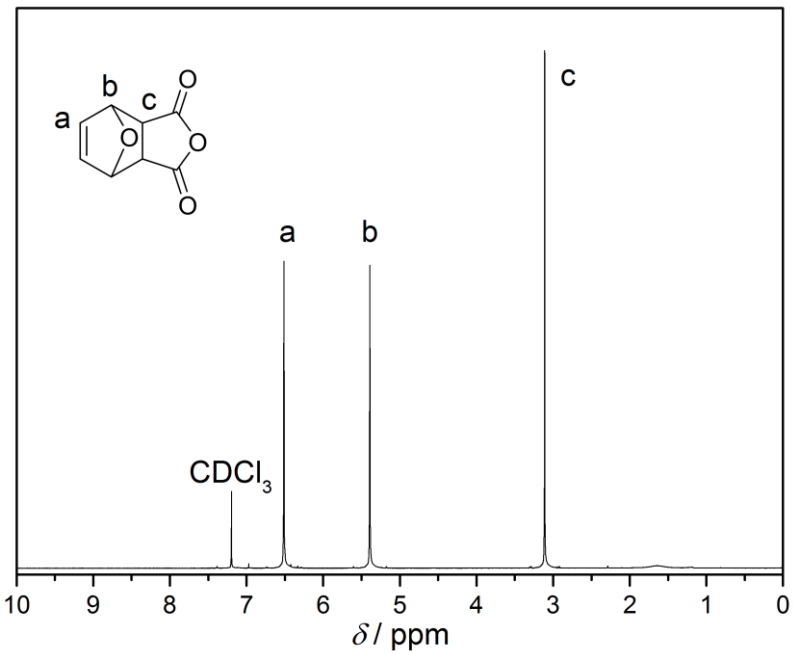

Figure 73: ^{1}H-NMR spectrum of MalPG (**19**) in $CDCl_3$.

5.3.15 *MalPG-OH (**20**)*

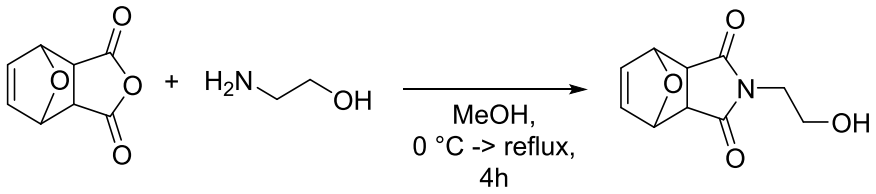

17.71 g (107.0 mmol, 1 eq.) MalPG (**19**) was suspended in 270 mL methanol and cooled to 0 °C. A solution of 6.47 g (106 mmol, 1 eq.) ethanolamine in 180 mL methanol was added drop wise within 10 min. The mixture was stirred for 5 min and subsequently refluxed for 4 h. The solution was concentrated *in* vacuo and stored in the freezer to yield yellowish crystals, which were isolated by filtration (m = 11.11 g, 53.5 mmol, 50% yield). The procedure was adapted from Mantovani *et al*.[210]

^{1}H-NMR (400 MHz, $CDCl_3$): δ (ppm) = 6.52 (s, 2H), 5.28 (s, 2H), 3.78-3.69 (m, 4H), 2.90 (s, 2H).

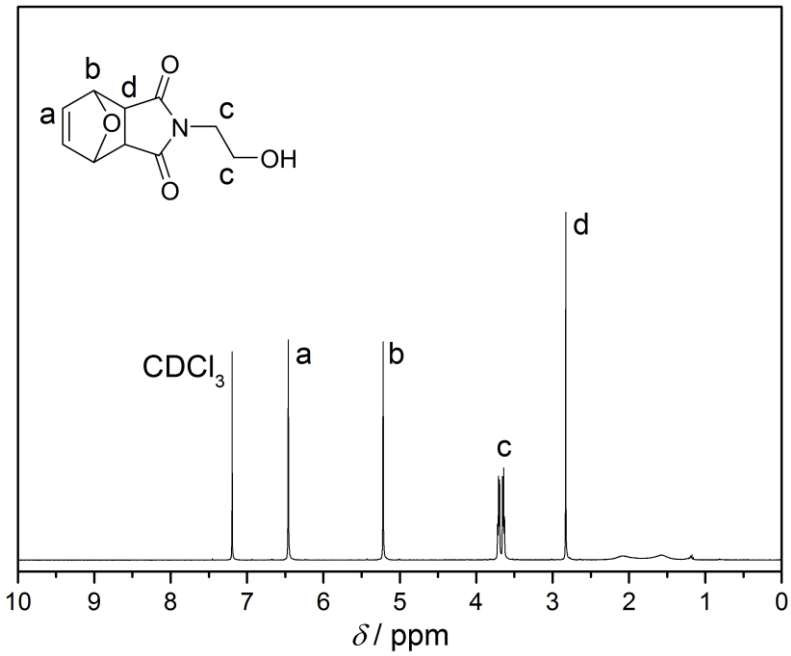

Figure 74: ^{1}H-NMR spectrum of MalPG (**20**) in $CDCl_3$.

5.3.16 *UPy-MalPG (**21**)*

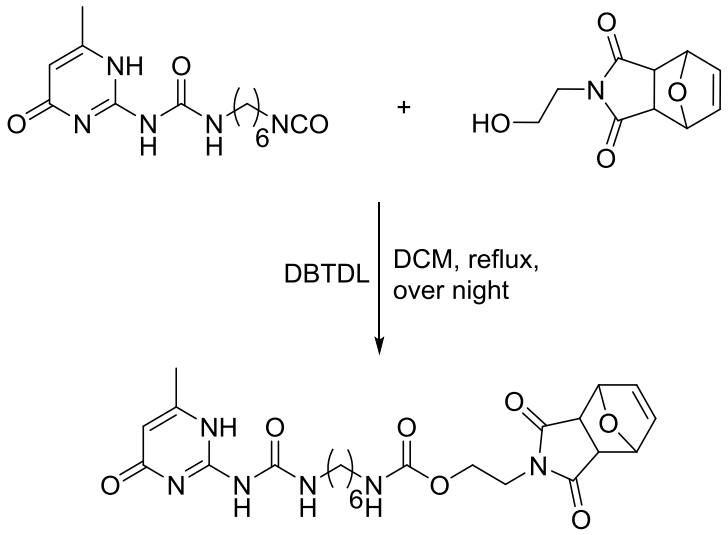

1.00 g (3.4 mmol, 1. eq.) UPy-NCO (**8**), 1.07 g (5.1 mmol, 1.5 eq.) MalPG-OH (**20**) and 1 drop DBTDL were suspended in 30 mL dry DCM and refluxed overnight. The solvent was removed *in vacuo*, the residual solid was washed with methanol and DCM and subsequently dried (1.21 g, 2.4 mmol, 70% yield).

^{1}H-NMR (400 MHz, $CDCl_3$): δ(ppm) = 13.04 (s, 1H), 11.79 (s, 1H), 10.08 (m, 1H), 6.43 (m, 2H), 5.77 (s, 1H), 5.20 (s, 2H), 4.89 (s, 1H), 4.12 (m, 2H), 3.76-3.51 (m, 2H), 3.28-2.88 (m, 4H), 2.19 (s, 3H), 1.63-1.08 (m, 8H).

^{13}C-NMR (400 MHz, $CDCl_3$): δ(ppm) = 175.93, 173.01, 156.55, 155.94, 154.69, 148.24, 136.48, 106.73, 80.90, 60.91, 47.48, 42.08, 39.78, 39.36, 38.43, 31.15, 29.58, 29.27, 26.25, 18.86.

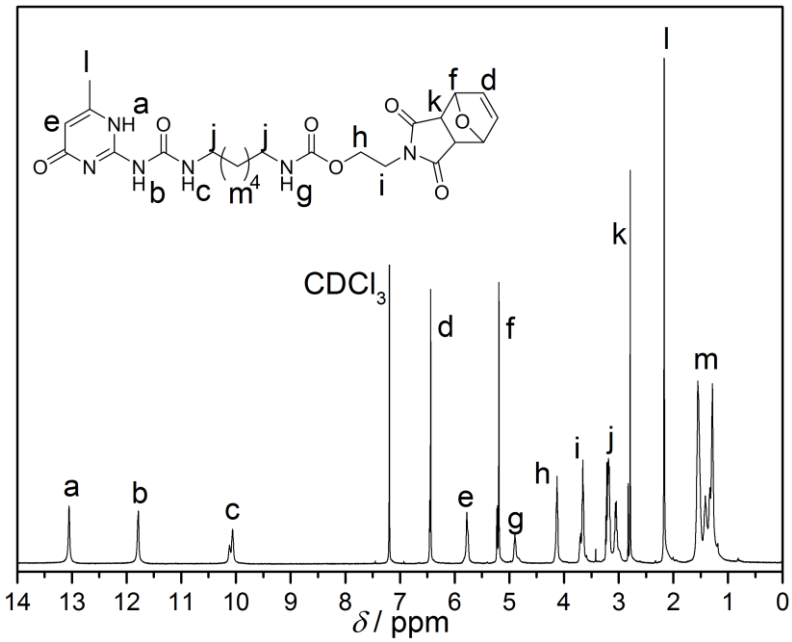

Figure 75: ^{1}H-NMR spectrum of UPy-MalPG (**21**) in $CDCl_3$.

5.3.17 *UPy-Mal (**22**)*

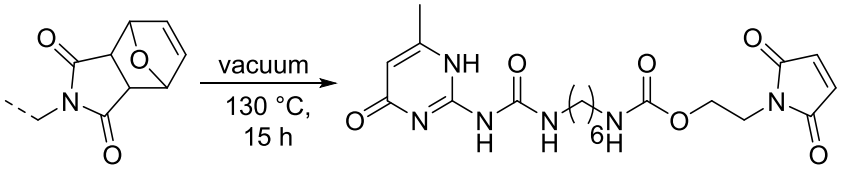

1.20 g (2.39 mmol, 1 eq.) UPy-MalPG (**21**) was kept in Schlenk vacuum at 130 °C for 15 h. With regard to ^{1}H-NMR analysis conversion was considered as complete (>97%).

^{1}H-NMR (400 MHz, $CDCl_3$): δ(ppm) = 13.04 (s, 1H), 11.79 (s, 1H), 10.08 (m, 1H), 6.62 (m, 2H) 5.77 (s, 1H), 5.20 (s, 2H), 4.89 (s, 1H), 4.12 (m, 2H), 3.70 (s, 2H), 3.26-2.99 (m, 4H), 2.17 (s, 3H), 1.60-1.12 (m, 8H).

m/z $([M+Na]^+)_{exp}$ = 457.42, $([M+Na]^+)_{theo}$ = 457.18, $([M_2+Na]^+)_{exp}$ = 890.83, $([M_2+Na]^+)_{theo}$ = 891.37. Values obtained with a LXQ mass spectrometer.

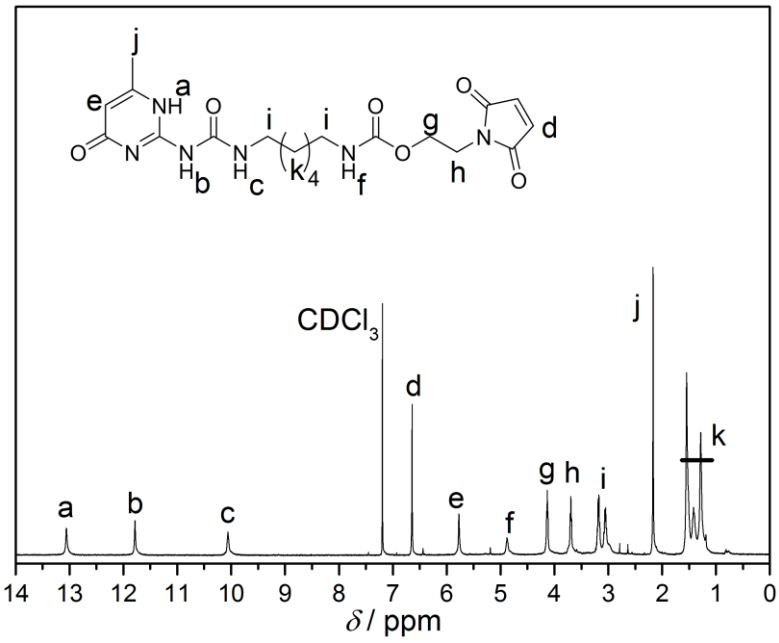

Figure 76: ^{1}H-NMR spectrum of UPy-Mal (**22**) in $CDCl_3$.

5.3.18 *UPy-CF_3 (**23**)*

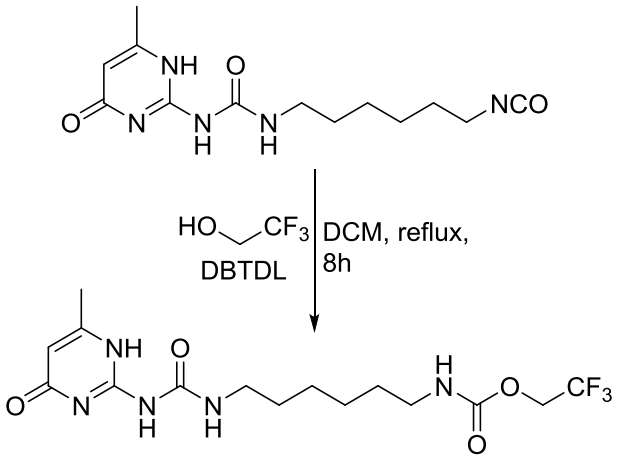

1.2 g (3.4 mmol, 1 eq.) UPy-NCO (**8**), 510.2 mg (5.1 mmol, 1.5 eq.) trifluoroethanol and 1 drop DBTDL were suspended in 60 mL dry DCM and refluxed for 8 h. For product isolation the solvent was removed *in vacuo* and the white powder was carefully washed with MeOH and acetone, resulting in product **23** (890 mg, 2.3 mmol, 68% yield).

^{1}H-NMR (400 MHz, $CDCl_3$): δ(ppm) = 13.07 (s, 1H), 11.80 (s, 1H), 10.00 (s, 1H), 5.79 (s, 1H), 5.51 (s, 1H), 4.47-4.30 (q, *J* = 8.6 Hz, 2H), 3.23-3.08 (m, 4H), 2.16 (s, 3H), 1.60-1.43 (m, 4H), 1.40-1.11 (m, 4H).

^{13}C-NMR (400 MHz, $CDCl_3$): δ(ppm) = 172.98, 156.27, 154.63, 148.06, 106,37, 40.69, 39.05, 29.15, 25.15, 18.54.

^{19}F-NMR (400 MHz, $CDCl_3$): δ(ppm) = -74.20.

m/z $([M+Na]^+)_{exp}$ = 416.25, $([M+Na]^+)_{theo}$ = 416.15, $([M_2+Na]^+)_{exp}$ = 808.75, $([M_2+Na]^+)_{theo}$ = 809.31. Values obtained with a LXQ mass spectrometer.

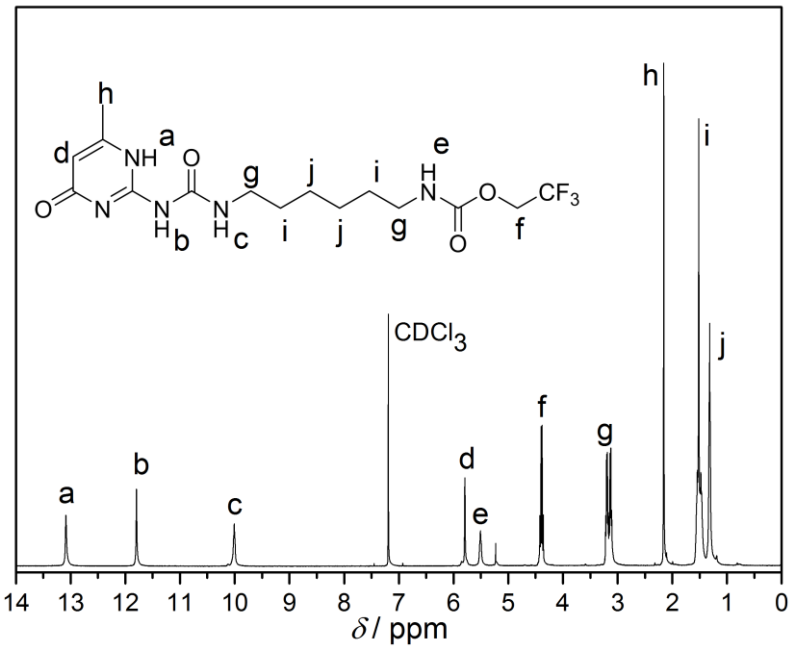

Figure 77: ^{1}H-NMR spectrum of UPy-CF_3 (**23**) in $CDCl_3$.

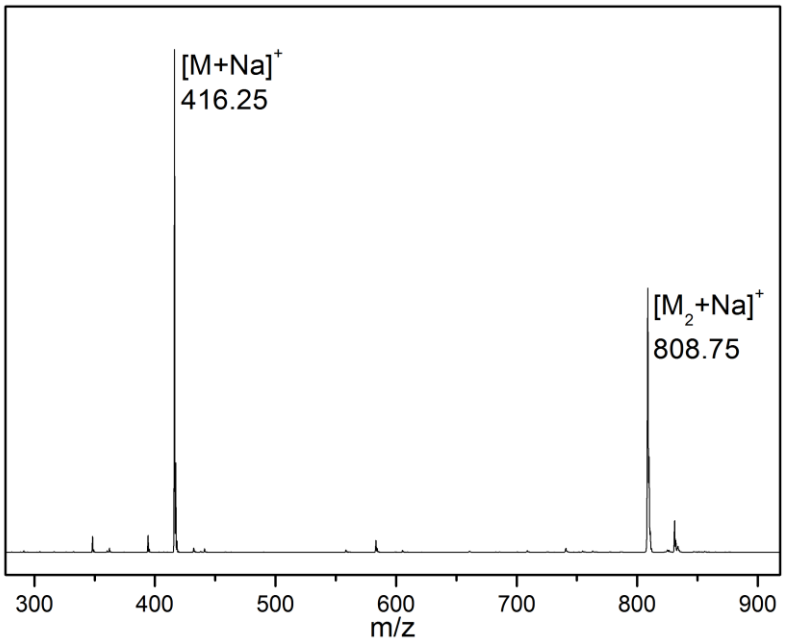

Figure 78: Mass spectrum of UPy-CF_3 (**23**) obtained by a LXQ mass spectrometer.

5.3.19 *UPy-Br (**24**)*

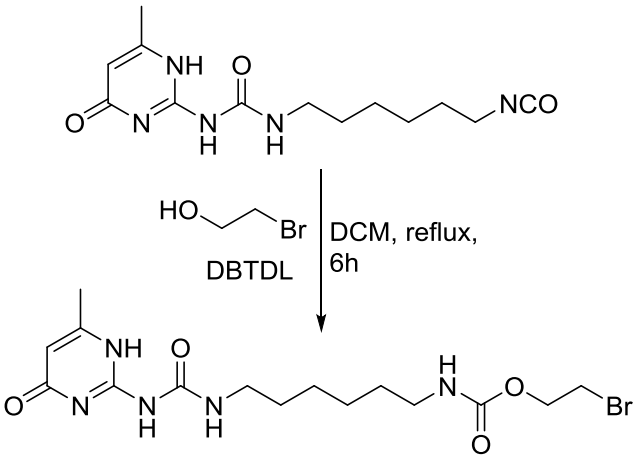

1.0 g (3.4 mmol, 1 eq.) UPy-NCO (**8**), 255 µL (0.450 mg, 3.6 mmol, 1.1 eq.) 2-bromoethanol and one drop DBTDL were suspended in 60 mL dry DCM and refluxed for 6 h. The solvent was removed under reduced pressure, the solid was washed with MeOH and EE and dried (0.941 g, 2.2 mmol, 65% yield).

^{1}H-NMR (400 MHz, $CDCl_3$): δ(ppm) = 13.04 (s, 1H), 11.75z (s, 1H), 10.00 (s, 1H), 5.78 (s, 1H), 5.09 (m, 1H), 4.39-4.38 (t, *J* = 5.8 Hz, 2H), 3.48-3.41 (t, *J* = 5.9 Hz, 2H), 3.28-3.01 (m, 4H), 2.16 (s, 3H), 1.60-1.43 (m, 4H), 1.40-1.22 (m, 4H).

^{13}C-NMR (400 MHz, $CDCl_3$): δ(ppm) = 173.21, 156.53, 155.78, 154.70, 148.29, 106.64, 64.15, 42.84, 40.68, 39.76, 31.17, 29.76, 29.35, 26.00, 18.93.

m/z $([M-Br+H+Na]^+)_{exp}$ = 362.24, $([M-Br+H+Na]^+)_{theo}$ = 362.18, $([M+Na]^+)_{exp}$ = 440.12/442.12 (1/1), $([M+Na]^+)_{theo}$ = 440.09/442.09 (1/1), $([M_2-Br_2+H_2+Na]^+)_{exp}$ = 701.00, $([M_2-Br_2+H_2+Na]^+)_{theo}$ = 701.37, $([M_2-Br+H+Na]^+)_{exp}$ = 778.88/708.88 (1/1), $([M_2-Br_2+H_2+Na]^+)_{theo}$ = 779.28/781.28 (1/1), $([M_2+Na]^+)_{exp}$ = 858.72, $([M_2+Na]^+)_{theo}$ = 859.19. Values obtained with a LXQ mass spectrometer.

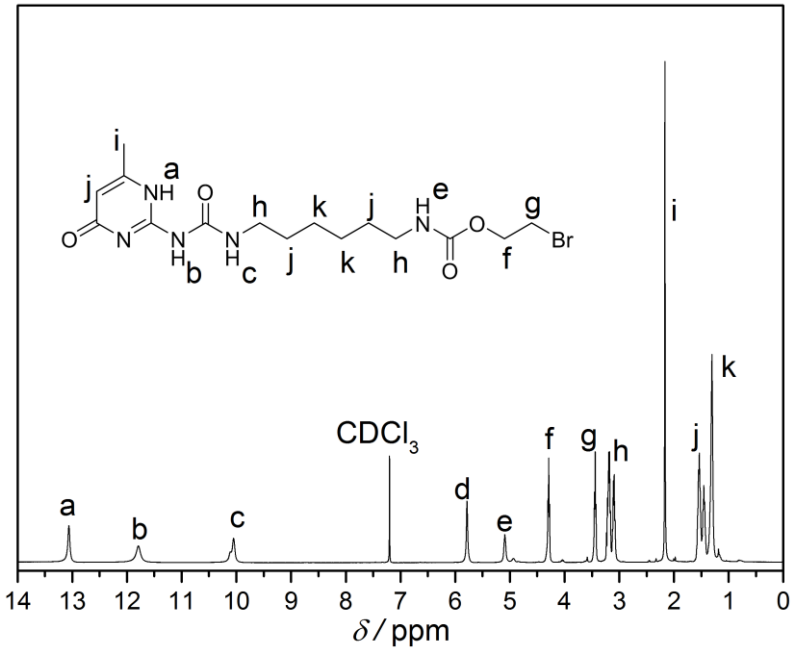

Figure 79: ^{1}H-NMR spectrum of UPy-Br (**24**) in $CDCl_3$.

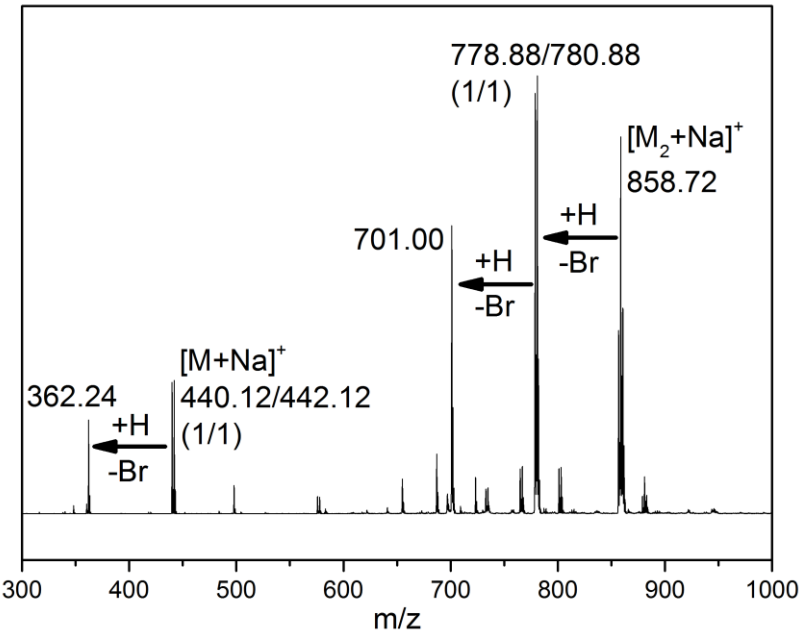

Figure 80: Mass spectrum of UPy-Br (**24**) recorded on a LXQ mass spectrometer.

5.3.20 *AOA-MalPG (**26**)*

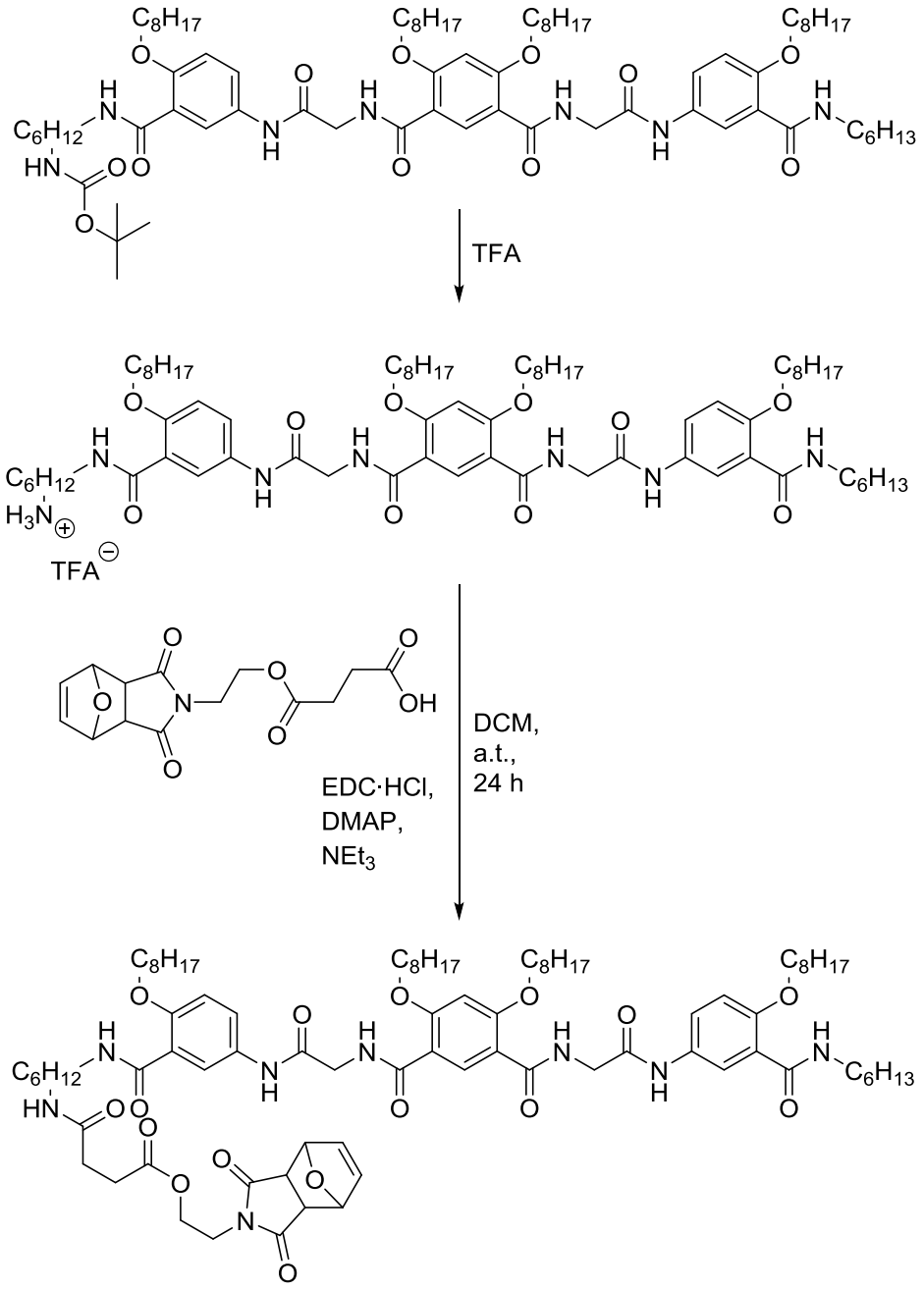

26 mg (20 μmol, 1 eq.) AOA-NHBoc (provided by Bernhard and coworkers, INSA-Lyon) were deprotected in TFA according to Montarnal *et al*.[153] and used without further purification or characterization.

The corresponding TFA ammonium salt, 9 mg (30 μmol, 1 eq.) MalPG-CO_2H (**25**) (provided by Kilian Wuest, KIT), 12 mg (60 μmol, eq.) EDC·HCl, 0.7 mg (6 μmol, 0.2 eq.) DMAP and 3.3 μL (2.4 mg, 24 μmol, 1 eq) NEt_3 were dissolved in 3 mL dry DCM under inert gas and stirred for 24 h. The solvent was removed *in vacuo* and the

crude product was purified *via* column chromatography (R_f = 0.29, DCM/MeOH 95/5) (12 mg, 8.0 mmol, 40% yield).

^{1}H NMR ($CDCl_3$, 400 MHz), δ (ppm) = 9.92-9.60 (s, 2H), 8.90 (s, 1H), 8.56-8.44 (m, 2), 8.25-7.95 (6H), 6.93-6.80 (m, 2H), 6.45-6.30 (3H), 5.17 (s, 2H), 4.43 (s, 4H), 4.20-3.95 (10H), 3.67 (t, J = 5.4 Hz, 4H), 3.50-3.35 (m, 2H), 3.20-3.10 (m, 2H), 2.81 (s, 2H), 2.56 (t, J = 7.0 Hz, 2H), 2.40 (t, J = 7.0 Hz, 2H), 2.03-1.73 (m, 8H), 1.70-1.10 (-CH_2-), 0.85-0.73 (m, 15H).

m/z $([M+Na]^+)_{exp}$ = 1525.7, $([M+Na]^+)_{theo}$ = 1525.9.

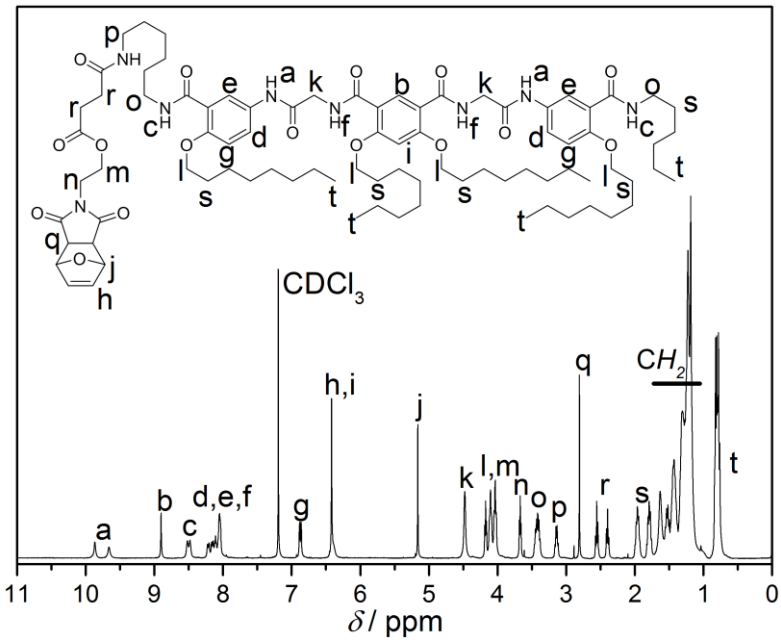

Figure 81: ^{1}H-NMR spectrum of AOA-MalPG (**26**) in $CDCl_3$.

5.3.21 *AOA-Mal (**27**)*

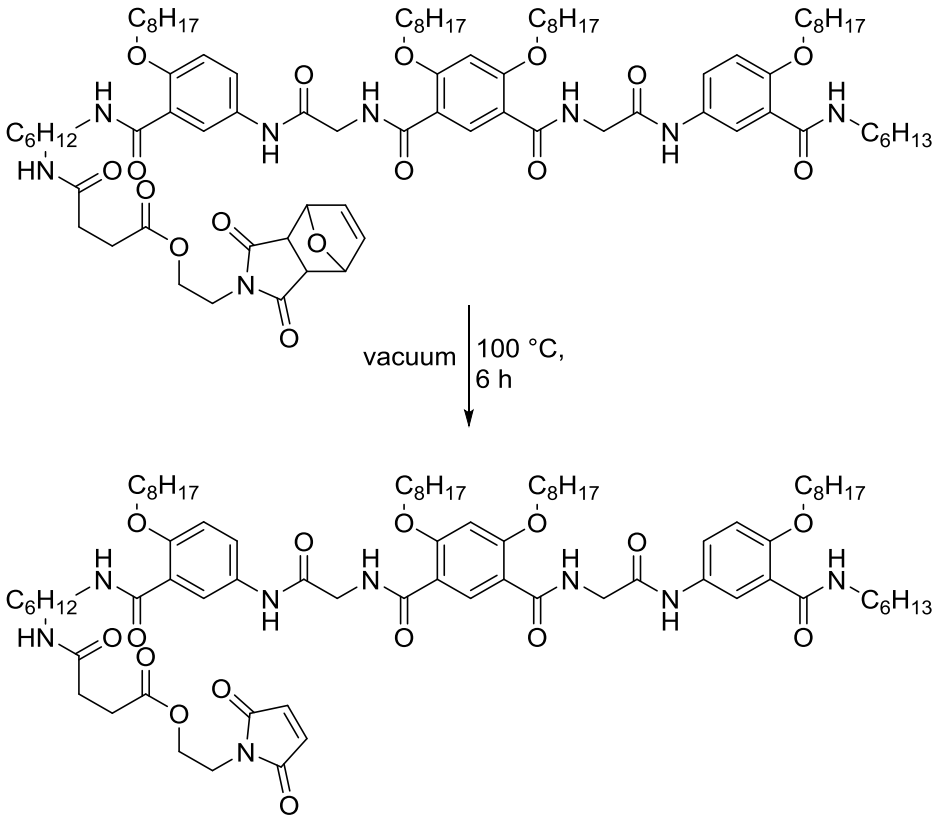

12 mg (8.0 mmol, 1 eq.) AOA-MalPG (**26**) was heated for 6 h at 100°C in a Schlenk tube to give a yellow solid that was used without further purification and yield was considered as very high (99% yield) with regard to the ^{1}H-NMR spectrum.

^{1}H NMR ($CDCl_3$, 400 MHz), δ (ppm) = 9.74-9.40 (2H), 8.90 (s, 1H), 8.55-8.40 (2), 8.25-7.95 (6H), 6.93-6.80 (m, 2H), 6.65 (s, 2H), 6.42 (s, 1H), 4.45 (s, 4H), 4.20-3.95 (m, 10H), 3.72 (t, J = 5.3 Hz, 2H), 3.50-3.35 (m, 2H), 3.20-3.10 (m, 2H), 2.56 (t, J = 7.1 Hz, 2H), 2.40 (t, J = 7.1 Hz, 2H), 2.03-1.73 (m, 8H), 1.70-1.10 (-CH_2-), 0.87-0.70 (m, 15H).

m/z $([M+Na]^+)_{exp}$ = 1458.0, $([M+Na]^+)_{theo}$ = 1457.9.

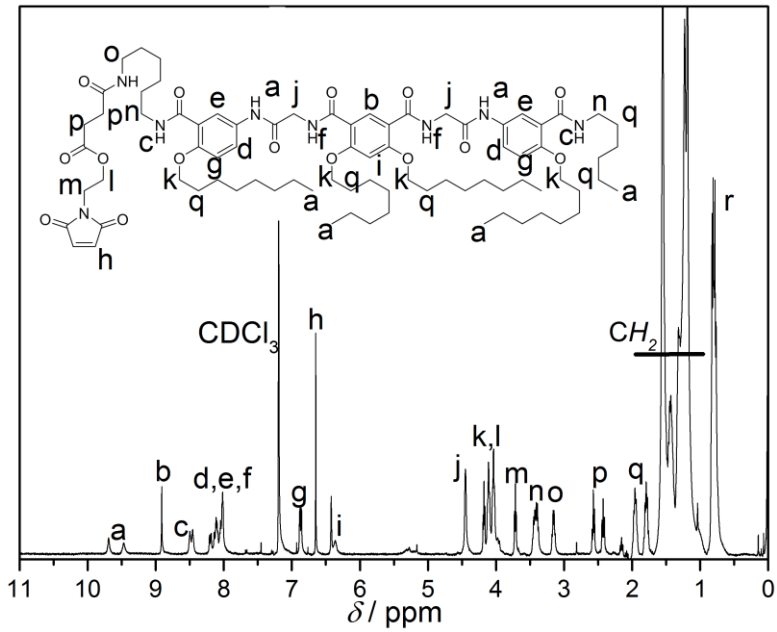

Figure 82: ^{1}H-NMR spectrum of AOA-Mal (**27**) in $CDCl_3$.

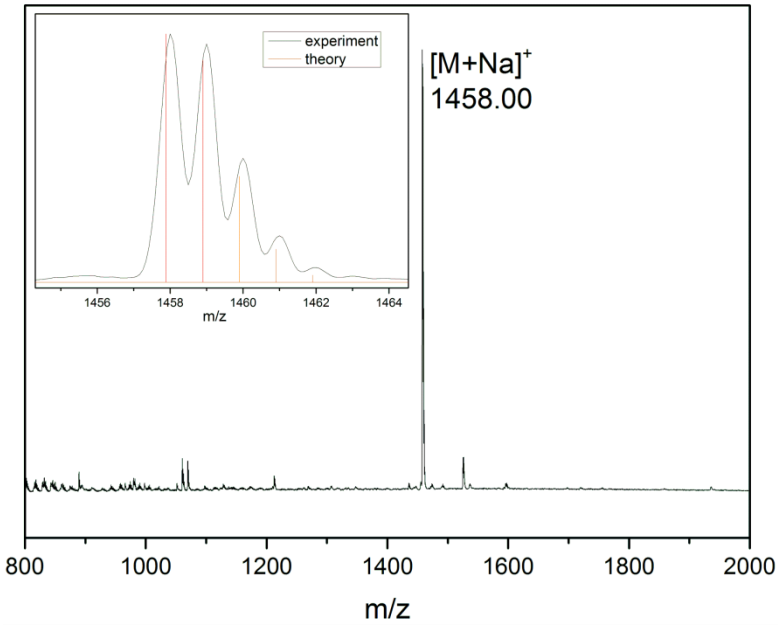

Figure 83: Mass spectrum of AOA-Mal (**27**) with the corresponding simulated isotopic pattern.

5.3.22 *Sorb$_2$ (**28**)*

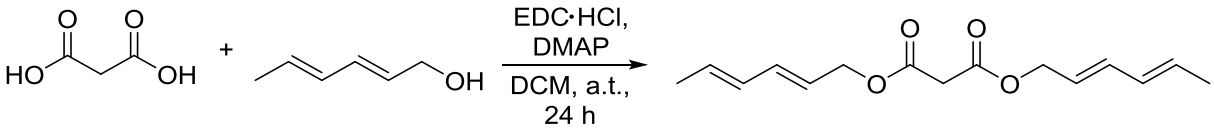

1.17 g (11.2 mmol, 1.0 eq) Malonic acid, 2.20 g (22.4 mmol, 2.0 eq.) sorbic alcohol, 6.23 g (5.1 mmol, 0.5 eq) DMAP and 6.84 g (35.7 mmol, 3.0 eq) EDC·HCl were dissolved in 90 mL dry DCM and stirred for 24 h at ambient temperature. The solution was extracted with 1M HCl, 1M KOH and H_2O, dried over $MgSO_4$ and evaporated under reduced pressure. The crude product was purified *via* purified by column chromatography (cyHex /EE 20/1) and obtained as pale yellow liquid (1.41 g, 5.3 mmol, 48% yield), which solidified in the fridge. The experiment was conducted by Thorsten Lückerath.

^{1}H-NMR ($CDCl_3$, 400 MHz), δ(ppm) = 6.24-6.14 (m, 2H), 6.03-5.92 (m, 2H,), 5.76-5.63 (m, 2H), 5.58-5.49 (m, 2H), 4.57 (m, 4H), 3.32 (s, 2H), 1.70 (m, 6H).

^{13}C-NMR ($CDCl_3$, 400 MHz), δ(ppm) = 166.27, 136.46, 131.46, 130.33, 122.92, 66.00, 41.60, 18.15.

m/z $([M+Na]^+)_{exp}$ = 287.12, $([M+Na]^+)_{theo}$ = 287.12, $([M_2+Na]^+)_{exp}$ = 551.26, $([M_2+Na]^+)_{theo}$ = 551.26.

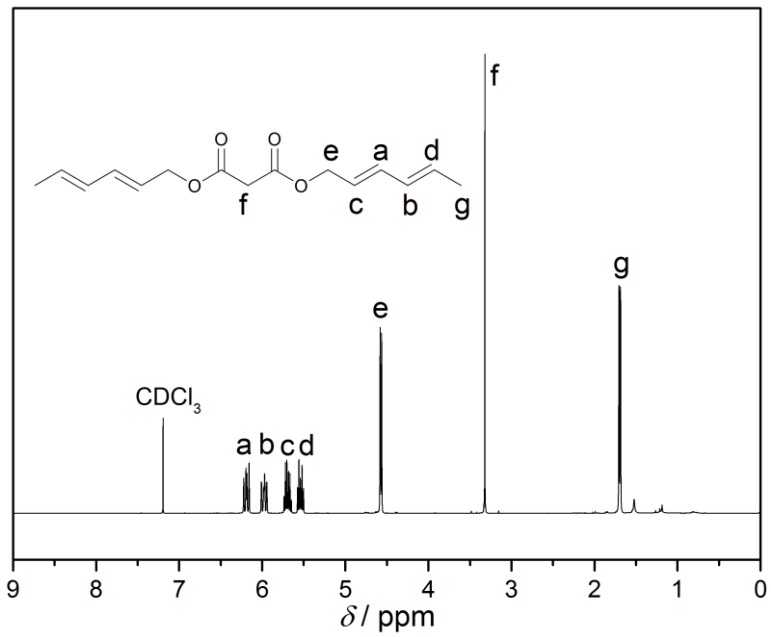

Figure 84: ^{1}H-NMR spectrum of $Sorb_2$ (**28**) in $CDCl_3$.

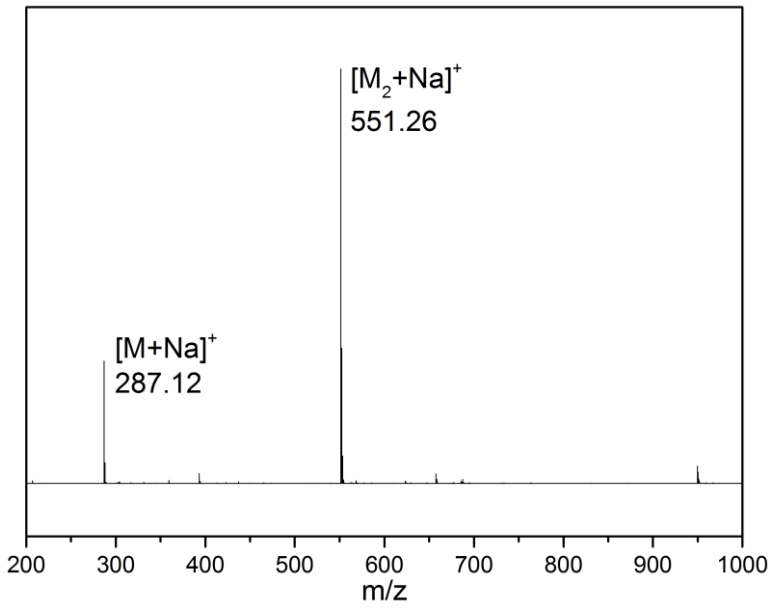

Figure 85: Mass spectrum of $Sorb_2$ (**28**).

5.4 Polymer Synthesis and Modification

5.4.1 *MeOEGMA$_{300}$-Br Star (**P1**)*

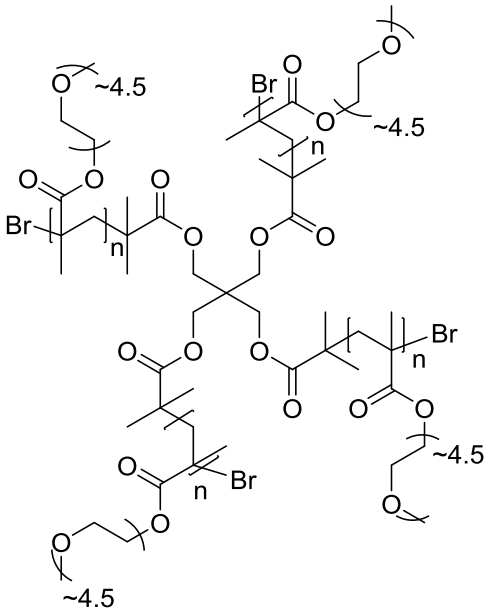

4f-Bib/6f-Bib, MeOEGMA$_{300}$, $CuBr_2$ and bPy were dissolved in DMF and the solution was degassed *via* three freeze-pump-thaw cycles. $Sn(EH)_2$ was added to the frozen reaction mixture and inert conditions were restored by exchanging the atmosphere 3 times. The polymerization was conducted for at 40 °C. The reaction was quenched with air and addition of 5 mL deionized water. The polymer was purified by dialysis in water (MWCO 2.000) and freeze dried resulting in a colorless oil.

^{1}H-NMR ($CDCl_3$, 400 MHz), δ(ppm) = 4.23 (s, 8H), 4.02 (s, 2nH), 3.81-3.37 (m, 16nH), 3.38-3.22 (s, 3nH), 1.97-1.63 (m, 2nH+24H), 1.08-0.68 (m, 3nH).

Polymer	4f-Bib (mg, mmol, eq.)	$MeOEGMA_{300}$ (g, mmol, eq.)	$CuBr_2$ (mg, mmol, eq.)	bPy (mg, mmol, eq.)	$Sn(EH)_2$ (μL, mg, mmol, eq.)	DMF (mL)	time (h)	SEC data (M_n, $Đ$)
$P1A_4$	146.6, 0.20, 1	4.032, 17.40, 87	8.9, 0.04, 0.2	31.2, 0.20, 1	38.4, 48.0, 0.12, 0.6	8	2	7.4 kDa, 1.2
$P1B_4$	293.2, 0.40, 1	7.200, 24.00, 60	8.9, 0.04, 0.1	31.2, 0.20, 0.5	38.4, 48.0, 0.12, 0.3	4	1	7.6 kDa, 1.2
$P1C_4$	146.6, 0.20, 1	4.032, 17.40, 87	8.9, 0.04, 0.2	31.2, 0.20, 1	38.4, 48.00, 0.12, 0.6	8	2.5	12.4 kDA, 1.2
$P1D_4$	58.6, 0.08, 1	28.800, 96.0, 1200	8.9, 0.04, 0.5	32.2, 0.20, 2.5	39.2, 48.10, 0.12, 1.5	8	3	28.0 kDa, 1.2
$P1_6$	(6f-Bib) 293.3, 0.26, 1	7.200, 24.00, 92	17.8, 0.08, 0.3	62.4, 0.40, 1.5	57.6, 72.10, 0.18, 0.6	8	1	7.0 kDa, 1.2
$P1_{el}$	146.6 0.20 1	2.016, 6.72, 34	4.48, 0.02, 0.1	15.6, 0.10, 0.5	19.2, 24.00, 0.06, 0.3	4	1	5.5 kDa, 1.2

Table 6: Reactants and reaction times for synthesis of $MeOEGMA_{300}$-Br Stars (**P1**).

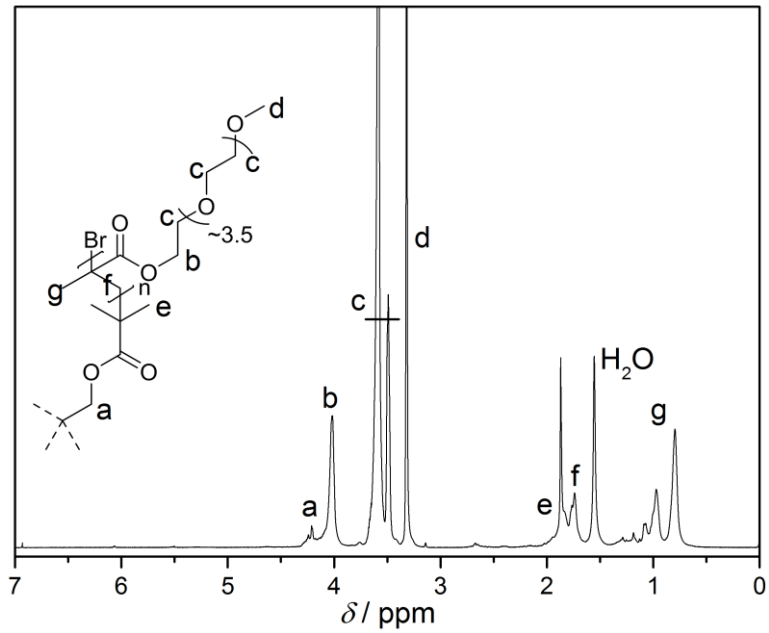

Figure 86: Representative ^{1}H-NMR spectrum of $MeOEGMA_{300}$-Br Star (**P1**) in $CDCl_3$.

5.4.2 *MeOEGMA$_{300}$-N$_3$ Star (**P2**)*

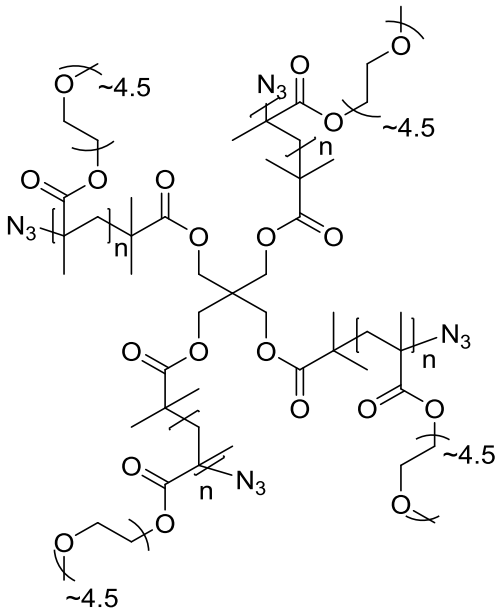

The precursor polymer **P1** and NaN_3 were dissolved in DMF, stirred for 3 d at ambient temperature, subsequently dialyzed against water (MWCO 2000) and isolated *via* freeze drying. The product was obtained as colorless oil. Functionalization was verified by IR analysis.

Polymer	Precursor (g, mmol, eq.)	NaN_3 (g, mmol, eq.)	DMF (mL)	SEC data (M_n, *Đ*)
P2A$_4$	**P1A$_4$** 1.257, 0.170, 1	1.090, 16.8, 99	25	7.0 kDa, 1.1
P2B$_4$	**P1B$_4$** 2.569, 0.338, 1	1.759, 27.0, 80	38	7.9 kDa. 1.2
P2C$_4$	**P1C$_4$** 2.770, 0.231, 1	1.160, 17.8, 77	25	11.0 kDa, 1.2
P2D$_4$	**P1D$_4$** 1.356, 0.0484, 1	251.8, 3.9, 80	5	34.1 kDa. 1.2
P2$_6$ (6 arms)	**P1$_6$** 1.590, 0.227, 1	1.770, 27.3, 120	40	7.4 kDa, 1.2
P2$_{el}$	**P1$_{el}$** 0.750, 0.140, 1	0.177, 2.7, 19	16	5.6 kDa, 1.1

Table 7: Synthesis of MeOEGMA$_{300}$-N_3 Stars (**P2**).

5.4.3 *MeOEGMA$_{300}$-UPy Star (**P3**)*

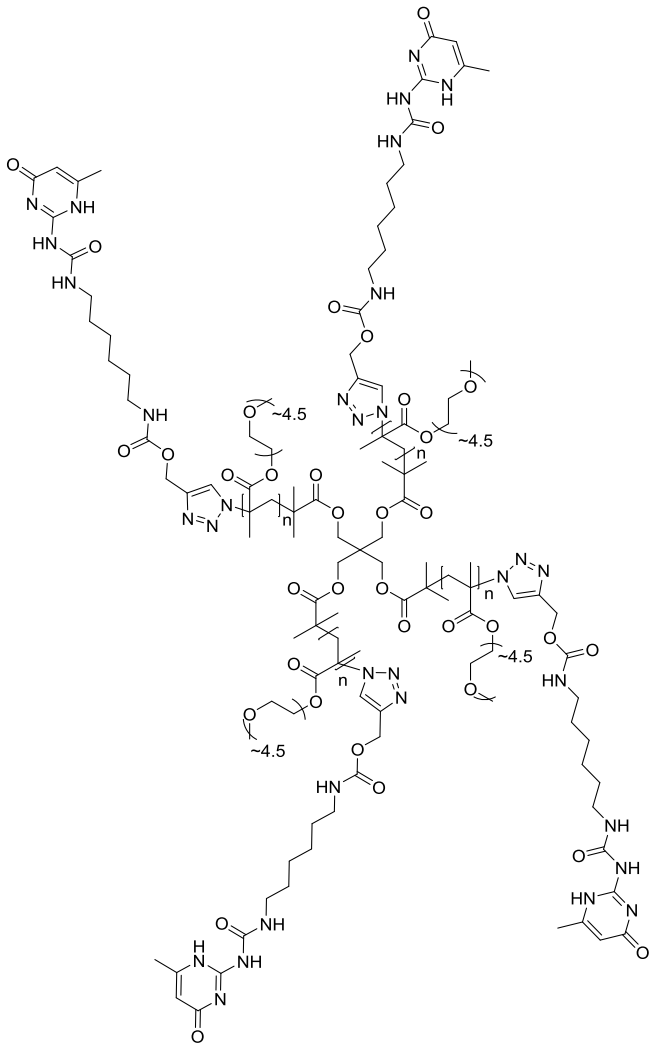

Precursor (**P2**), UPy-Urethane-Alkyne (**9**) and PMDTA were dissolved in DMF. The solution was degassed by four freeze-pump-thaw cycles. CuBr and a pinch of ascorbic acid was added to the frozen solution and the inert conditions were restored. The reaction mixture was stirred for 24 h at ambient temperature, changing its color from light violet to green. The product was purified by dialysis (MWCO 2000) and isolated by freeze drying, yielding a dark green solid. Additionally to ^{1}H-NMR analysis functionalization was verified by the disappearance of the N_3-Band in the corresponding IR spectrum. For removal of the Cu-contamination the polymers were purified by electrolysis in aqueous solution.

^{1}H-NMR ($CDCl_3$, 400 MHz), δ(ppm) = 13.03 (s, 4H), 11.78 (s, 4H), 10.03 (s, 4H), 7.78 (s, 4H), 5.77 (s, 4H), 5.17-5.00 (m, 12H), 4.23 (8H), 4.02 (s, 2nH), 3.81-3.37 (10nH),

3.38-3.22 (s, 3nH) 3.15-3.01 (m, 16H), 2.16 (s, 12H), 1.97-1.63 (2nH+24H), 1.29 (), 1.18 (), 1.08-0.68 (3nH, CH_3).

Polymer	Precursor (g, mmol, eq.)	**9** (mg, mmol, eq.)	PMDTA (μL, mg, mmol, eq.)	CuBr (mg, mmol, eq.)	DMF (mL)	SEC data (M_n, *Đ*)
P3A$_4$	**P2A$_4$** 0.926, 0.132, 1	177.4, 0.529, 4	110.5, 91.7, 0.529, 4	82.6 0.529, 4	20	7.0 kDa, 1.2
P3B$_4$	**P2B$_4$** 2.336, 0.552, 1	804.8, 2.400, 4.4	501.2, 416.0, 2.400, 4.4	348.0, 2.228, 4.0	35	8.8 kDa, 1.2
P3C$_4$	**P2C$_4$** 2.358, 0.214, 1	316.0, 0.942, 4.4	196.7, 163.3, 0.942, 4.4	147.0, 0.942, 4.4	35	12.1 kDa, 1.2
P3D$_4$	**P2D$_4$** 1.390, 0.050, 1	100.0, 0.298, 6.0	200.0, 241.0, 1.391, 28.0	150.0, 0.960, 19.3	20	48.0 kDa, 2.0
P3$_6$ (6 arms)	**P3$_6$** 1.244, 0.168, 1	369.0, 1.100, 6.5	230.0, 190.9, 1.102, 6.6	158.0, 1.011, 6.0	16	7.3 kDa, 1.3
P3$_{el}$	**P2$_{el}$** 0.646 0.120, 1	173.0, 0.520, 4.3	107.9, 89.5, 0.520, 4.3	83.6, 0.540, 4.5	15	6.1 kDa, 1.2

Table 8: Synthesis of MeOEGMA$_{300}$-UPy Stars (**P3**).

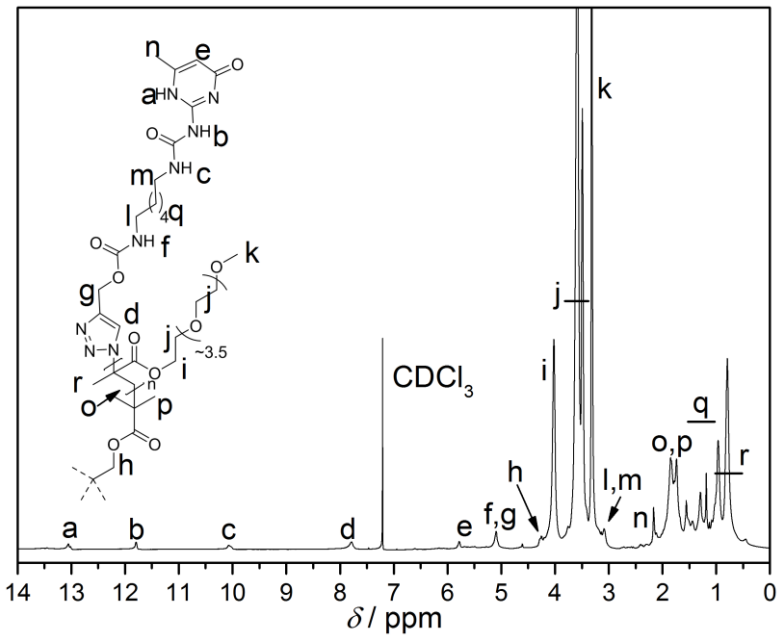

Figure 87: Representative ^{1}H-NMR spectrum of MeOEGMA$_{300}$-UPy Star (**P3**) in $CDCl_3$.

5.4.4 *Electrolysis of **P3** (**P3***)*

MeOEGMA$_{300}$-UPy Star (**P3**) was dissolved in deionized water with a concentration c(UPy) = 0.0134 mmol·mL^{-1} and electrolysis was performed with platinum electrodes applying a voltage of 12 V until the aqueous solution was discolored (24 h). After electrolysis the aqueous solution was lyophilized and the purified polymer **P3*** was characterized by ^{1}H NMR and SEC to exclude degradation events. Since degradation was not observed, analytic data of all polymers **P3*** is identical to **P3** and, therefore, not presented.

5.4.5 *MeOEGMA$_{300}$-**11/12**-Copolymers (**P4**)*

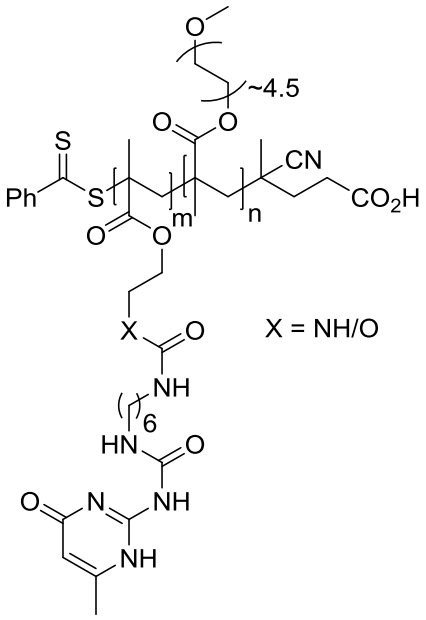

MeOEGMA$_{300}$, **11/12**, AIBN, 4-Cyano-4-(phenylcarbonothioylthio)pentanoic acid were dissolved in dry DMSO, degassed with an Ar stream and polymerized at 65 °C. The polymer was purified by dialysis against water and isolated by lyophilization.

^{1}H-NMR (400 MHz, DMSO-d$_6$): δ(ppm) = 11.51 (s, 1H), 9.64 (s, 1H,), 7.83 (m, 2H), 7.64 (t, *J* = 6.9 Hz, 1H), 7.47 (t, *J* = 7.2 Hz, 2H), 6.91(s, 1H), 5.76 (s, 1H), 4.18-3.90 (4mH+2nH), 3.67-3.38 (m, -OCH$_2$-), 3.44- (s,), 3.25 (s, 3nH), 3.16-2.91 (4mH), 2.18 (s, 3nH), 1.99-1.51(2nH+2mH), 1.51-1.09 (8mH+3H), 1.06-0.52 (3nH+3mH+4H).

Polymer	$MeOEGMA_{300}$ (g, mmol, eq.)	UPy-monomer (mg, mmol, eq., mol% monomer)	AIBN (mg, μmol, eq.)	CTA (mg, mmol, eq.)	DMSO (mL)	time (h)	Copolymer (M_n, $Đ$, mol% UPy)
P4$^{NH}_{10}$	2.740, 9.1, 180	**12** 580.0, 1.40, 27, 13%	0.8, 5, 0.1	14.2, 0.05, 1	8	11	38.8 kDa, 1.4, 10%
P4$^{O}_{10}$	‖	**11** 580.0, 1.40, 27, 13%	‖	‖	‖	‖	34.2 kDa, 1.3, 10%
P4$^{NH}_{3}$	2.700, 9.0, 177	**12** 290.0, 0.69, 13.5, 7%	‖	‖	‖	22	28.5 kDa, 1.6, 3%
P4$^{O}_{5}$	‖	**11** 290.0, 0.69, 13.5, 7%	‖	‖	‖	21	23.8 kDa, 1.2, 5%

Table 9: Amounts of reactants, solvent and polymerization time for the RAFT polymerization of **P4** and SEC and ^{1}H-NMR evaluation of the final polymers.

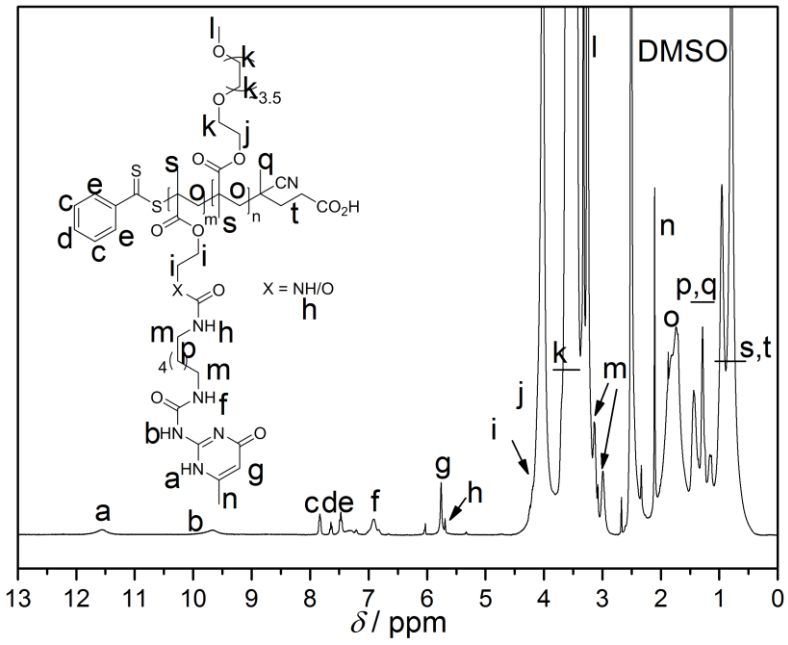

Figure 88: Representative ^{1}H-NMR spectrum of **P4** in DMSO-d_6. Copolymer composition was calculated with resonances g and r.

5.4.6 *MeOEGMA$_{500}$-**13**-Copolymers (**P5**)*

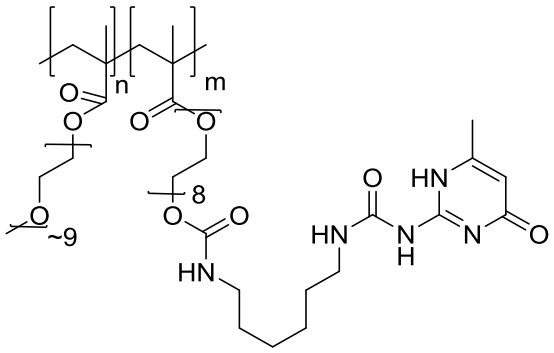

MeOEGMA$_{500}$ and UPy-OEG-MA (**13**) were dispersed in DMF and heated to 65 °C until the dispersion became clear. AIBN was added at ambient temperature and the mixture was degassed with an argon stream for 30 min. For polymerization the solution was heated to 65 °C and the copolymer was isolated *via* dialysis against water, subsequent centrifugation, and lyophilization.

^{1}H-NMR (400 MHz, $CDCl_3$): δ(ppm) =13.04 (s, 1mH), 11.80 (s, 1mH), 10.04 (s, 1mH), 5.78 (s, 1mH), 4.92 (s, 1mH), 4.40-3.81 (m, 4mH+2nH), 3.87-3.37 (m, 8mH+6nH), 3.30 (s, 3nH), 2.23-2.95 (m, 4mH), 2.25-1.55 (m, 2mH+2nH), 2.19 (s, 3mH), 1.61-1.10 (m, 8mH), 1.10-0.52 (m, 3mH+3nH).

Polymer	$MeOEGMA_{500}$ (g, mmol)	UPy-OEG-MA (**13**) (g, mmol, mol%)	DMF (mL)	AIBN (mg, µmol)	reaction time (h)	Copolymer (M_n, $Đ$, mol% UPy)
$P5_0$	6.39, 12.8	-	40	0.2, 1.3	23	364 kDa, 2.2, 0 %
$P5_{10}$	5.44, 10.9	1.138, 1.9, 14.8	‖	‖	‖	161 kDa, 2.2, 10.4%
$P5_{14}$	54.4, 109.0	11.4, 19.0, 14.8	400	2.1, 13	‖	339 kDa, 1.8, 14 %
$P5_{20}$	44.8, 89.6	23.0 g, 38.4, 30.0	‖	‖	‖	414 kDa, 1.7, 20 %

Table 10: Masses (m), moles (n) and volumes (V) of employed reactants and solvents for synthesis of **P5**. Copolymer composition was calculated from ^{1}H-NMR resonances d and i.

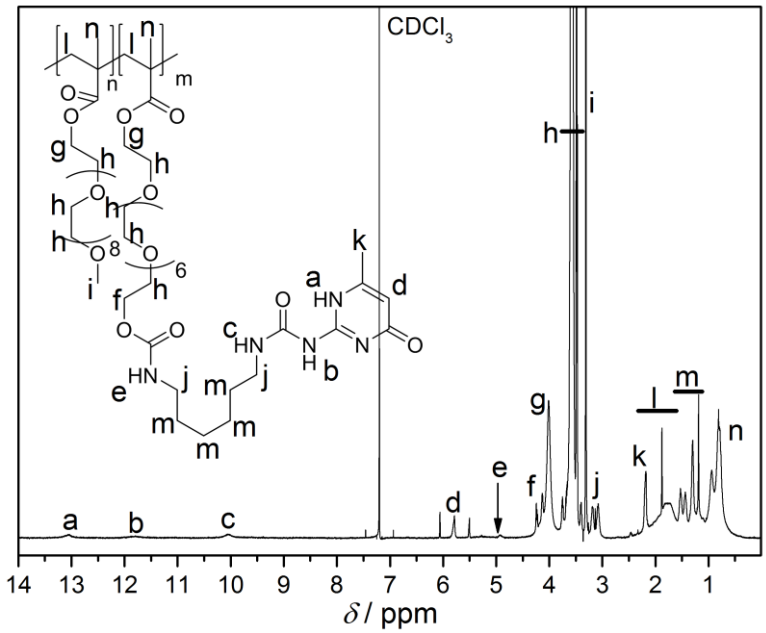

Figure 89: Representative ^{1}H-NMR spectrum of a copolymer of $MeOEGMA_{500}$ and UPy-OEG-MA (**13**) in $CDCl_3$. Copolymer compositions (mol% UPy) were calculated employing resonances d and i.

5.4.7 *MeOEGMA$_{500}$-**15**-**16**-Copolymer (**P6**)*

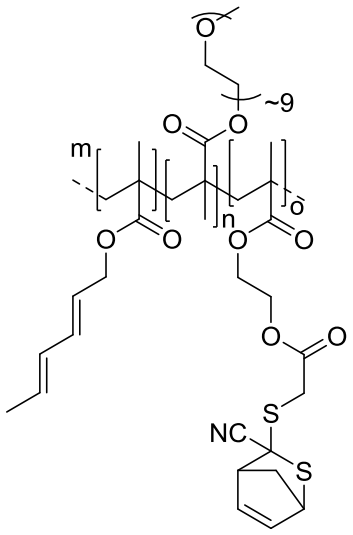

10.6 g (21.2 mmol, 180 eq.) MeOEGMA$_{500}$, 196 mg (1.2 mmol, 10 eq.) Sorb-MA (**16**), 420 mg (1.2 mmol, 10 eq.) CDTE-MA (**15**), 19.4 mg (0.12 mmol, 1 eq.) AIBN were dissolved in 10.5 mL dioxane, degassed for 20 min with an argon stream and heated to 65 °C for 5.5 h. The polymer was isolated *via* aqueous dialysis and subsequent lyophilization, yielding a yellow viscous liquid. The HDA polymer **P6** was analyzed *via* ^{1}H-NMR and SEC and stored as aqueous solution, since it cross-linked at ambient temperature over several days (M_n = 127.2 kDa, $Đ$ = 2.3, 6 mol% **15**, 4 mol% **16**).

^{1}H-NMR ($CDCl_3$, 400 MHz), δ(ppm) = 6.7-6.3 (m, 1oH), 6.2-5.4 (4mH+1oH), 4.4-4.0 (m, 5oH+2nH+2mH), 4.0-3.4 (m, 3oH+32nH), 3.30 (s, 3nH), 2.1-1.7 (m, 4oH+5mH+2nH), 1.1-0.7 (m, 3oH+3mH+3nH).

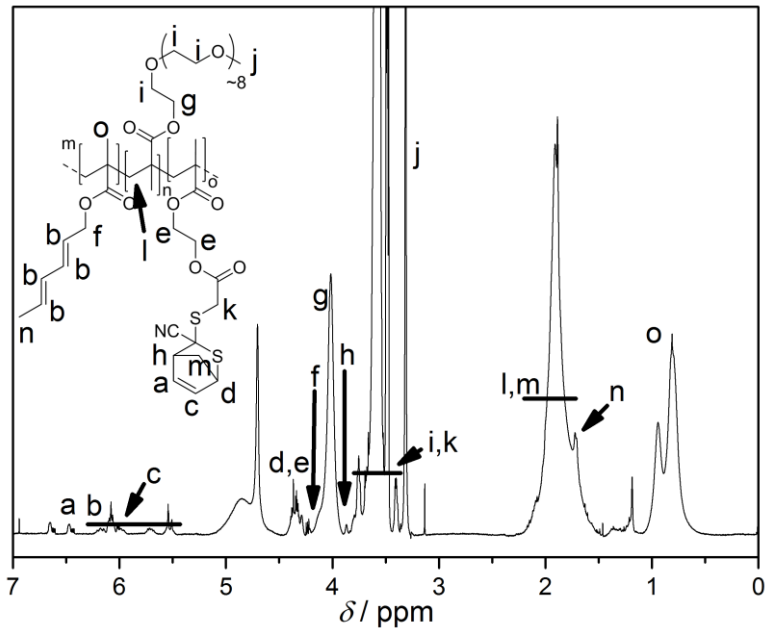

Figure 90: ^{1}H-NMR spectrum of **P6** in $CDCl_3$.For calculation resonances a and (b-c) have been employed.

5.4.8 *BMA-**10**-TFEMA (**P7**)*

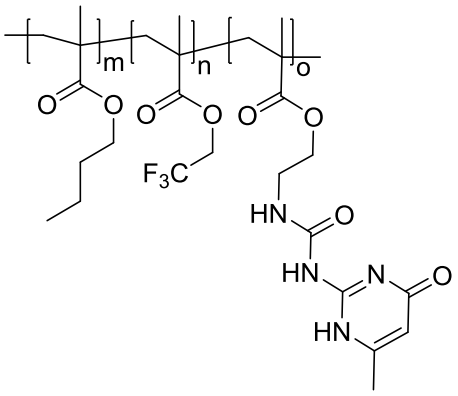

168 mg (1.0 mmol, 1.9 eq.) TFEMA, 1.278 g (9.0 mmol, 17.0 eq.) BMA, 280 mg (1.0 mmol, 1.9 eq.) UPy-MA (**10**), 87 mg (0.53 mmol, 1 eq.) AIBN were suspended in 20 mL DMSO, degassed and heated to 60 °C for 24 h. The polymer was precipitated in MeOH, dissolved in $CHCl_3$ and precipitated two more times, subsequently the precipitate was dried (M_n = 63.0 kDa, $Đ$ = 1.4, 4 mol% UPy, 8 mol% CF_3).

^{1}H-NMR (400 MHz, $CDCl_3$): δ(ppm) = 12.92 (s, 1oH), 11.890 (s, 1oH), 10.44 (s, 1oH), 5.77 (s, 1oH), 4.27 (s, 2nH), 4.12-3.63 (m, 2mH+2oH), 3.44 (m, 2oH), 2.32-2.07 (m, 3oH), 2.04-1.63 (m, 4mH+2nH+2oH), 1.54 (s, 2mH), 1.33 (s, 3mH+3nH+3oH), 1.06-0.63 (m, 3mH).

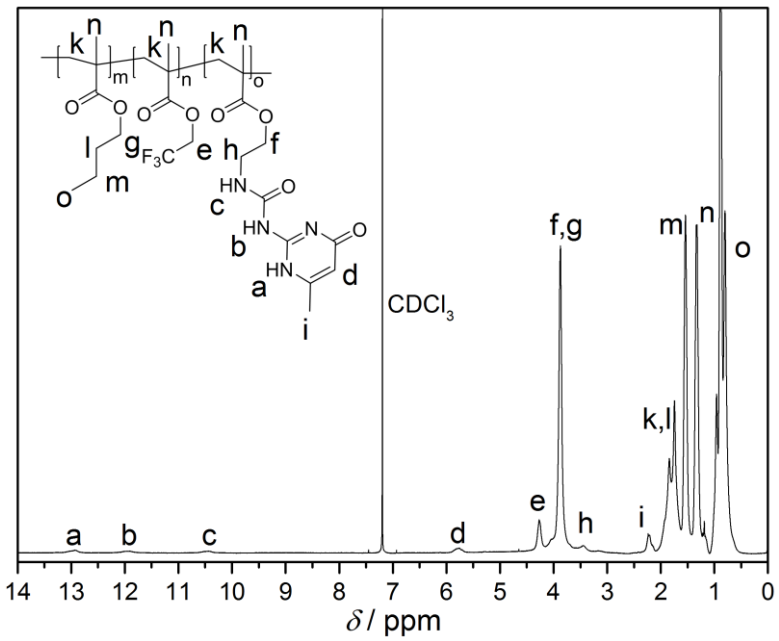

Figure 91: ^{1}H-NMR spectrum of BMA-**10**-TFEMA (**P7**) in $CDCl_3$.

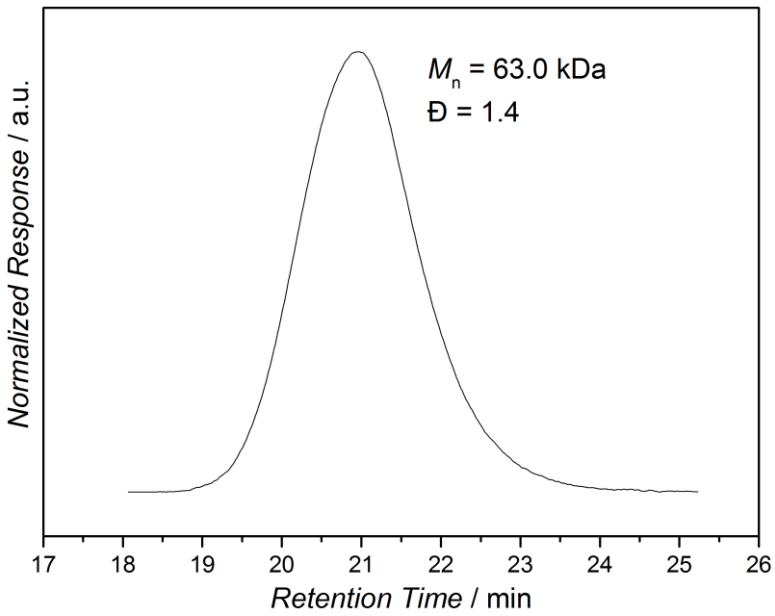

Figure 92: SEC elugram of BMA-**10**-TFEMA (**P7**).

5.4.9 *MMA-**15** RAFT-Copolymers (**P8**)*

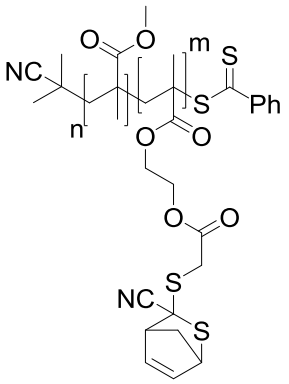

In a typical experiment, MMA, CDTE-MA (**15**), CPDB (11.0 mg, 0.5 mmol, 1 eq) AIBN (1.64 mg, 0.1 mmol, 0.2 eq) and dioxane were combined in schlenk tube and degassed *via* three freeze-pump-thaw cycles. The polymerization was carried out under inert gas at 60 °C. After polymerization the mixture was cooled to ambient temperature and precipitated in cold cyclohexane (20 mL). The resulting pink solid was dissolved in DCM (1 mL) and precipitation was repeated twice. The final polymer was characterized *via* SEC and ^{1}H-NMR.

^{1}H-NMR ($CDCl_3$, 400 MHz), δ(ppm) = 6.7-6.3 (m, 1mH), 6.1-6.0 (m, 1mH), 4.4-4.2 (m, 5mH), 3.9-3.6 (m, 3mH), 3.5 (s, 3nH), 2.1-1.7 (m, 2nH+4mH), 1.1-0.7 (m, 3mH+3nH).

Polymer	MMA (mg, mmol, eq., mol% monomer)	**15** (mg, mmol, eq., mol% monomer)	dioxane (mL)	time (h)	SEC data (M_p, $Đ$)	^{1}H-NMR Data (mol% **15**)
P8A	626, 62.5, 125, 83%	424, 12.5, 25, 17%	0.6	40	13.8 kDa, 1.3,	17%
P8B	901, 90.0, 180, 90%	339. 10.0, 20, 10%	0.6	16	10.0 kDa, 1.3	10%
P8C	500, 50.0, 100, 83%	339, 10.0, 20, 17%	0.5	16	9.8 kDa, 1.3	17%

Table 11: Amounts of reactants, solvent and polymerization time for the RAFT polymerization of **P8** including the corresponding SEC and ^{1}H-NMR evaluation of the final polymer

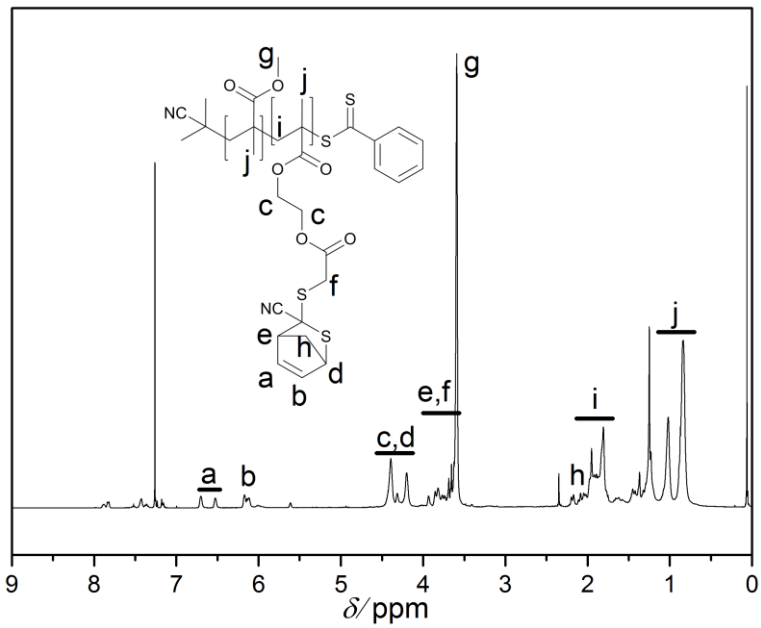

Figure 93: Representative ^{1}H-NMR spectrum of **P8** in $CDCl_3$.

5.4.10 *MMA-**15** FRP-Copolymer (**P8FRP**)*

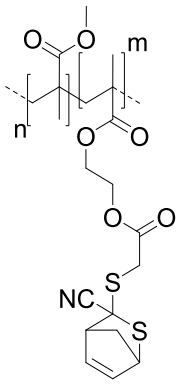

668.6 mg MMA (6.7 mmol, 170 eq), 400 mg CDTE-MA (**15**) (1.2 mmol, 30 eq), 6.5 mg AIBN (0.04 mmol, 1 eq) and 3.5 mL dioxane were combined in a schlenk tube and degassed *via* three freeze-pump-thaw cycles. The polymerization was carried out under inert gas at 60 °C for 5 h. After polymerization the mixture was cooled to ambient temperature and precipitated in cold cyclohexane (20 mL). The white solid was dissolved in DCM (1 mL) and precipitation was repeated twice (M_P = 47.8 kDa, $Đ$ = 1.6, 15 mol% **15**).

^{1}H-NMR ($CDCl_3$, 400 MHz), δ(ppm) = 6.7-6.3 (m, 1mH), 6.1-6.0 (m, 1mH), 4.4-4.2 (m, 5mH), 3.9-3.4 (m, 3mH), 3.5 (3nH), 2.1-1.7 (m, 2nH+4mH), 1.1-0.7 (m, 3mH+3nH).

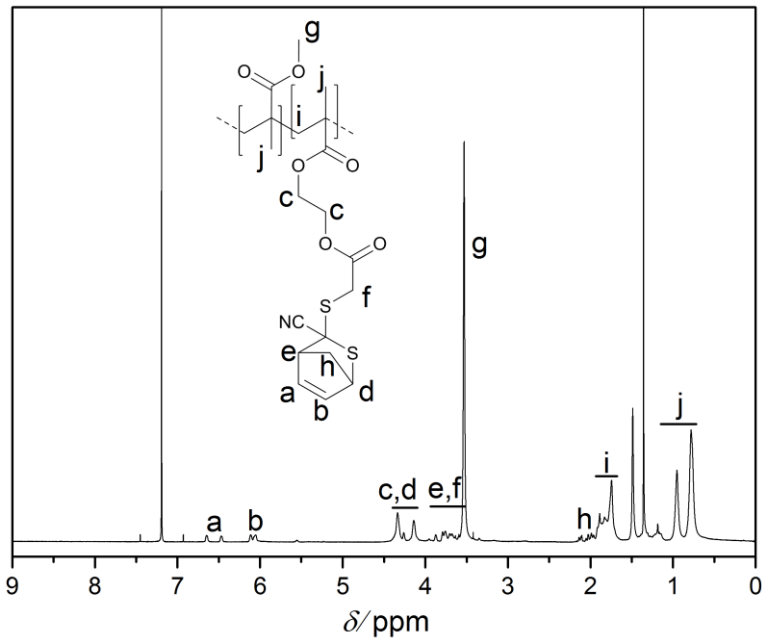

Figure 94: ^{1}H-NMR spectrum of **P8FRP** in $CDCl_3$. Polymer composition was calculated with resonances a and g.

5.4.11 *Folding of **P8** (**P8$_f$**)*

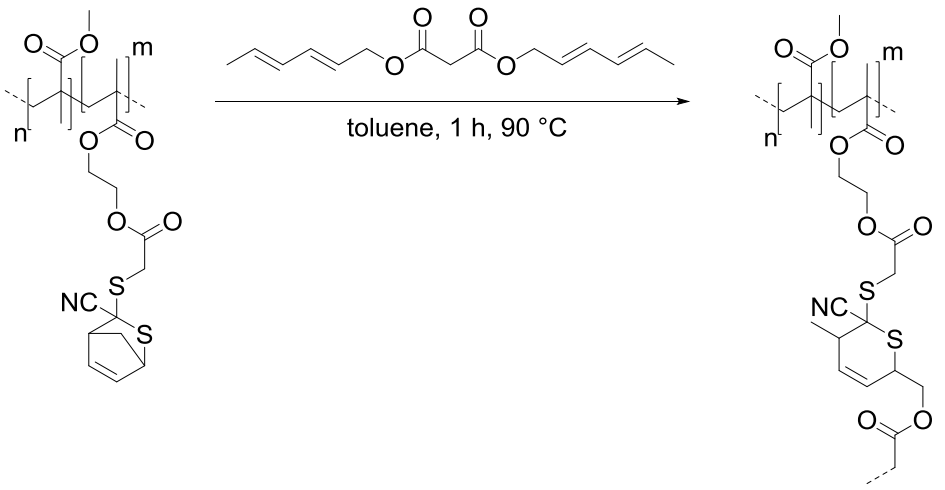

60 mg Polymer **P8A-C**,**FRP** was dissolved in toluene (300 mL) and 0.5 eq (per CDTE unit) $Sorb_2$ (**28**) was added. The solution was stirred for 1 d at 90 °C. To isolate the SCNP, the reaction volume was decreased under reduced pressure to approx. 2~3 mL and the SCNP was precipitated in cold cyclohexane (20 mL) and received as grayish powder after drying. The SCNPs (**P8A-C$_f$,FRP$_f$**) were characterized by comparative SEC measurement and ^{1}H-NMR.

^{1}H-NMR ($CDCl_3$, 400 MHz), δ(ppm) = 6.2-5.6 (2mH), 4.4-4.2 (m, 6mH), 3.9-3.4 (m, 5mH+3nH),3.0-2.6 (1mH), 2.1-1.7 (m, 2nH+2mH), 1.08-0.68 (m, 6mH+3nH).

Precursor Polymer (M_n, M_p, $Đ$, mol% **15**)	mmol CDTE (per 60 mg precursor)	**28** (mg, mmol, eq.)	SCNP (M_p, $Đ$, ΔM_p, $\Delta\%M_p$)
P8A, 10.0 kDa, 13.8 kDa, 1.3, 17%	0.071	9.4, 0.036, 0.5	**P8A$_f$**, 11.7 kDa, 1.2, -2.1 kDa, -15%
P8B, 7.9 kDa, 10.0 kDa, 1.3, 10%	0.048	6.4, 0.024, 0.5	**P8B$_f$**, 9.0 kDa, 1.2, -1.0 kDa, -10%
P8C, 8.1 kDa, 9.8 kDa, 1.3, 17%	0.071	9.4, 0.036, 0.5	**P8C$_f$**, 8.3 kDa, 1.2, -1.5 kDa, -15%
P8FRP, 28.7 kDa, 47.8 kDa, 1.6, 15%	0.066	8.8, 0.032, 0.5	**P8FRP$_f$**, 38.5 kDa, 1.5, -9.3 kDa, -19%

Table 12: Precursors and reactants in single chain folding of **P8** to **P8$_f$** including the corresponding SEC evaluation of the final SCNPs

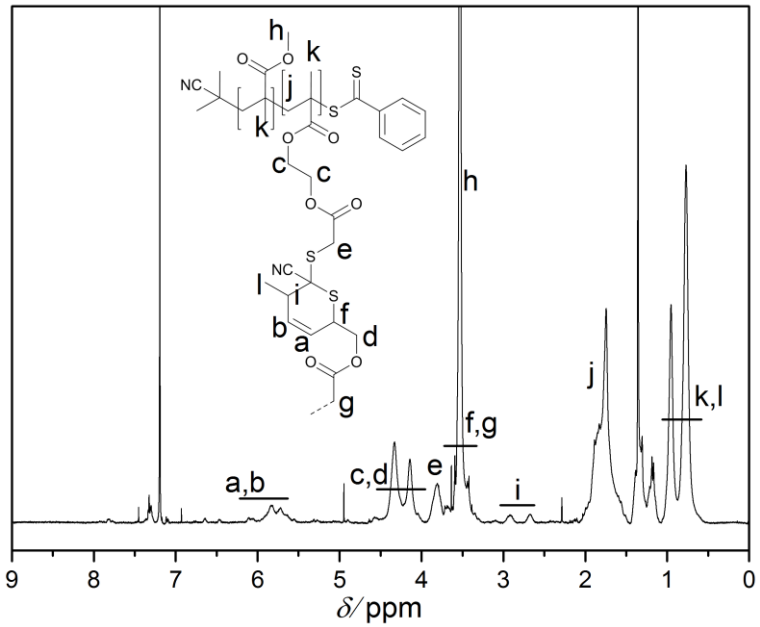

Figure 95: Representative ^{1}H-NMR spectrum of **P8$_f$** in $CDCl_3$.

5.4.12 *Unfolding of **P8A$_f$** (**P8A$_{uf}$**)*

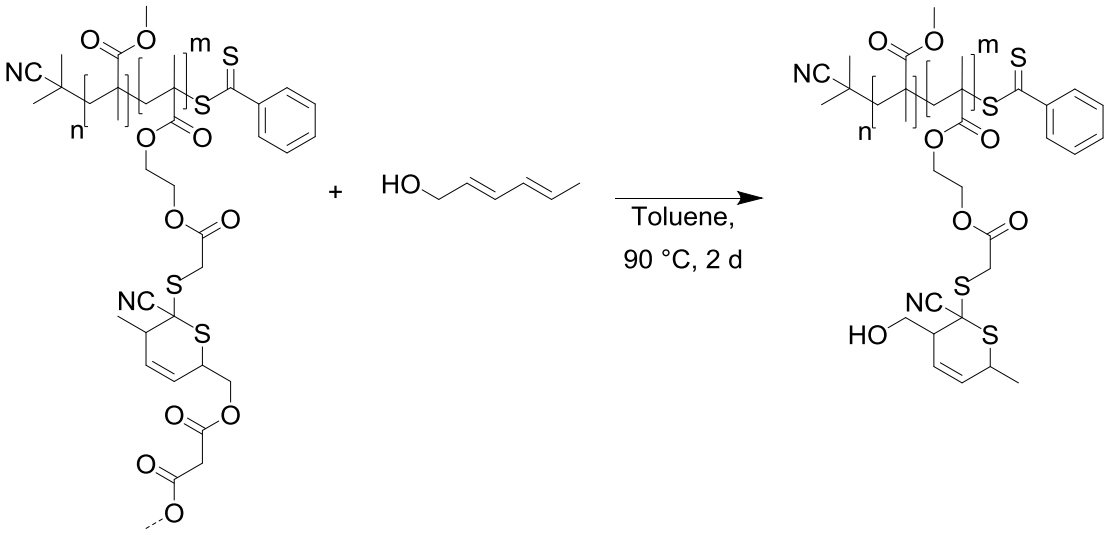

30 mg **P8A$_f$** (0.003 mmol, 0.036 mmol CDTE) was dissolved in toluene (150 mL) and 17.5 mg sorbic alcohol (0.18 mmol) was added. The reaction mixture was heated to 90 °C and stirred for 2 d. For isolation the reaction volume was reduced to 2~3 mL *in vacuo* and precipitated in cold cyclohexane (20 mL). The grayish powder **P8A$_{uf}$** was characterized by comparative SEC, DLS and ^{1}H-NMR measurements.

^{1}H-NMR ($CDCl_3$, 400 MHz), δ(ppm) = 6.1-5.6 (2mH), 4.4-4.2 (m, 4mH), 3.9-3.4 (m, 5mH+3nH),3.0-2.6 (1mH), 2.1-1.7 (m, 2nH+2mH), 1.08-0.68 (m, 6mH+3nH).

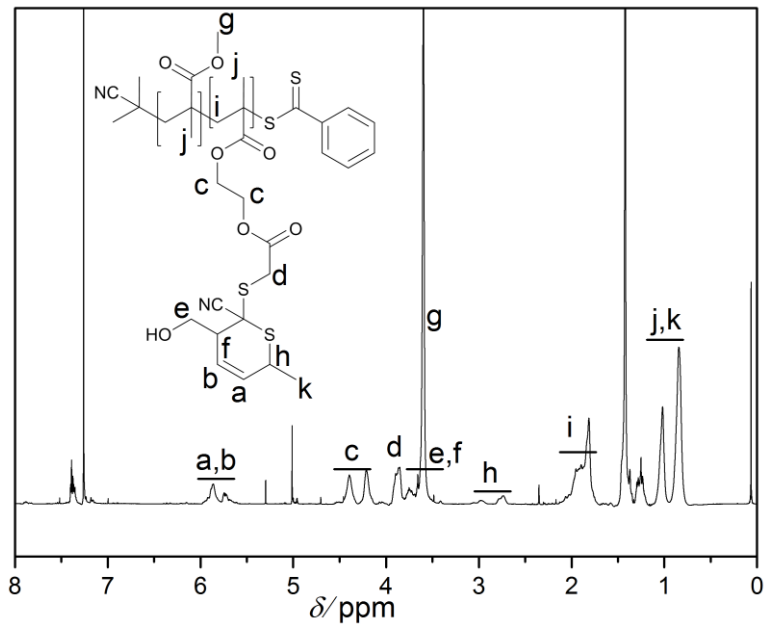

Figure 96: ^{1}H-NMR spectrum of **P8A$_{uf}$** in $CDCl_3$.

5.5 Surface Modification

5.5.1 *Tet-Si (**S1**)*

The neat silicon wafer was activated in H_2O_2/conc. H_2SO_4 (1/2) for 2 h at 100 °C. The wafer was extensively washed with MilliQ water and dried in an argon stream. Subsequently, the activated wafer was covered with a solution of Tet-Silane (**18**) in dry toluene (5 mg·mL), heated to 50°C for 1 h and stored at ambient temperature overnight. Unreacted **18** was removed by washing with toluene (HPLC grade), and the wafer was dried in an argon stream and used without further characterization.

5.5.2 *UPy-Si (**S2**)*

Surface **S1** was mounted in a sample holder and immersed in a filtered, saturated solution of UPy-Mal (**22**) in dry DMSO, and irradiated with an Arimed B6 lamp for 22 h. The surface was removed from the solution and the sample holder and extensively washed with THF, acetone, MeOH and DCM and dried in a N_2 stream. ToF-Sims analysis reveals spatially resolved immobilization of UPys indicated by a specific fragment (Figure 47).

5.5.3 *General Procedure to Immobilize UPys on UPy-Si (**S3**)*

Surface **S2** was immersed in a filtered solution of UPy (**23**, **P7**) in $CHCl_3$, heated to 50 °C for 15 min and kept 1 h at ambient temperature subsequently and washed. ToF-SIMS analysis and washing procedures are summarized in Table 3.

5.5.4 *AOA-Si (**S4**)*

Surface **S1** was mounted in a sample holder with a shadow mask and immersed in a solution of AOA-Mal (**27**) in dry DCM (c = 0.6 g·mL). The solution was degassed for 15 min in an ice bath and the surface was irradiated for 24 h with an Arimed B6 lamp. The surface was removed from the solution and the sample holder and extensively washed with DCM and dried in a N_2 stream. The surface was used for immobilization of SOA-PMMA without further analysis.

5.5.5 *Immobilization of SOA-PMMA (**S5/S5***)*

The washed surface **S4/S4*** was immersed in a filtered solution of SOA-PMMA, which was prepared according to a literature procedure and provided by Bernard and coworkers,[153] in dry toluene (c = 0.6 g·mL) for 10 min. The surface **S5** was washed extensively with toluene to remove any physisorbed SOA-PMMA and subsequently dried in a N_2 stream.

5.5.6 *Removal of H-bonded SOA-PMMA from Surfaces (**S4***)*

The surface **S5** was washed with 10 mL of 10% MeOH in $CHCl_3$ and dried in an N_2 stream.

6 BIBLIOGRAPHY

1. Odian, G., In *Principles of polymerization*, Wiley-Interscience: Hoboken, New Jersey, 2004; Vol. 4, p 302.

2. Currey, J. D. *Proc. R. Soc. B* **1977,** *196*, 443.

3. Diels, O.; Kurt, A. *Justus Liebigs Ann. Chem.* **1928,** *460*, 98.

4. Woodward, R. B.; Hoffmann, R. *J. Am. Chem. Soc.* **1965,** *87*, 395.

5. Klopman, G. *J. Am. Chem. Soc.* **1968,** *90*, 223.

6. Salem, L. *J. Am. Chem. Soc.* **1968,** *90*, 543.

7. Fleming, I., *Grenzorbitale und Reaktionen organischer Verbindungen*. VCH Verlagsgesellschaft mbH: Weinheim, 1983; Vol. 1.

8. Yang, N. C.; Rivas, C. *J. Am. Chem. Soc.* **1961,** *83*, 2213.

9. Whittell, G. R.; Hager, M. D.; Martin, U. S. *Nat. Mater.* **2011,** *10*, 176.

10. Pahnke, K.; Brandt, J.; Gryn'ova, G.; Lindner, P.; Schweins, R.; Schmidt, F. G.; Lederer, A.; Coote, M. L.; Barner-Kowollik, C. *Chemical Science* **2015,** *6*, 1061.

11. Hoffmann, R.; Woodward, R. B. *J. Am. Chem. Soc.* **1965,** *87*, 2046.

12. Woodward, R. B.; Hoffmann, R. *Angew. Chem. Int. Ed. Engl.* **1969,** *8*, 781.

13. Porter, G.; Tchir, M. F. *Journal of the Chemical Society D: Chemical Communications* **1970**, 1372.

14. Houk, K. N. *J. Am. Chem. Soc.* **1973,** *95*, 4092.

15. Kwart, H.; Burchuk, I. *J. Am. Chem. Soc.* **1952,** *74*, 3094.

16. Gandini, A. *Prog. Polym. Sci.* **2013,** *38*, 1.

17. Rulíšek, L.; Šebek, P.; Havlas, Z.; Hrabal, R.; Čapek, P.; Svatoš, A. *J. Org. Chem.* **2005,** *70*, 6295.

18. Tesoro, G. C.; Sastri, V. R. *Industrial & Engineering Chemistry Product Research and Development* **1986,** *25*, 444.

19. Middleton, W. J. *J. Org. Chem.* **1965,** *30*, 1390.

20. McGregor, W. M.; Sherrington, D. C. *Chem. Soc. Rev.* **1993,** *22*, 199.

21. Vedejs, E.; Eberlein, T. H.; Mazur, D. J.; McClure, C. K.; Perry, D. A.; Ruggeri, R.; Schwartz, E.; Stults, J. S.; Varie, D. L. *J. Org. Chem.* **1986,** *51*, 1556.

22. König, B.; Martens, J.; Praefcke, K.; Schönberg, A.; Schwarz, H.; Zeisberg, R. *Chem. Ber.* **1974,** *107*, 2931.

23. Vedejs, E.; Stults, J. S. *J. Org. Chem.* **1988,** *53*, 2226.

24. Mlostoń, G.; Grzelak, P.; Mikina, M.; Linden, A.; Heimgartner, H. *Beilstein Journal of Organic Chemistry* **2015,** *11*, 576.

25. Vyas, D. M.; Hay, G. W. *Journal of the Chemical Society D: Chemical Communications* **1971**, 1411.

26. Beslin, P.; Metzner, P. *Tetrahedron Lett.* **1980,** *21*, 4657.

27. Vyas, D. M.; Hay, G. W. *Can. J. Chem.* **1971,** *49*, 3755.

28. Oehlenschlaeger, K. K.; Guimard, N. K.; Brandt, J.; Mueller, J. O.; Lin, C. Y.; Hilf, S.; Lederer, A.; Coote, M. L.; Schmidt, F. G.; Barner-Kowollik, C. *Polym. Chem.* **2013,** *4*, 4348.

29. Kirby, G. W.; McGregor, W. M. *J. Chem. Soc., Perkin Trans. 1* **1990**, 3175.

30. Inglis, A. J.; Stenzel, M. H.; Barner-Kowollik, C. *Macromol. Rapid Commun.* **2009,** *30*, 1792.

31. Inglis, A. J.; Sinnwell, S.; Stenzel, M. H.; Barner-Kowollik, C. *Angew. Chem. Int. Ed.* **2009,** *48*, 2411.

32. Glassner, M.; Delaittre, G.; Kaupp, M.; Blinco, J. P.; Barner-Kowollik, C. *J. Am. Chem. Soc.* **2012,** *134*, 7274.

33. Sinnwell, S.; Inglis, A. J.; Davis, T. P.; Stenzel, M. H.; Barner-Kowollik, C. *Chem. Commun.* **2008**, 2052.

34. Schenzel, A. M.; Klein, C.; Rist, K.; Moszner, N.; Barner-Kowollik, C. *Advanced Science* **2016,** *3*, n/a.

35. Zhou, J.; Guimard, N. K.; Inglis, A. J.; Namazian, M.; Lin, C. Y.; Coote, M. L.; Spyrou, E.; Hilf, S.; Schmidt, F. G.; Barner-Kowollik, C. *Polym. Chem.* **2012,** *3*, 628.

36. Huisgen, R. *Angew. Chem.* **1963,** *75*, 742.

37. Kolb, H. C.; Finn, M. G.; Sharpless, K. B. *Angew. Chem. Int. Ed.* **2001,** *40*, 2004.

38. Barner-Kowollik, C.; Du Prez, F. E.; Espeel, P.; Hawker, C. J.; Junkers, T.; Schlaad, H.; Van Camp, W. *Angew. Chem. Int. Ed.* **2011,** *50*, 60.

39. Huisgen, R.; Knorr, R.; Möbius, L.; Szeimies, G. *Chem. Ber.* **1965,** *98*, 4014.

40. Buckley, G. D. *Journal of the Chemical Society (Resumed)* **1954**, 1850.

41. Meldal, M.; Tornøe, C. W. *Chem. Rev.* **2008,** *108*, 2952.

42. Horne, W. S.; Yadav, M. K.; Stout, C. D.; Ghadiri, M. R. *J. Am. Chem. Soc.* **2004,** *126*, 15366.

43. Xie, J.; Seto, C. T. *Biorg. Med. Chem.* **2007,** *15*, 458.

44. Zinzalla, G.; Milroy, L.-G.; Ley, S. V. *Organic & Biomolecular Chemistry* **2006,** *4*, 1977.

45. Derbré, S.; Roué, G.; Poupon, E.; Susin, S. A.; Hocquemiller, R. *ChemBioChem* **2005,** *6*, 979.

46. Roice, M.; Johannsen, I.; Meldal, M. *QSAR & Combinatorial Science* **2004,** *23*, 662.

47. Bock, V. D.; Speijer, D.; Hiemstra, H.; van Maarseveen, J. H. *Organic & Biomolecular Chemistry* **2007,** *5*, 971.

48. Voit, B. *New J. Chem.* **2007,** *31*, 1139.

49. Chen, G.; Tao, L.; Mantovani, G.; Ladmiral, V.; Burt, D. P.; Macpherson, J. V.; Haddleton, D. M. *Soft Matter* **2007,** *3*, 732.

50. Guo, Z.; Lei, A.; Liang, X.; Xu, Q. *Chem. Commun.* **2006**, 4512.

51. Ranjan, R.; Brittain, W. J. *Macromolecules* **2007,** *40*, 6217.

52. O'Reilly, R. K.; Joralemon, M. J.; Hawker, C. J.; Wooley, K. L. *Chem. Eur. J.* **2006,** *12*, 6776.

53. Kempe, K.; Krieg, A.; Becer, C. R.; Schubert, U. S. *Chem. Soc. Rev.* **2012,** *41*, 176.

54. Golas, P. L.; Tsarevsky, N. V.; Sumerlin, B. S.; Matyjaszewski, K. *Macromolecules* **2006,** *39*, 6451.

55. van Steenis, D. J. V. C.; David, O. R. P.; van Strijdonck, G. P. F.; van Maarseveen, J. H.; Reek, J. N. H. *Chem. Commun.* **2005**, 4333.

56. Díaz, D. D.; Punna, S.; Holzer, P.; McPherson, A. K.; Sharpless, K. B.; Fokin, V. V.; Finn, M. G. *J. Polym. Sci., Part A: Polym. Chem.* **2004,** *42*, 4392.

57. Van Camp, W.; Germonpré, V.; Mespouille, L.; Dubois, P.; Goethals, E. J.; Du Prez, F. E. *React. Funct. Polym.* **2007,** *67*, 1168.

58. Hasneen, A.; Kim, S. J.; Paik, H.-j. *Macromolecular Research* **2007,** *15*, 541.

59. Durmaz, H.; Dag, A.; Altintas, O.; Erdogan, T.; Hizal, G.; Tunca, U. *Macromolecules* **2007,** *40*, 191.

60. Golas, P. L.; Matyjaszewski, K. *QSAR & Comb. Sci.* **2007,** *26*, 1116.

61. Opsteen, J. A.; Hest, J. C. M. v. *Chem Commun (Camb)* **2005**, 57.

62. Agard, N. J.; Prescher, J. A.; Bertozzi, C. R. *J. Am. Chem. Soc.* **2004,** *126*, 15046.

63. Li, Z.; Seo, T. S.; Ju, J. *Tetrahedron Lett.* **2004,** *45*, 3143.

64. Huisgen, R.; Seidel, M.; Sauer, J.; McFarland, J.; Wallbillich, G. *J. Org. Chem.* **1959,** *24*, 892.

65. Eckell, A.; Huisgen, R.; Sustmann, R.; Wallbillich, G.; Grashey, D.; Spindler, E. *Chem. Ber.* **1967,** *100*, 2192.

66. Clovis, J. S.; Eckell, A.; Huisgen, R.; Sustmann, R.; Wallbillich, G.; Weberndörfer, V. *Chem. Ber.* **1967,** *100*, 1593.

67. Huisgen, R.; Sustmann, R.; Wallbillich, G. *Chem. Ber.* **1967,** *100*, 1786.

68. Wang, Y.; Rivera Vera, C. I.; Lin, Q. *Org. Lett.* **2007,** *9*, 4155.

69. Song, W.; Wang, Y.; Qu, J.; Madden, M. M.; Lin, Q. *Angew. Chem. Int. Ed.* **2008,** *47*, 2832.

70. Madden, M. M.; Rivera Vera, C. I.; Song, W.; Lin, Q. *Chem. Commun.* **2009**, 5588.

71. Li, Z.; Qian, L.; Li, L.; Bernhammer, J. C.; Huynh, H. V.; Lee, J.-S.; Yao, S. Q. *Angew. Chem. Int. Ed.* **2016,** *55*, 2002.

72. Suketaka, I.; Yumo, T.; Akikazu, K.; Ken-ichi, K. *Bull. Chem. Soc. Jpn.* **1976,** *49*, 1920.

73. Moderhack, D. *Journal für Praktische Chemie/Chemiker-Zeitung* **1998,** *340*, 687.

74. Dimroth, O.; Merzbacher, S. *Berichte der deutschen chemischen Gesellschaft* **1907,** *40*, 2402.

75. Weinberg, P.; Csongár, C.; Grummt, U.-W. *Journal of Photochemistry and Photobiology A: Chemistry* **1989,** *50*, 11.

76. Lohse, V.; Leihkauf, P.; Csongar, C.; Tomaschewski, G. *J. Prakt. Chem.* **1988,** *330*, 406.

77. Blasco, E.; Sugawara, Y.; Lederhose, P.; Blinco, J. P.; Kelterer, A.-M.; Barner-Kowollik, C. *ChemPhotoChem* **2016**, n/a.

78. Wang, Y.; Hu, W. J.; Song, W.; Lim, R. K. V.; Lin, Q. *Org. Lett.* **2008,** *10*, 3725.

79. Hiltebrandt, K.; Pauloehrl, T.; Blinco, J. P.; Linkert, K.; Börner, H. G.; Barner-Kowollik, C. *Angew. Chem. Int. Ed.* **2015,** *54*, 2838.

80. Rodriguez-Emmenegger, C.; Preuss, C. M.; Yameen, B.; Pop-Georgievski, O.; Bachmann, M.; Mueller, J. O.; Bruns, M.; Goldmann, A. S.; Bastmeyer, M.; Barner-Kowollik, C. *Adv. Mater.* **2013,** *25*, 6123.

81. Yu, Z.; Ho, L. Y.; Wang, Z.; Lin, Q. *Bioorg. Med. Chem. Lett.* **2011,** *21*, 5033.

82. Lederhose, P.; Wust, K. N. R.; Barner-Kowollik, C.; Blinco, J. P. *Chem. Commun.* **2016,** *52*, 5928.

83. Willenbacher, J.; Wuest, K. N. R.; Mueller, J. O.; Kaupp, M.; Wagenknecht, H.-A.; Barner-Kowollik, C. *ACS Macro Letters* **2014,** *3*, 574.

84. de Silva, A. P.; Gunaratne, H. Q. N.; Lynch, P. L. M. *Journal of the Chemical Society, Perkin Transactions 2* **1995**, 685.

85. Houk, K. N.; Sims, J.; Watts, C. R.; Luskus, L. J. *J. Am. Chem. Soc.* **1973,** *95*, 7301.

86. Zhang, Y.; Liu, W.; Zhao, Z. *Molecules* **2014,** *19*, 306.

87. Feng, W.; Li, L.; Yang, C.; Welle, A.; Trapp, O.; Levkin, P. A. *Angew. Chem. Int. Ed.* **2015,** *54*, 8732.

88. Song, W.; Wang, Y.; Qu, J.; Lin, Q. *J. Am. Chem. Soc.* **2008,** *130*, 9654.

89. Hufendiek, A.; Barner-Kowollik, C.; Meier, M. A. R. *Polym. Chem.* **2015,** *6*, 2188.

90. Tischer, T.; Rodriguez-Emmenegger, C.; Trouillet, V.; Welle, A.; Schueler, V.; Mueller, J. O.; Goldmann, A. S.; Brynda, E.; Barner-Kowollik, C. *Adv. Mater.* **2014,** *26*, 4087.

91. Arndt, S.; Wagenknecht, H.-A. *Angew. Chem. Int. Ed.* **2014,** *53*, 14580.

92. de Hoog, H.-P. M.; Nallani, M.; Liedberg, B. *Polym. Chem.* **2012,** *3*, 302.

93. Sugawara, Y.; Jasinski, N.; Kaupp, M.; Welle, A.; Zydziak, N.; Blasco, E.; Barner-Kowollik, C. *Chem. Commun.* **2015,** *51*, 13000.

94. Mueller, J. O.; Guimard, N. K.; Oehlenschlaeger, K. K.; Schmidt, F. G.; Barner-Kowollik, C. *Polym. Chem.* **2014,** *5*, 1447.

95. Zydziak, N.; Feist, F.; Huber, B.; Mueller, J. O.; Barner-Kowollik, C. *Chem. Commun.* **2015,** *51*, 1799.

96. Wedler-Jasinski, N.; Delbosc, N.; Virolleaud, M.-A.; Montarnal, D.; Welle, A.; Barner, L.; Walther, A.; Bernard, J.; Barner-Kowollik, C. *Chem. Commun.* **2016,** *52*, 8753.

97. Prins, L. J.; Reinhoudt, D. N.; Timmerman, P. *Angew. Chem. Int. Ed. Engl.* **2001,** *40*, 2382.

98. Sijbesma, R. P.; Meijer, E. W. *Chem. Commun.* **2003,** *0*, 5.

99. Beijer, F. H.; Sijbesma, R. P.; Vekemans, J. A. J. M.; Meijer, E. W.; Kooijman, H.; Spek, A. L. *J. Org. Chem.* **1996,** *61*, 6371.

100. Sherrington, D. C.; Taskinen, K. A. *Chem. Soc. Rev.* **2001,** *30*, 83.

101. Nernst, W. *Z. Phys. Chem.* **1892,** *8*, 110.

102. Bernal, J. D.; Megaw, H. D. *Proc. R. Soc. A* **1935,** *151*, 384.

103. Taylor, R.; Kennard, O.; Versichel, W. *J. Am. Chem. Soc.* **1984,** *106*, 244.

104. Tsubomura, H. *Bull. Chem. Soc. Jpn.* **1954,** *27*, 445.

105. Kollman, P. A.; Allen, L. C. *Chem. Rev.* **1972,** *72*, 283.

106. Bell, D. A.; Anslyn, E. V. *J. Org. Chem.* **1994,** *59*, 512.

107. Sartorius, J.; Schneider, H.-J. *Chem. Eur. J.* **1996,** *2*, 1446.

108. Hammes, G. G.; Park, A. C. *J. Am. Chem. Soc.* **1968,** *90*, 4151.

109. Hirschberg, J. H. K. K.; Beijer, F. H.; van Aert, H. A.; Magusin, P. C. M. M.; Sijbesma, R. P.; Meijer, E. W. *Macromolecules* **1999,** *32*, 2696.

110. Söntjens, S. H. M.; Sijbesma, R. P.; van Genderen, M. H. P.; Meijer, E. W. *Macromolecules* **2001,** *34*, 3815.

111. Folmer, B. J. B.; Sijbesma, R. P.; Meijer, E. W. *J. Am. Chem. Soc.* **2001,** *123*, 2093.

112. Konrat, R.; Tollinger, M.; Kontaxis, G.; Kräutler, B. *Monatsh. Chem.* **1999,** *130*, 961.

113. Nieuwenhuizen, M. M. L.; de Greef, T. F. A.; van der Bruggen, R. L. J.; Paulusse, J. M. J.; Appel, W. P. J.; Smulders, M. M. J.; Sijbesma, R. P.; Meijer, E. W. *Chem. Eur. J.* **2010,** *16*, 1601.

114. Botterhuis, N. E.; van Beek, D. J. M.; van Gemert, G. M. L.; Bosman, A. W.; Sijbesma, R. P. *J. Polym. Sci., Part A: Polym. Chem.* **2008,** *46*, 3877.

115. Kuo, S.-W.; Tsai, H.-T. *J. Appl. Polym. Sci.* **2012,** *123*, 3275.

116. Zeng, H.; Miller, R. S.; Flowers, R. A.; Gong, B. *J. Am. Chem. Soc.* **2000,** *122*, 2635.

117. Zhu, B.; Jasinski, N.; Benitez, A.; Noack, M.; Park, D.; Goldmann, A. S.; Barner-Kowollik, C.; Walther, A. *Angew. Chem. Int. Ed.* **2015,** *54*, 8653.

118. Wyler, R.; de Mendoza, J.; Rebek, J. *Angew. Chem.* **1993,** *105*, 1820.

119. Ghadiri, M. R.; Granja, J. R.; Milligan, R. A.; McRee, D. E.; Khazanovich, N. *Nature* **1993,** *366*, 324.

120. Brunsveld, L.; Folmer, B. J. B.; Meijer, E. W.; Sijbesma, R. P. *Chem. Rev.* **2001,** *101*, 4071.

121. Zhang, Y.; Anderson, C. A.; Zimmerman, S. C. *Org. Lett.* **2013,** *15*, 3506.

122. Altintas, O.; Artar, M.; ter Huurne, G.; Voets, I. K.; Palmans, A. R. A.; Barner-Kowollik, C.; Meijer, E. W. *Macromolecules* **2015,** *48*, 8921.

123. Altintas, O.; Barner-Kowollik, C. *Macromol. Rapid Commun.* **2012,** *33*, 958.

124. Terashima, T.; Mes, T.; De Greef, T. F. A.; Gillissen, M. A. J.; Besenius, P.; Palmans, A. R. A.; Meijer, E. W. *J. Am. Chem. Soc.* **2011,** *133*, 4742.

125. Yamauchi, K.; Lizotte, J. R.; Long, T. E. *Macromolecules* **2003,** *36*, 1083.

126. Kokil, A.; Saito, T.; Depolo, W.; Elkins, C. L.; Wilkes, G. L.; Long, T. E. *J. Macromol. Sci., Part A: Pure Appl. Chem.* **2011,** *48*, 1016.

127. Neikirk, C. C.; Chung, J. W.; Priestley, R. D. *RSC Advances* **2013,** *3*, 16686.

128. Celiz, A. D.; Lee, T.-C.; Scherman, O. A. *Adv. Mater.* **2009,** *21*, 3937.

129. Li, S.-L.; Xiao, T.; Xia, W.; Ding, X.; Yu, Y.; Jiang, J.; Wang, L. *Chem. Eur. J.* **2011,** *17*, 10716.

130. De Greef, T. F. A.; Kade, M. J.; Feldman, K. E.; Kramer, E. J.; Hawker, C. J.; Meijer, E. W. *J. Polym. Sci., Part A: Polym. Chem.* **2011,** *49*, 4253.

131. Hosono, N.; Gillissen, M. A. J.; Li, Y.; Sheiko, S. S.; Palmans, A. R. A.; Meijer, E. W. *J. Am. Chem. Soc.* **2012,** *135*, 501.

132. Berda, E. B.; Foster, E. J.; Meijer, E. W. *Macromolecules* **2010,** *43*, 1430.

133. Kieltyka, R. E.; Pape, A. C. H.; Albertazzi, L.; Nakano, Y.; Bastings, M. M. C.; Voets, I. K.; Dankers, P. Y. W.; Meijer, E. W. *J. Am. Chem. Soc.* **2013,** *135*, 11159.

134. Appel, W. P. J.; Portale, G.; Wisse, E.; Dankers, P. Y. W.; Meijer, E. W. *Macromolecules* **2011,** *44*, 6776.

135. Ohkawa, H.; Ligthart, G. B. W. L.; Sijbesma, R. P.; Meijer, E. W. *Macromolecules* **2007,** *40*, 1453.

136. de Greef, T. F. A.; Ercolani, G.; Ligthart, G. B. W. L.; Meijer, E. W.; Sijbesma, R. P. *J. Am. Chem. Soc.* **2008,** *130*, 13755.

137. Wong, C.-H.; Chan, W.-S.; Lo, C.-M.; Chow, H.-F.; Ngai, T.; Wong, K.-W. *Macromolecules* **2010,** *43*, 8389.

138. Feldman, K. E.; Kade, M. J.; Meijer, E. W.; Hawker, C. J.; Kramer, E. J. *Macromolecules* **2010,** *43*, 5121.

139. Wrue, M. H.; McUmber, A. C.; Anthamatten, M. *Macromolecules* **2009,** *42*, 9255.

140. Hentschel, J.; Kushner, A. M.; Ziller, J.; Guan, Z. *Angew. Chem. Int. Ed.* **2012,** *51*, 10561.

141. Park, T.; Zimmerman, S. C. *J. Am. Chem. Soc.* **2006,** *128*, 14236.

142. Söntjens, S. H. M.; Renken, R. A. E.; van Gemert, G. M. L.; Engels, T. A. P.; Bosman, A. W.; Janssen, H. M.; Govaert, L. E.; Baaijens, F. P. T. *Macromolecules* **2008,** *41*, 5703.

143. Dankers, P. Y. W.; van Leeuwen, E. N. M.; van Gemert, G. M. L.; Spiering, A. J. H.; Harmsen, M. C.; Brouwer, L. A.; Janssen, H. M.; Bosman, A. W.; van Luyn, M. J. A.; Meijer, E. W. *Biomaterials* **2006,** *27*, 5490.

144. Li, J.; Lewis, C. L.; Chen, D. L.; Anthamatten, M. *Macromolecules* **2011,** *44*, 5336.

145. Elkins, C. L.; Viswanathan, K.; Long, T. E. *Macromolecules* **2006,** *39*, 3132.

146. Chen, Y.; Ballard, N.; Bon, S. A. F. *Polym. Chem.* **2013,** *4*, 387.

147. Lewis, C. L.; Anthamatten, M. *Soft Matter* **2013,** *9*, 4058.

148. Cui, J.; Wang, D.; Koynov, K.; del Campo, A. *ChemPhysChem* **2013,** *14*, 2932.

149. Shokrollahi, P.; Mirzadeh, H.; Scherman, O. A.; Huck, W. T. S. *Journal of Biomedical Materials Research Part A* **2010,** *95A*, 209.

150. Biyani, M. V.; Foster, E. J.; Weder, C. *ACS Macro Letters* **2013,** *2*, 236.

151. Feldman, K. E.; Kade, M. J.; Meijer, E. W.; Hawker, C. J.; Kramer, E. J. *Macromolecules* **2009,** *42*, 9072.

152. Gong, B. *Polym. Int.* **2007,** *56*, 436.

153. Montarnal, D.; Delbosc, N.; Chamignon, C.; Virolleaud, M.-A.; Luo, Y.; Hawker, C. J.; Drockenmuller, E.; Bernard, J. *Angew. Chem. Int. Ed.* **2015,** *54*, 11117.

154. Yang, X.; Hua, F.; Yamato, K.; Ruckenstein, E.; Gong, B.; Kim, W.; Ryu, C. Y. *Angew. Chem. Int. Ed.* **2004,** *43*, 6471.

155. Zeng, H.; Ickes, H.; Flowers, R. A.; Gong, B. *J. Org. Chem.* **2001,** *66*, 3574.

156. Kojima, Y.; Usuki, A.; Kawasumi, M.; Okada, A.; Kurauchi, T.; Kamigaito, O. *J. Polym. Sci., Part A: Polym. Chem.* **1993,** *31*, 983.

157. Kawasumi, M. *J. Polym. Sci., Part A: Polym. Chem.* **2004,** *42*, 819.

158. Jang, B. N.; Costache, M.; Wilkie, C. A. *Polymer* **2005,** *46*, 10678.

159. Caruso, F.; Spasova, M.; Susha, A.; Giersig, M.; Caruso, R. A. *Chem. Mater.* **2000,** *13*, 109.

160. Vaia, R. A.; Wagner, H. D. *Mater. Today* **2004,** *7*, 32.

161. Pavlidou, S.; Papaspyrides, C. D. *Prog. Polym. Sci.* **2008,** *33*, 1119.

162. Di Maio, E.; Iannace, S.; Sorrentino, L.; Nicolais, L. *Polymer* **2004,** *45*, 8893.

163. Zhang, Q.-X.; Yu, Z.-Z.; Yang, M.; Ma, J.; Mai, Y.-W. *J. Polym. Sci., Part B: Polym. Phys.* **2003,** *41*, 2861.

164. Mu, B.; Wang, Q.; Wang, H.; Jian, L. *J. Macromol. Sci., Part B: Phys.* **2007,** *46*, 1093.

165. Li, L.; Li, C. Y.; Ni, C.; Rong, L.; Hsiao, B. *Polymer* **2007,** *48*, 3452.

166. Rittigstein, P.; Torkelson, J. M. *J. Polym. Sci., Part B: Polym. Phys.* **2006,** *44*, 2935.

167. Merkel, T. C.; Freeman, B. D.; Spontak, R. J.; He, Z.; Pinnau, I.; Meakin, P.; Hill, A. J. *Science* **2002,** *296*, 519.

168. Pluta, M.; Jeszka, J. K.; Boiteux, G. *Eur. Polym. J.* **2007,** *43*, 2819.

169. Paul, D. R.; Robeson, L. M. *Polymer* **2008,** *49*, 3187.

170. Hofmann, U. *Angew. Chem. Int. Ed. Engl.* **1968,** *7*, 681.

171. Ogawa, M.; Handa, T.; Kuroda, K.; Kato, C. *Chem. Lett.* **1990,** *19*, 71.

172. Barthelat, F.; Tang, H.; Zavattieri, P. D.; Li, C. M.; Espinosa, H. D. *J. Mech. Phys. Solids* **2007,** *55*, 306.

173. Song, F.; Zhou, J.; Xu, X.; Xu, Y.; Bai, Y. *Phys. Rev. Lett.* **2008,** *100*, 245502.

174. Song, F.; Soh, A. K.; Bai, Y. L. *Biomaterials* **2003,** *24*, 3623.

175. Smith, B. L.; Schaffer, T. E.; Viani, M.; Thompson, J. B.; Frederick, N. A.; Kindt, J.; Belcher, A.; Stucky, G. D.; Morse, D. E.; Hansma, P. K. *Nature* **1999,** *399*, 761.

176. Wang, R. Z.; Suo, Z.; Evans, A. G.; Yao, N.; Aksay, I. A. *J. Mater. Res.* **2001,** *16*, 2485.

177. Barthelat, F.; Li, C.-M.; Comi, C.; Espinosa, H. D. *J. Mater. Res.* **2006,** *21*, 1977.

178. Espinosa, H. D.; Rim, J. E.; Barthelat, F.; Buehler, M. J. *Prog. Mater Sci.* **2009,** *54*, 1059.

179. Krishnamoorti, R. *MRS Bull.* **2007,** *32*, 341.

180. Vaia, R. A.; Giannelis, E. P. *Macromolecules* **1997,** *30*, 7990.

181. Sahoo, N. G.; Rana, S.; Cho, J. W.; Li, L.; Chan, S. H. *Prog. Polym. Sci.* **2010,** *35*, 837.

182. Shen, Z.; Simon, G. P.; Cheng, Y.-B. *Polymer* **2002,** *43*, 4251.

183. Panwar, A.; Choudhary, V.; Sharma, D. K. *J. Reinf. Plast. Compos.* **2011,** *30*, 446.

184. Almqvist, N.; Thomson, N. H.; Smith, B. L.; Stucky, G. D.; Morse, D. E.; Hansma, P. K. *Mater. Sci. Eng., C* **1999,** *7*, 37.

185. Mavila, S.; Eivgi, O.; Berkovich, I.; Lemcoff, N. G. *Chem. Rev.* **2016,** *116*, 878.

186. Altintas, O.; Barner-Kowollik, C. *Macromol. Rapid Commun.* **2016,** *37*, 29.

187. Sanchez-Sanchez, A.; Pérez-Baena, I.; Pomposo, J. *Molecules* **2013,** *18*, 3339.

188. Kuhn, V. W.; Majer, H. *Die Makromolekulare Chemie* **1956,** *18*, 239.

189. Merrifield, R. B. *J. Am. Chem. Soc.* **1963,** *85*, 2149.

190. Danilov, D.; Barner-Kowollik, C.; Wenzel, W. *Chem. Commun.* **2015,** *51*, 6002.

191. Moreno, A. J.; Lo Verso, F.; Sanchez-Sanchez, A.; Arbe, A.; Colmenero, J.; Pomposo, J. A. *Macromolecules* **2013,** *46*, 9748.

192. Aiertza, M. K.; Odriozola, I.; Cabañero, G.; Grande, H.-J.; Loinaz, I. *Cellular and Molecular Life Sciences* **2012,** *69*, 337.

193. Wojtecki, R. J.; Meador, M. A.; Rowan, S. J. *Nat Mater* **2011,** *10*, 14.

194. Rowan, S. J.; Cantrill, S. J.; Cousins, G. R. L.; Sanders, J. K. M.; Stoddart, J. F. *Angew. Chem. Int. Ed.* **2002,** *41*, 898.

195. Black, S. P.; Sanders, J. K. M.; Stefankiewicz, A. R. *Chem. Soc. Rev.* **2014,** *43*, 1861.

196. Murray, B. S.; Fulton, D. A. *Macromolecules* **2011,** *44*, 7242.

197. Buruaga, L.; Pomposo, J. A. *Polymers* **2011,** *3*, 1673.

198. Maddipatla, M. V. S. N.; Wehrung, D.; Tang, C.; Fan, W.; Oyewumi, M. O.; Miyoshi, T.; Joy, A. *Macromolecules* **2013,** *46*, 5133.

199. Müller-Dethlefs, K.; Hobza, P. *Chem. Rev.* **2000,** *100*, 143.

200. Gillissen, M. A. J.; Voets, I. K.; Meijer, E. W.; Palmans, A. R. A. *Polym. Chem.* **2012,** *3*, 3166.

201. Lu, J.; ten Brummelhuis, N.; Weck, M. *Chem. Commun.* **2014,** *50*, 6225.

202. Morishima, Y.; Nomura, S.; Ikeda, T.; Seki, M.; Kamachi, M. *Macromolecules* **1995,** *28*, 2874.

203. Mackay, M. E.; Dao, T. T.; Tuteja, A.; Ho, D. L.; Van Horn, B.; Kim, H.-C.; Hawker, C. J. *Nat Mater* **2003,** *2*, 762.

204. Huerta, E.; Stals, P. J. M.; Meijer, E. W.; Palmans, A. R. A. *Angew. Chem. Int. Ed.* **2013,** *52*, 2906.

205. Perez-Baena, I.; Loinaz, I.; Padro, D.; Garcia, I.; Grande, H. J.; Odriozola, I. *J. Mater. Chem.* **2010,** *20*, 6916.

206. Zhu, B.; Sun, S.; Wang, Y.; Deng, S.; Qian, G.; Wang, M.; Hu, A. *Journal of Materials Chemistry C* **2013,** *1*, 580.

207. Oria, L.; Aguado, R.; Pomposo, J. A.; Colmenero, J. *Adv. Mater.* **2010,** *22*, 3038.

208. Jasinski, N.; Lauer, A.; Stals, P. J. M.; Behrens, S.; Essig, S.; Walther, A.; Goldmann, A. S.; Barner-Kowollik, C. *ACS Macro Letters* **2015,** *4*, 298.

209. Dietrich, M.; Delaittre, G.; Blinco, J. P.; Inglis, A. J.; Bruns, M.; Barner-Kowollik, C. *Adv. Funct. Mater.* **2012,** *22*, 304.

210. Mantovani, G.; Lecolley, F.; Tao, L.; Haddleton, D. M.; Clerx, J.; Cornelissen, J. J. L. M.; Velonia, K. *J. Am. Chem. Soc.* **2005,** *127*, 2966.

211. Wedler-Jasinski, N.; Lueckerath, T.; Mutlu, H.; Goldmann, A. S.; Walther, A.; Stenzel, M. H.; Barner-Kowollik, C. *Chem. Commun.* **2017**.

212. Mansfeld, U.; Hager, M. D.; Hoogenboom, R.; Ott, C.; Winter, A.; Schubert, U. S. *Chem. Commun.* **2009**, 3386.

7 APPENDIX

7.1 List of Publications

Publications arising from this thesis are marked with an asterisk.

*[6]** *Dynamic Covalent Single Chain Nanoparticles based on Hetero Diels-Alder Chemistry* Wedler-Jasinski, N.; Lückerath, T.; Mutlu, H.; Goldmann, A. S.; Walther, A.; Stenzel, M. H., Barner-Kowollik, C. *Chem. Commun.* ***2017****, in press.*

*[5]** *Recodable Surfaces Based on Switchable Hydrogen Bonds* Wedler-Jasinski, N.; Delbosc, N.; Virolleaud, M.-A.; Montarnal, D.; Welle, A.; Barner, L.; Walther, A.; Bernard, J.; Barner-Kowollik, C., *Chem. Commun.* **2016**, *52*, 8753-8756.

[4] *Maleimide-Functionalized Poly(2-ethyl-2-oxazoline): Synthesis and Reactivity,*Wendler, F.; Rudolph, T.; Görls, H.; Jasinski, N.; Trouillet, V.; Barner-Kowollik, C.; Schacher, F. H. *Polym. Chem.* **2016**, *7*, 2419-2426.

[3] *Light-Driven Nitrile Imine-Mediated Tetrazole-Ene Cycloaddition as a Versatile Platform for Fullerene Conjugation,* Sugawara, Y.; Jasinski, N.; Kaupp, M.; Welle, A.; Zydziak, N.; Blasco, E.; Barner-Kowollik, C. *Chem. Commun.* **2015**, *51*, 13000-13003.

[2] *Hierarchical Nacre-Mimetics with Synergistic Mechanical Properties by Control of Molecular Interactions in Self-Healing Polymers,* Zhu, B.; Jasinski, N.; Benitez, A.; Noack, M.; Park, D.; Goldmann, A. S.; Barner-Kowollik, C.; Walther, A. *Angew. Chem. Int. Ed.* **2015**, *4*, 8653-8657.

*[1]** *Cleaning the Click: A Simple Electrochemical Avenue for Copper Removal from Strongly Coordinating Macromolecules,* Jasinski, N.; Lauer, A.; Stals, P. J. M.; Behrens, S.; Essig, S.; Walther, A.; Goldmann, A. S.; Barner-Kowollik, C. *ACS Macro Lett.* **2015**, *4*, 298–301.

7.2 List of Figures

7.3 List of Schemes

7.4 List of Tables

7.5 List of Abbreviations

4f-Bib ..... Pentaerythritol tetrakis(2-bromoisobutyrate)
6f-Bib ..... Dipentaerythritol hexakis(2-bromoisobutyrate)
ACN ..... Acetonitrile
AES ..... Atomic Emission Spectrometry
AGET ATRP ..... Activators Generated by Electron Transfer
..... Atom Transfer Radical Polymerization
AIBN ..... Azobis(isobutyronitril)
AlOx ..... Aluminum Oxide
AOA ..... Asymmetrical Oligo Amides
APTES ..... (3-Aminopropyl)triethoxysilane
ATRP ..... Atom Transfer Radical Polymerization
BMA ..... Butyl methacrylate
Boc ..... *t*-Butoxy carbonyl
Boc_2O ..... Di-*tert*-butyl dicarbonate
bPy ..... 2,2´-Bipyridine
CA ..... Cycloaddition
Cbz ..... Carboxybenzyl
CDI ..... Carbonyldiimidazole
CDTE ..... Cyanodithioester
Cp ..... Cyclopentadiene
CuAAc ..... Copper(I)-Catalyzed Azide-Alkyne Cycloaddition,
DA ..... Diels-Alder
DCC ..... N,N´-Dicylcohexylcarbodiimide
DCM ..... Dichloromethane
DHTP 3,6-Dihydro-*2H*-thiopyrane
DLS ..... Dynamic Light Scattering
DMAP 4-Dimethylaminopyridine
DMF ..... Dimethylformamide
DMSO ..... Dimethyl sulfoxide
CPDB ..... 2-Cyano-2-propyl benzodithioate
EDC·HCl ..... 1-(3-Dimethylaminopropyl)-3-ethylcarbodiimide hydrochloride
EDTA ..... Ethylenediaminetetraacetic acid
FMO ..... Frontier Molecular Orbitals

FRP ..... Free Radical Polymerization
HBTU ..... 2-(1*H*-Benzotriazol-1-yl)-1,1,3,3-tetramethyluronium-hexafluorphosphat
HDA ..... Hetero Diels-Alder
HEMA ..... Hydroxyethylmethacrylate
HOMO ..... Highest Occupied Molecular Orbital
IC ..... Internal Conversion
IR ..... Infrared
ISC ..... Intersystem crossing
LUMO ..... Lowest Unoccupied Molecular Orbital
MeOEGMA ..... Poly(ethylene glycol) methyl ether methacrylate
MeOH ..... Methanol
mg ..... Milligramm
MO ..... Molecular Orbital
MRFA ..... Met-Arg-Phe-Ala acetate
NaPy 2,7-Diamido-1,8-naphthyridine
NC ..... Nano-composite
NITEC ..... Nitrile imine-mediated tetrazole-ene cycloaddition
nm ..... Nanometer
OEGMA ..... Poly(ethylene glycol) methacrylate
pH ..... Power of Hydrogen
PMDTA ..... *N*,*N*′,*N*″,*N*″-Pentamethyldiethylenetriamine
RAFT ..... Reversible Addition-Fragmentation Chain-Transfer
rDA ..... Retro Diels-Alder
SCNP ..... Single-chain nano-particle
SEC ..... Size Exclusion Chromatography
SOA ..... Symmetrical Oligo Amide
TEM ..... Transmission Electron Microscopy
TFA ..... Trifluoroacetic Acid
TFEMA ..... 2,2,2-Trifluoroethyl methacrylate
TLC ..... Thin-layer Chromatography
ToF-SIMS ..... Time-of-Flight Secondary Ion Mass Spectrometry
UPy 2-Ureido-4-pyrimidone
VR ..... Vibrational relaxation
WH ..... Woodward-Hoffmann

wt ..... Weight

XRD ..... X-ray Diffraction

δ ..... Chemical Shift

7.6 Acknowledgements

Zum Ende dieser Arbeit möchte ich persönlich all denen danken, die mich während meiner Promotion unterstützt und begleitet haben.

Zuerst möchte ich mich bei meinem Doktorvater Prof. Dr. Christopher Barner-Kowollik, für die Möglichkeit meine Arbeit unter seiner Anleitung anzufertigen, bedanken. Die ausgezeichnete und angenehme Betreuung, die Bereitstellung aller benötigten Materialien, sowie der Verweis auf sinnvolle Ansprechpartner und Analytiker waren von großer Hilfe für mich.

Weiter bedanke ich mich bei meinen Kooperationspartnern Prof. Dr. Andreas Walther, Dr. Baolei Zhu und Saskia Gröer für die angenehme Zusammenarbeit, die Herstellung und Messung der Nanokomposite, sowie die Hilfe bei der Interpretation der Messdaten.

Ein großes Dankeschön geht an Dr. Anja Goldmann für ihre herausragende und freundliche Unterstützung in vielerlei Lagen sowie das Korrekturlesen dieser Arbeit.

Bei der VW Stiftung bedanke ich mich für die finanzielle Unterstützung meiner Promotion und die Einladung zum Statussymposium.

Vielen Dank an Maria Schneider, Evelyn Stühring, Vincent Schüler und Katharina Elies für die großartige administrative und technische Unterstützung während meiner Promotion.

Bei Andrea Lauer bedanke ich mich dafür, dass ich ihre herausragende Masterarbeit betreuen durfte und für ihre Hilfe und Anregungen im Bereich der Matrixsynthese.

Desweiteren danke ich Thorsten Lückerath für seine großartige Masterarbeit und seine umfassende und tatkräftige Hilfe im Feld der Hetero Diels-Alder Chemie.

Ich bedanke mich bei Tobias Fischer für seine Hilfe im Rahmen seiner Zeit als studentische Hilfskraft.

Ein großes Dankeschön geht an Dr. Silke Behrens und Sarah Essig für die AES Messungen.

Bei Dr. Alexander Welle bedanke ich mich für die vielen ToF-SIMS Messungen und dafür, dass er mir die damit verbundene Logistik immer so einfach wie möglich gestaltet hat.

I thank Dr. Julien Bernard and Dr. Damien Montarnal for providing the SOA/AOA precursors and compounds employed in this current thesis.

Ein großes Dankeschön geht an Kilian Wüst für die großzügige Bereitstellung von Chemikalien und das ausführliche Korrekturlesen des Kapitels über SCNPs.

Dr. Hatice Mutlu danke ich für die schnellen und unkomplizierten DLS Messungen und ihre hilfreiche Korrektur des Kapitels über UPy-Matrix Polymere.

Bei Dr. Eva Blasco bedanke ich mich für ihre Unterstützung in der Tetrazolsynthese und das umfassende Korrekturlesen des Oberflächen-Kapitels meiner Dissertation.

Mein Dank geht an Alexander Schenzel für den bis-Cp Linker und die Korrektur von Abstract, Introduction und Discussion dieser Arbeit.

Ich danke Jan Steinkönig für das Korrekturlesen des Kapitels über Hetero Diels-Alder Matrices.

Ein riesen Dankeschön geht an meine Kommilitonen und Freunde Kai, Niklas und Patrick für unsere großartige gemeinsame Zeit am KIT und darüber hinaus.

Ich bedanke mich besonders bei meinen Eltern, meiner Familie und Schwiegereltern für ihre Unterstützung und ihr Verständnis, wenn ich wieder mal zu wenig Zeit für sie hatte.

Ein besonderer Dank gebührt meiner Frau Nadin, die mit mir nicht nur die Freuden und die Unwägbarkeiten des Lebens schulterte, sondern auch immer geduldig und verständnisvoll war, wenn ich mal wieder spät abends, früh morgens oder am Wochenende arbeiten musste. Weil ohne sie nicht eine einzige Zeile dieser Arbeit geschrieben worden wäre, habe ich meine Dissertation ihr gewidmet.